# G-FLOWS Stage 3: Hydrogeological conceptual understanding of the Anangu Pitjantjatjara Yankunytjatjara (APY) Lands groundwater system including the Lindsay East Palaeovalley

Andrew Love, Adrian Costar, Carmen Krapf, Yueqing Xie, Ilka Wallis, Tessa Lane, Mark Keppel, Kent Inverarity, Zijiuan Deng, Tim Munday and Neville Robinson

Goyder Institute for Water Research
Technical Report Series No. 20/06

www.goyderinstitute.org

**Goyder Institute for Water Research Technical Report Series ISSN: 1839-2725**

The Goyder Institute for Water Research is a partnership between the South Australian Government through the Department for Environment and Water, CSIRO, Flinders University, the University of Adelaide, and the University of South Australia. The Institute enhances the South Australian Government's capacity to develop and deliver science-based policy solutions in water management. It brings together the best scientists and researchers across Australia to provide expert and independent scientific advice to inform good government water policy and identify future threats and opportunities to water security.

The following Associate organisations contributed to this report:

Enquires should be addressed to: Goyder Institute for Water Research
Level 4, Rundle Mall Plaza, 50 Rundle Mall,
Adelaide, SA 5000
tel: 08 8313 5020
e-mail: enquiries@goyderinstitute.org

**Citation**

Love A., Costar A., Krapf C., Xie Y., Wallis I., Lane T., Keppel M., Inverarity K., Deng Z., Munday T. and Robinson N. (2020) *G-FLOWS Stage 3: Hydrogeological conceptual understanding of the APY Lands groundwater system including the Lindsay East Palaeovalley*. Goyder Institute for Water Research Technical Report Series No. 20/06.

# Contents

# Figures

# Tables

# Executive summary

The scarcity of reliable and useable water resources is one of the most significant limitations on health, wellbeing and economic development in the semi-arid and arid regions of South Australia. The Anangu Pitjantjatjara Yankunytjatjara (APY) Lands in the north-western part of South Australia are an example where water resources are almost entirely reliant on shallow, typically low yielding (and often saline) groundwater systems. Communities in this region rely upon these groundwater resources to supply water for their community supplies as well as economic purposes including road building, pastoral, agriculture and mining industries (although to date there are no mining developments in the APY Lands).

There has been considerable investment in airborne electromagnetic (AEM) and other geophysical surveys in this region that are primarily used in mineral exploration. These data sets may help in the investigation, identification and targeting of other potential aquifer systems, most notably the hidden palaeovalley systems (that are located tens of meters below today's land surface). Very little information on the water quality and quantity is available on these currently unexplored systems.

The Goyder Institute for Water Research "Facilitating Long-term Outback Water Solutions" (G-FLOWS) is a research project which incorporates a suite of tasks to specifically determine and test the usefulness of these geophysical data to provide information on groundwater resources.

This report describes the project work conducted to enhance the conceptual hydrogeological understanding, both at the regional scale (referred to as the study area) and at a hydrogeological control site located at what is known as the Lindsay East Palaeovalley. However, it should be noted that this is the current understanding and as future studies and investigations continue to collect, analyse and interpret more data, the conceptualisation will evolve.

A major part of this report is the development of a novel conceptual hydrogeological groundwater numerical model, its conceptualisation and the environmental tracers (groundwater age dating) that underpins this conceptualisation. The model indicates that a number of local recharge and discharge features occur throughout the study area, which were tested and confirmed by numerical modelling along two main transects that span the study area. The plausibility of these local and occasionally intermediate flow systems has been confirmed by numerical modelling experiments. Only very small undulations in the watertable will drive these flow cells, resulting in considerably more vertical flow than has been previously recognised.

Groundwater recharge and local discharge features occur throughout the mountainous terrain of the Musgrave Ranges. Recharge to the palaeovalley system occurs where these palaeovalleys abut the more resistive fractured rock units. A good example of this process is the area in the vicinity of Umuwa which is located on the foothills of the Musgrave Ranges. It was also determined that groundwater recharge only occurs where rainfall events exceed 60-70 mm/month and groundwater discharge occurs mainly through transpiration processes from groundwater-dependent plants.

This project discovered hidden groundwater resources within the Lindsay East Palaeovalley. These resources have both high yield and low groundwater salinity making them potentially ideal for future potential resource development. Future work is required to determine the sustainability of these resources.

Drilling near the centre of the Lindsay East Palaeovalley at the hydrogeological control site DH1 in the vicinity of Kaltjiti (Fregon) suggests there are at least three groundwater bearing horizons, one of which is quite significant. This zone consists of coarse-grained sandstone (which overlays a lacustrine mudstone) and shows promise as a productive aquifer, with development yields up to 15 L/s and salinities (TDS) <1000 mg/L.

The project was successful in finding a significant hidden water resource. However, this is a first pass and more extensive work needs to be undertaken to more fully understand the palaeovalley system at the Lindsay East Palaeovalley and other palaeovalleys within the APY Lands beyond the hydrogeological control site. Nevertheless, the find so far is very promising and these resources, hidden from the surface and away from historical drilling areas, may represent the most significant find of groundwater in South Australia for at least the last 50 years.

# Acknowledgments

We would like to acknowledge the traditional owners of the Anangu Pitjantjatjara Yankunytjatjara (APY) Lands, the Pitjantjatjara, Yankunytjatjara and Ngaanyatjarra people. In particular we would like to thank Mr Witjiti George, Mr Maxi Stevens, Mr Robert Stevens, Bruce, Frank, Lee, and many others for undertaking on-country site inspections.

We would also like to acknowledge the work undertaken by the APY Consultation, Land & Heritage Unit, including Ms Charmaine Jones, Ms Cecilia Tucker, Mr Noah Pleshet, and Mr Andrew Cawthorn, who facilitated the necessary clearance approval to undertake this program of works within the APY Lands.

Saeed Ghaderi is also acknowledged for helping with the collection of groundwater samples which aided the environmental tracer analysis conducted as a part of this work.

Finally, we would like to thank APY General Manager Mr Richard King and the entire APY Executive Board who were supportive of the G-FLOWS project.

Parts of this report are taken directly from other unpublished grey literature such as G-FLOWS Stage 3 drilling program planning documents, drilling report with permission from Goyder Institute authors. Recently published MESA Journal articles (Costar et al 2019 and Krapf et al 2019) which document immediate findings from the drilling program conducted in 2018 have also been included where relevant. We thank the South Australian Department for Energy and Mining for their support.

The authors would like to acknowledge Professor Adrian Werner and Professor Paul Shand for their comprehensive review of this report.

# 1 Introduction

## 1.1 Background

Reliable water availability is critical to sustaining community water supplies and determining economic development opportunities. In many cases, particularly in remote and arid areas such as in the Anangu Pitjantjatjara Yankunytjatjara (APY) Lands in the far northwest of South Australia, groundwater is the only viable source of water.

However, there is limited knowledge of the groundwater resources in these remote regions; and the Musgrave Province, where the APY Lands is located, is no exception. Consequently, there is a need to identify and determine the potential of groundwater resources in regions – such as the APY Lands – to supplement their community water supplies and to provide water for economic development which leads to employment opportunities.

The South Australian Water Corporation (SA Water) provide and manage water infrastructure services to a number of remote indigenous communities in the APY Lands and as such have engaged South Australian Department for Environment and Water (DEW), as well as a number of consultants, to lead various groundwater investigations over the past 30 years. However, these investigations have tended to be focussed on the various individual community water supplies within the much more extensive APY Lands.

Road building and road upgrades by South Australia's Department for Planning, Transport and Infrastructure (DPTI) to improve living standards in the local APY community by providing better access to essential services and facilities, reduced travel times and vehicle operating costs and increase safety, have also relied upon suitable groundwater resources at various locations near road infrastructure.

The Goyder Institute Facilitating Long-term Outback Water Solutions (G-FLOWS) project is a collaboration between CSIRO and Flinders University (FU), managed through DEW with support from the Department for Energy and Mining (DEM) via the Geological Survey of South Australia (GSSA).

Commencing in 2011 with Stage 1, the G-FLOWS suite of research projects (Stages 1, 2 and 3) have developed new techniques to interpret airborne electromagnetic (AEM) geophysical data, coupled with hydrogeological techniques, to identify groundwater resources buried by deep sedimentary cover which is a major constraint to identifying water sources in the northern parts of South Australia. Stage 3 involves a targeted program of data acquisition, interpretation and mapping of palaeovalley systems (potential groundwater resources) in the Musgrave Province, APY Lands. The research is applying new and innovative geophysical techniques developed in the previous G-FLOWS projects (Stages 1 and 2) combined with field evaluation techniques to map potential sources and identify deep groundwater resources.

Part of the Stage 3 program of works is to extend the AEM geophysical interpretation process by establishing a hydrogeological control test site. This site contained a number of newly constructed water wells with the aim of reducing uncertainty in the interpretation of AEM data, thereby identifying deep potential groundwater resources in the palaeovalley system. It is this hydrogeological control site where the majority of the new field work and associated investigations has been conducted and is pivotal to the hydrogeological understanding and conceptualisation.

## 1.2 Study area

The study area for the project work is centred on the indigenous APY Lands located approximately 1,100 km northwest of Adelaide, in the far north-western corner of South Australia. The study area covers an area estimated to be 26,600 $km^2$ within the central region of the APY Lands and encompasses a number of communities and homelands including Amata, Pukatja (Ernabella), Yunyarinyi (Kenmore Park), Kaltjiti (Fregon), Mimili and the administrative centre of Umuwa (Figure. 1-1).

It is estimated that an Indigenous population of between 2,000 and 2,500 currently lives in the APY Lands (Australian Bureau of Statistics, ABS, 2016). According to the ABS (2017), the main industry and largest employer in the APY Lands is education and training, although with respect to income generation, the pastoral industry (i.e. cattle) is of importance. Retail trade, arts and recreation are also notable employers and generators of income. In particular, the arts industry is expanding at a rapid rate with galleries being established across Australia.

Topography in the study area varies considerably. The northern part is dominated by the Musgrave Ranges, which host the highest elevation point in South Australia, Mount Woodroffe, at 1,435 m AHD (Australian Height Datum, i.e. sea level) located approximately 40 km west of Pukatja (Figure. 1-1). The Everard Ranges dominate the southern margins of the study area near Mimili. Lying between the Musgrave and Everard ranges are extensive plains and rangelands (~550 m AHD), dominated by aeolian sand dunes and dunefields, sandplains and alluvial plains. A few creeks drain the Musgrave Ranges to the south and the centre of the study area. Officer Creek is the most prominent watercourse into which smaller tributaries such as Currie Creek and Ernabella Creek feed into (Figure. 1-1). For most of the year, these creeks are dry and only flow under episodic high rainfall conditions. Currently, flow in these creeks and watercourses is not being monitored.

The climate of the region is semi-arid to arid, typically with very hot summers and cool winters. Rainfall has a large range in variability from 50 to 1000 mm/year with mean annual rainfall of around 250 mm/year (Bureau of Meteorology (BOM2019)). The community of Pukatja (Ernabella) reports an annual mean rainfall of 279 mm (BOM, 2019) and a mean annual temperature of 27 °C (BOM, 2018), with most of the rain occurring in the summer (December–January) months (BOM, 2018). In general terms rainfall is very infrequent but intense and is predominately influenced by the monsoons from the north of the continent. Rainfall in the north of the study area in the mountainous area is much greater than rainfall in the southern flatter topographic region. Vegetation cover comprises predominantly grassland, shrub land and open woodlands.

Two hydrogeological control sites were selected (DH1 and S22), however, this work primarily focused on site DH1 and the main palaeovalley system known as the Lindsay East Palaeovalley.

Site DH1 (DH1) is located on the Fregon-Mimili road approximately 6 kilometres southeast of Kaltjiti (Fregon) (Fig. 1-1). DH1 was selected due to its proximity to the mapped extent of the Lindsay East Palaeovalley as depicted by the AEM geophysical data and location adjacent to a main road, which aided site access and clearance.

The topography at DH1 is generally flat, with relief primarily provided by sand dunes that were 3-5 metres in height. Vegetation largely consists of grassland and sparse woodland and soils are largely composed of aeolian sand and silt. Some calcrete mounds are present within the sandplain.

Site 22 (S22) is located adjacent to the Umuwa-Fregon road approximately 9 kilometres north of Kaltjiti (Fregon) (Fig. 1-1). S22 was selected to aid in the understanding of the phreatic (shallow) groundwater system where many of the community water supplies source water. Additionally, S22 also spans part of a shallow palaeovalley tributary system.

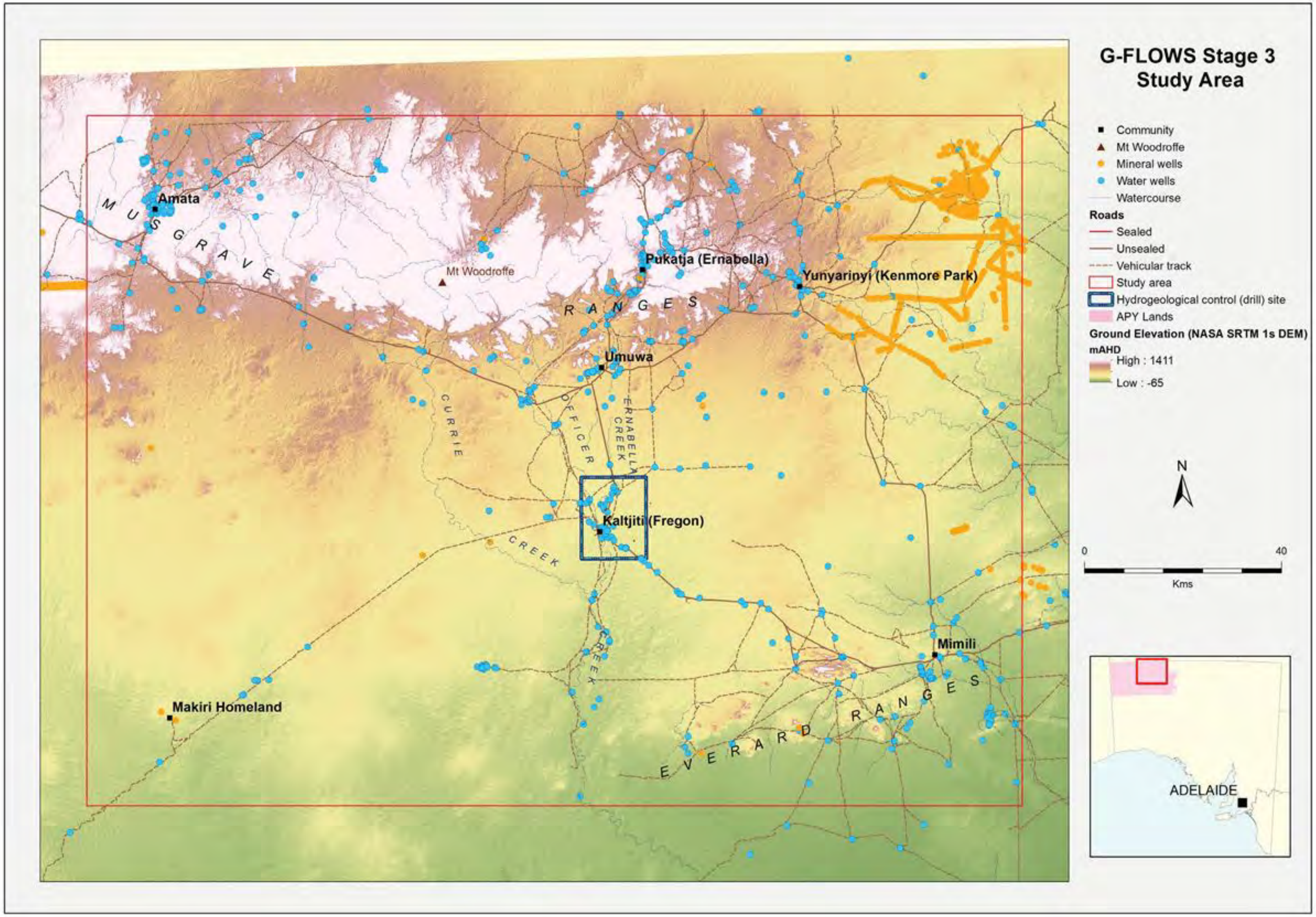


Figure 1-1. Regional study area located in the APY Lands. Blue rectangle depicts location of hydrogeological control site where drilling and sampling was conducted for the project.

## 1.3 Previous studies

DEW, and its predecessors has had an involvement locating water supplies within the APY Lands over the past 60 years. At that time there were a few shallow wells completed in the alluvium (unconfined aquifer system) and they were mainly used for stock supply. The deeper fractured rock system was not viewed as being a viable target for drilling at the time. A comprehensive review of available data was conducted by the Dept. for Water (Watt and Bernes 2011).Since then, a number of major drilling programs have been conducted the latest being the DEW drilling program in the APY for SA Water and DPTI during 2015-2017 (Howles et al., 2017).

In addition to this program, various other research organisations have commissioned investigative projects in the last six years across the APY Lands. These include the Goyder Institute for Water Research (Goyder Institute) through G-FLOWS (Stage 1) and the Non-Prescribed Areas project under DEW's Groundwater Program.

In 2011, the G-FLOWS Stage 1 project proposed to reprocess and provide further research in analysing the extensive existing AEM datasets for water resource and supply options over the area, which were originally commissioned for mineral exploration purposes. Then in 2013, the non-prescribed program commissioned a small hydrogeochemical investigative study that focussed on groundwater recharge within the eastern APY Lands (Kretschmer and Wohling 2014).

A project worth noting due to the groundwater sampling of environmental tracer analysis, is that undertaken from 1997-1999 by Dodds et al. (2001), which aimed to evaluate the sustainability of groundwater resources for nine of the larger communities where there was concern for sustainability of water supply.

The following is a list of reports deemed to be the most relevant and recent to the hydrogeological component of G-FLOWS Stage 3 and upon which to build conceptualisation. These reports contain literature reviews and references to other reports, and are therefore a good summary of the current hydrogeological data and information available in the project area:

- Community water supplies in the Anangu Pitjantjatjara Lands, South Australia: sustainability of groundwater resources (Dodds et al. 2001)
- G-FLOWS Stage 1 suite of reports (Varma 2012, Leaney et al 2013, Munday et al. 2013)
    - Hydrogeological Framework
    - Groundwater Assessment and Aquifer Characterisation in the Musgrave Province, South Australia
    - Groundwater recharge characteristics across key priority areas
    - Hydrogeological review of the Musgrave Province, South Australia
- Groundwater recharge in the eastern APY Lands (Kretschmer and Wohling 2014)
- APY Lands and Yalata Water Search (DEWNR TN 2015-17, Howles et al 2017)
- Musgrave Geological (desktop) Study (commissioned by the DEW for the 2015-17 program, Pawley and Krapf 2017)

The first analyses of geochemical tracer data in the APY was presented by Dodds et al (2001) and reported by Creswell et al (2002).These studies mentioned above have attempted to estimate groundwater recharge across the various areas of the APY: the sustainability study (data collected 1999), G-FLOWS Stage 1 (data collected 2012) and the DEW recharge study (data collected 2013). The G-FLOWS Stage 1 project sampled and analysed 21 wells across the entire APY whereas the DEW recharge study, which focused on the eastern APY (the western boundary approximately 25 kilometres west of Kaltjiti), sampled and analysed 29 sites but included existing data from Leaney et al. (2013) and Custance (2012) therefore the study reported on 60 sites in total (Fig. 1-2).

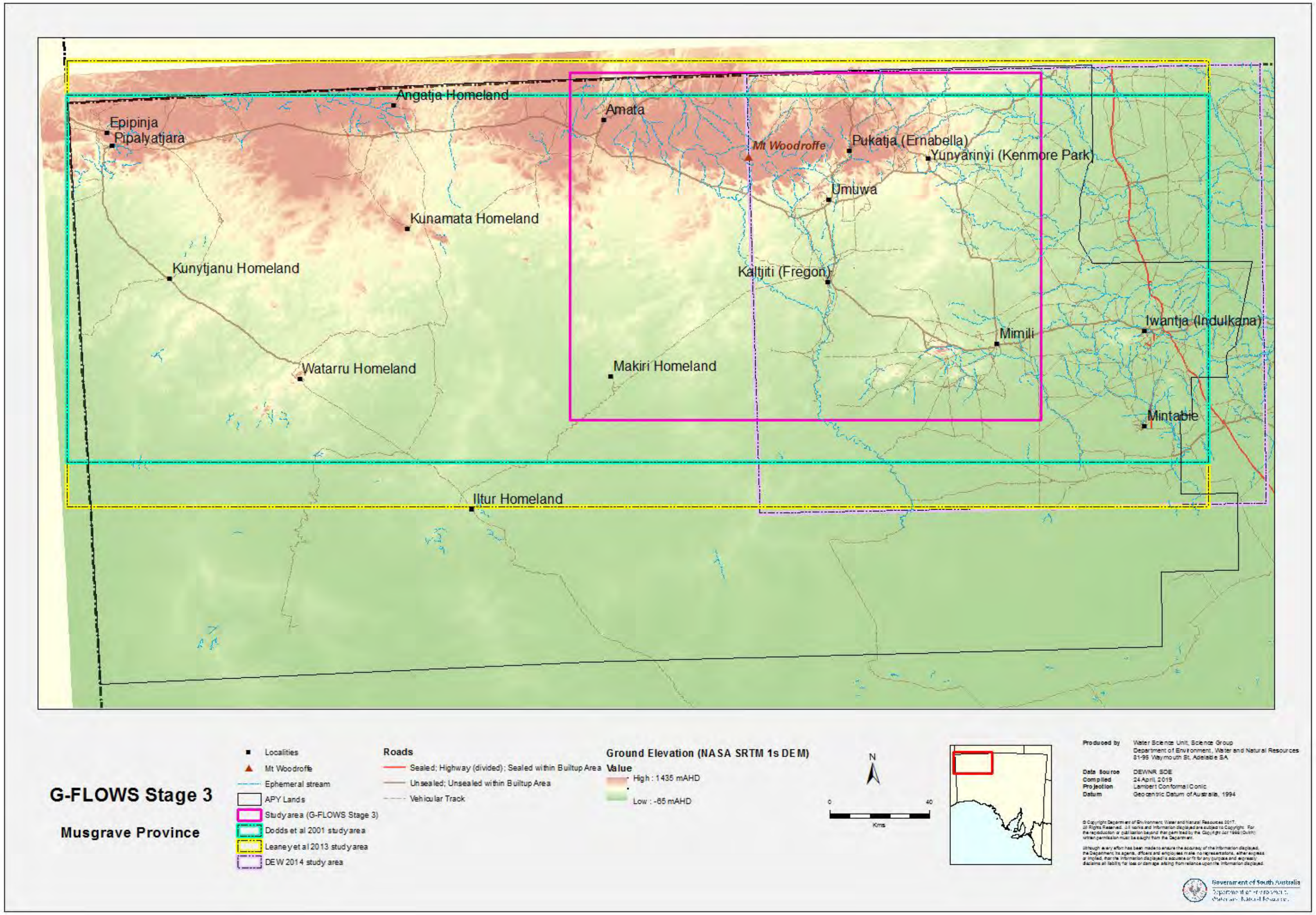


Figure 1-2. Footprint of groundwater sampling and hydrochemical analysis conducted in the APY Lands (2001, 2012, 2013, and 2014).

While a comprehensive range of chemical and isotopic analyses were performed to aid estimation of recharge, results from these studies appear to be inconclusive. Although hydrochemistry-based methodologies for recharge calculations suffer from technical limitations, these studies did not appear to consider or discuss more fundamental limitations such as well construction and the effect this may have on sampling suitability and representation. It is not clear from the reporting available whether any of the following were considered:

- Discrete well screens (i.e. short lengths)
- Position of the screened interval within the strata (i.e. does the zone span several systems)
- Well construction integrity (i.e. how old is the well and therefore construction and the ability to sample a discrete system).

Additionally, the contrasting results between recharge rates obtained using the chloride mass balance (CMB) approach compared to those obtained using other analytes, strongly suggest that greater consideration of the fractured rock aquifer environment is required when examining results. In general, groundwater dating techniques using radio carbon and chlorofluorocarbons (CFC's) indicated relatively modern water (<50 years) whereas recharge rates calculated using the CMB approach indicate rates <1 mm/year which would imply much older water (>50 years). This apparent discrepancy requires detailed investigation that considers well construction and the integrity of the groundwater sample itself.


**Figure 1-3. Watertable surface contours (Varma, 2012).**

In addition to recharge calculations, two attempts have been made to construct a groundwater level (watertable) surface for the APY Lands, which is fundamental to determining groundwater flow direction (Varma 2012, Kretschmer and Wohling 2014). The watertable surface of Varma (2012) (Fig. 1-3), shows a general groundwater flow direction from the northwest to the southeast with slight mounding to the south of Kaltjiti as well as to the south and east of Mimili. The other watertable surface of Kretschmer and Wohling (2014) (Fig. 1-4), shows a major groundwater divide in the Musgrave Ranges partitioning groundwater flow towards the north and also groundwater flow towards the south east, and south. However, due to similar issues concerning well construction discussed above, current watertable surface interpretations are problematic, with issues centred on limited groundwater level data and the common absence of accurate ground elevation surveys.

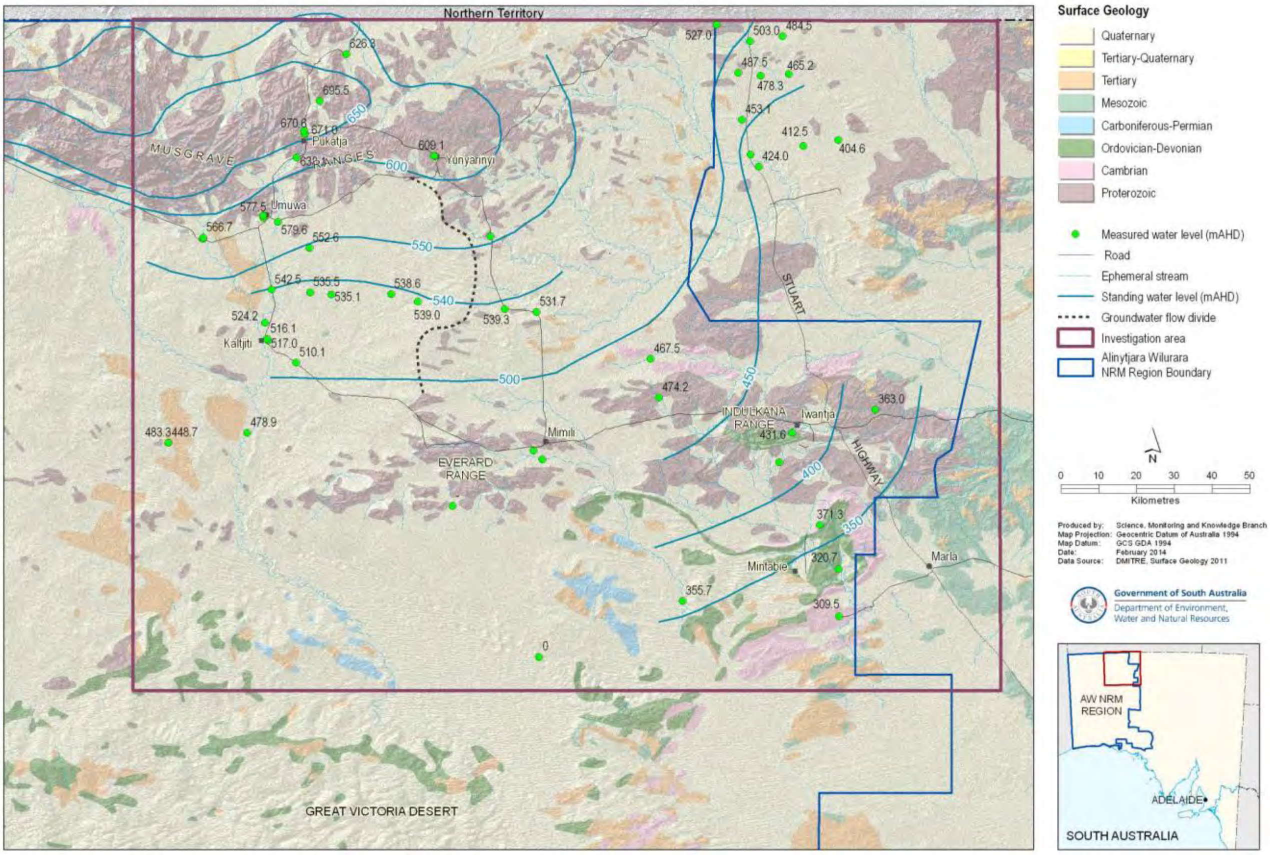


Figure 1-4. Watertable surface contours (Kretschmer and Wohling, 2014).

In 2015, both the SA Water and DPTI engaged DEW to locate new groundwater supplies (including well replacement) and complete a program of works to design, drill and construct new groundwater wells in various parts of the state's indigenous communities but primarily the APY Lands (Howles et al. 2017). This study also used flow accumulation models and structural geology results from GFLOWS 1 (Munday et al 2013).

Specifically, SA Water required new community water supplies at the communities of Amata, Kaltjiti, Iwantja (Indulkana), Mimili and Pukatja while DPTI required groundwater supplies for road construction at regular intervals in order to upgrade the road from Iwantja to Pukatja (Fig. 1-5).

Data sources for this program stemmed primarily from a GSSA study commissioned at the request of DEW to provide information and geological support to establish potential alternative water resources around the communities in the APY Lands. This study entitled "Investigating the potential for bedrock aquifers in the APY Lands", used a range of existing datasets, such as pre-existing geological data, total magnetic intensity (TMI), gravity data, ortho-images, digital elevation models, Landsat imagery, and earthquake data. This study provides a new detailed structural interpretation of the solid geology in the vicinity of the main communities, however, no ground-truthing was conducted (Pawley and Krapf 2017).

Traditionally, water is sourced from palaeovalley sands, calcrete, and alluvial and aeolian sediments as well as from the on-lapping sediments of the Officer Basin in the south-eastern part of the APY Lands (Bell et al. 2012, Magee 2009). The GSSA study examined the geology in the vicinity of the main communities Amata, Kaltjiti (Fregon), Iwantja, Mimili, Pukatja and Yunyarinyi (Kenmore Park) and provided a new interpretation for bedrock structures that can potentially act as aquifers (Pawley and Krapf 2016). These include faults and breccia zones, where the fractured rock is permeable, allowing water to flow and be stored in potentially usable quantities. As these types of aquifers have not been extensively exploited, they have potential to offer a valuable additional water resource for the region.

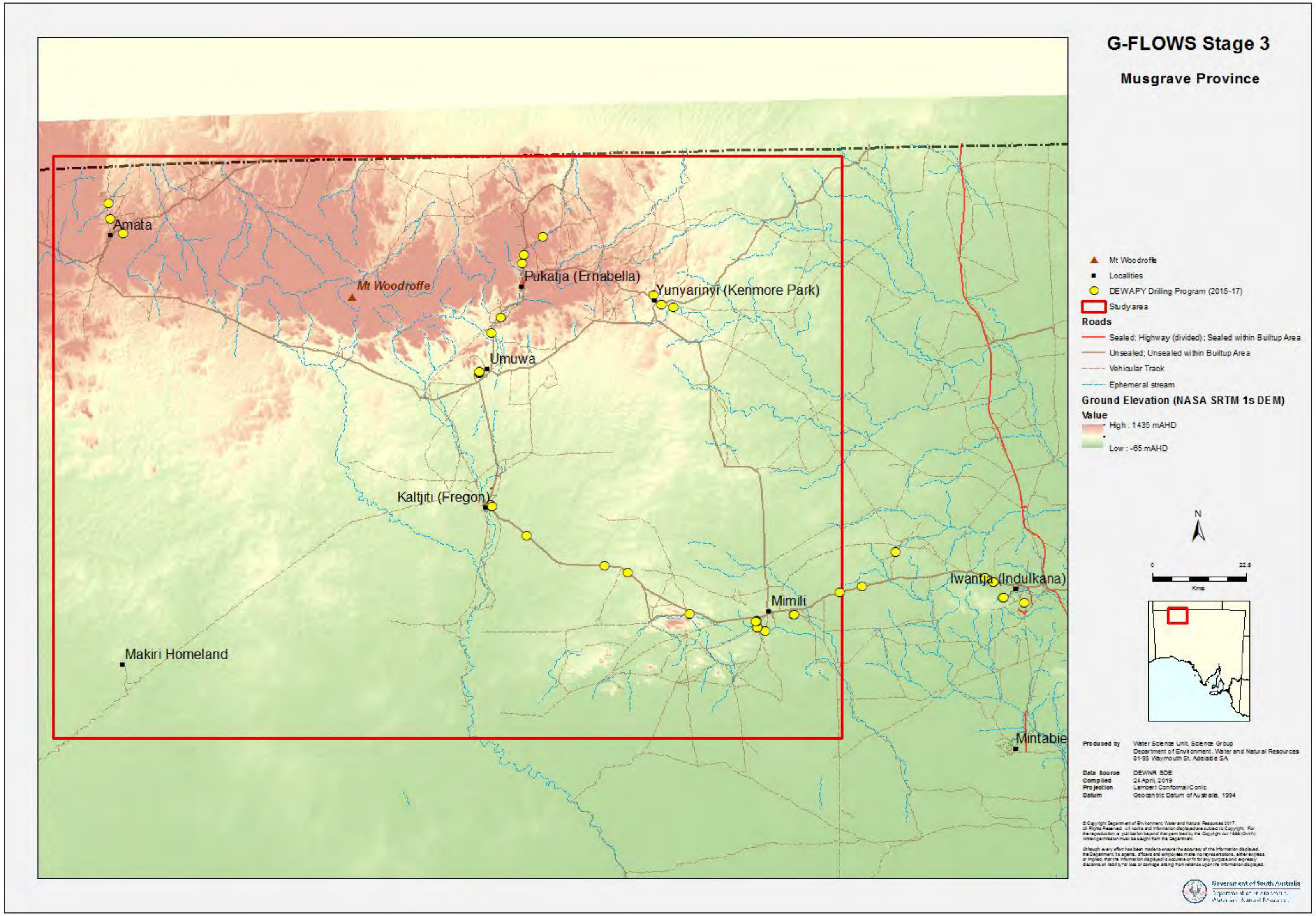


**Figure 1-5. Recent (2015-17) drilling conducted by DEW for community water supply and road building in APY Lands.**

Stage 1 of the G-FLOWS project developed a new hydrogeological framework for the Musgrave Province. Two conceptualisations of the landscape evolution for the pre-Pliocene and contemporary landscape are schematically showed in Figures 1-6a and b. These two schematics represent a summary of some of the major outcomes of G-FLOWS Stage 1. They were developed using a comprehensive analyses of hydrogeological results as well as previous AEM and geological interpretation. For a comprehensive review, the reader is referred to the work of Munday et al. (2013). G-FLOWS Stage 3 provides more data and knowledge to determine the extent and significance of the palaeovalley system; in particular, the Lindsay East Palaeovalley in the Musgrave Province.

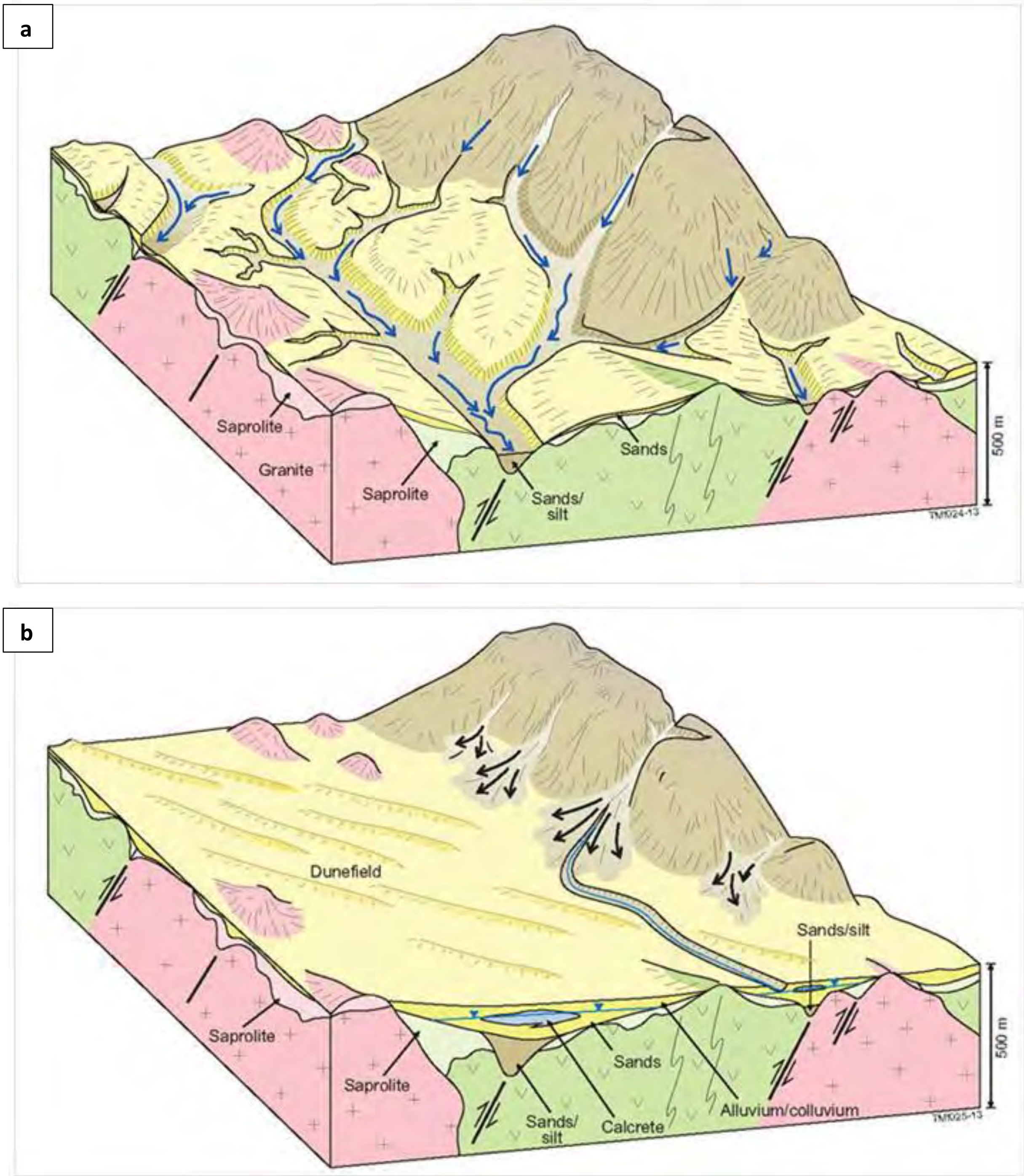


**Figure 1-6. Previous conceptual model for the NW and central parts of the Musgrave Province developed from AEM, TMI and DEM interpretation (Munday et al. 2013): (a) pre-Pliocene landscape (b) contemporary landscape.**

## 1.4 Methods, objectives and investigations

G-FLOWS Stage 3 added to new knowledge and understanding by conducting a suite of on-ground field investigations which included targeted drilling in the palaeovalley (including core retrieval), construction of new wells targeting the water bearing zones within the palaeovalley sequence, age dating the strata from the core, age dating of the groundwater and aquifer testing of the palaeovalley.

A brief description of the various G-FLOWS Stage 3 specific field investigations is presented below which inform the hydrogeological conceptualisation of the control site and the wider study area.

### 1.4.1 GEOPHYSICS

Approximately two-thirds of the APY Lands was captured in an AEM survey conducted in 2016 comprising 17,395 line kilometres (Heath, Wilcox and Davies 2017). AEM is a non-invasive, fast and effective method, particularly in remote areas where ground access can be challenging, for assisting in mapping the location and geometry of aquifer systems including palaeovalleys, which constitute an important groundwater resource for local communities, industry and the environment. It presents the opportunity to gain information about the subsurface in an otherwise data poor area (Munday et al. 2020).

The survey was flown with a line spacing of 2 kilometres in a north–south direction and employed two-time domain AEM systems (Fig. 1-7). The western part of the area was flown with fixed wing aircraft employing the TEMPEST system, while the eastern part used the SkyTEM system flown by helicopter (Soerensen et al. 2017).

The AEM data acquired across the area uncovered an extensive palaeovalley drainage system (Soerensen et al. 2017; Costar et al. 2018). The conductivity depth sections inverted from AEM data revealed a complex, well-defined and relatively narrow set of palaeovalleys that contrast with those depicted in the contemporary landscape of today (Munday et al. 2013; Soerensen et al. in press). Although these palaeovalleys have been previously recognised (Rogers 1995; Magee 2009) and mapped (Bell et al. 2012; Hou et al. 2012), the AEM data enabled the mapping of the palaeovalley network in more detail and at higher spatial accuracy (Krapf et al. 2019) in comparison to previous interpretations.

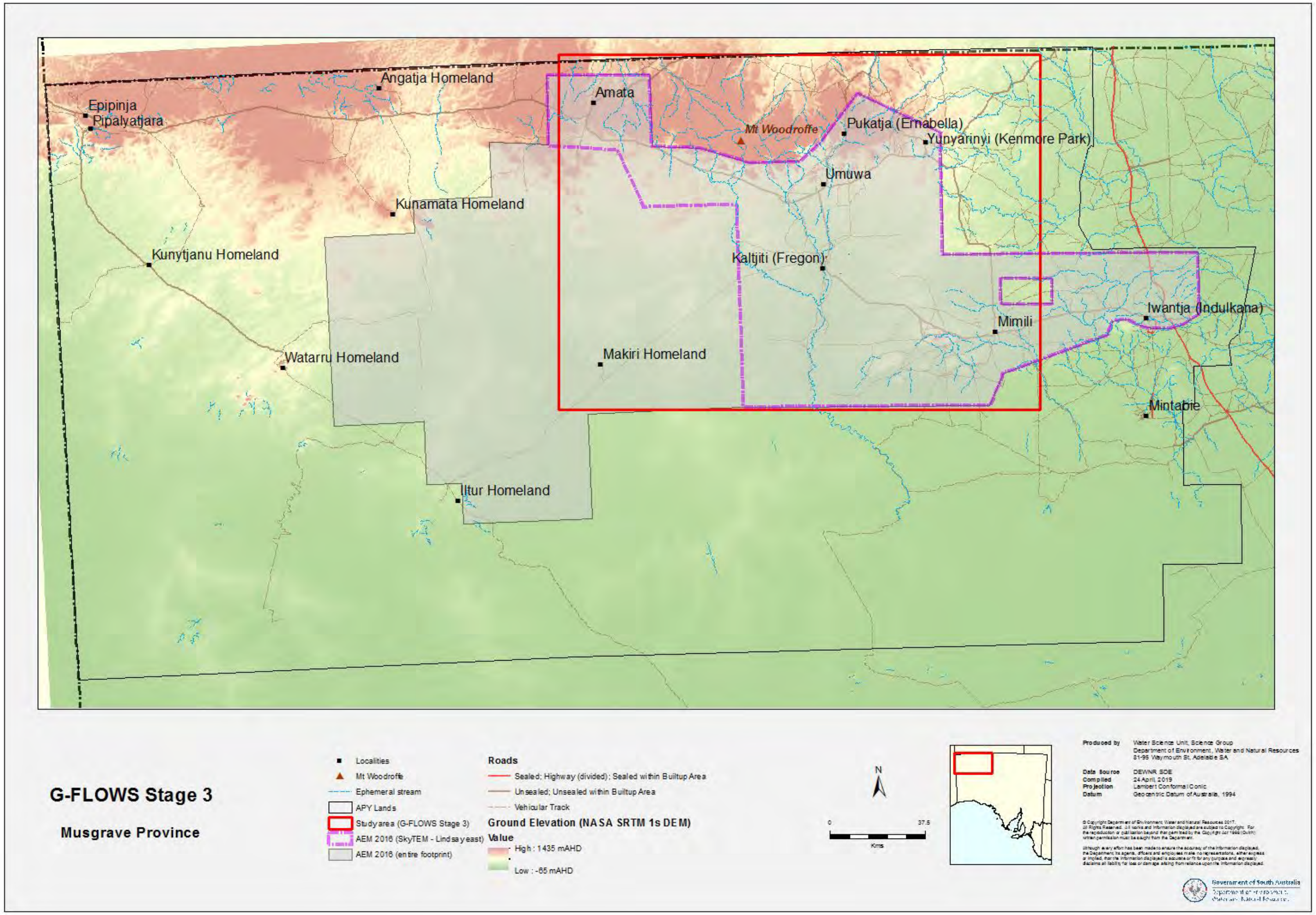


Figure 1-7. Footprint of AEM survey conducted in 2016. The pink outline shows the SkyTEM system coverage which covers much of the study area.

### 1.4.2 WELL SURVEY AND DATABASE

A groundwater well survey (bore audit) was conducted between 10 and 20 October 2017 to identify and confirm groundwater infrastructure (i.e. water wells) and the condition of such infrastructure to aid in establishing monitoring and field investigation requirements such as drilling and groundwater sampling.

The State's groundwater database identified 573 water wells (739 drillholes) as of 1 May 2017 spread across the G-FLOWS Stage 3 study area. Work on the database included a review of all geological and drillers logs as well as a review of well completion intervals. During the field survey it was not practical to visit every well in part due to strict access requirements.

The bore audit was undertaken by navigating to the identified well location using a hand-held GPS, where the following well attributes were surveyed for 39 wells (Fig. 1-8):

- Spatial coordinates (accuracy verification) using a differential global positioning system (DGPS);
- ground elevation using DGPS;
- well casing condition (material, diameter, headworks, surface seal);
- cap identification;
- standpipe condition and cementing;
- reference point type and elevation (above ground level);
- depth to water;
- total well depth;
- current status and purpose of use;
- presence of logging devices;
- access constraints;
- suitability for monitoring and sampling; and
- multiple digital photographs describing the location and condition of the well.

Due to resourcing, budget and time constraints, sampling was not undertaken at this time as a routine component of this audit, however, a pump was used opportunistically for sampling basic salinity if a measurement was not recorded at all in the database.

The bore audit provided valuable information for planning of future field activities and input into numerical groundwater modelling tasks as part of the G-FLOWS project, including:

- verification of well location and status for planning and design of drilling and sampling programs;
- water level data for developing potentiometric surfaces, to aid initial groundwater modelling and the design of well drilling programs (i.e. design length and position of screen); and
- identification of access issues/feasibility for future ground-based activities such as geophysical surveys and drilling operation.

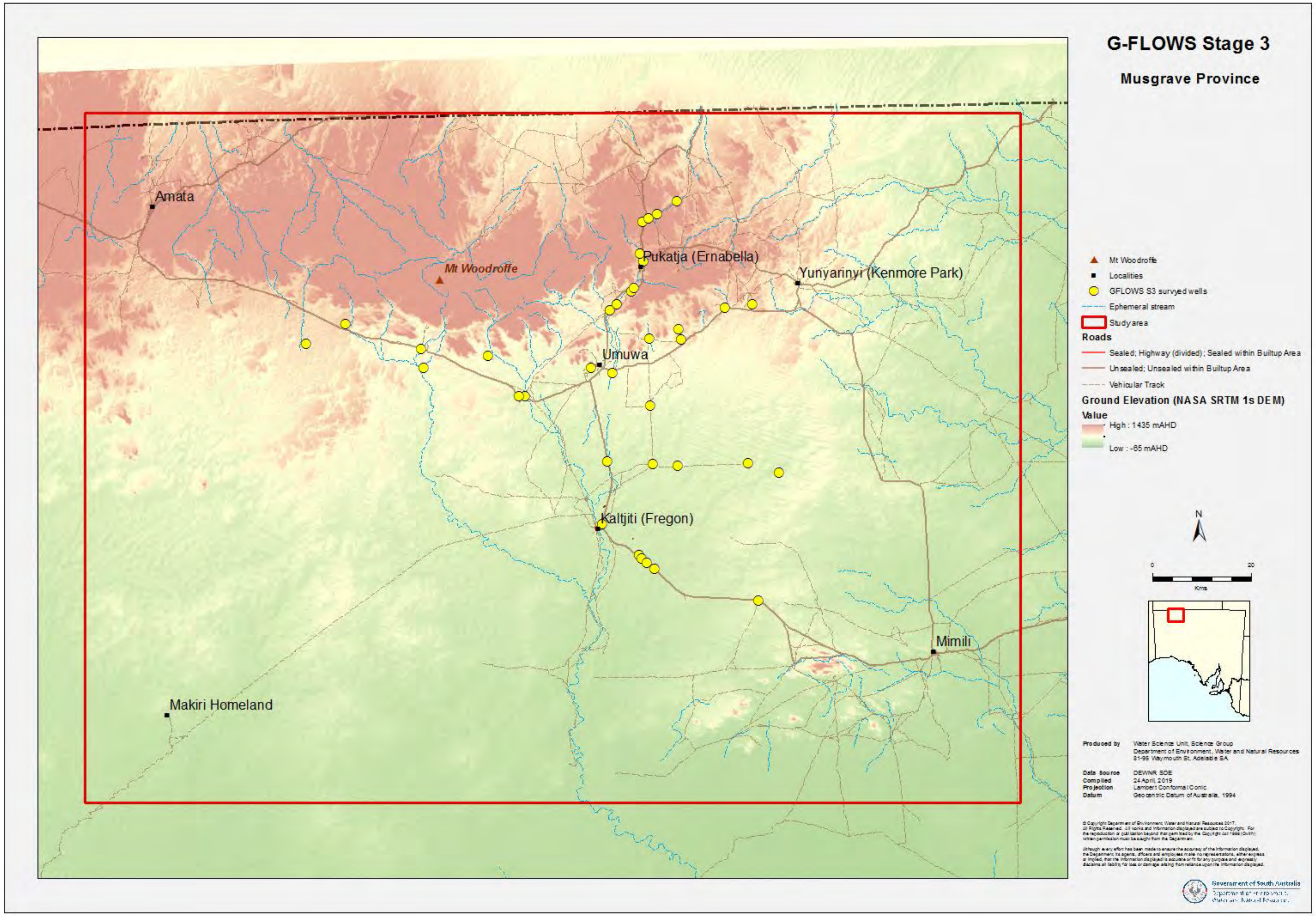


**Figure 1-8. Well survey (bore audit) conducted in the initial stages of the project.**

### 1.4.3 DRILLING AND AQUIFER TESTING

A drilling program conducted in 2018 (Keppel et al. 2019) established a hydrogeological control test site within the spatial extent of the Lindsay East Palaeovalley (site DH1). Seven groundwater wells were constructed at this site to assist in the development of geophysical and hydrogeological conceptualisation of the palaeovalley groundwater flow system.

Site DH1 is located on the Fregon-Mimili road, approximately 6 kilometres southeast of Kaltjiti. This location was selected for drilling investigations due to its proximity to the mapped extent of the Lindsay East Palaeovalley (Fig. 1-1). This extent was identified from AEM survey data and is located adjacent to a main road, which aided site access and clearance. Investigation drilling and well construction at site DH1 was designed to enable palaeovalley aquifer testing. In addition to the seven wells and one cored hole that were initially planned, an additional well was installed to replace well 1a, which encountered construction issues after coring.

The DH1 site configuration incorporated the following aspects:

1. The main site was located south of the Fregon-Mimili road and centred on the Lindsay East Palaeovalley. One cored hole (DH1a) and four wells (DH1a2, c, d and e) were completed. DH1a was plugged (no screen) and replaced by DH1a2.
2. A second site was located north of the Fregon-Mimili road, approximately 100 m north of the main site. One well (DH1b) was completed.
3. A third site was located approximately one kilometre north of the main site, adjacent to the Fregon-Mimili road. Two wells (DH1f and g) were completed.

Drillholes at DH1 were situated in order to target geological features and water bearing zones hosted within the palaeovalley sediments as inferred from the AEM. Wells were constructed to allow aquifer testing of any water bearing zones encountered.

Investigation drilling was also undertaken at an additional site (S22) over four locations (i.e. S22a-d) situated 7-10 km to the north of site DH1. Investigations at site S22 were intended to aid the understanding of the phreatic (shallow) groundwater system. However, as discussed later in this report, no aquifer testing was conducted at site S22 but may be undertaken beyond G-FLOWS Stage 3.

Aquifer hydraulic testing was conducted between 14 and 18 March 2019 as part of the G-FLOWS Stage 3 suite of on-ground field programs. These programs were designed specifically to provide the necessary data required to ground-truth and validate the existing hydrogeophysical interpretation and thereby aid in reducing uncertainty in geophysics-based outputs. Time-drawdown data derived from aquifer testing was used to estimate hydraulic parameters of the Lindsay East Palaeovalley aquifer. This will inform future conceptual and numerical modelling of this and other palaeovalley flow systems in the APY Lands (Costar et al. 2020).

### 1.4.4 GROUNDWATER FIELD SAMPLING

Groundwater sampling was conducted during the drilling and airlifting phase (two samples – pre- and post-development) of the drilling program but was restricted to field measurements and major and minor solutes.

In November 2018 (3 months post drilling), a dedicated environmental tracer program was conducted. This involved collecting groundwater samples for the following environmental tracers:

- Tritium ($^{3}H$)
- Carbon isotopes ($^{14}C$ and $^{13}C$)
- Stable isotopes
- Major and minor solutes/elements

These samples were sent to laboratories (ANSTO, GNS Science (NZ) and CSIRO) for analysis in early January 2019 with results received in March to September 2019.

While G-FLOWS Stage 3 focused on the Lindsay East Palaeovalley this sampling and analysis complimented the historical sampling mentioned in the previous sections.

### 1.4.5 TASK AIMS AND OBJECTIVES

The primary objectives of this work were to:

- Review existing data to develop a regional scale hydrogeological conceptual model
- Confirm the stratigraphy and depth of the Lindsay East Palaeovalley including the identification of water bearing zones within the palaeovalley
- Help validate the AEM geophysical data
- Obtain a first pass hydrogeological conceptualisation of the previously unknown palaeovalley at the hydrogeological control site DH1. This new conceptualisation is underpinned by a dedicated drilling program (including core), aquifer testing, environmental tracer analyses and numerical modelling.

# 2 Regional groundwater conceptualisation

## 2.1 Introduction

The development of numerical models to simulate a groundwater system requires, in the first instance, an understanding or conceptualisation of the system. Conceptualising the hydrogeological processes in a groundwater system is an important step and includes some key elements which address characterisation of the system. These include, but are not limited to, the:

- Geological setting (including structural features and stratigraphy)
- Groundwater salinity and yield
- Hydrostratigraphy –the hydraulic nature of the system such as aquifer testing and measures of porosity; aquifer interconnectivity
- Architecture – identification of aquifer systems (water bearing zones), their geometry, location within the landscape and their relationship with one another
- Flow systems –groundwater flow direction(s) through various investigations including groundwater level measurements
- Recharge and discharge processes – where are these processes potentially located in the landscape and what are their recharge and discharge rates

This project collated a number of different scientific tools which have been used to obtain a greater understanding of the system. These tools/datasets included AEM, surveying, geochemistry, environmental tracers and aquifer testing. It is important to understand that conceptualisation (and numerical modelling) is an iterative process, meaning as new information and data becomes available there is a need to revisit the conceptualisation and update where necessary. However, the process of starting conceptualisation is extremely useful since it can identify knowledge gaps and therefore target investigations.

The aim of this report is to provide a summary of the best understanding (to date) of groundwater conceptualisation in data sparse areas. This chapter specifically examines the regional groundwater conceptualisation.

## 2.2 Regional geology

The G-FLOWS Stage 3 study area occurs within the south-eastern portion of the Musgrave geological Province (Musgrave Province). The Paleo- to Mesoproterozoic Musgrave Province consists predominantly of gneissic rocks of the Birksgate Complex, which were deformed and metamorphosed as well as intruded by granitic plutons of the Pitjantjatjara Supersuite during the province-wide c. 1220–1120 Ma Musgravian Orogeny (Edgoose et al. 2004; Howard et al. 2011; Major and Conor 1993; Smithies et al. 2011). These basement rocks were intruded by mafic rocks of the Giles Complex, during the c. 1085–1030 Ma Giles Event, including dykes of the Alcurra Dolerite (Close, et al 2002; Edgoose et al. 2004, Glikson et al. 1996; Howard et al. 2011; Woodhouse and Gum 2003). Following the Giles Event, the c. 825 Ma Amata Dolerite intruded the rocks of the Musgrave Province (Werner et al. 2018).

The Musgrave Province is overlain or bordered by a number of sedimentary basins, including the Neoproterozoic to Early Carboniferous Amadeus Basin to the north, the Ordovician to Early Cretaceous Canning Basin to the west and the Neoproterozoic to Late Devonian Officer Basin to the south (Figure 2-1). To the east, the Musgrave Province abuts a few stacked basins that are separated by major unconformities. These eastern basins include the Cambro-Ordovician Warburton Basin, the Permo-Carboniferous Arckaringa and Pedirka basins and the Mesozoic Great Artesian Basin (Eromanga Basin).

The region in general is highly deformed by a series of major east-west shear zone systems, the most important being the Hinckley, Mann-Ferdinand, Lindsay, Wintiginna and Woodroffe systems. Metamorphic and initial structural deformation is interpreted to have begun during the Musgravian Orogeny between 1220 and 1120 Ma, when intrusion of felsic magmas associated with the Pitjantjatjara Supersuite occurred. However, the bulk of the high strain deformation is thought to have occurred during the Late Neoproterozoic Petermann Orogeny (~550 Ma) when a number of mylonites and ultra-mylonites were formed (Woodhouse and Gum, 2003). Between the Musgravian and Petermann orogenies, the 1085-1040 Ma Giles Event resulted in the intrusion of mafic, ultra-mafic and minor felsic igneous rocks as well as the deposition of bimodal volcanic rocks, followed by the intrusion of a number of dolerite dyke suites.

One of the most prominent geological features within the study area is the Woodroffe Thrust, which is a zone of sheared gneiss, mylonite and pseudotachylite that occurs within the Musgrave Ranges (Fig. 2-1). The Woodroffe Thrust demarcates the Musgrave Province into the northern Mulga Park Subdomain and the southern Fregon Subdomain (Pawley and Krapf, 2016). The south-dipping Woodroffe Thrust is interpreted to have accommodated the exhumation of the Fregon Domain (Korsch and Kositcin, 2010)

Another important related structural feature within the study area is the Levenger Graben, which represents a reactivation of the Mann Fault during the Cambrian (~542-488 Ma) (Fig. 2-1). The Levenger Graben occurs south of the Musgrave Ranges, between Amata and Kaltjiti (Fregon). The shape and thick accumulation of sedimentary clastic fill, called the Levenger Formation, within the Levenger Graben suggests this reactivation formed a wrench pull-apart basin (Major and Conor, 1993).

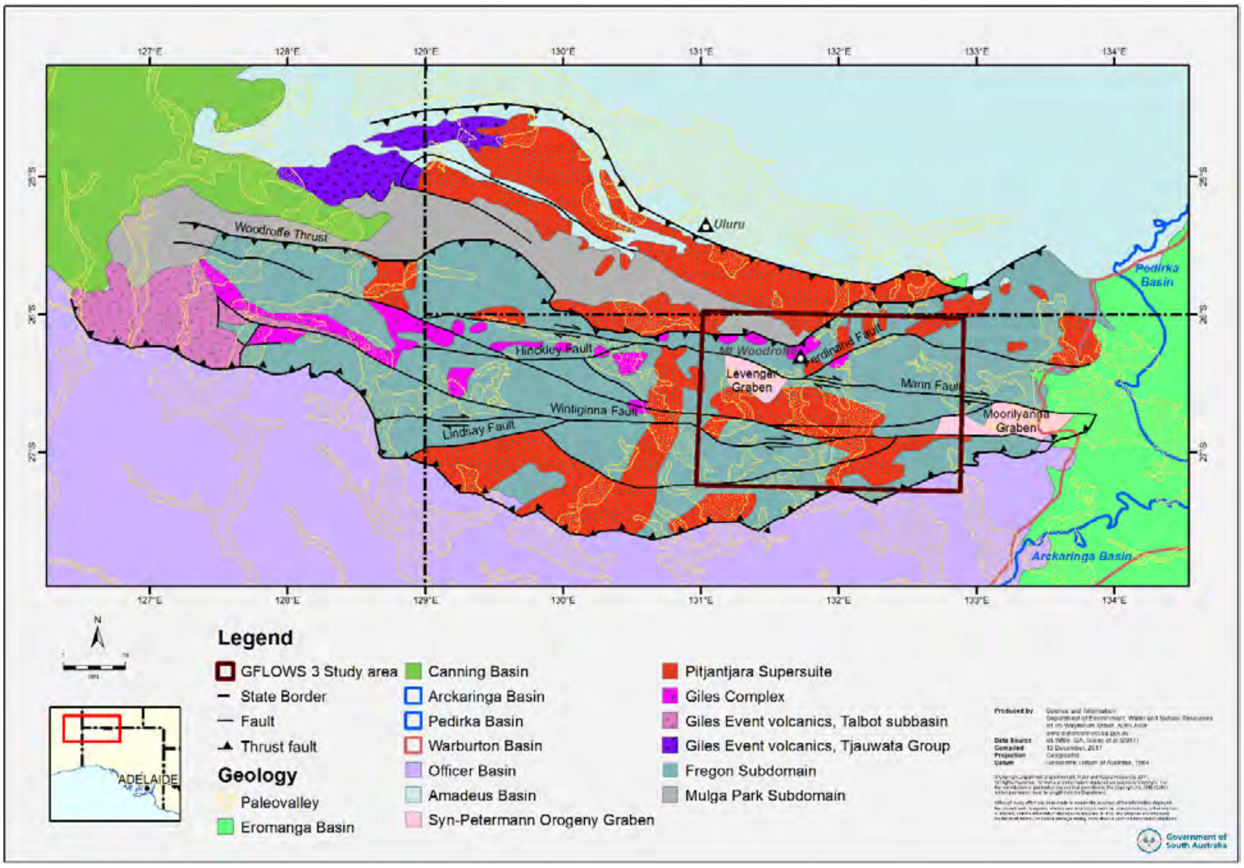


Figure 2-1. Simplified regional structural geology of the Musgrave geological Province, surrounding sedimentary basins and location of palaeovalleys in the far north western regions of South Australia near the Western Australian and Northern Territory borders. Developed after Glorie et al. (2017), and Geoscience Australia.

The Musgrave Ranges is an up-thrusted crystalline basement complex that has been modified by orogenic uplifted and subsequent erosion and sedimentation of younger units. The oldest unit is the Birksgate Complex is sequence of clastic rocks that have been highly metamorphosed mainly into gneisses. These were deformed and metamorphosed as well as intruded by granitic plutons of the Pitjantjatjara Supersuite during the province-wide c. 1220–1120 Ma Musgravian Orogeny (Edgoose et al. 2004; Howard et al. 2011; Major and Conor 1993; Smithies et al. 2011). These basement rocks were intruded by mafic rocks of the Giles Complex, during the c. 1085–1030 Ma Giles Event, including dykes of the Alcurra Dolerite (Close, Edgoose and Scrimgeour 2003; Edgoose et al. 2002; Glikson et al. 1996; Howard et al. 2011; Quentin de Gromard et al. 2017; Woodhouse and Gum 2003). Following the Giles Event, the c. 825 Ma Amata Dolerite intruded the rocks of the Musgrave Province (Werner et al. 2018). These are overlain by Adelaidean-aged meta-sedimentary shale, siltstone and sandstones that make up the basin fill of the Levenger and Moorilyanna Grabens.

Within the study area and relevant to this study are a few more recent geological events and associated sedimentary untis, most notable the palaeovalleys and their associated sedimentary fill. These palaeovalleys have their headwaters in the Musgrave Ranges, generally flow to the south (Fig. 2-1 and 2-3) and can be incised into the underlying basement up to 70 m deep (Pawley and Krapf, 2016). Palaeovalleys of note within or near the study area include the Lindsay East and West, Serpentine, Mermangye palaeovalleys and the Hamilton Basin. A map of the palaeovalley distribution and thawleg profiles was produced via a combination geological interpretation and the AEM data (Krapf et al. 2020). These palaeovalleys largely formed during the Late Paleogene and Early Neogene and were subsequently filled during a warmer and wetter subtropical to tropical climate in the Mid to Late Neogene with clastic sediments including alluvial, fluvial, and lacustrine sediments composed of clay, sandy clay, mixed sand-clay deposits, and lenses of coarse sand and gravel (Rogers 1995; Magee 2009). Preceding palaeovalley development was a period of intense chemical weathering that resulted in the development of a deep weathering profile of up to 100 m that affected the underlying basement rocks (Pawley and Krapf, 2016).

Increasing aridity during the Quaternary led to today's surface (Fig. 2-2) dominated by aeolian and ephemeral alluvial processes, leading to a landscape of sand plains, alluvial plains and creeks as well as aeolian dunes and dunefields.

To further understand the geology at depth two geological cross-sections where prepared. One orientated in a NW-SE direction from Amata near the ranges to Mimili on the plains and the other in a N-S direction from Pukatja near the ranges to Kaltjiti (Fregon) on the plains (Fig. 2-4). The cross-section locations were chosen largely in part due to the density of geological and hydrogeological data available. They were also chosen based on the previous watertable surfaces (Varma 2012 and Kretschmer and Wohling 2014 reproduced in Chapter 1) which indicated the potential direction of groundwater flow towards the south east and south. These cross-sections will play an important role in understanding groundwater flow. This is discussed in greater detail later in this chapter. Furthermore, these two transects were modelled for groundwater flow and groundwater age distribution. Cross-sections were based on geological interpretation from existing lithological drillhole logs as well as recent AEM interpretation through conductivity depth profiles.

AEM interpretation for each geological cross-section is shown in a qualitative scale on Figure 2-5 and 2-6. In these sections, blue represents zones of low conductivity grading into increasingly higher values of conductivity from green to yellow to orange and finally to the most conductive zones of red. As observed, low conductivity zones correspond to the most resistive rocks of the fractured rock and other basement rocks. The orange and red areas define the location of the Quaternary and Tertiary sediments composed of sands silts and clays. The palaeovalleys can be clearly defined in these two sections.

Figures 2-7 and 2-8 form the finalised geological cross-sections by combining the AEM and lithological information. The AEM data helps to interpret between drillhole locations. These cross-sections show that the basement rocks predominately consist of the gneissic rocks of the Birksgate Complex, which have been intruded by y granitoids of the Pitiantjatjara Supersuite and to a lesser extent by ultramafis of the Giles Complex.

A number of faults have been mapped on these cross-sections; however, it is worth noting that this is an interpretation only and may also include other contacts caused by younger intrusions. No hydraulic information is available on the type of faulting and none on hydraulic conductivity information of the various basement and fractured rock units.

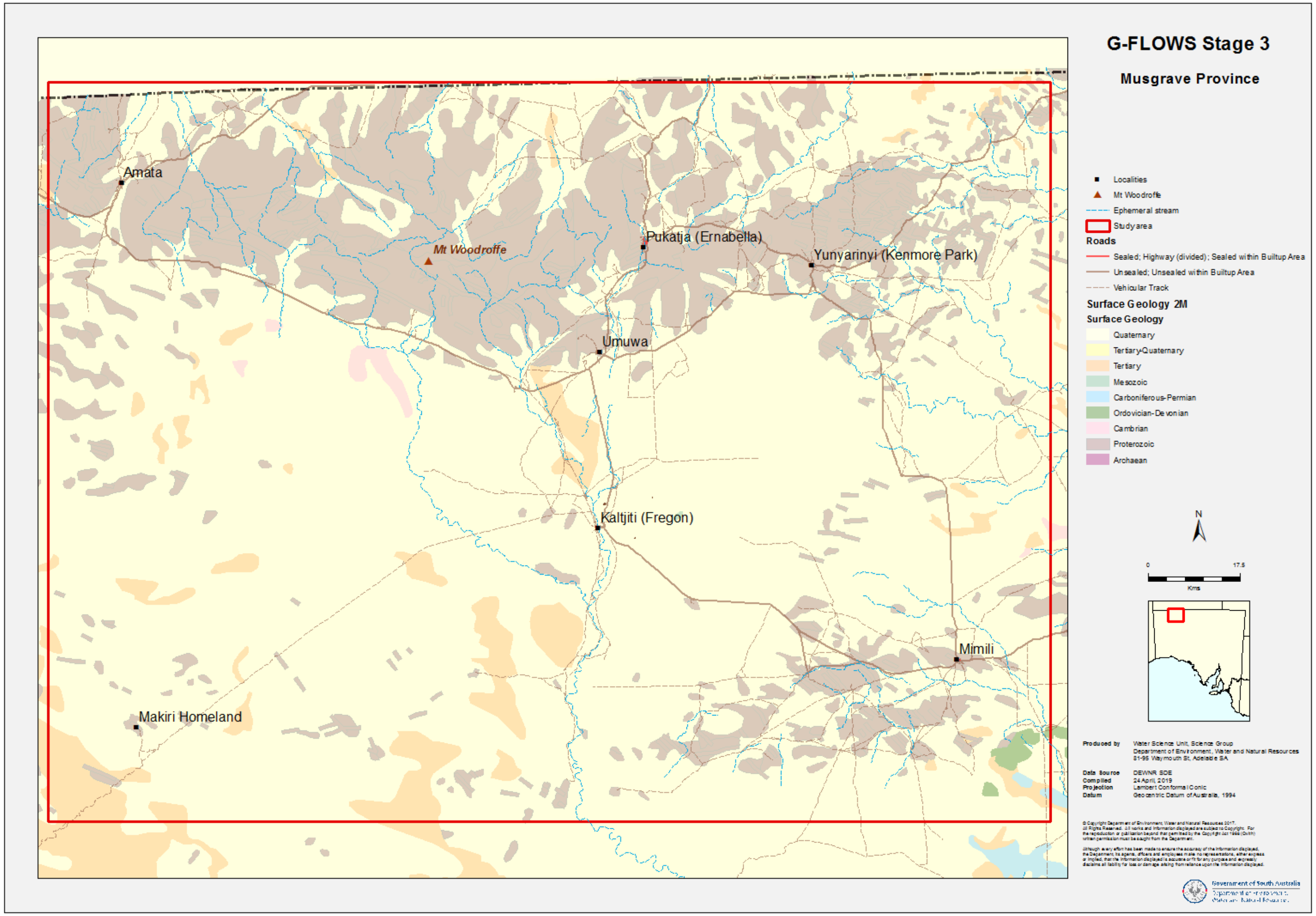


**Figure 2-2. Simplified surface geology across the study area.**

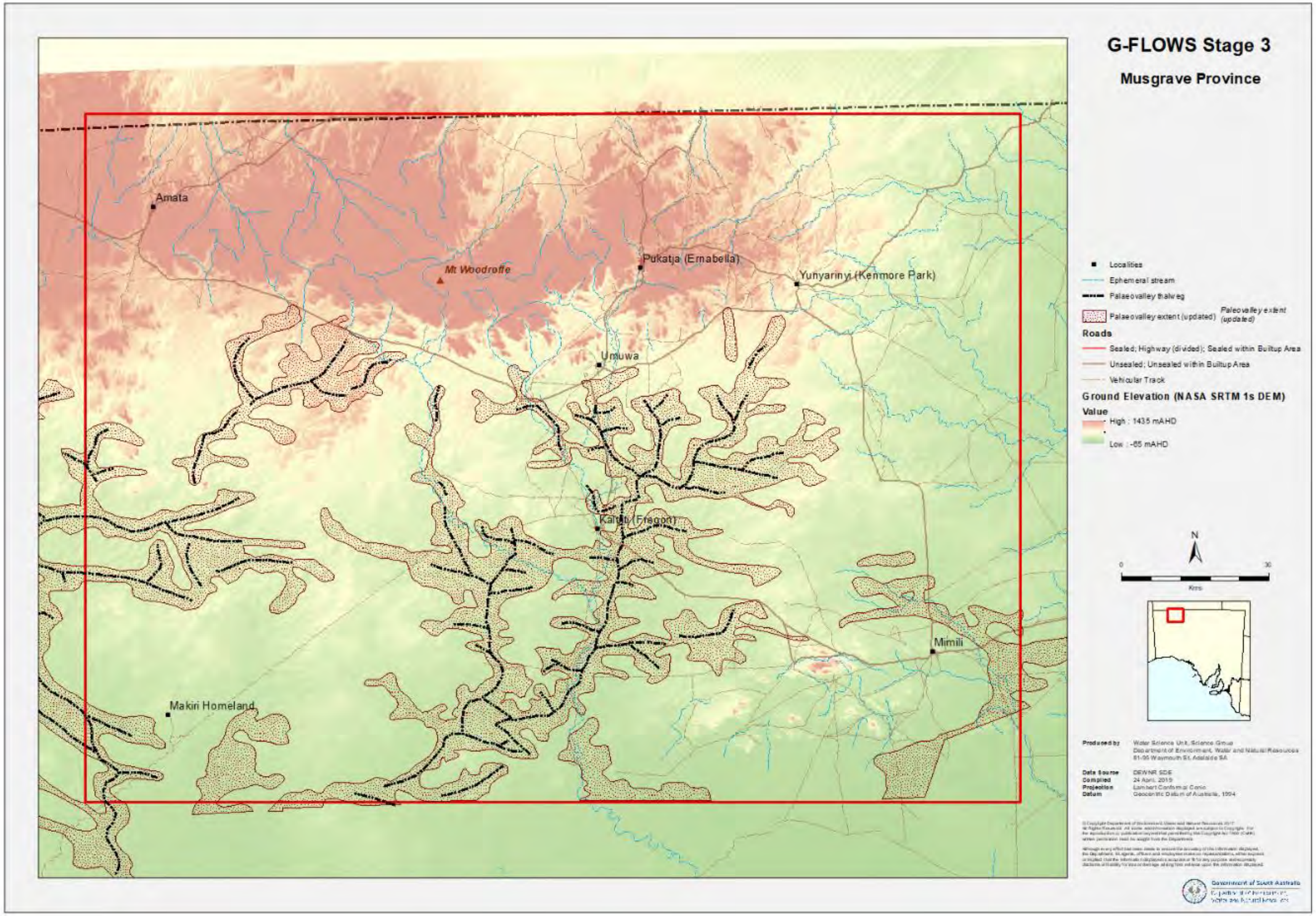


**Figure 2-3. Palaeovalley mapped extent (Krapf et al. 2020) across study area.**

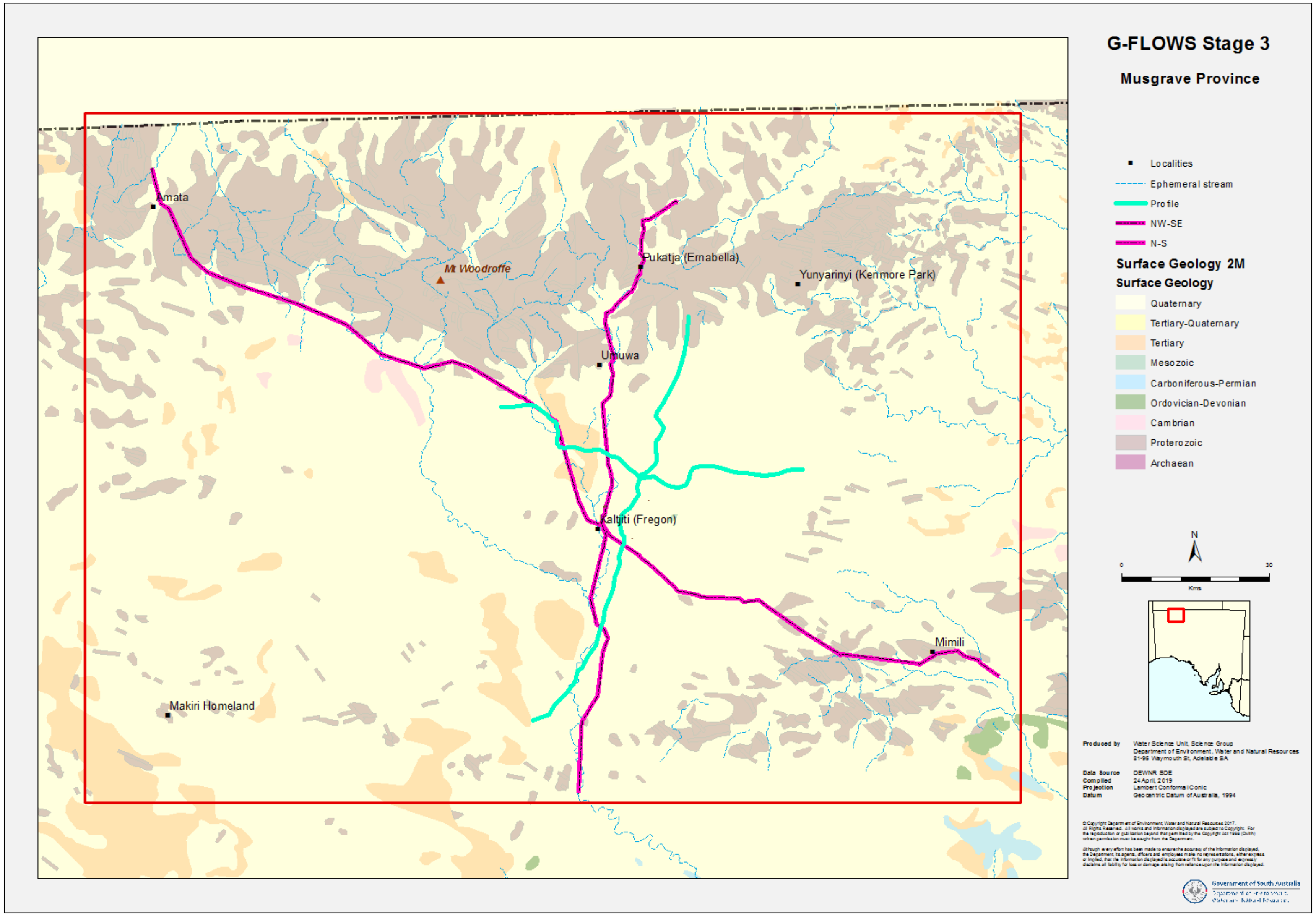


Figure 2-4. Locations of geological cross-section transects across study area.

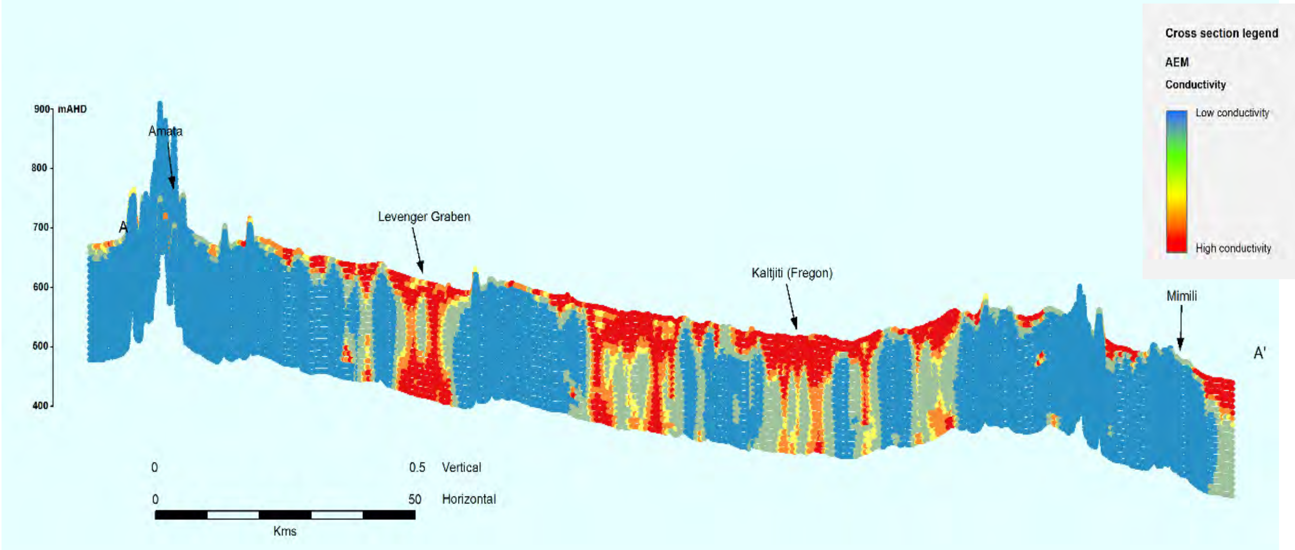


Figure 2-5. AEM Conductivity depth section  interpretation for the NW-SE transect using AEM (SkyTEM) data (see Fig. 2-4 for transect locations).

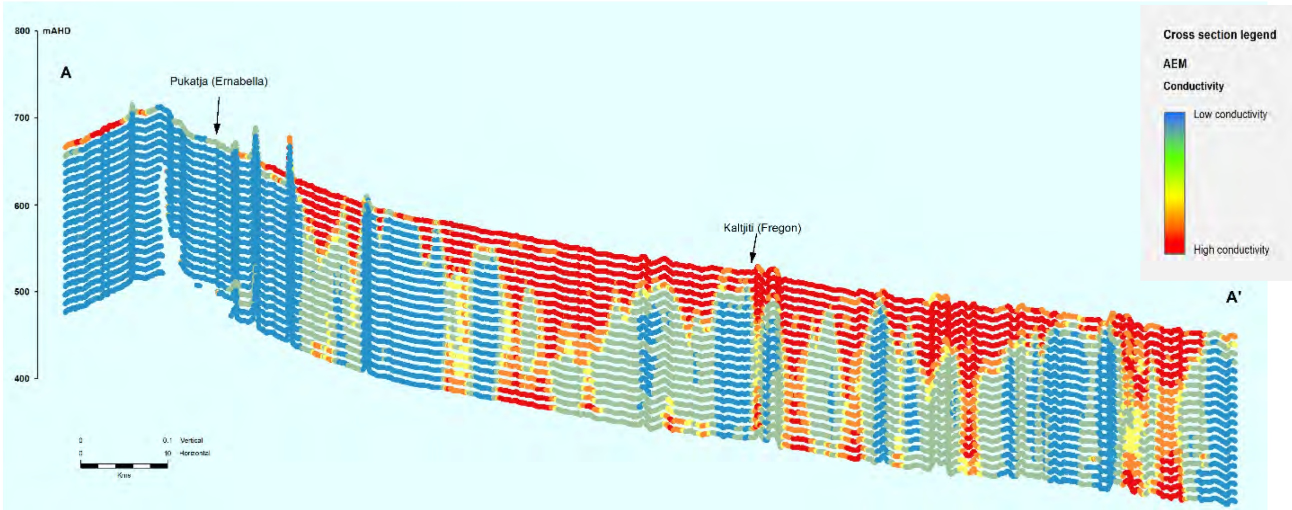


Figure 2-6. AEM Conductivity depth section interpretation for the N-S transect using AEM (SkyTEM) data (see Fig. 2-4 for transect locations).

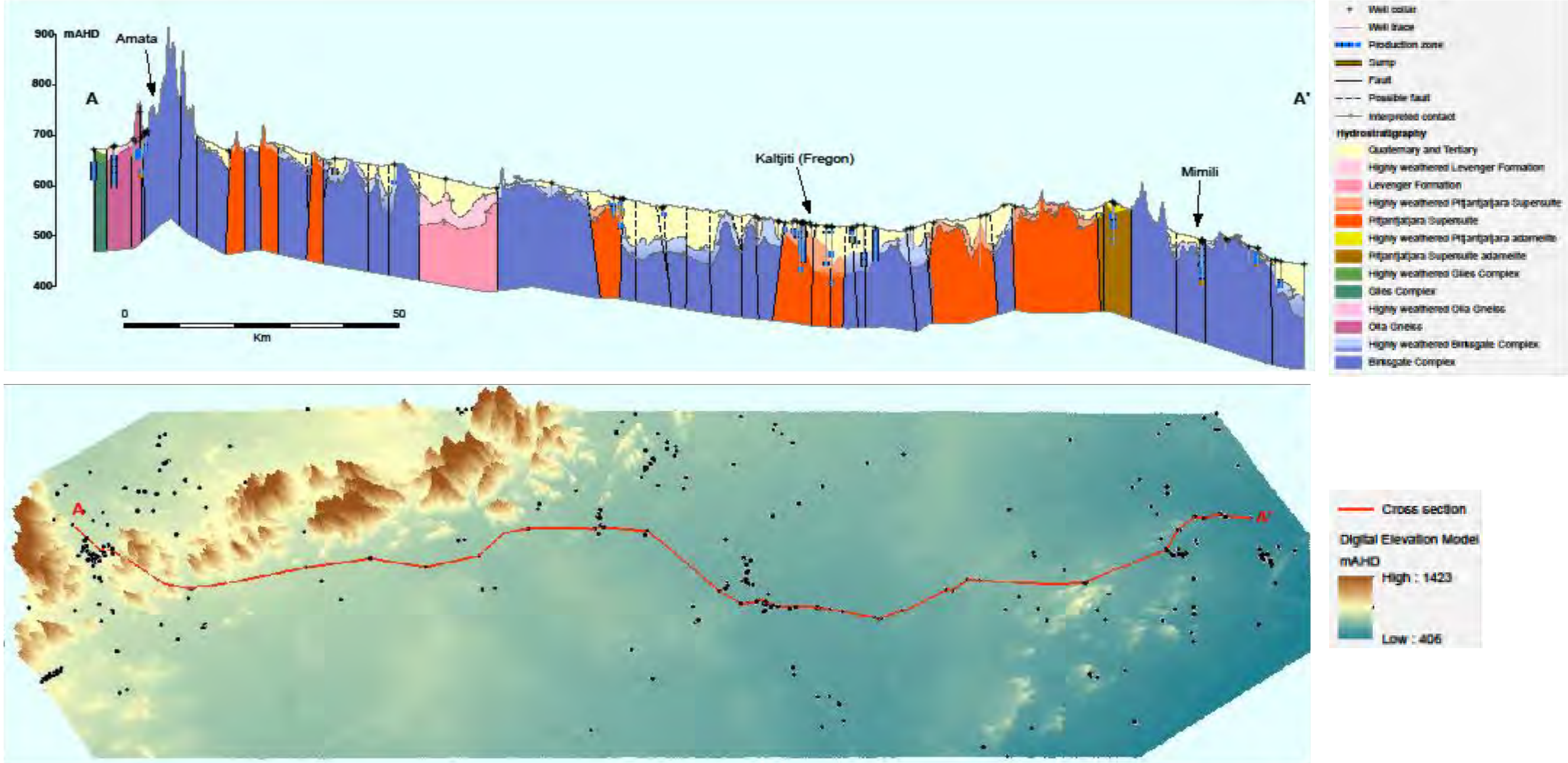


**Figure 2-7. Final Interpreted NW-SE transect geological cross-section using existing drillhole information and geophysics.**

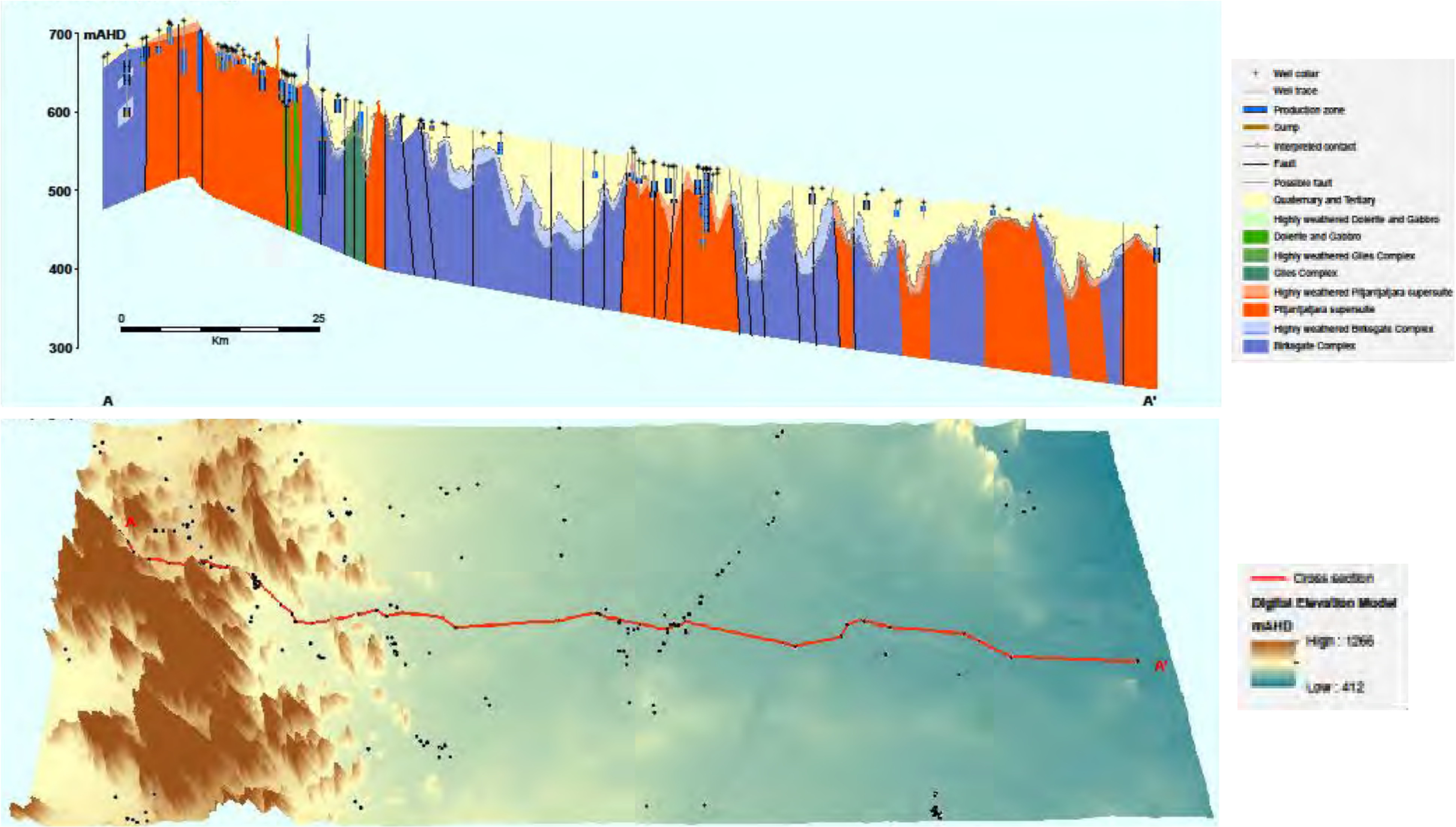


**Figure 2-8. Final Interpreted N-S transect geological cross-section using existing drillhole information and geophysics.**

Overlying the low conductivity (resistive) basement rocks is the weathered basement. The weathered basement consists of fractured rock aquifers grading into in-situ weathered basement. The separation of these two zones occurs around a conductivity of ~20 mS/m, while the upper boundary of the weathered basement zone that separates the upper porous media occurs at ~50 mS/m. This interpretation of the weathered zone is based on the geology (representing the top of the weathered fractured rock, see Section 2.4.1).

## 2.3 Regional hydrogeology

The hydrogeology of the region is complex in terms of both the hydrostratigraphy and the groundwater flow systems. Data is limited as it is a remote area which is difficult to access (special permits and permissions are required to enter the APY Lands), and as such, the understanding of hydrogeological processes are often general.

Most of the hydrogeological information comes from basic investigations into water supplies for the communities, road building and special research projects such as G-FLOWS. The occurrence and distribution of water wells is quite sparse throughout the vast area of the APY Lands and monitoring and maintenance of wells in this remote area is challenging.

Broad-scale geology and hydrogeology of the region has received some recent attention through investigations focused on small-scale localised water supplies for road building (Pawley and Krapf 2016,) which has also delivered new insight into the hydrostratigraphy. Previous studies have suggested that the Musgrave Ranges and the headwaters of the drainage channels originating in the ranges, are important recharge areas (Leaney et al. 2013).

Faulting is widespread across the APY Lands and the region is known to be still tectonically active with evidence of many small-scale seismic events and earthquakes (Pawley and Krapf 2016). The specific impact of faulting on localised groundwater flow patterns within the study area is currently difficult to discern given the lack of data. However, given the prevalence of deformation, it is likely to be important. The general east-west trend of structural deformation, which is perpendicular to the north-south or northwest-southeast direction of the palaeovalley development, regional surface drainage and groundwater flow suggests that tectonic uplift or sagging is generally more important than the influence of shearing on the groundwater system.

Figure 2-9 displays the average depth weighted AEM horizontal slice from 45.3 to 53.8 m below natural surface (mBNS) superimposed onto the total magnetic intensity (TMI). The red colour denotes zones of high conductivity while the blue zones denote zones of low conductivity and more resistive rock. Overlaying these two geophysical layers is an interpretation of potential east-west orientated faults in the region by Pawley and Krapf (2016). These faults can often correspond to rapid changes in the values of conductivity or magnetic intensity which is inferred to represent changes in lithology of the rocks, which often correspond to juxposting of geological units.

While the AEM shows tributaries of the main palaeovalley drainage system are aligned east-west, the course of the main palaeovalley 'channel' is only affected in small area (where it actually crosses the east-west structures) and follows the natural topographic gradient from north to south (Krapf et al. 2019).

The potential influence of the east-west structural deformation on the groundwater flow systems can be observed in the AEM. This perpendicular relationship may also indicate a potential for localised development of lateral flow barriers, or preferential flow pathways (Krapf et al. 2019). Additionally, reactivation of older structures may have an important influence on the architecture of present-day drainage and palaeovalleys. Such an architecture is interpreted between Pukatja and Kaltjiti where the accumulation and thickness of Quaternary and Tertiary alluvial sediments appears to be impacted by dip-slip movement along east-west fault planes (Krapf et al. 2019).

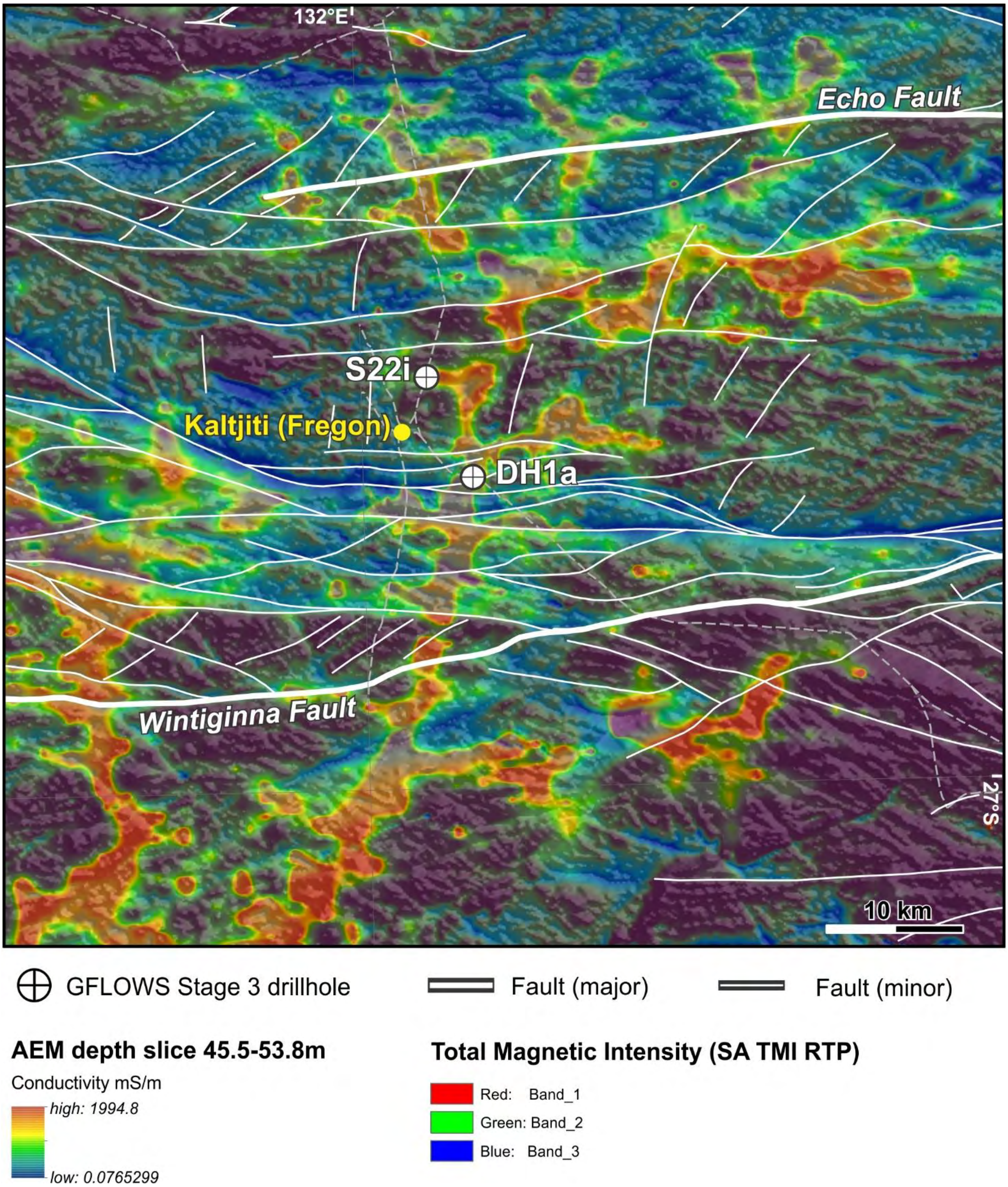


**Figure 2-9. AEM depth slice 45.3 to 53.8 mBNS draped over TMI data (texture). TMI shows E-W structures.**

### 2.3.1 SALINITY AND YIELD

Groundwater salinity and yield spatially vary considerably across the region (Fig. 2-10 and 2-11).

Electrical conductivity (EC) from WaterConnect was converted to salinity (TDS) by the formula TDS = EC *0.55. Groundwater samples were collected at the time of drilling as per the well construction reporting requirements on newly constructed wells. Samples were also collected from wells during dedicated sampling events or as part of town water supply routine sampling. In order to maximise data Figure 2-10 uses the latest data that is available for that well with the vast majority of data from the time of drilling.

As with salinity groundwater yields from WaterConnect were measured at the time of drilling. Approximately 40% of the data is from wells open to the upper porous media units while the remaining 60% is from wells open to the fractured rock and the weathered zone.

Salinity varies considerably from 140 mg/L to in excess of 13,000 mg/L but is generally <2,000 mg/L. The spatial distribution of salinity can also be extremely variable with values doubling or even changing by an order of magnitude within a 5 km radius of the drill site. The lowest values of salinity occur in the fractured rock region, although in these regions rapid increase in salinity over small spatial areas is still observed. The low values of salinity in the Musgrave Ranges reflects zones of rapid recharge. This rapid recharge is thought to occur from infrequent high monsoonal rainfall events that originate from the north of the continent. A similar recharge mechanism has been proposed to occur on the margin of the Great Artesian Basin (Love et al. 2013 and Fulton et al. 2013). Regions with higher values of salinity are more commonly associated with zones of diffuse recharge or even possibly zones of discharge. The extreme variability of salinity from adjacent wells suggest that a simple flow path of uniform distributed recharge is not present.

A similar pattern occurs for yield(s) where large spatial variability is observed over short distances. Yields are generally low ranging from zero yield (dry well) to up to 10 L/s but generally < 2 L/s. Prior to the project's dedicated drilling program, no wells had intersected the palaeovalley at depth across the study area. However, the Nyikukura palaeovalley near the SA-WA border (to the west of the study area) intersected sand horizons at a depth of 120 m with fresh groundwater of 500 mg/L of and relatively high yields of 4-6 L/s (Rockwater 2012).

The absence of any strong spatial distribution of salinity and yield is also reflected in the distribution of these two variables versus depth. Figure 2-12, shows the depth relationship for salinity and yield for the shallow sedimentary (porous media) aquifer. Salinity is highly variable with most wells being fresh to brackish. Yield varies from a dry well to approximately 7 L/s, with the vast majority of wells having a yield <2 L/s. Both graphs show a wide scatter in data points indicating no relationship to depth.

Salinity for the fractured rock aquifer is <2600 mg/L (except for one outliner at 4,600 mg/L). This range is smaller than the one observed in the shallow sedimentary aquifer. The range in groundwater yield is larger for fractured rock varying from a dry well up to 10 L/s. The yield of the fractured rock appears to decrease with depth and reaches very low yields at 120 m. It approaches values of around 0.3 L/s which is close to the measurement error and would only represent a thin trickle from air lifting. Below this depth it is likely hydraulic conductivity is low and may represent hydraulic basement for numerical modelling purposes.

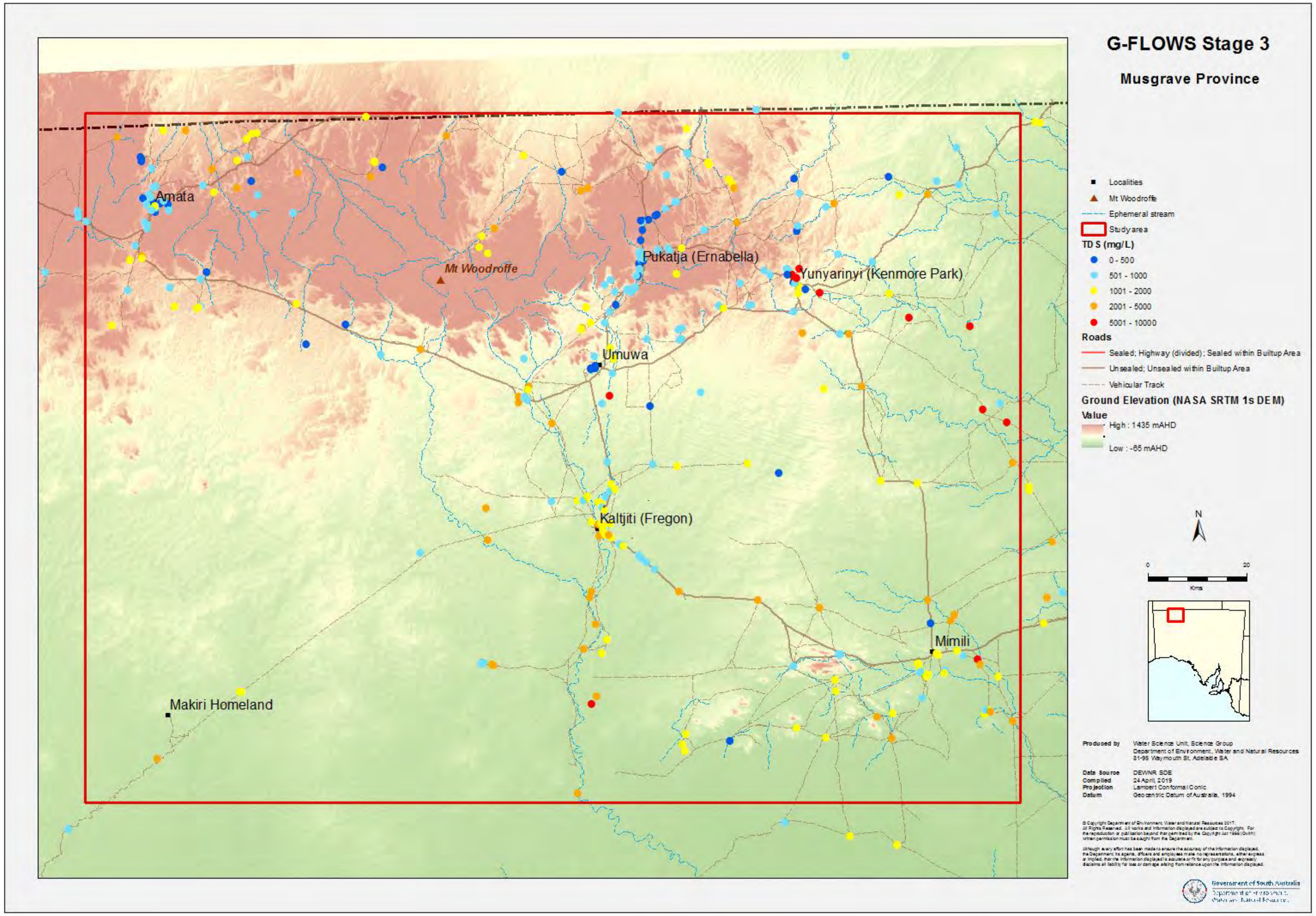


**Figure 2-10. Spatial distribution of salinity (TDS) across the study area (upper porous and lower fractured rock aquifers based on available screen interval and lithological information).**

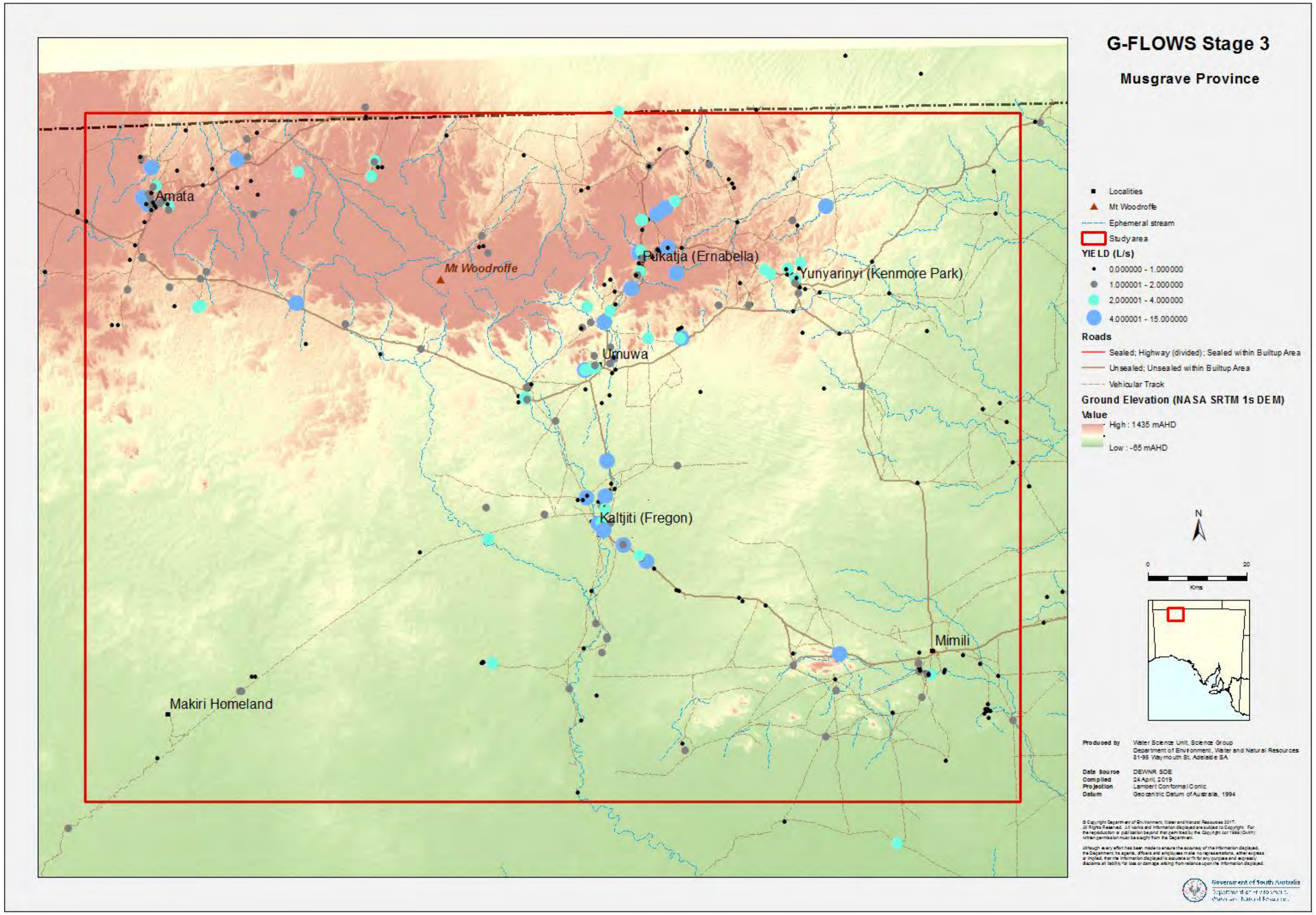


**Figure 2-11. Spatial distribution of yield across the study area (upper porous and lower fractured rock aquifers based on available screen interval and lithological information).**

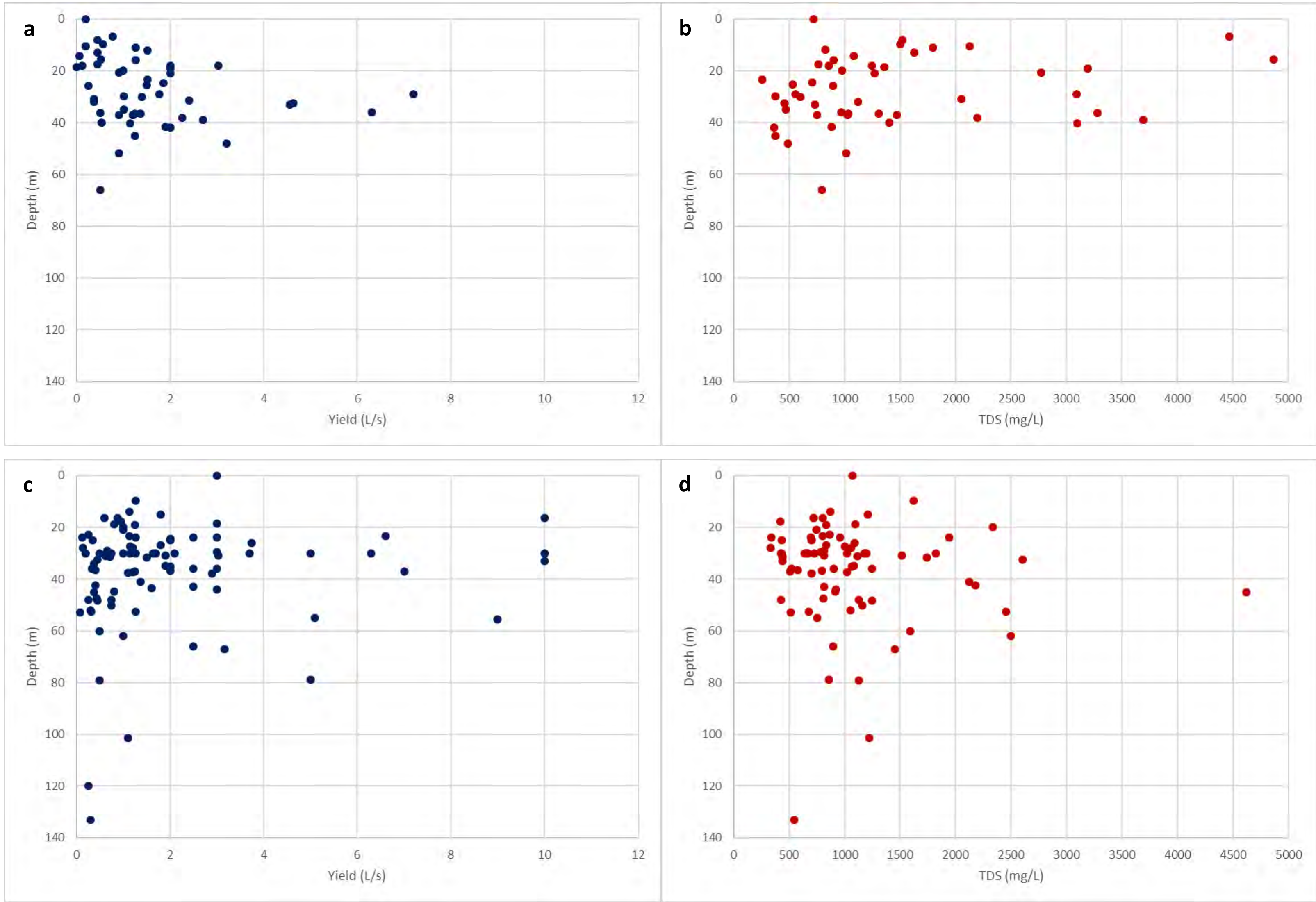


**Figure 2-12. Salinity and yield as function of depth; (a) yield from the porous media and (b)TDS from the porous media; (c) yield fractured rock aquifer and (d) TDS fractured rock aquifer (based on available screen interval and lithological information).**

## 2.4 Regional hydrostratigraphy and architecture

### 2.4.1 HYDROSTRATIGRAPHY

The broad scale geology of the region is relatively well known (Conor et al. 2006; Woodhouse and Gum 2003), however, the hydrostratigraphy is not. Based on the distribution of the Quaternary and Tertiary cover deposits as well as many geological logs throughout the region, the hydrostratigraphy can be broadly divided into four units.

- **Unit 1: Porous media unit.** Quaternary and Tertiary units. This unit consists of sands, silts and clays. The distribution of any inter-beds of this horizon is not known with any certainty. Based purely on the lithology it is estimated that the hydraulic conductivity varies by 3-5 orders of magnitude.
- **Unit 2: Weathered fractured rock aquifer.** This unit is highly weathered. Recent drilling has encountered this unit containing yields of up to 15 L/s.
- **Unit 3: Fractured rock aquifer.** Generally consolidated basement rock containing fractures of unknown distribution and orientation. Hydraulic conductivity is anticipated to be low.
- **Unit 4: Basement.** Unweathered/fresh basement that is dominantly crystalline basement rock that is part of the fractured rock aquifer but would have a lower hydraulic conductivity than the layer immediately above.

Although the four units described above can be recognised in some geological logs and an interpretation has been provided to inform the AEM vertical conductivity depth profiles in the two geological cross sections (Fig. 2-7 and 2-8), the units cannot be extrapolated across the entire study area. For example it is difficult to distinguish between Unit 1 and Unit 2 without a detailed geological log and in some cases downhole geophysical logs. It is very rare to have this information as most information in the state groundwater database is based on driller's logs alone; no further interpretation offered. However, the AEM data enables separation of Unit 1 (porous media unit) from Unit 2 (weathered fractured rock aquifer) using a conductivity value threshold. The threshold (separating these two horizons) has been interpreted to be at a conductivity value near 50 mS/m; meaning values >50 mS/m represent the porous medium horizon while values of conductivity <50 mS/m represent weathered fractured rock and fractured rock basement below.

### 2.4.2 ARCHITECTURE

The interpretation of the division between Unit 1 and Unit 2, using AEM data detailed in the previous section, has enabled regional-scale analysis and a series of mapping products; thickness of the porous media (Fig. 2-14), thickness of the porous media and weathered fractured rock (Fig. 2-15) and fractured rock basement (Fig. 2-16). The methodology used is described in Figure 2-13.

Data displayed in Figures 14-16 contain AEM data from two survey systems, Zone A in the east of the study area uses SkyTEM data flown using a helicopter, with a pixel size of approximately 90 m, while Zone B in the west of the study area used the TEMPEST data was flown with a fixed wing plane and a pixel size of approximately 800 m. The western boundary of all three maps were cut off at an easting value of 707 0000. This was done to eliminate the upper northern mountainous region of the study area where data control is poor.

Thickness of the porous media (Fig. 2-14) reveals that the greatest thickness is associated with the palaeovalleys (Lindsay East and Lindsay West). The porous media is absent in the east and north of the study area where the fractured rock aquifer either outcrops or subcrops. As discussed previously, the boundary between the base of the porous media and top of the weathered fractured rock has been defined as the AEM conductivity value of 50 mS/m. This represents a conservative value when calculating aquifer volume. The total number of raster cells within the map frame is 69,595,184. Given a cell size of 90 m x 90 m, this yields a predicted volume of 564 $km^3$. Assuming 40% of the volume is clay and 60% sand with a porosity of 20%, this volume equates to 67.7 $km^3$ (67,700 GL). This corresponds to a volume equal to 134 Sydney Harbours. While this value is not precise and represents many assumptions, the exercise is useful as it provides an indication, or at least a first pass, of the potential size of the porous media groundwater resource across the area. The true thickness of the actual porous media and its volume could be larger. This is because part of the weathered bedrock could represent porous media but has not been included therefore the volume could be somewhat conservative.

The volume of the total aquifer thickness porous media plus fractured rock aquifer has not been attempted. For modelling purposes hydrogeologist often require a definition of hydraulic basement, that is the depth at which fractures are closed and theoretical hydraulic conductivity is close to zero. To determine the hydraulic basement, the distribution of yield versus depth (Fig. 2-12) was considered. This indicated that yields were close to zero at approximately 120 metres. A greater distribution of yields would be required to firm up this estimate.

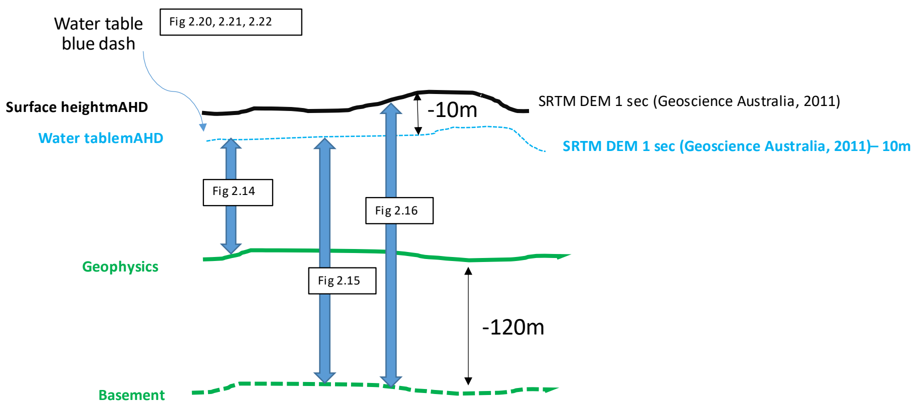


Fig 2.20, 2.21, 2.22 Water Table contour cut at 7070000 eastings
Fig 2.14 Interpreted thickness of the p[porous media
Fig 2.15 Total predicted Aquifer Thickness
Fig 2.16 Depth to assumed Basement, structural contour

**Figure 2-13. Schematic of interpreted aquifer thicknesses and structural contours using GIS (not to scale). Map (1) refers to Fig. 2-20, 2-21 and 2-22; Map 2 (thickness of porous medium) refers to Fig. 2-14, Map 3 (total aquifer thickness) refers to Fig. 2-15; Map 4 (depth to basement) refers to Fig. 2-16.**

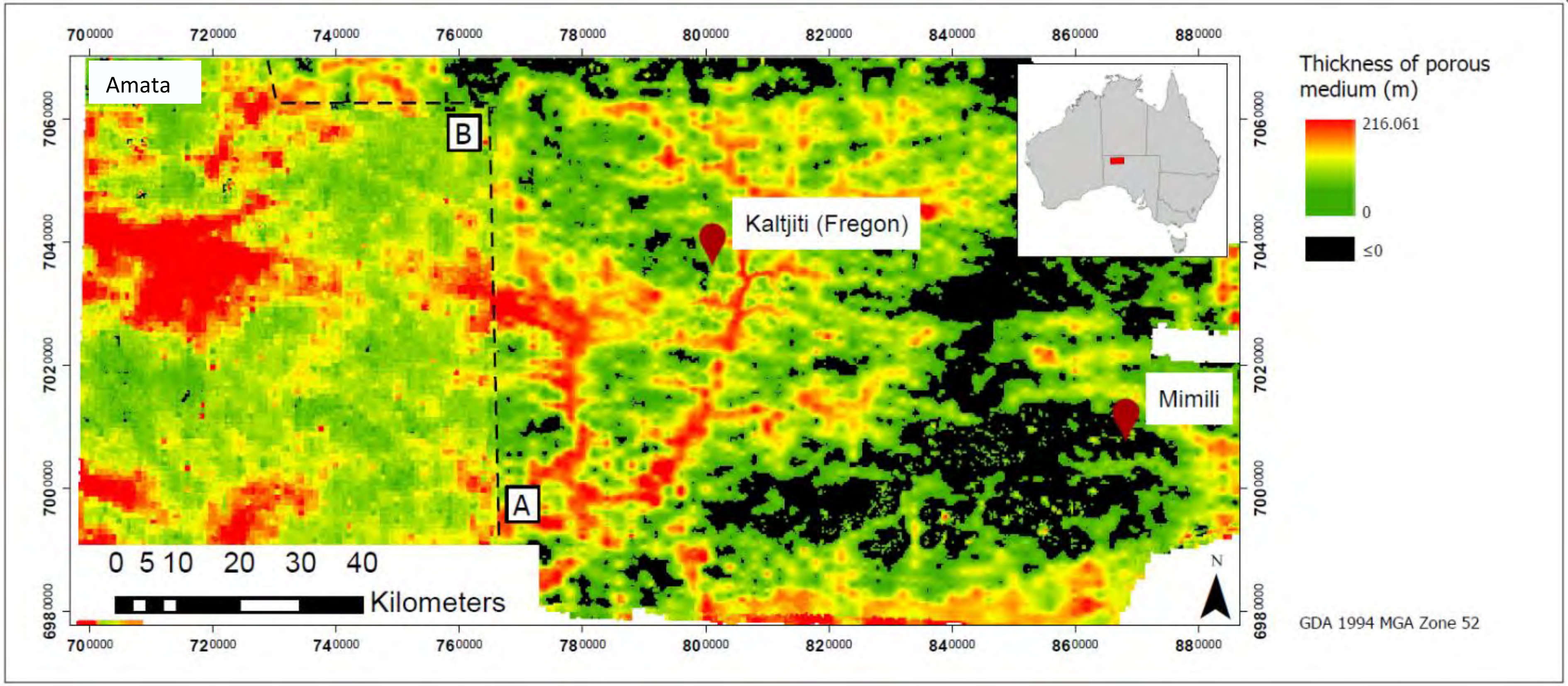


**Figure 2-14. Thickness map of the porous media aquifer across the study area. A/B boundary is the boundary between the SkyTEM and TEMPEST AEM systems.**

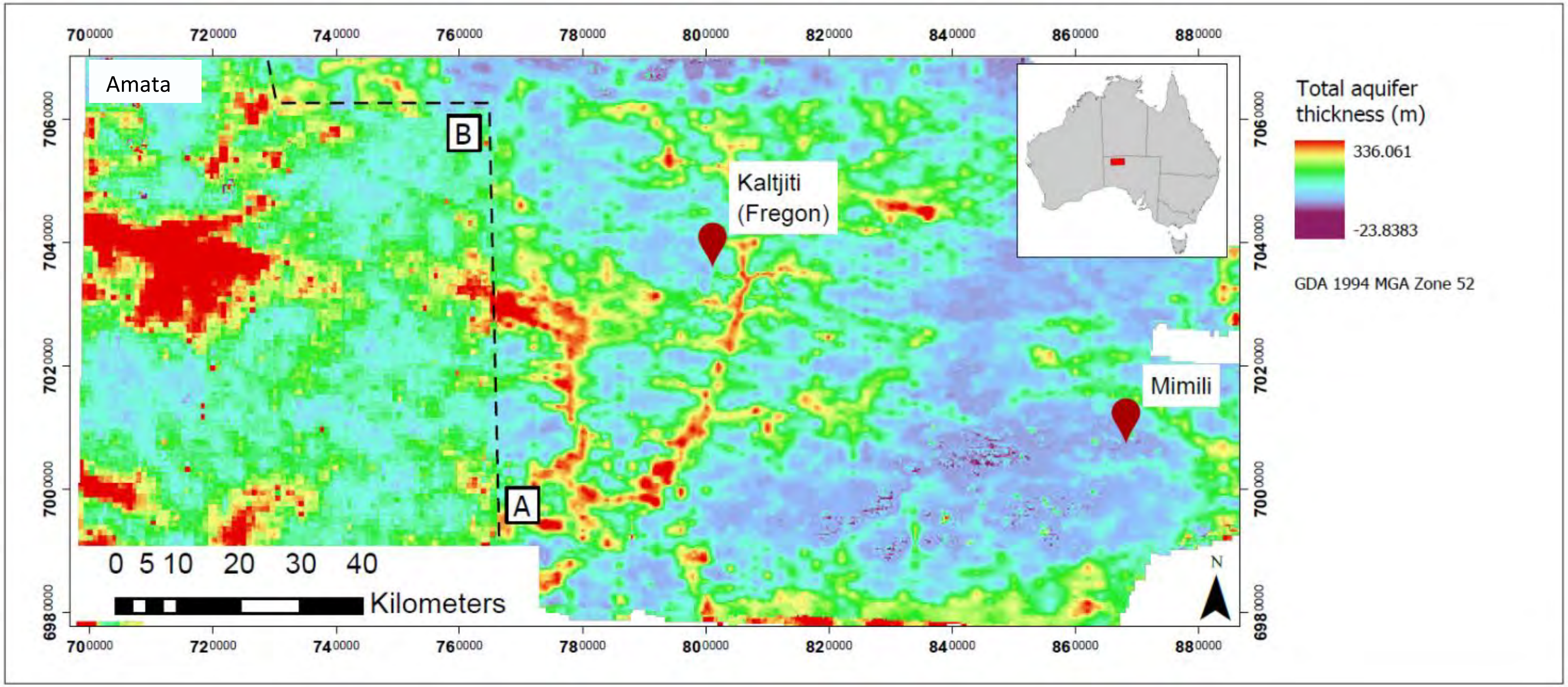


**Figure 2-15. Total thickness map of the aquifer (porous media and weathered fractured rock) across the study area. A/B boundary is the boundary between the SkyTEM and TEMPEST AEM systems.**

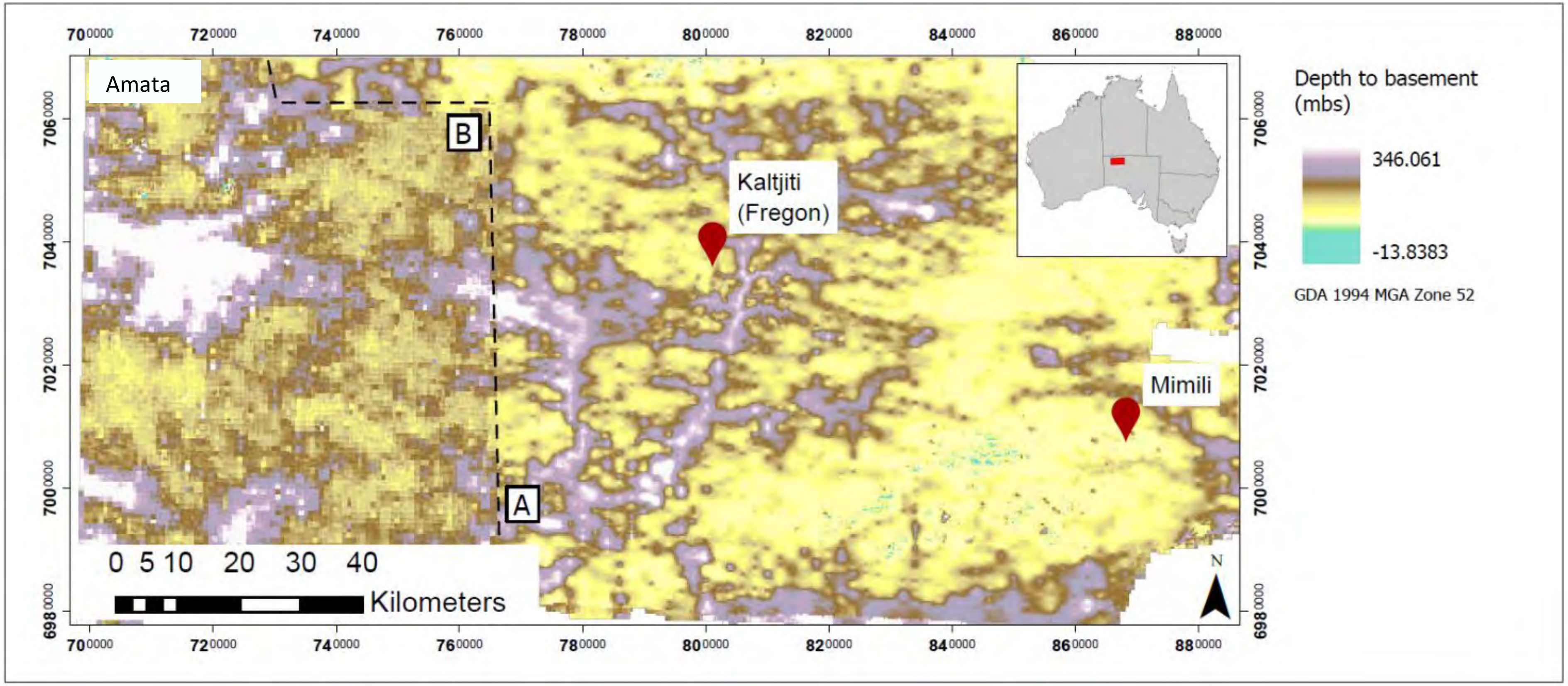


**Figure 2-16. Depth to assumed hydraulic basement map (from ground surface) across the study area. A/B boundary is the boundary between the SkyTEM and TEMPEST AEM systems.**

## 2.5 Groundwater flow systems

The watertable surface is an important element in informing the groundwater flow systems. This project explored two different methodologies. The first was a watertable surface map presented by Keppel et al. (2020) (repeated here in Fig. 2-17). This surface was constructed using traditional techniques and was considerably improved on previous surfaces (Varma 2012 and Kretschmer and Wohling 2014) through more thorough data validation, and increased data collection including ground and well elevations (see Chapter 1.4).

Groundwater elevation levels vary from approximately 800 m AHD in fractured rock aquifers near Mount Woodroffe in the Musgrave Ranges, to approximately 320 m AHD in sedimentary aquifers south of the Everard Ranges. Topographic highs (Musgrave and Everard ranges) appear to be the largest influence on the watertable surface, a surface that is a subdued reflection of the topography. Generally, the water level data appears to indicate that groundwater flow follows topography. In general, groundwater flow radiates away from the highland areas, particularly those of the Musgrave Ranges, into low-lying areas between the Musgrave and Everard Ranges and to the east and north of the study area. The watertable contours indicate that groundwater is flowing in a south-easterly direction originating from the Amata area. However, directly north of Kaltjiti the flow direction is almost north–south and parallel to Ernabella Creek. In this location the upper sand aquifer is more continuous. Several groundwater flow reversals can be observed throughout the study region, these can be observed by mounding of the watertable, an example of this mounding can be observed in the Everard Ranges. This may also form a zone of recharge.

Structural influence on groundwater flow is not evident in current groundwater level data due to the sparseness of measurements, however, such evidence could possibly be found at more localised scales than what is currently permitted by the existing well network.

This traditional methodology for determining watertable and potentiometric surfaces is well established and used by hydrogeologist throughout the globe. This method is particularly useful and accurate where there is a large amount of data points; however, in this process, there is a bias to the shallow system as there are inherently is a larger density of wells in the shallow horizons. The major limitation of the potentiometric surface interpretation is the number and distribution of water wells within the study area. Areas where there are few, if any data points are more prone to be erroneous. Such areas include the south-western portion of the study area between Amata and the Makiri Homeland and northwest of Mimili (Figure. 2-17).

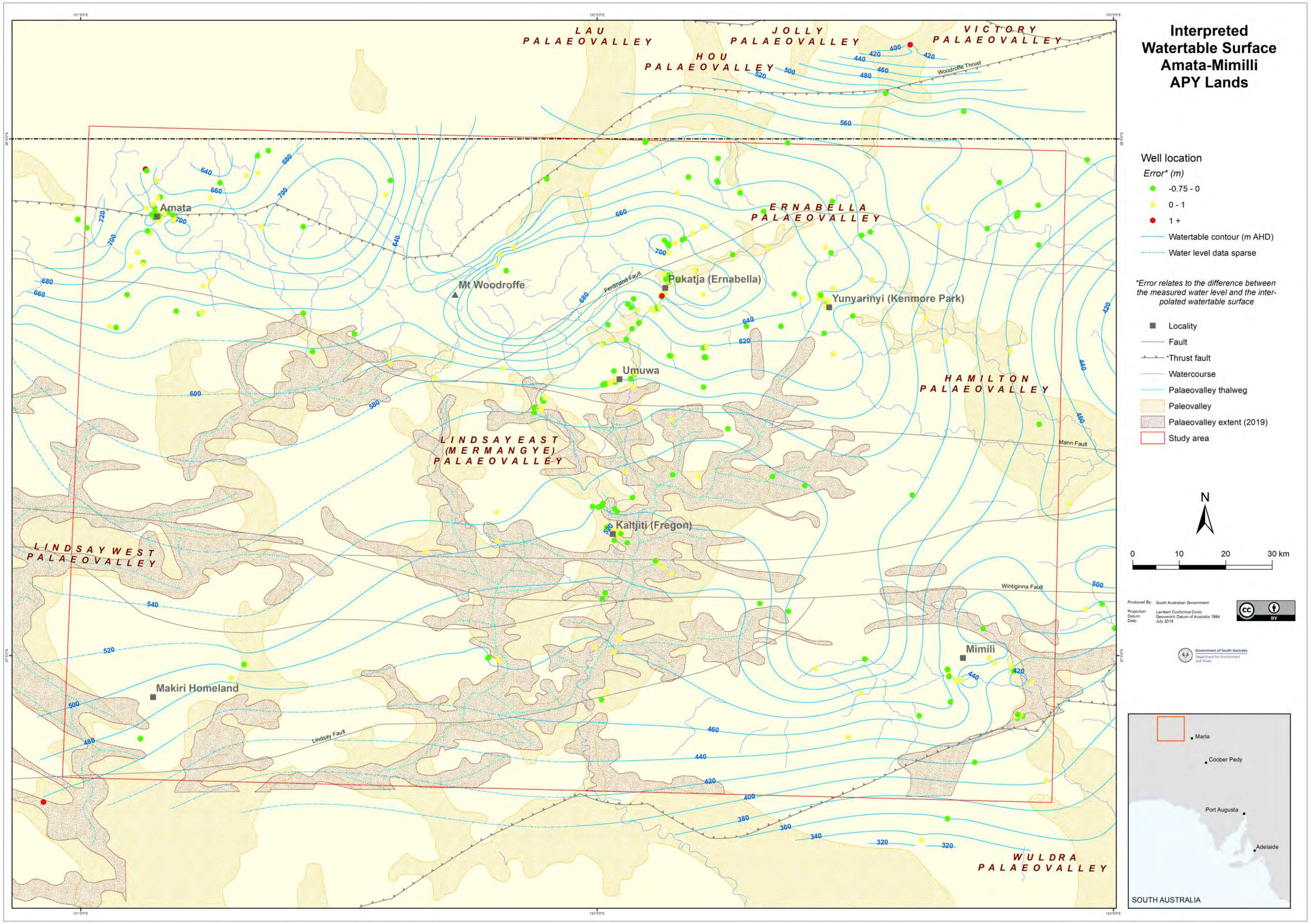


Figure 2-17. Newly interpreted watertable surface map across the study area (20 metre contours).

Figures 2-18 and 2-19 represent the N-S and NW-SE geological cross-sections and show the relationship between topography and depth to water. These show that the depth to water below the topography is relatively shallow with an average depth of 11.2 m for the NW-SE transect and 8.5 m for the N-S transect.

The line of best fit for the depth to water observed measurements was fitted with a cosine Fourier series to obtain a complete watertable map across the whole study area (Fig. 2-20). The cosine Fourier series is given by:

$$W = C_0 + \sum_{m=1}^{N} C_m \cos\left(m\pi x / L\right)$$

where *W* is the watertable elevation (m), $C_0$ is the base elevation (m), *L* is the length (m), *x* is the distance from the origin (m), $C_m$ is the coefficient, *N* is the number of coefficients used. It was found that when *N* equals 35, fitting to the watertable in both cross-sections is reasonable.

Figure 2-18 clearly shows that the watertable follows a subdued form of the topography. The groundwater flow system is a gravity driven system controlled by the distribution of the groundwater level. The NW-SE transect shows several undulations of the watertable (variations in amplitude against the regional slope) suggesting the potential for flow reversals as well as a number of different flow cells. At first glance we would suggest that this transect is controlled by local flow systems where both vertical and horizontal flow are important. In this scenario, a number of recharge and discharge zones can be identified with recharge occurring on the hill tops and potential discharge zones occurring in the adjacent valleys. In comparison, the N-S transect shows a smoother profile with only very small variations in the amplitude of any undulations. We would infer that this profile has larger flow systems such as regional flow paths compared to the NW-SE profile. This profile would follow more of a distributed recharge zone with limited discharge. This N-S transect also contains a thicker more continuous porous medium aquifer. This hypothesis of gravity driven Tóthian Flow systems is further explored by numerical modelling; as outlined in Chapter 2.7.

The major control on the hydrogeology of the unconfined/fractured rock aquifer is thought to be the distribution of the watertable. This is a widely accepted phenomenon in hydrogeology (Tóth, 1963 and 2009). We expect that head variations are more likely to reflect flow changes (i.e., recharge and discharge variations) rather than changes in aquifer hydraulic properties. e.g. due to faulting and other geological effects.

Since the watertable follows a subdued form of the topography and is relatively shallow we have been able to produce a second map of the watertable (Fig. 2-20). The watertable map produced in this conceptualisation was achieved by subtracting the average depth to water from the topography. For simplification, the watertable was assumed to have an average depth of approximately 10 mBNS and then subtract from the digital elevation model to produce the second watertable map for the study area.

The northern part of the study area in the ranges has been removed by splicing the map at 707 000 00 easting as the depth to the water is variable above this depth.

Figure 2-20 displays the map in plan-view where the watertable is presented in intervals of 20 m. This map shows variations in the watertable that mirrors the topography with the dark blue representing areas of low and the brown areas representing zones of high watertables. Groundwater flows at right angles to these contour intervals. However, the map is difficult to read and so we have produced the same data in different views (Fig. 2-21 and 2-22).

Figure 2-21 shows a 3D image of the watertable. This map was produced using an inverse distance weighting smoothing algorithm with a 100 times vertical exaggeration. Broad-scale features of the watertable can be observed including an undulating watertable throughout, which suggest several local and possibly some intermediate groundwater flow systems. The local systems appear to be more dominant in the northern portion of the study area as well as immediate east of Mimili. A larger more regional flow system may be associated with Officer Creek and Ernabella Creek.

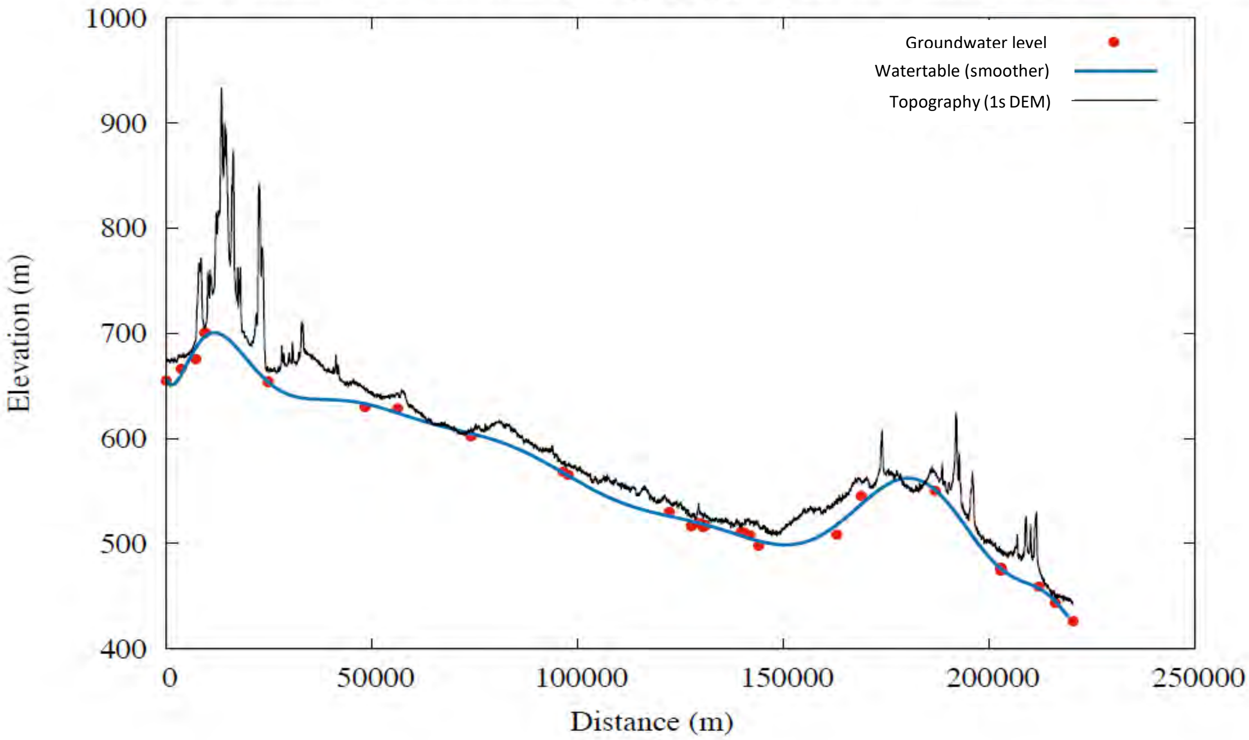


Figure 2-18. Plot of the topography and groundwater level (water table - smoothed) across the NW-SE transect.

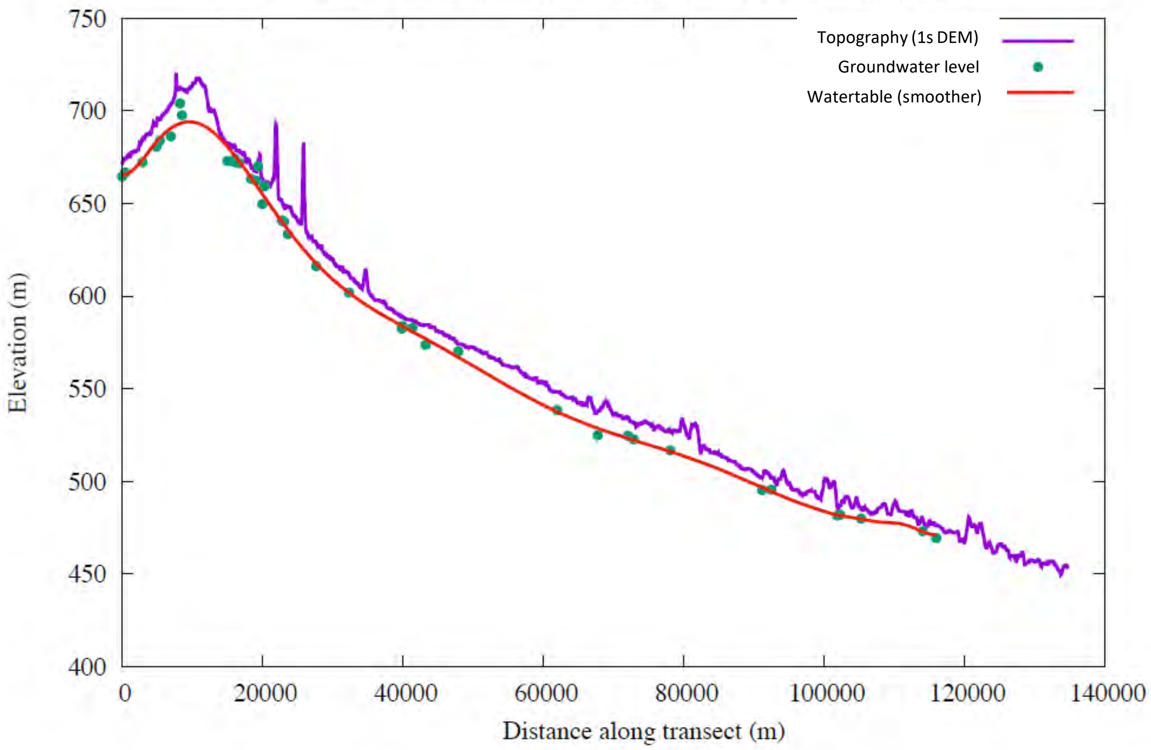


Figure 2-19. Plot of the topography and groundwater level (water table - smoothed) across the N-S transect.

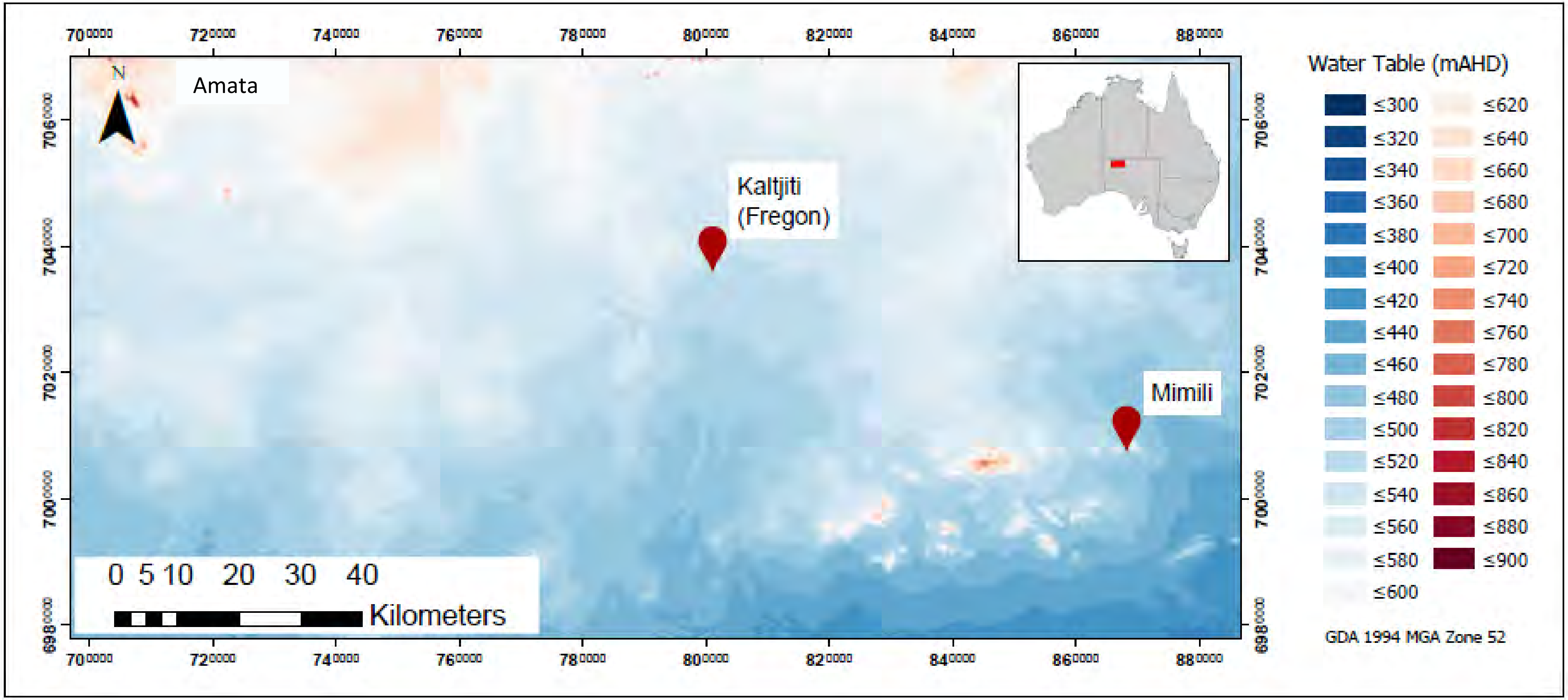


**Figure 2-20 Watertable surface derived from the 1 sec DEM across the study area.**

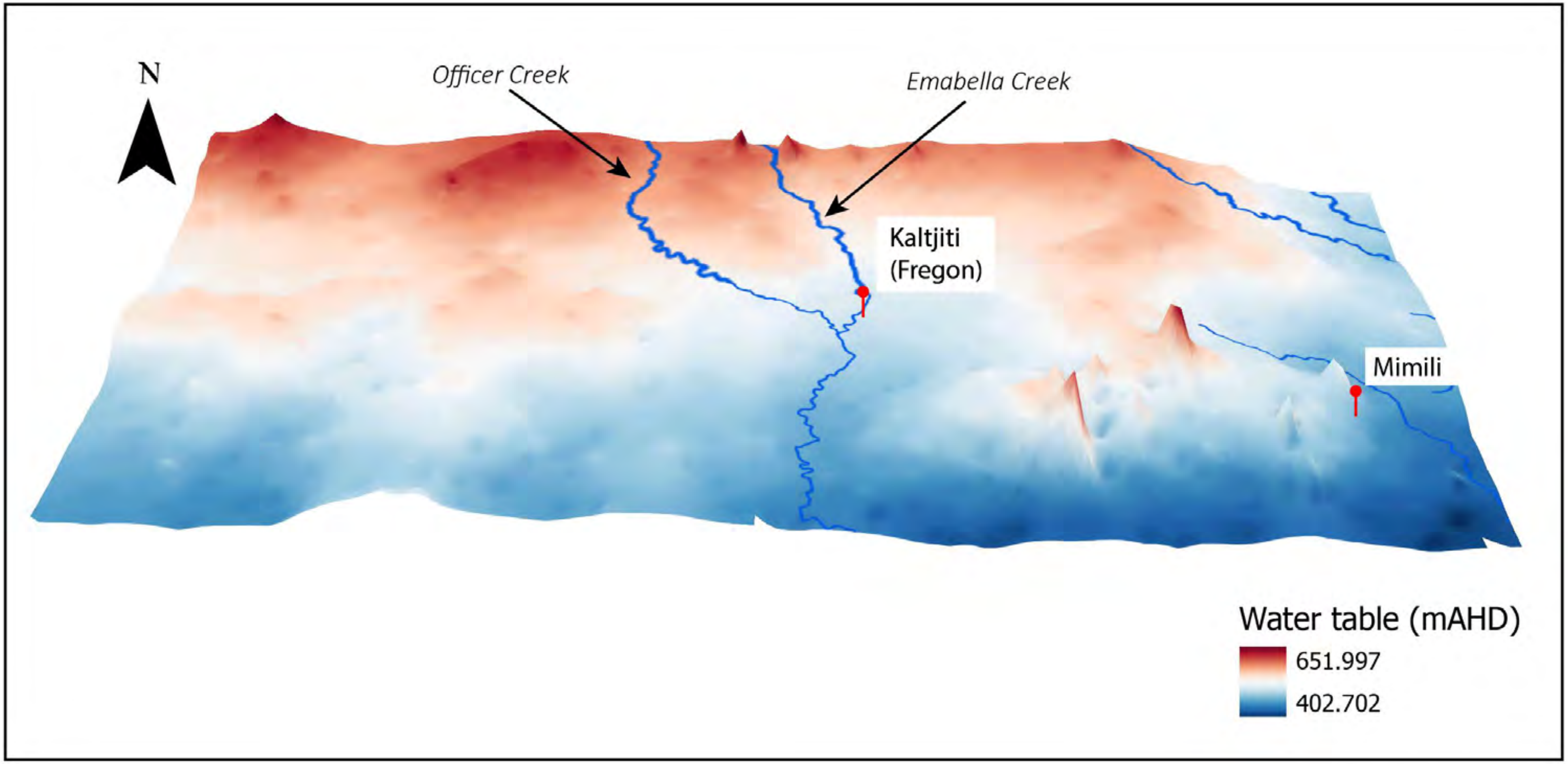


**Figure 2-21. Smoothed 3D watertable surface derived from the 1 sec DEM across the study area. Map view is looking north towards the Musgrave Ranges.**

Finally, the data is presented as a raw surface without any smoothing with a 50 times vertical exaggeration (Fig. 2-22). Watertable contours have also been added at 5 m intervals. More detail of variations in the watertable can be observed in this projection. This includes a general slope of the watertable towards the south, however, this is superimposed by several local groundwater flow cells as indicated by large and small scale watertable undulations. In these local areas, groundwater will flow from high zones to low zones which corresponds to zones of potential recharge and discharge, respectively.

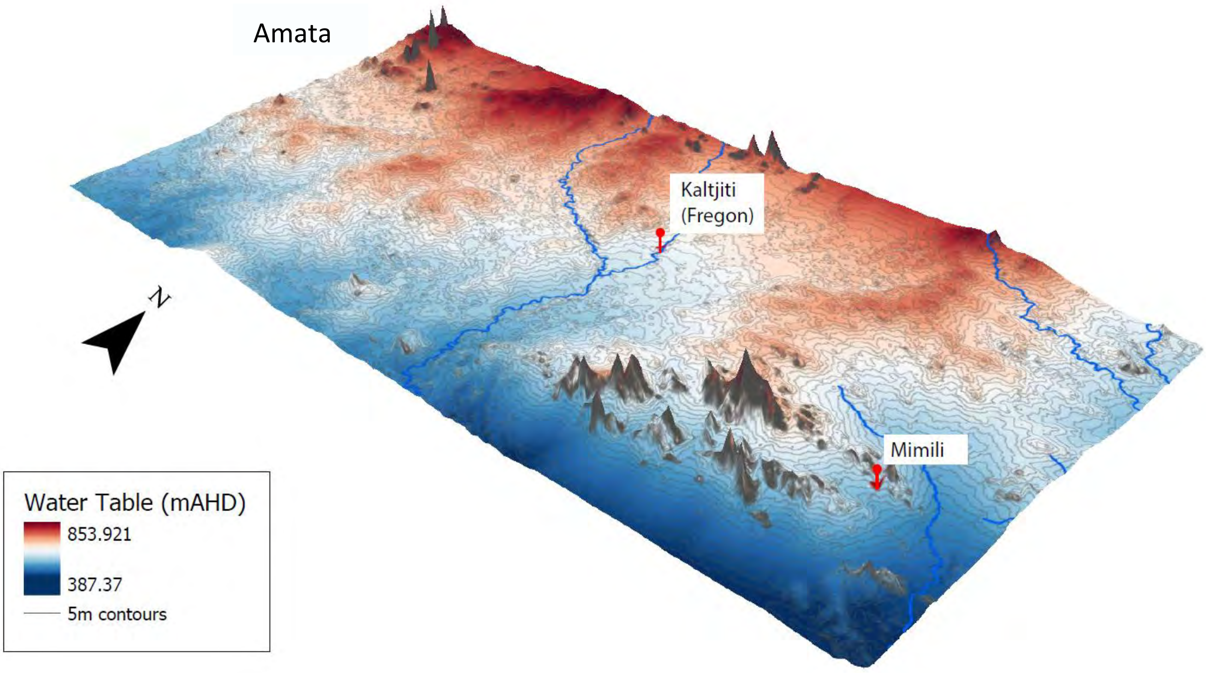


**Figure 2-22. Unsmoothed 3D watertable surface with 50 times vertical exaggeration applied.**

## 2.6 Regional tracers and chemistry

Environmental tracers included stable and radioactive isotopes of the water molecule, the major solute chloride, radioactive solutes and gases as well as dissolved gases such as noble gases and anthropogenic contaminants. As these tracers are introduced in the recharge process they can serve as hydrological tracers. For example, under ideal circumstances a vast array of information about groundwater recharge, discharge and groundwater flow, to mention a few, can be deduced from these tracers.

Previous studies in the APY Lands and throughout central Australia have concentrated on groundwater recharge processes using the distribution of stable isotopes (Harrington et al. 2002, Leaney et al. 2013, Fulton et al. 2013, Love et al. 2013, Kretschmer and Wohling 2014). Groundwater recharge has previously been estimated using CMB, and groundwater age distribution has been determined using radiocarbon, tritium and chlorine 36 (Love et al. 2000, Harrington et al. 2002, Creswell et al. 1999). Specifically, work on environmental tracers and chemistry in the APY lands has occurred through projects associated with Geoscience Australia (Dodds et al. 2001, Creswell et al. 2002), the Goyder Institute for Water Research, GFLOWS 1 Project (Leaney et al. 2013) and the Department for Environment and Water (Kretschmer and Wohling 2014).

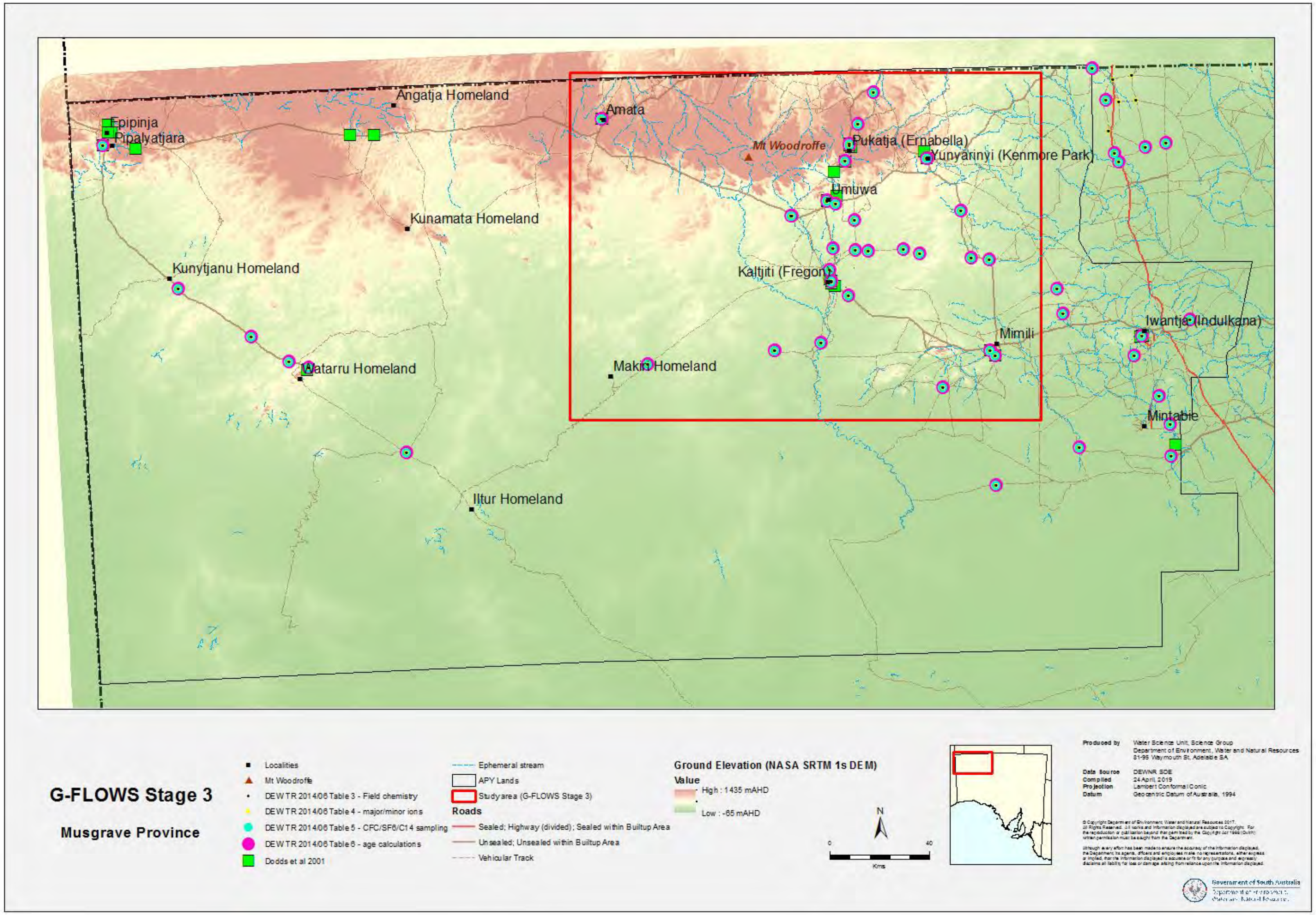


**Figure 2-23. Footprint of groundwater sampling and hydrochemical analysis conducted in the APY Lands (2001, 2012, 2013 and 2014).**

The regional hydrochemistry has been discussed extensively by previous authors (Leaney et al. 2013, Kretschmer and Wohling 2014) and therefore only a brief summary is presented here. Groundwater salinity is variable ranging from fresh to brackish with saline groundwater in a few places. The overall chemistry of the waters generally has an evolution form Ca-$HCO_3$ towards Na-Cl along flow paths, typical of many groundwater systems in central Australia (Leaney et al. 2013, Kretschmer and Wohling 2014).

Many of the local communities source groundwater from the cover sedimentary aquifer of Quaternary and Tertiary age as well as the weathered fractured rock aquifer. Some local water supply wells from community wells have high levels of salinity nitrate and fluoride that exceeds world health thresholds (Dodds et al. 2001).

The distribution of groundwater chemistry and environmental isotopes can provide information on potential groundwater flow systems. In the following we discuss the distribution of salinity (TDS) as well as the distribution of radiocarbon.

### 2.6.1 CHLORIDE

In the following, we assume that chloride (Cl) is chemically conservative. This is a reasonable assumption as there are no known halite deposits in the region and Cl has a positive correlation with many of the other major ions (Chapter 3). In this way, changes in Cl concentrations can only occur by physical processes such as evaporation, transpiration, or mixing of different water bodies with different Cl concentrations or diffusion processes. Therefore, variations of Cl provide insights into the groundwater flow system. For example, in the Otway Basin, it has been shown that rapid variations in the concentration of Cl reflect variations from local recharge to local discharge systems (Love et al. 1993). While in the Murray Mallee variations in Cl along assumed groundwater transects represent variations in past climates (Leaney et al. 2003).

For the samples with full analyses, a relationship between Cl and TDS was derived. This relationship was then applied to the entire DEW chemical data base where values of TDS were recorded. This resulted in a significant increase in the number of Cl values (Figure. 2-24).

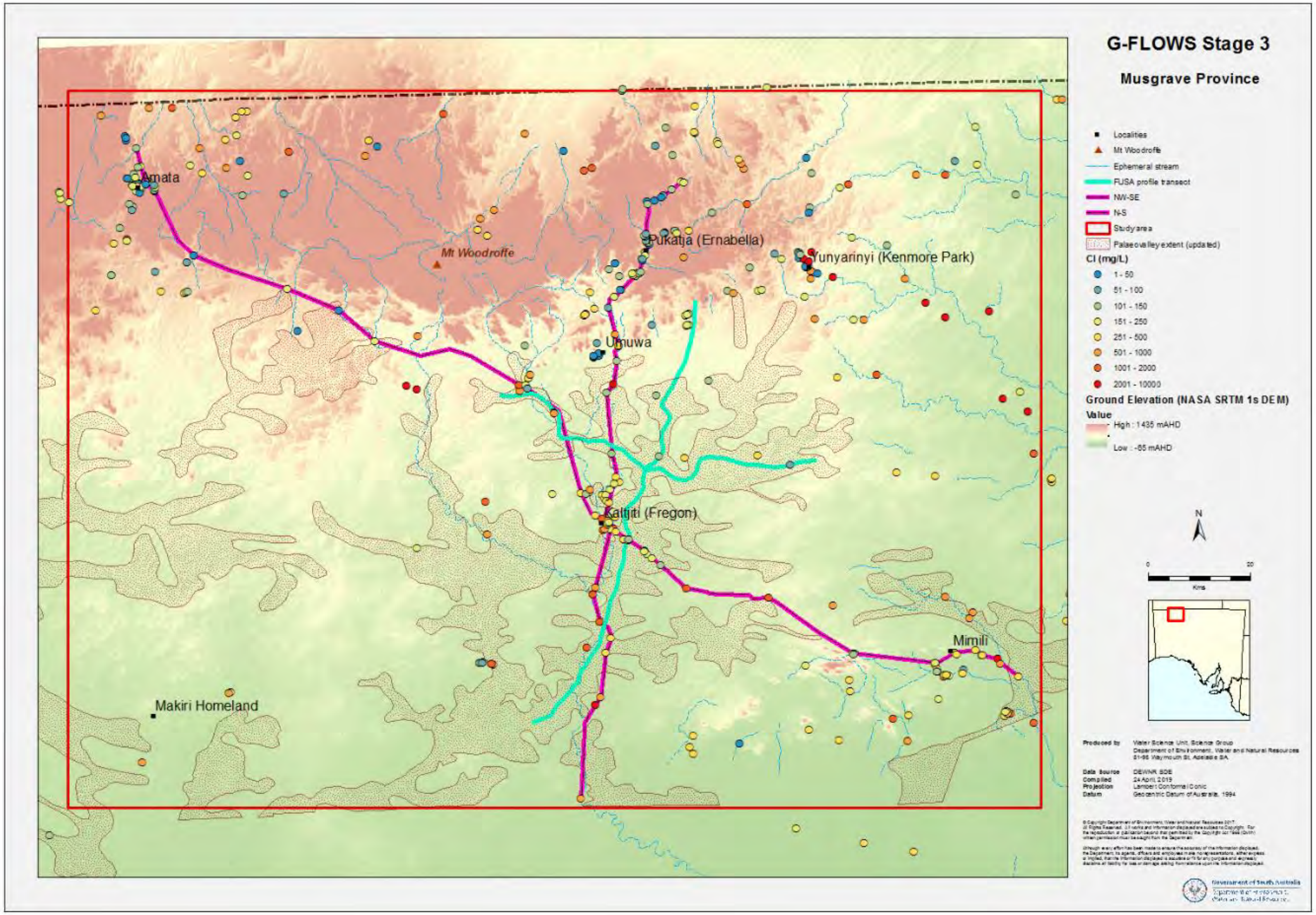


**Figure 2-24. Spatial distribution of Cl (mg/L) across the study area.**

As discussed previously, as Cl is assumed to be chemically conservative in the APY Lands, then its spatial distribution can provide insights into the groundwater flow systems. Cl concentrations in the study area vary from 26 mg/L to 1,900 mg/L, with an average value of 336 mg/L. Cl shows a high amount of spatial variability with large variations in Cl occurring over small spatial scales. For example, large spatial variability, can be observed for the fractured rock aquifers near Amata and Pukatja (Ernabella), where the colour scale of Cl ranges in the map show steep concentration gradients. However, despite this dominant feature of large spatial variability, some general patterns do emerge, with notable patterns listed below.

1. Lower concentrations of Cl are associated with the fractured rock aquifers of the Musgrave region and those near Mimili.

   Low concentrations of Cl in the mountains region, strongly suggests relatively high recharge rates (note these zones also have high $^{14}C$ discussed below). Slightly more concentrated values of Cl in the adjacent flats and drainage within the mountains region, supports the concept of lower recharge rates in these zones. Alternatively, these lower elevation regions, close to today's drainage patterns, may also represent local discharge zones through evapotranspiration.

2. There is large variation in the concentration of Cl across the landscape (from low concentrations to higher and then lower concentrations). This can be observed by the variation in colours across the landscape. A good example of this can be observed in both NW-SE and N-S transects.

   This pattern of alternating Cl concentrations does not suggest a simple groundwater flow system with constant distributed recharge. Rather the data suggest either a) differential recharge rates due to different soil properties or alternating zones of recharge and discharge.

3. Higher values of Cl occur to the south in the Officer Basin possibly reflecting greater evaporation during diffuse recharge.

The higher Cl concentrations may indicate low rates of diffuse recharge. Alternatively, these high Cl zones may indicate groundwater discharge through evapotranspiration. A similar pattern of the distribution of Cl occurs throughout the APY Lands.

### 2.6.2 CARBON 14

Carbon-14 ($^{14}C$) is a measure of the time that $^{14}C$ has been isolated from the atmosphere. If we assume that the water molecule travels at the same speed as the radiocarbon, then inferences about groundwater residence times and recharge rates can be inferred. In this section we present the radiocarbon data uncorrected as pMC (percent modern carbon). Values of $^{14}C$ > 90-100 pMC (background levels for southern hemisphere) would indicate a thermonuclear component. Above background atmospheric levels of $^{14}C$ occurred in the 1950s and 1960s due to nuclear weapon testing, above background levels were recorded in 1955, with peak values in 1965. Thus, groundwater's with activities above background must have a component of recharge since 1955 (i.e. <65 year old before present (BP)). In simple terms, groundwater with a value of 50 pMC would represent the decay of one-half life with an age of 5730 years. These radiocarbon "ages" represent the maximum possible groundwater ages as they have not been corrected for any possible water rock interactions. However, if any correction is required for closed system dissolution of the carbonate then the actual groundwater ages would be younger (refer to Chapter 3). In Chapter 3 we discuss this, and geochemical corrections, at the Lindsay East Palaeovalley site.

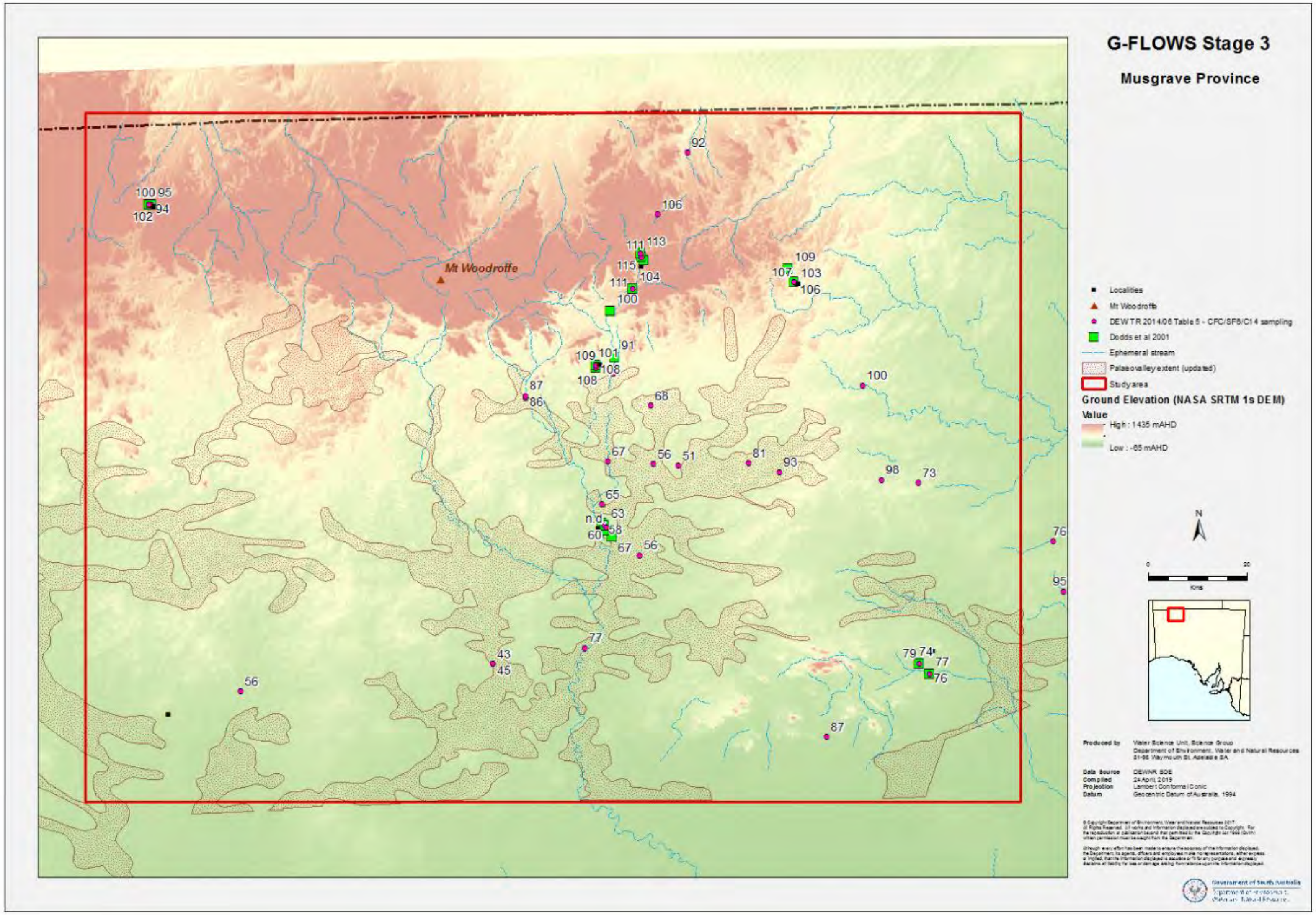


**Figure 2-25. Spatial distribution of $^{14}C$ in pMC across the study area.**

The spatial distribution of radiocarbon is shown in Figure 2-25. High activities of $^{14}C$ above natural background levels occur throughout the Musgrave Ranges, indicating that these fractured rock groundwater's have a thermonuclear component[1] and have been recharged in the last 65 years these. Many of these wells also have CFC, $^{36}Cl$ and $^{3}H$ concentrations consistent with modern recharge (Creswell et al. 2002 and Dodds et al. 2001). From this we can make a first order estimate of recharge from the following equation:

$$R = V\theta$$

where *R* = recharge *V* = vertical velocity and $\vartheta$ = porosity. If we assume that the environmental tracers are in equilibrium with the atmosphere and there is no decay of $^{14}C$ or degradation of CFCs.

This is a reasonable assumption when the watertable is shallow. Furthermore, if we assume a porosity of 0.2 and that the midpoint of the well screen varies between 2 and 10 m this would convert to a first order estimate of recharge between 4 to 80 mm/year. Using these event markers to estimate recharge is a good first order approach and gives a reasonable comparison to the work of Cresswell et al. (2002), who established similar a result.

High $^{14}C$ activities also correspond to outcropping or sub cropping fractured rock aquifers of the Birksgate and Pitjantjatjara Super Group near Mimili and on the eastern flank of our study area again inferring relatively young groundwater's with relatively high recharge rates. We can also observe high $^{14}C$ values on the boundary of the fractured rock aquifer and the palaeovalleys suggesting that these may represent zones of recharge. Groundwater within the upper palaeovalley sequence is older than those on the boundary and those in the fractured rock (this is discussed in greater detail in Chapter 3).

One of the unresolved questions from the previous conceptualisation is the question of whether the recharge in the plains emanated from the mountainous fractured rock aquifer to the north. However, most of the groundwater in the plains is far too young to be derived from the mountain front/block. The oldest groundwater's on the plains have values of ~45-55 pMC, which converts to uncorrected ages of approximately one half-life of 5730 years (note this is a maximum groundwater age). Assuming this age, we can calculate a minimum groundwater velocity of ~16 m/year assuming that the distance to the mountain front is ~80 km. This is a very large velocity for this kind of system and lithology and is out of the common range that we could expect. We conclude that it is very unlikely for any groundwater recharged in the mountains to travel to the edge of the study area. If this was to occur it would be a very small component.

### 2.6.3 STABLE ISOTOPES OF THE WATER MOLECULE

Under ideal conditions the stable isotopes of the water molecule deuterium ($\delta^{2}H$) and oxygen 18 ($\delta^{18}0$) can be used to provide a vast array of information on recharge and discharge process.

A plot of $\delta^{2}H$ –$\delta^{18}O$ space shows the distribution of these isotopes in rainfall and groundwater (Fig. 2-26). This figure is taken from Kretschmer and Wohling (2014). A similar figure was also produced from GFLOWS 1 (Leaney at al. 2013) but is not repeated here. We have superimposed groundwater samples from our study on to this figure. These groundwater samples were sampled from the control site DH1 and S22. These are discussed briefly in Chapter 3.

The groundwater data is referenced to Alice Springs rainfall the nearest isotopic rainfall collection site. The local meteoric water line (LMWL) of Alice Springs is displayed along with the weighted mean precipitation

[1] A thermonuclear component means that groundwater contains radiocarbon, tritium or 36 chloride that was introduced at elevated levels due to nuclear weapons testing in 1950s and 1960s that was released into the atmosphere and subsequently groundwater.

amounts for Alice Springs. The groundwater data plot just below the LMWL with a similar slope suggesting that much of the groundwater has been recharge with little evaporation.

Previous researchers in the arid zone of central Australia have estimated a rainfall threshold for of in excess of 80 mm/year and 60-100 mm/year for recharge to occur (Leaney et al. 2013 and Kretschmer and Wohling 2014, respectively). This is based on the interception between the groundwater trend and the Alice Springs (or local) meteoric water line. This corresponds to January to March weighted mean rainfall values for Alice Springs. These $\delta^2$H –$\delta^{18}$O values are in the range of samples collected adjacent to the Finke River which have corresponding high values of $^{14}$C.

A similar recharge mechanism occurs for the high rainfall events in the Musgrave Ranges as that of the Finke River. High rainfall events correspond to low Cl in groundwater, depleted stable isotopes of the water molecule and young groundwater ages as indicated by radiocarbon data.

The concept of a single threshold value of recharge does not apply in the APY Lands. This is because the difference in slope between the LMWL and the groundwater data is very small and does not indicate a single threshold value of recharge followed by partial evaporation, i.e. slopes are close to parallel. Rather the data suggests multiple threshold values for groundwater recharge if rainfall events are greater than 60 mm/month. The line of best fit for the groundwater data shows a wide scatter of data with many values of deuterium plotting either above or below the LMWL by up to 10 ‰. It is difficult therefore to extrapolate back to the LMWL to determine a threshold single threshold value for recharge. This indicates multiple sources of rainfall would result in this distribution. Rainfall events much less 100 mm/month or even greater than this could result in recharge to the groundwater system.

The spatial distribution of $\delta^2$H –$\delta^{18}$O across the wider APY Lands (as well as our study area) show the characteristic spatial variability of other tracers such as TDS, Cl and $^{14}$C. Despite this, we can still tease out the following characteristics. The higher elevation areas in the Musgrave Ranges have the most depleted values (ranging from -10 to -6 ‰; average ~ -8 ‰). In the plains we get a more enriched ranges from approximately -8 to -4.5 ‰ (average ~ -5.8 ‰). Whilst the most southerly samples, close to the Officer Basin have the most enriched with values, ranging from -7.4 to -4.2 ‰.

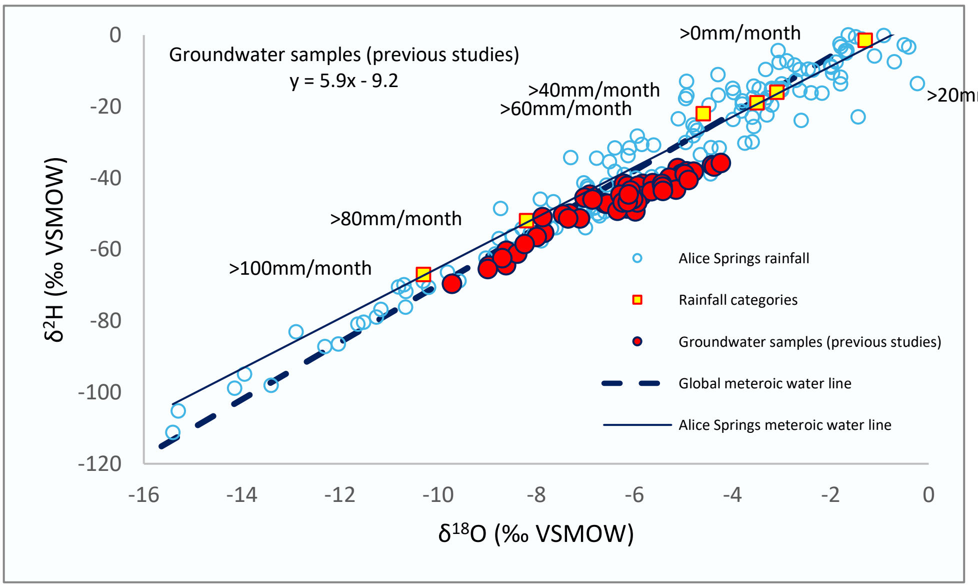


**Figure 2-26. Groundwater stable isotope ratio relative to amount weighted-mean monthly rainfall volume categories.**

This distribution of data is consistent with our model of higher rainfall events resulting in rapid recharge in the mountains, followed by less recharge with a greater increase in patrial evaporation or transpiration in the lower elevation zones in the plains. However, Kretschmer and Wohling (2014) suggested that the distribution of $\delta^{18}$O may also be partly a result of an orographic effect where stable isotopes become more depleted with altitude. This is different from our model where we suggest that the depletion in the isotopes is due to the continental effect where the isotopes become progressively depleted due to rainout effects. As with the Finke River recharge work, the most likely source for this is monsoons in the north of the continent that travel across the vast interior of Australia which results in large episodic summer rainfall. The exact weighting of each mechanism, i.e. local orographic effects versus continental rain out, cannot be determined. Additional isotopic weather stations would need to be established to determine this. From a practical point of view this may not be important.

### 2.6.4 TRACER – TRACER PLOTS

Tracer versus tracer plots can be useful indicators of processes for example residence time indictor such as $^{14}C$ compared with stable isotopes of the water molecule can be useful in some circumstances in finger printing what mechanisms are occurring during recharge and discharge (Love et al. 1993).

For a plot of $^{14}C$ versus Cl, although there is scatter, there is a trend of increasing Cl concentration with decreasing $^{14}C$ (Fig. 2-27a). Younger groundwater corresponds to high recharge rates with low Cl values while, corresponding to recharge zones. Slightly older groundwater as indicated by lower activities of $^{14}C$, show an increase in concentration of Cl. A common explanation for this would be that as TDS increases with groundwater residence time and as Cl is positively correlated with TDS, then this would indicate evolution along the flow path. However, as Cl is chemically conservative in the study area, any increases in Cl are a result of either a) differential recharge due to different soil zones with varying degrees of evaporation or, b) local groundwater flow systems with concentration increases as a result of evapotranspiration process.

The work to this point suggests that evapotranspiration is an important process in concentrating Cl in the groundwater, but it is difficult to distinguish between the two processes. A plot of $\delta^{18}O$ vs Cl is very instructive, as trends of both evaporation and transpiration can be observed. At low Cl concentrations, $\delta^{18}O$ values are depleted and as Cl becomes concentrated then the stable isotope becomes enriched, showing a slight partial evaporation trend. At around -5 to -6 ‰, $\delta^{18}O$ remains relatively constant with a rapid concentration in the Cl anion. This clearly indicates a trend of transpiration causing an increase in Cl , beacuse $\delta^{18}O$ is not fractionated during the process of plant transpiration. It is important to note that both evaporation and transpiration processes can occur in both recharge and discharge processes.

The depth to the watertable in the region has an average of 10 m. It is highly likely that the native vegetation is groundwater dependent and has access to the watertable uptake during the transpiration process. Thus transpiration is an important process in groundwater discharge zones that occur throughout the landscape. We suggest that many of the shallow groundwater discharge zones, occur in the relatively flat lying regions between topographic lows. Many of these zones would represent the terminal zones of the local flow systems. A number groundwater's sampled in the plains have a signature of transpiration. We suggest that these zones represent zones of discharge and not recharge as previously assumed by previous authors.

This supports our hypothesis of the region being dominated by local and to a lesser extent intermediate flow systems. There are few if any long scale regional groundwater flow systems. Future work should include methodologies to map local groundwater flow systems as they manifest themselves on the surface topography.

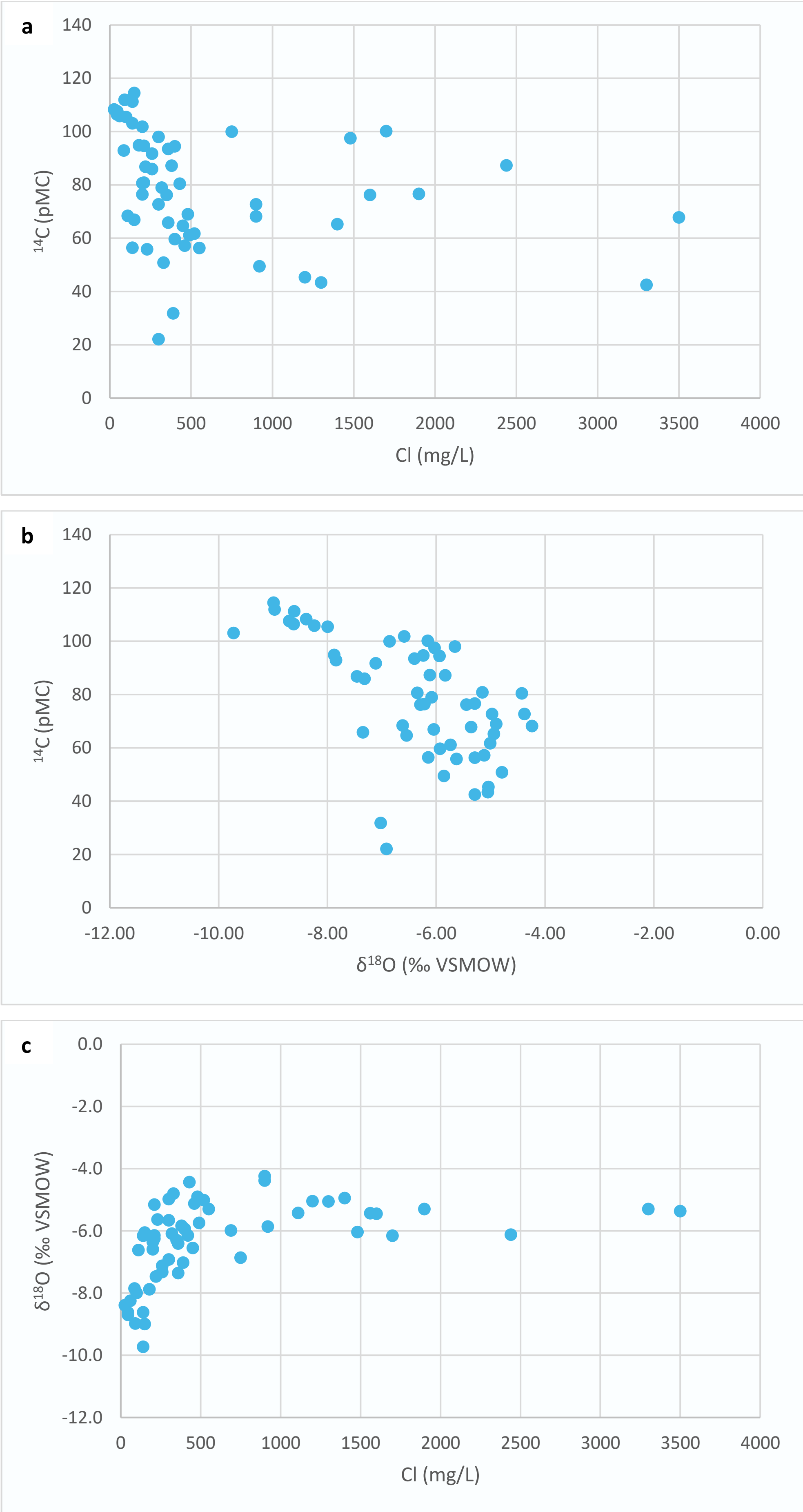


**Figure 2-27. Tracer - tracer plots: (a) $^{14}C$ vs Cl; (b) $^{14}C$ vs $\delta^{18}O$; c) $\delta 1^{8}O$ vs Cl.**

Previous work in the arid zone has postulated that an increase in Cl can be a result of total evaporation followed by a build-up of salts in the unsaturated zone. Eventually this build-up of salts would be flushed to the watertable by intense rainfall events. This would result in a similar pattern as Figure 2-27c where an increase in Cl without fractionation of $\delta^{18}O$ is observed. However, this process does not account for groundwater discharge. Beyond the mountain front in the APY Lands, the groundwater system has an aspect ratio of greater than 1:100 and relatively shallow watertables (<10 m). Under this scenario it is entirely feasible that groundwater discharge occurs. We propose that the majority of this discharge occurs through transpiration as supported by the data.

## 2.7 Groundwater recharge

### 2.7.1 CHLORIDE MASS BALANCE

Chloride mass balance (CMB) methods have been used by a number of researchers in the past to provide a reasonable estimation of recharge rates (Eriksson and Khunakasem 1969, Scanlon 2000, and Scanlon et al. 2002). The groundwater recharge rate can be expressed as:

$$R = \frac{Cl_P P}{Cl_{GW}}$$

where $R$ = recharge, $Cl_P$ = Cl concentration in precipitation, $P$ = annual precipitation, $Cl_{GW}$ = Cl concentration in groundwater.

The CMB method is subjected to a number of assumptions including,

- Cl is conservative and is not added to the system from water rock interactions
- Cl is deposited in the groundwater by aerosal particles in precipitation
- Steady state conditions apply

Recent studies have concentrated on estimating recharge by this method (Leaney et al. 2013, Kretschmer and Wohling 2014). The Leaney et al. (2013) study was across the entire APY Lands, while Kretschmer and Wohling (2014) concentrated on the eastern APY (Fig. 2-23).

Leaney and co-workers in the GFLOWS Stage 1, used the Cl deposition maps expressed in kg/ha/year to determine the input concentrations of $Cl_p$ (2011). While, Kretschmer and Wohling used the value of Cl measured in rainfall from Alice Springs, $Cl_p$ equals 0.72 mg/L (Crosby et al. 2012). Both studies used a value of $P$ equal to 250 mm/year for rainfall. The GFLOWS Stage 1 estimated recharge rates that ranged from " < 0.1 mm/year to 29 mm/year, and from < 0.1 mm/year to 52 mm/year, for the fractured rock and Quaternary and Tertiary wells respectively, using the lower 95% prediction interval range" (Leaney et al. 2013). Leaney et al. and co-workers compared recharge rates determined from CMB to the multi valley flat bottom flatness index. This essentially defines the areas of higher elevation to the flat lying areas where today's drainage pattern can be clearly identified. For their study recharge in the fractured rock was generally >5 mm/year, while the adjacent valleys had rates of <2 mm/year.

Kretschmer and Wohling (2014) found similar results for point estimates of recharge rates but did not record the high values of Leaney and co-workers. In the Musgrave Ranges, recharge rates varied between 0.5 mm/year and 7.2 mm/year. Recharge to the plains averaged 0.5 mm/year but varied between 0.05 and 2 mm/year. Slightly higher recharge rates of ~0.5 mm/year occurred in the Everard Ranges. These results were volumetrically scaled up based on land type and geological type into a number of different zones that included elements of a regolith (near surface) mapping including sheet flow deposits, aeolian sediments, transported sediments as well as classes of highly and moderately weathered bedrock, to name the major divisions (Krapf et al. 2012). This scaled up to a value of 56,500 ML/year over the entire APY Lands while a recharge volume of 15,000 ML/year for their eastern APY Lands study site (Fig. 2-23).

In summary, recharge rates varied from <0.1 to 30 mm/year for both studies. However, for both studies the rates are generally low (<1 mm/year). Higher values of recharge are found in the Musgrave Mountain corresponding to fractured rock aquifers. These higher recharge rates support our hypothesis of two recharge mechanisms, with rapid recharge occurring through the fractured rock system and slower more diffuse recharge occurring to the porous media aquifer.

One of the limitations of the CMB approach is that there are no values of Cl concentrations in rainfall throughout the APY Lands. In particular future studies could establish rainfall stations both in the mountains and in the plains. In the following, recharge rates are re-examined using the above data as well as an additional data set from concentrations of Cl in rainfall taken from Melita Keywood's PhD thesis (Keywood 1995). This includes data from Alice Springs to the north as well as Wintanna station ~100 km to the south of Coober Pedy (Keywood 1995). The mean weighted Cl concentration for Alice Springs was calculated to be $Cl_p$ =0.62 mg/L while for Wintanna the mean weighted $Cl_p$ = 0.5 mg/L. Using these concentrations decreases the value of recharge relative to the estimates of Kretschmer and Wohling (2014). This illustrates that for more accurate results Cl concentrations in the field site would be desirable.

One of the main limitations of the above is that it assumes recharge occurs across the landscape and this ignores potential groundwater discharge. If discharge does indeed exist then previous estimates of recharge, based on CMB, may need to be re-evaluated. This may suggest local discharge occurs throughout this relatively shallow unconfined/fractured rock aquifer driven by local topographic flow.

### 2.7.2 AGE TRACERS

Environmental "age tracers" can, under ideal situations, provide information on recharge rates, groundwater velocity, groundwater age as well providing greater understanding of the flow systems (Solomon and Cook 1997, Cook et al. 2000, Love et al. 1993, 1994).

Previous studies in the Musgrave Ranges have estimated that recharge determined using $^{3}H$ and $^{36}Cl$ varies from 10 to 30 mm/year as a result of intense rainfall events (Creswell et al. 2002). In the same study, , it was estimated based on $^{14}C$ that all groundwater was <5000 years old. As well as this, it was suggested that rainfall in excess of 150 mm/year was required for recharge to occur (Cresswell et al. 2002). This study also showed large variability of recharge with higher values in the fractured rock aquifers in the mountains and lower rates in the adjacent sandy flats. This variability is consistent with this study and GFLOWS Stage 1 (Leaney et al. 2013).

In this study, we have estimated groundwater recharge by using the Vogel method (Vogel 1967). In his seminal work, Vogel described the analytical solution to the distribution of groundwater age in an ideal aquifer. The method of Vogel and variations of it have been used by many researchers in the past 30 years as documented in numerous texts (e.g. Cook and Bothke 2000 and Love et al. 1993).

Vogel used the distribution of groundwater ages from radiocarbon and $H^3$ data in an ideal aquifer to determine recharge rates. From the relationship between the "groundwater age" at a certain depth, one can determine the groundwater recharge rate. The Vogel model assumes constant distributed recharge, constant porosity and hydraulic conductivity, and a no-flow boundary at the upstream limit of the flow path, and an impermeable basement.

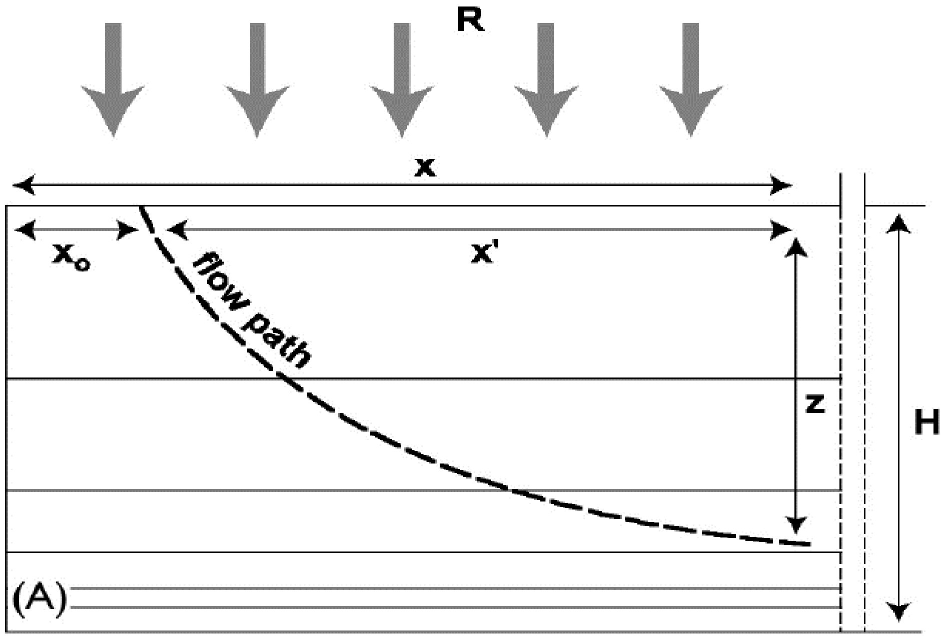


**Figure 2-28. Groundwater age distribution in an unconfined aquifer.**

If the recharge rate is constant across the top of the aquifer then the age isochrones will be horizontal, with age increasing with depth (Fig. 2-27).

The groundwater age can be determined from the folowing equation:

$$t = \frac{H\theta}{R} ln\left(\frac{H}{H-z}\right)$$

where *t* = groundwater age, *H* is the aquifer thickness, *ϑ* is the porosity and *z* is the depth of the sample. The bottom of the aquifer is considered to be an aquiclude. Rearanging the equation above the recharge rate can be determined by the following:

$$R = \frac{H\theta}{t} ln\left(\frac{H}{H-z}\right)$$

If the depth of the sampling interval (*z*) below the watertable is small relative to the thickness of the aquifer (*H*) then recharge can be approximated by the following:

$$\mathrm{R} = \frac{\mathrm{z\theta}}{\mathrm{t}}$$

It is widely accepted that short well screens and nested piezometer profiles (Cook and Herczeg 2000) deliver the most reliable environmental tracer analysis results to estimate groundwater recharge. However, unless specific nested piezometer networks are drilled this information is rarely available.

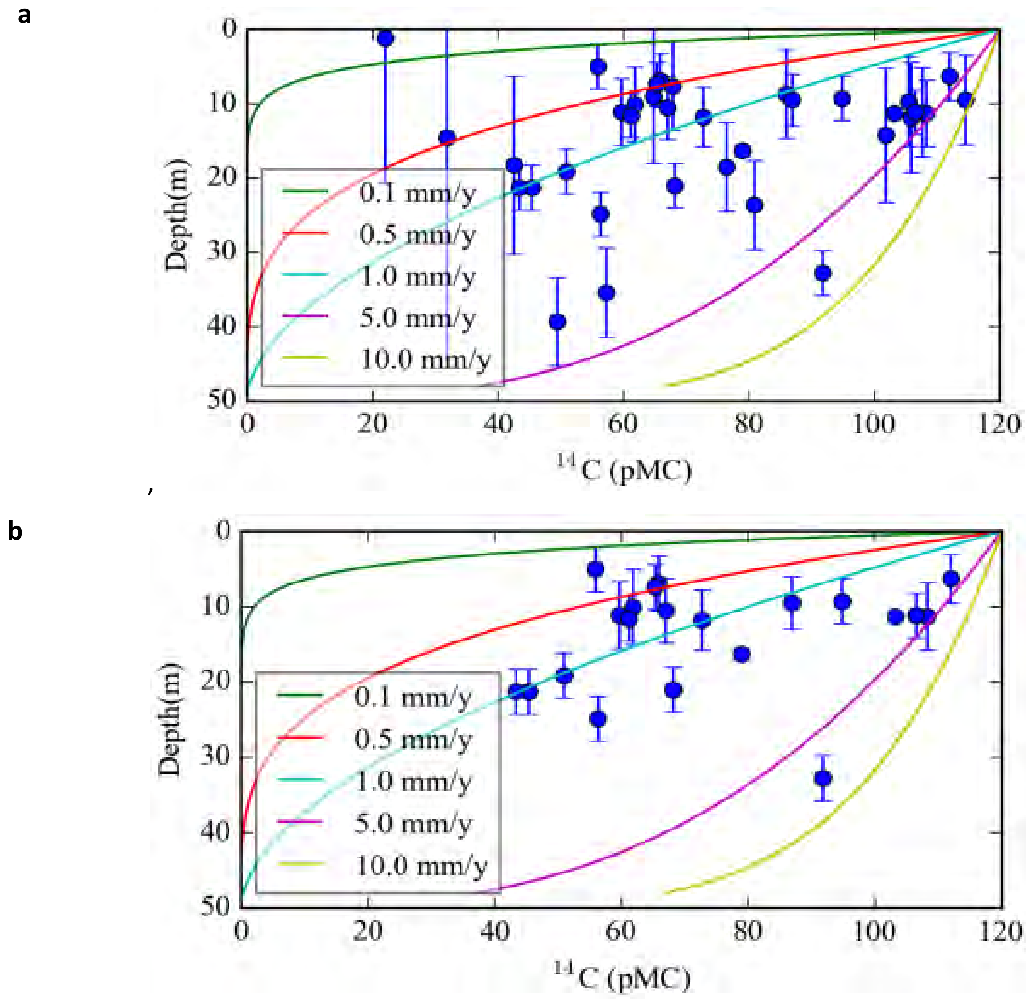


**Figure 2-29. Results from the Vogel model for $^{14}$C data across the study area with (a) all data; b) modified data set for short (<10 m) well screens.**

Results for $^{14}$C are displayed in Figure 2-29. The plot shows a wide range of recharge rates varying from <0.1 to 10 mm/year. In addition to the wide scatter of data, the long well screens suggest that mixing of groundwater of different ages may be sampled and so accurate recharge values maybe difficult to determine. The data set was then reduced to include only recently drilled wells so that the completion intervals were more likely to be competent thus reducing the potential for leakage around the casing. Furthermore, only wells with screens <10 m is displayed. The smaller the well screen, then the more accurate the recharge rates. This provides more reliable results with recharge rates having a smaller band around 0.5 to 5 mm/year. The major limitations to this approach are that we are assuming a simplified groundwater system and that $^{14}$C has not been corrected for any water-rock interactions. This means that we observe maximum groundwater ages but minimal recharge rates.

## 2.8 Numerical slice modelling

### 2.8.1 INTRODUCTION

Two numerical models were constructed in FEFLOW to understand groundwater flow and age distribution in two different directions including Northwest-Southeast (NW-SE) and North-South (N-

S) cross-sections. These cross-sections represent two primary flow directions identified in the study region.

Both models are fully saturated with the watertable as the model top boundary and have a uniform thicknerss of 100 m in thickness uniformly. We first fitted discrete watertable measurements with a cosine Fourier series to obtain complete watertable. The cosine Fourier series is given by:

$$W = C_0 + \sum_{m=1}^{N} C_m \cos\left(m\pi x / L\right)$$

where $W$ is the watertable elevation (m), $C_0$ is the base elevation (m), $L$ is the length (m), $x$ is the distance from the origin (m), $C_m$ is the coefficient, $N$ is the number of coefficients used. We found that when $N$ equals 35, fitting to the watertable in both cross-sections is reasonable.

Apart from the top boundary, all the other sides were specified with no-flow boundary conditions. As we do not know the exact boundaries for both cross-sections, the no-flow boundary conditions will affect groundwater flow. However, they are not expected to change the overall patterns of streamlines.

The models were performed in steady state for both groundwater flow and mean age simulations. Hydraulic conductivity and porosity were required for simulating the age. In this study, a hydraulic conductivity of 1.0 m/day and a porosity of 0.3 were used. Both parameters were not important for the flow simulation but are critical for the age simulation.

### 2.8.2 RESULTS

The modelling results show that independent cellular flow cells are developed in the NW-SE transect due to the undulation of the watertable (Fig. 2-30). This is in accordance with the seminal work of Joe Tóth (Tóth 1962, 1963). The results show nine individual flow cells and one larger intermediate or regional flow cell. The stream lines (or direction of groundwater flow) travel from areas of high hydraulic head to areas of lower hydraulic head. A number of groundwater flow reversals can also be observed. This is again consistent with the theory of regional gravitational flow (Tóth 1962, 1963, 2009), sometimes noted as Tóthian Flow in the literature. The most important aspect of this theory is that the watertable closely mimics the topography.

In comparison, much larger flow cells can be found in the N-S transect (Fig. 2-31). This is because the watertable is sloping without strong undulation. Trivial watertable undulation can still cause the development of local flow cells in the shallow part of the aquifer domain and affect the degree of the smoothness of streamlines.

Groundwater age is strongly affected by streamlines (Fig. 2-32 and 2-33). The groundwater age is usually much larger in valley bottoms than in hillslopes. As the watertable is generally inclined as well as undulated, groundwater discharge is also accompanied by groundwater recharge. This co-existence of both recharge and discharge result in sharp changes in the groundwater age underneath these regions. However, when a low-elevation area acts as a discharge zone only, the groundwater age can be found to increase gradually towards both directions.

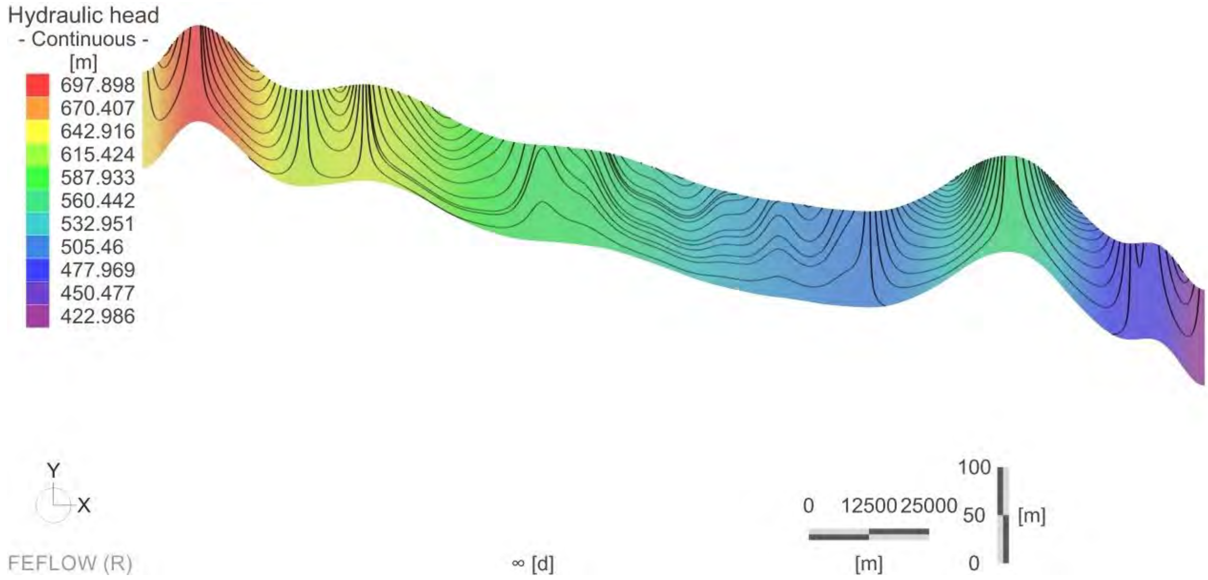


**Figure 2-30. Hydraulic head (graduated scale) and streamlines for the NW-SE transect.**

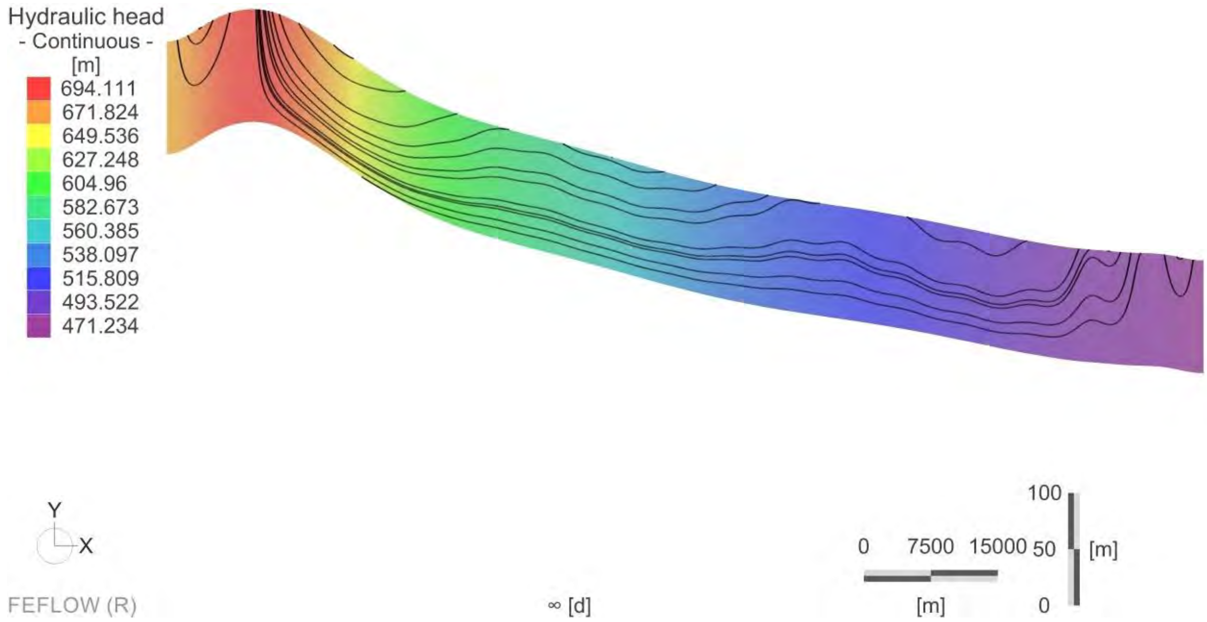


**Figure 2-31. Hydraulic head (graduated scale) and streamlines for the N-S transect.**

The purpose of the strip modelling is to obtain a greater conceptual understanding of the groundwater flow systems across the study area. The models are not designed to be used for any sustainability or pumping scenarios. The main features that can be observed are the presence of many local and, to a lesser extent, intermediate flow systems. These local and intermediate flow systems show characteristic groundwater flow reversals (Figs. 2-29, 2-30, 2-31, 32 and 2-33). It is interesting to note, that even for a relatively flat watertable (Fig. 2-31 and 2-33) with small undulations of the watertable surface, that local and intermediate flow systems can occur (Love et al. 2020).

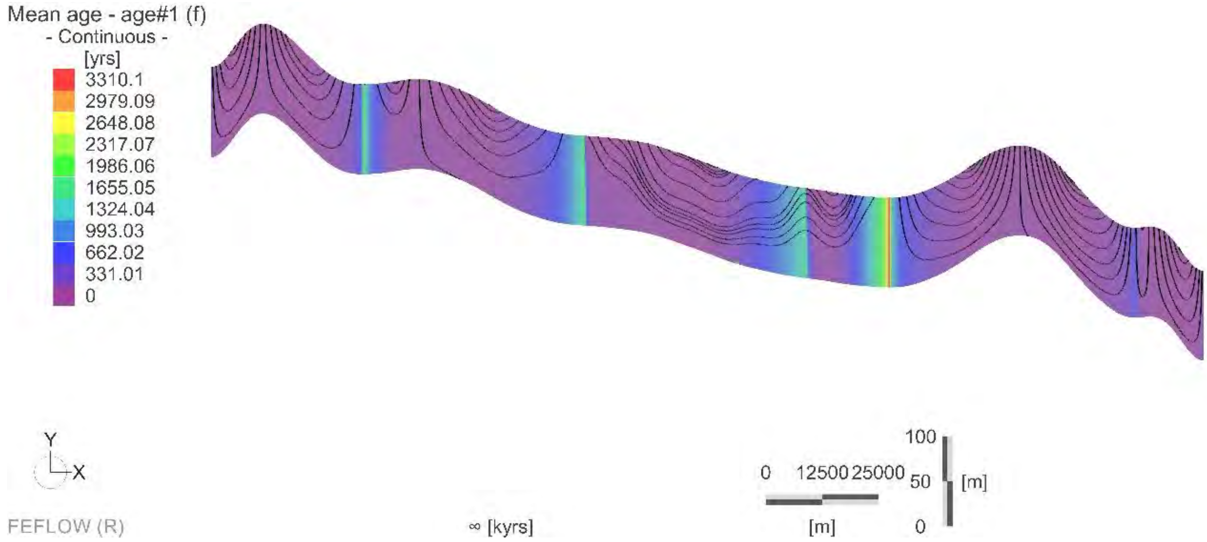


**Figure 2-32. Groundwater age and streamlines for the NW-SE transect. The hydraulic conductivity and porosity were given 1.0 m/day and 0.3 m/day respectively over the entire section for simplicity. It should be noted that the groundwater age is linearly proportional to the hydraulic conductivity and the porosity.**

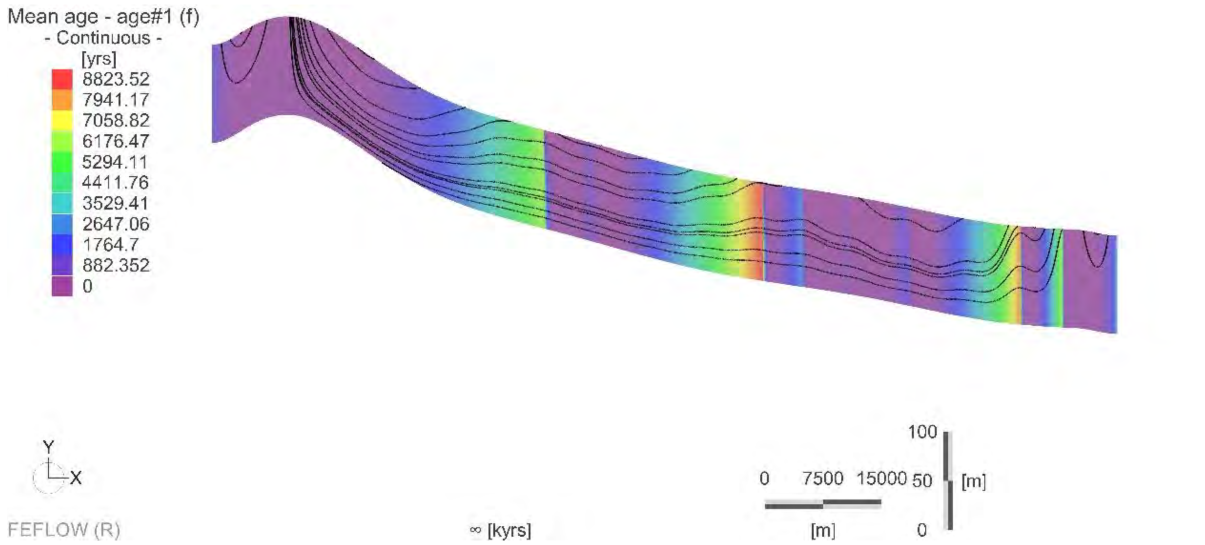


**Figure 2-33. Groundwater age and streamlines in the N-S transect. The hydraulic conductivity and porosity were given 1.0 m/day and 0.3 m/day respectively over the entire section for simplicity. It should be noted that the groundwater age is linearly proportional the hydraulic conductivity and the porosity.**

There is also one possible regional flow system that originates in a groundwater divide in the vicinity of Pukatja that extends south of Kaltjiti (Fregon) (Fig. 2-17). This follows the valley of Ernabella Creek which is dominated by coarse grain river sediments. Above this regional system we still observe both local and intermediate flow systems.

# 3 Hydrogeological control site, Lindsay East Palaeovalley

## 3.1 Geology of the Lindsay East Palaeovalley

### 3.1.1 CORING THE PALAEOVALLEY

The drilling program conducted during 2018 as a part of this project provided the opportunity to acquire a diamond drill core taken from the thickest part of the sedimentary infill of the Lindsay East Palaeovalley and, ideally, also including the top of the underlying basement. Notably, this core is one of a limited few drilled in sedimentary cover in the APY Lands and certainly the only core taken through the centre of a palaeovalley system. As discussed at length in Keppel et al. (2018), Costar et al. (2019) and Krapf et al. (2019), drillhole DH1a was designed for this purpose and thereby tested the AEM data and geophysical model of Munday et al. (2020).

Drill core was successfully retrieved from drillhole DH1a to a depth of 93.4 mBNS. This drillhole intersected three main sandy successions with the lower two separated by a thick interval of mud (Fig. 3-1). No core material could be recovered from below 93.4 mBNS depth due to continued core loss. Successive rotary mud drilling produced cuttings up to a depth of 117 mBNS with the palaeovalley fill and basement contact intersected at ~108 mBNS.

The contact between weathered basement and the overlying, also intensively weathered, palaeovalley fill sediments is not very distinctive in the drill cuttings, which is also reflected in the diffuse boundary seen in the AEM model (Munday et al. 2020). However, thorough inspection of the cuttings identified a noticeable change of quartz grain morphology with depth. Above ~108 m, quartz grains are mainly subangular to subrounded, indicating that the grains have experienced mechanical abrasion during sedimentary transport. Below ~108 mBNS, quartz grains display more angular to subangular morphologies and are interpreted to be *in situ* within the weathered basement (Krapf et al. 2019), likely granites of the Pitjantjatjara Supersuite (Pawley and Krapf 2016).

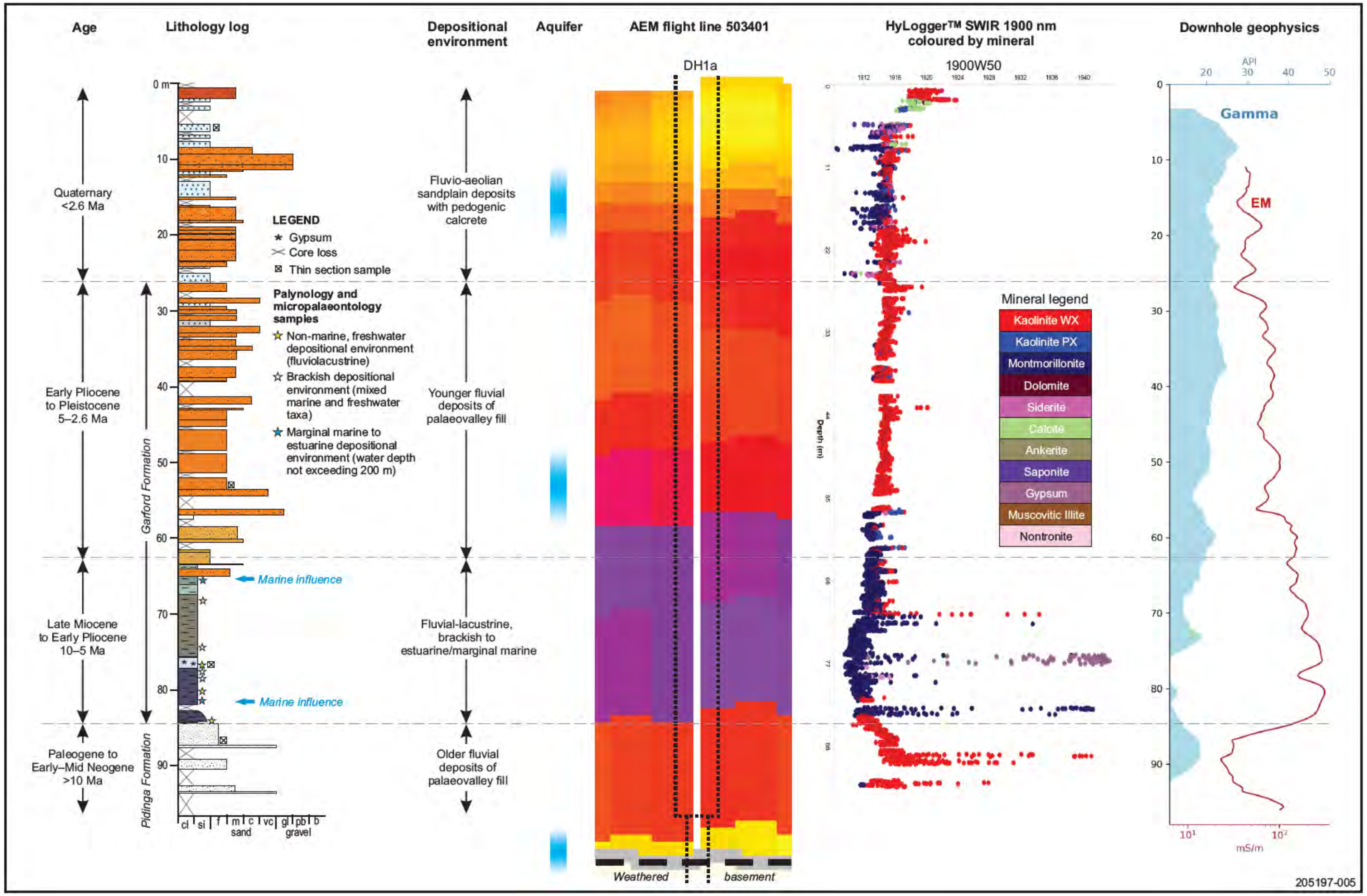


**Figure 3-1. Lithostratigraphic log of drill core DH1a, showing palynology sample points, depositional environment interpretation, AEM profile, HyLoggerTM spectral data, and downhole geophysics (from Krapf et al. 2019).**

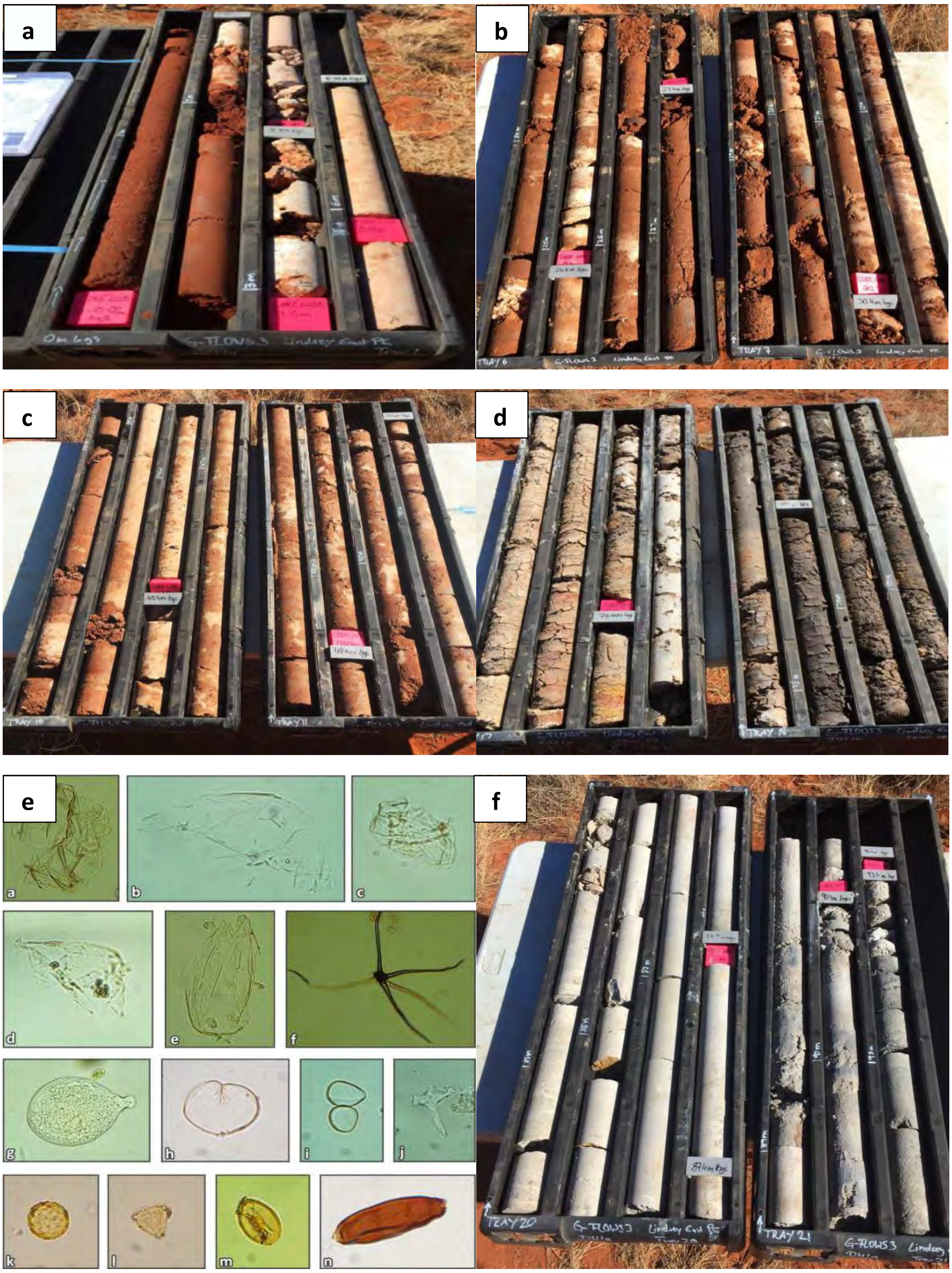

**Figure 3-2. DH1a Core (a) Fluvio-aeolian sandplain deposits with pedogenic calcrete at 0-6 mBNS:; (b) Transition between sandplain deposits and fluvial deposits of the upper palaeovalley fil at 24-32 mBNS l; (c) Fluvial deposits at 44-46 mBNS; (d) Lacustrine to brackish to marginal marine deposits with distinct 1 m thick gypsum horizon (white) at 70-78 mBNS; (e) Palynomorphs extracted from core sample (f) 85-94m: Older fluvial deposits of the palaeovalley at 70-78 mBNS.**

The basal part of the sedimentary palaeovalley fill is ~23 metres thick (85–108 mBNS). It is composed of highly weathered, semi-consolidated, poorly to moderately sorted, coarse-grained, quartz-rich, kaolinitic sandstones that grade upward into consolidated, massive, more mature, moderately to well sorted, fine-grained, quartz-rich sandstones (Fig 3-2f).

This sandstone succession is overlain by a ~20 metres thick succession of distinctive brown-black organic-, sulfidic- and clay-rich basal muds that are separated from olive-green muds higher up in the succession by a 1.25 m thick massive gypsum layer (Figs 3-2d and 3-4a). This mud-dominated interval (from 85 to 65 mBNS) corresponds to a prominent conductive zone in the AEM dataset (Munday et al. 2020, Keppel et al. 2020, Krapf et al. 2019). This zone represents a confining bed (Fig. 3-4b).

The mud interval is overlain by a second, ~38 m thick (65–27 mBNS) sandy succession characterised by partly massive, moderately sorted, fine- to coarse-grained, quartz-rich sands and sandstones, which in parts have intercalations of clay and gravel layers (Fig. 3-2a, 3-2b, 3-3a). The consolidation and cementation of these sandy deposits is highly variable, ranging from compact sandstones to free flowing unconsolidated sands. The depth interval 65 to 60 mBNS is composed of interbedded mud and coarse-grained sand, which shows no or only weak calcification. Higher up in the core, calcification increases within this sandy unit. The calcified part shows dissolution features resulting in cellular-like calcite veining patterns in parts of the core. Root casts are also common in the upper part of this unit. The transition into the overlying uppermost sandy succession is very gradational as its composition is similar to the underlying sandy unit. This is also reflected in the AEM data with no distinct conductivity variations visible within the combined upper sandy interval above the high conductivity mud unit.

From ~27 mBNS, distinctive up to 50 cm thick pedogenic calcrete horizons (Fig.3-2a, 3-3b) occur within semi-consolidated, moderately sorted, fine- to coarse-grained sands. Hyperspectral mineralogy data acquired via HyLoggerTM reflect this by a change in clay mineralogy from kaolinite in the upper sandy interval to montmorillonite in the overlying sandplain deposits (Fig.3-1).


**Figure 3-3. Hydrogeological Units (a) Major unconfined aquifer in the palaeovalley - fluvial deposits of massive, moderately sorted, fine- to coarse-grained, quartz-rich sandstones interbedded with gravel layers (52-56 mBNS); (b) Upper unconfined aquifer unit - red-brown sandplain deposits and white pedogenic calcrete at 0–7 mBNS.**

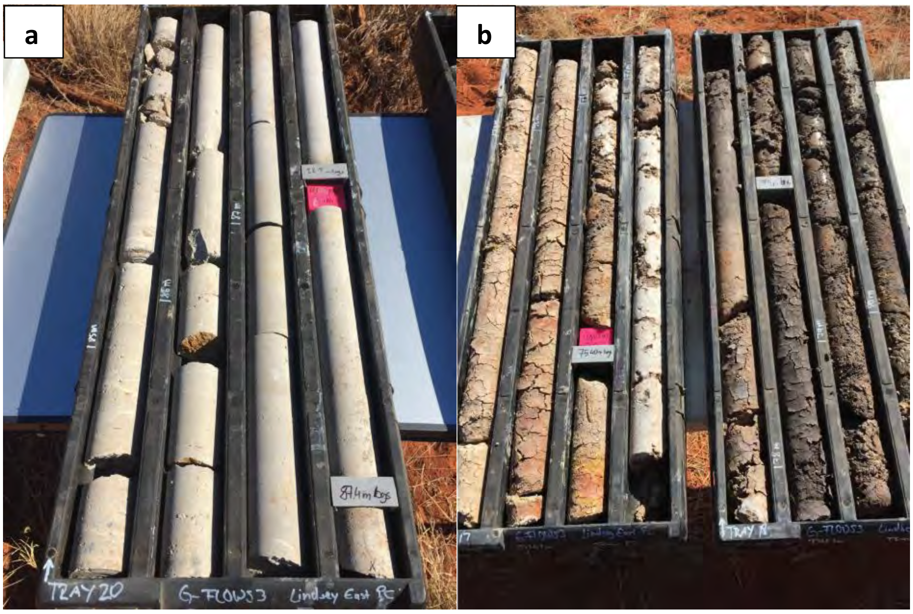


**Figure 3-4. Hydrogeological Units a) Confined aquifer - consolidated, massive, moderately to well sorted, fine-grained, quartz-rich, mature sandstones of the lower fluvial palaeovalley fill succession, 84.77–88.9 mBNS; b) Confining bed- lower brown-black muds (right), separated from upper olive-green-brown muds (left) by a 1.25 m thick white gypsum layer, 73.25–80.63 mBNS. This interval corresponds to the prominent conductive zone in the AEM dataset (Fig. 3-1).**

### 3.1.2 SEDIMENTOLOGY AND DEPOSITIONAL ENVIRONMENT

The quartz-dominated sands and sandstones of the palaeovalley fill overall are lacking sedimentary structures and have limited compositional and grain-size variation (no clasts greater than granule size). This can be attributed to the source material of the palaeovalley fill, which was dominated by felsic gneisses and granites that have been intensively weathered to kaolinitic saprolite with residual quartz grains. Quartz-rich sands that possess compositional and grain-size properties similar to the sediments within the palaeovalley also dominate channel sediments of modern creeks in the APY Lands, such as Officer Creek. Hence, the basal and upper sandstone units that compose the major part of the fill of the Lindsay East Palaeovalley in drillhole DH1a are both interpreted to be of fluvial origin (Krapf et al. 2019).

The clay-rich muds were likely deposited in a quiescent environment within the palaeovalley. The brown-black basal muds between 75 and 85 m depth is organic-rich and sulfidic, indicating that the depositional environment was anoxic and permanently covered with water during mud deposition. The development of a gypsum layer between the basal dark coloured and the overlying lighter coloured muds indicates that the palaeovalley became temporarily dry, before deposition returned to mainly subaqueous conditions in a more oxidising and ephemeral environment, comparable to the conditions in a playa lake.

The sand unit overlying the palaeovalley fill sediments is characterised by multiple up to 50 cm thick pedogenic calcrete horizons. These calcrete-bearing sandy sediments record the change from a fluvial-dominated environment during the filling of the palaeovalley to the formation of a semi-arid to arid sandplain landscape dominated by sheetwash and aeolian processes with only minor fluvial activity.

The sedimentary fill of the tributary channel intersected in drillhole S22i is overall compositionally less mature than that of the main palaeovalley fill in drillhole DH1a, reflecting the distality of the tributary within the palaeovalley system and its proximity to exposed basement, which outcrops just ~5 km upstream (i.e. NW) from drillhole S22i. The absence of lacustrine muds, as intersected in drillhole DH1a, also reflects the distality of this tributary channel to the main trunk of the Lindsay East

Palaeovalley and indicates that back-flooding of the main palaeovalley during the deposition of the thick mud layer did not extend upstream into this tributary.

### 3.1.3 GEOLOGICAL MODEL OF THE PALAEOVALLEY

The evolution of the palaeovalley system in the APY Lands, particularly the Lindsay East Palaeovalley located at hydrogeological control site DH1, is well documented in Krapf et al. (2019). Krapf et al. (2019) produced the following figures (Fig. 3-5 a-e) and used knowledge and information derived from the core at drillhole DH1a.

Drilling the full thickness of the Lindsay East Palaeovalley provided for the first-time evidence that the palaeovalley was incised up to 40 m into the underling weathered crystalline bedrock (Fig. 3-5a). A combination of data captured by DH1a and the AEM dataset, enabled extension of the findings beyond the control site, which suggest that this incision depth may also apply to other palaeovalleys in the wider Musgrave Province region.

The time of incision and hence the formation of the palaeovalleys in South Australia, including the Musgrave region, is debated. Hou et al. (2008) consider that the formation of the majority of the Eucla Basin palaeovalleys happened in the Mesozoic as their lower reaches contain sediments of the Early Cretaceous Madura Formation.

Infilling of the palaeovalley began with the deposition of a sandy fluvial succession (Fig. 3-5a and 3-5b). The identification of two marginal marine to estuarine intervals within the mud unit of drill core DH1a based on palynological constraints (Krapf et al. 2019) suggests that the Lindsay East Palaeovalley periodically experienced marine influences with the sea transgressing far inland beyond the coastal margin and wetlands areas of the Eucla Basin (Fig. 3-5b). The combined effects of a warm and humid climate and a rising sea level accompanied by subsidence and orogenic movements during the Late Miocene (Hou et al. 2008) can explain the presence of marginal marine deposits in the Lindsay East Palaeovalley at the foothills of the Musgrave Ranges more than 300 km NNE of the palaeocoastline.

The base of the mud-rich interval intersected in drill core DH1a records a first marine incursion, where the deeply incised valleys became flooded to form a large inland estuary system. The marine influence gradually faded and a brackish to freshwater lake occupied the valley floor or parts of it as indicated in the palynology from marine to brackish to freshwater taxa. The organic-rich and sulfidic black muds are indicative of a depositional environment that was anoxic and permanently covered with water. Evaporation caused the temporary drying out of this waterbody leading to the deposition of a gypsum layer (Fig. 3-5c). After this evaporation event, conditions returned to mainly subaqueous deposition in a more oxidising and ephemeral lacustrine environment, comparable to the conditions in a playa lake. However, palynology indicates brackish conditions for this upper part of the mud succession and near the top the palynomorphs assemblage documents a second marine incursion.

After the mud-dominated subaqueous deposition phase in the Late Miocene to Early Pliocene, the interior of the palaeovalley changed back to a dominantly fluvial environment leading to the successive infill of the palaeovalley with quartz-rich sands containing minor clay and gravel intercalations (Fig. 3-5d). This final infill phase may be related to wetter conditions in the catchment area and thus increased water and sediment inflow into the palaeovalley.

Deposition continued after infilling of the palaeovalley. However, with increasing aridity the depositional environment gradually switched from fluvial-dominated to sheetwash- and aeolian-dominated leading to the formation of extensive sheet-like sandplain deposits. These sediments were locally indurated by carbonate or silica forming calcrete and chalcedonic silcrete horizons within them (Fig. 3-5e).

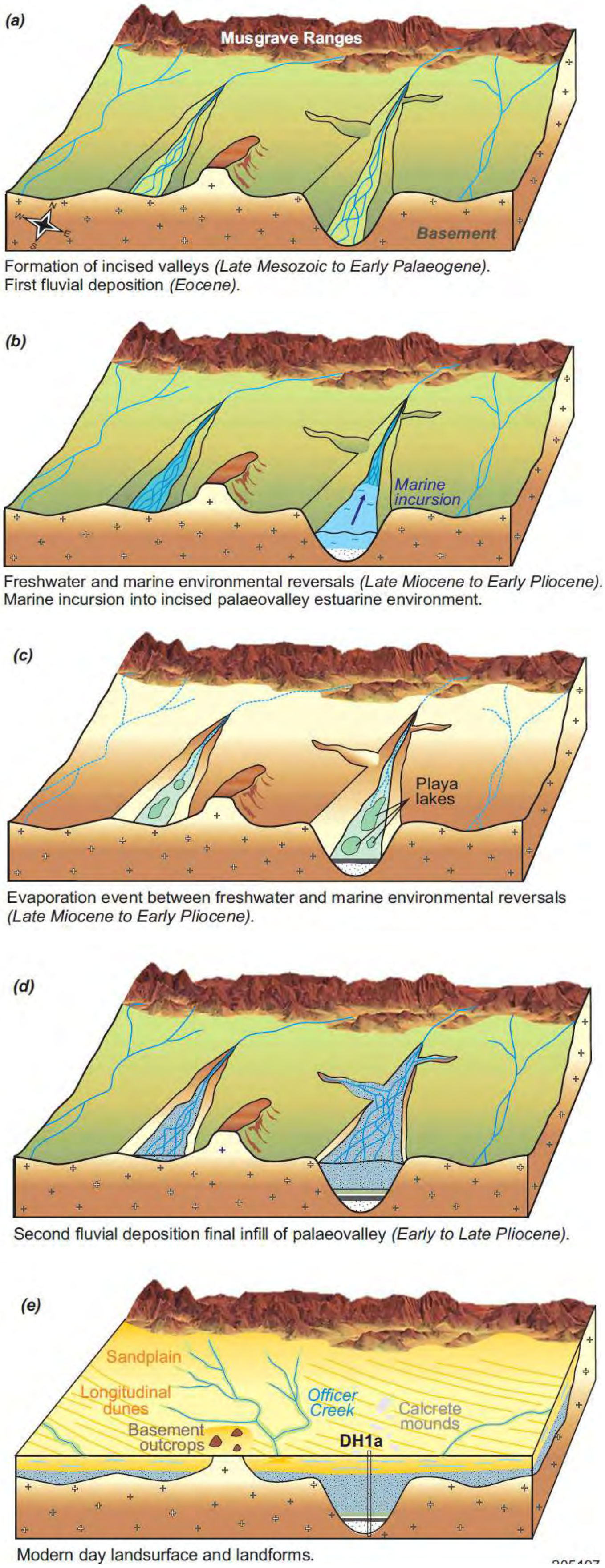


**Figure 3-5. Geological evolution model of the Lindsay East Palaeovalley (reproduced from Krapf et al. 2019).**

The modern day landscape is characterised by extensive sandplains and dunefields with minor creeks. Pedogenic calcretes and chalcedonic silcretes, which have widely formed within the sandplain deposits, are frequently cropping out as resistant mounds in low-lying areas (Fig. 3-5e).

### 3.1.4 HYDROGEOLOGICAL UNITS

Identification of the major hydrogeological units is well documented in Costar et al. (2019). Whilst specific groundwater quality assessments are required before it can be used for any specific purpose, they are dependent on the desired use of the water source. Salinity is a useful and preliminary water quality indicator that can be used to determine the potential for groundwater use. The well yield is also an important factor when considering the significance of a groundwater source.

The hydrogeological control site DH1 is located ~5 km southeast from Kaltjiti, centred on the Lindsay East Palaeovalley. This was the first time that deep palaeovalley sediments have been used as water targets and drilled to investigate their potential as a suitable groundwater resource in the APY Lands. The sediments within the Lindsay East Palaeovalley can be divided broadly into four major units based on their hydrogeological characteristics:

- **Units 1a and 1b: Unconfined aquifer** (well DH1e, unit no. 5344-83). This unit encompasses the dune and underlying sandplain system (~30 m thick) beneath which lies the hydraulically connected fluvial palaeovalley fill sand deposit with an estimated thickness of 35 m (Krapf et al. 2019). Groundwater is encountered at ~8 mBNS. Salinities in the top 30 m are ~1,000–1,500 mg/L and yields are estimated to be <1 L/s. However, for the target-water-bearing palaeovalley zone (55–65 m deep), salinities are lower (~870 mg/L), with much higher yields of 10–18 L/s (wells DH1b, DH1c, DH1d; unit no. 5344-89, 5344-80, 5344-82). Transmissivity values are ~120 m/day (Costar et al. 2020). Hydraulic parameters were estimated by conducting step drawdown tests and a constant rate discharge test (12-hour continuous pumping).
- **Unit 2: Confining bed.** This unit consists of a 20 m thick sequence of mud (silty clay).
- **Unit 3: Confined aquifer.** This unit represents the basal palaeovalley fill sediments (wells DH1a, DH1a2, unit no 5344-87, 5344-78; note DH1a has no screen interval and was replaced by DH1a2) consisting of sand but with a slightly higher salinity range (1,200 mg/L). Yields are <2 L/s which is much less than that of the target-water-bearing palaeovalley zone. Thickness is ~10–15 m, grading into a weathered basement sequence at the bottom (which overlies fractured rock and a consolidated fresh basement).
- **Unit 4a: Weathered basement** (well DH1f, unit no. 5344-85). This unit is located ~700 m to the west of the centre of the palaeovalley. Yields are extremely low (<1 L/s) with salinities of ~1,000 mg/L. **Fresh basement forms Unit 4b** but this has not been intersected in the drilling.

**Table 1. Summary of groundwater parameters for the palaeovalley sediments**

| Unit | Aquifer characteristics | Depth (m) | Salinity (mg/L) | Yield (L/s) | Hydraulic conductivity (m/day) | DTW (m) | Lithological description |
|---|---|---|---|---|---|---|---|
| 1 | Unconfined | 8–55 | 1,000–1,500 | <1 | NA | 7.7 | Sandplain system |
| 1b | Unconfined | 55–65 | 870 | 10–18 | 50 | 7.6 | Main water-bearing zone within the palaeovalley sediments<br>(i.e. target-water-bearing palaeovalley zone) |
| 2 | Confining bed | 65–85 | NA | NA | NA | NA | Silty clay (mud) |
| 3 | Confined | 85–108 | 1,200 | <2 | NA | 8 | Basal palaeovalley sediments |
| 4a | Weathered basement | 108–117+ | 1,000 | <1 | NA | 8 | Weathered rock (saprolite) |
| 4b | Fresh basement | >117 | NA | NA | NA | Na | Fresh rock with possible fractures |

NA – not available

Encountering a groundwater resource with well yields of 10 L/s (at a minimum) and salinities of <1,000 mg/L is a significant find. This water is suitable for many purposes including community water supply and possible economic development, such as stock watering and irrigation.

According to recent aquifer tests, the target-water-bearing palaeovalley zone is capable of yields up to 18 L/s, but a more conservative yield of 10 L/s ensures a long-term sustainable supply (Costar et al. (in press)). This rate equates to a volume of ~1 ML per day.

The AEM conductivity depth slice at 40–50 mBNS provides a spatial conductivity distribution across the entire survey footprint (Fig. 3-6). Conductivity depth slices of the AEM data at regular intervals is a typical output from processed AEM data; however, data can also be represented as a conductivity depth profile (Fig. 3-6) which can aid in defining the basic geometric architecture of the palaeovalley. Figure 3-7 illustrates an interpreted geometry of the palaeovalley fill sediments (blue) over the underlining fractured bedrock basement (grey) across site DH1 in the centre of the Lindsay East Palaeovalley (wells DH1a, 1a2, b, c, d and with wells DH1f and DH1g (unit no. 5344-86) located outside the palaeovalley extent. Figure 3-7 has also been annotated with relevant groundwater information from the recent drilling program.

This is a small but crucial step in characterising the groundwater in this area and the first step in verifying AEM data.

From these early findings it is evident how data acquired at the hydrogeological control site (DH1) can be used to verify the AEM data. Whilst drilling provides real observations of the subsurface as a point data source, the validated AEM data can be very useful in upscaling point source groundwater and lithological data to a regional scale (i.e. the entire footprint of the AEM survey) and provide a useful tool for targeting water-bearing zones across the region where AEM data exists.

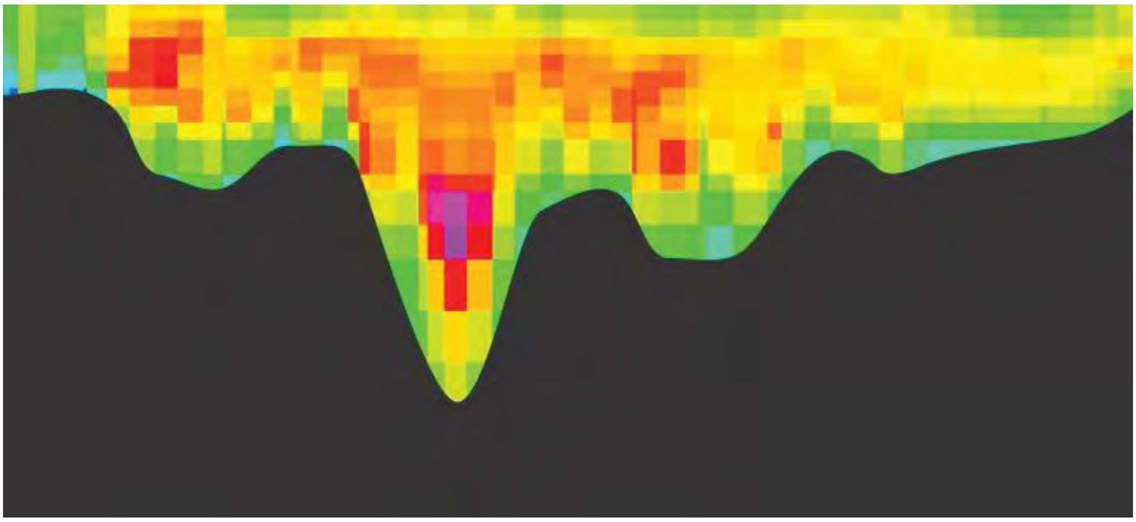

Figure 3-6. Conductivity depth profile derived from the AEM dataset across hydrogeological control site DH1.

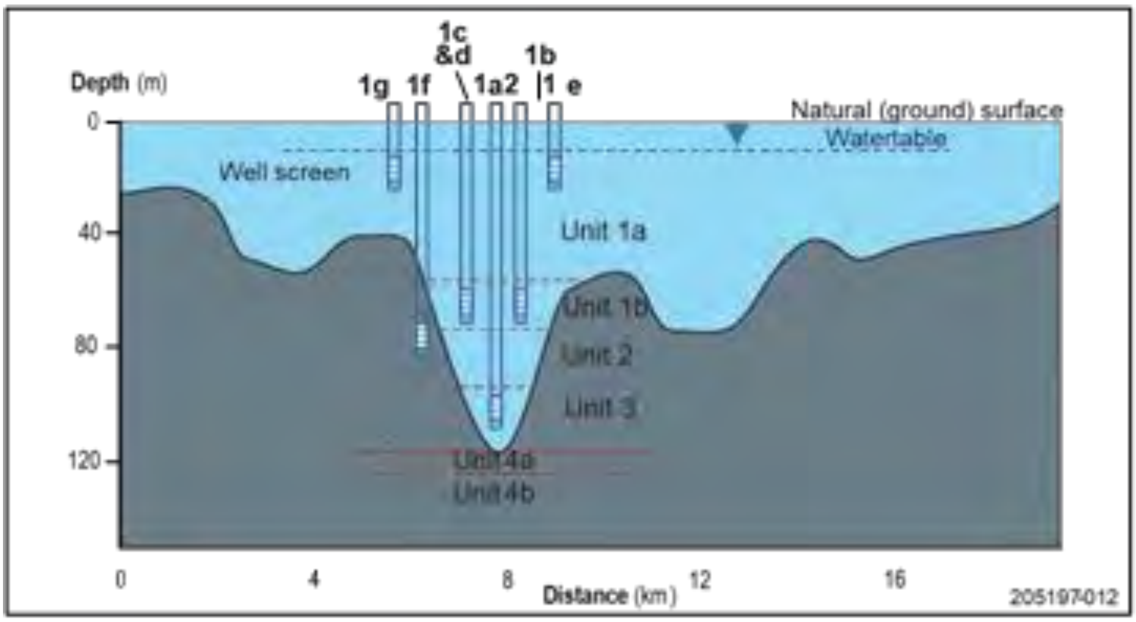


Figure 3-7. Basic schematic across hydrogeological control site DH1 showing well locations and indicative screen depths.

### 3.1.5 AQUIFER TEST

Aquifer (or pumping) tests were conducted at site DH1 to determine hydraulic parameters and to provide some preliminary estimates of long term pumping sustainability (Costar et al. 2020). These tests consisted of step tests on two wells (DH1b and DH1d) with one site (DH1d) coupled by a constant rate discharge (CRD) test of 12 hours continuous pumping. Step tests were used to calculate the indicative long-term pumping rate for the CRD test, stress the pumping rate of the sequence and to provide some preliminary aquifer parameters. The CRD test (while short) provided longer term pumping rates and more surety on hydraulic parameters. During the CRD test neighbouring wells DH1b, 1c, 1e, 1f and 1g were used as observation wells. The observed drawdowns for each well is shown in Figure 3-8.

DH1d was completed between 55 to 65 m (thought to be the more productive zone during drilling) in the centre of the Lindsay East Palaeovalley. The CRD test performed on this well used a pumping rate of 10L/s coupled with 12 hours of continuous pumping followed by recovery. Large drawdown occurred for early time indicating a large component of well loss, then the drawdown rate slowed until a final drawdown of 17.5 m was recorded at the end of pumping (700 minutes). Full recovery occurred after only 100 minutes. No hydraulic boundary conditions were observed during the test.

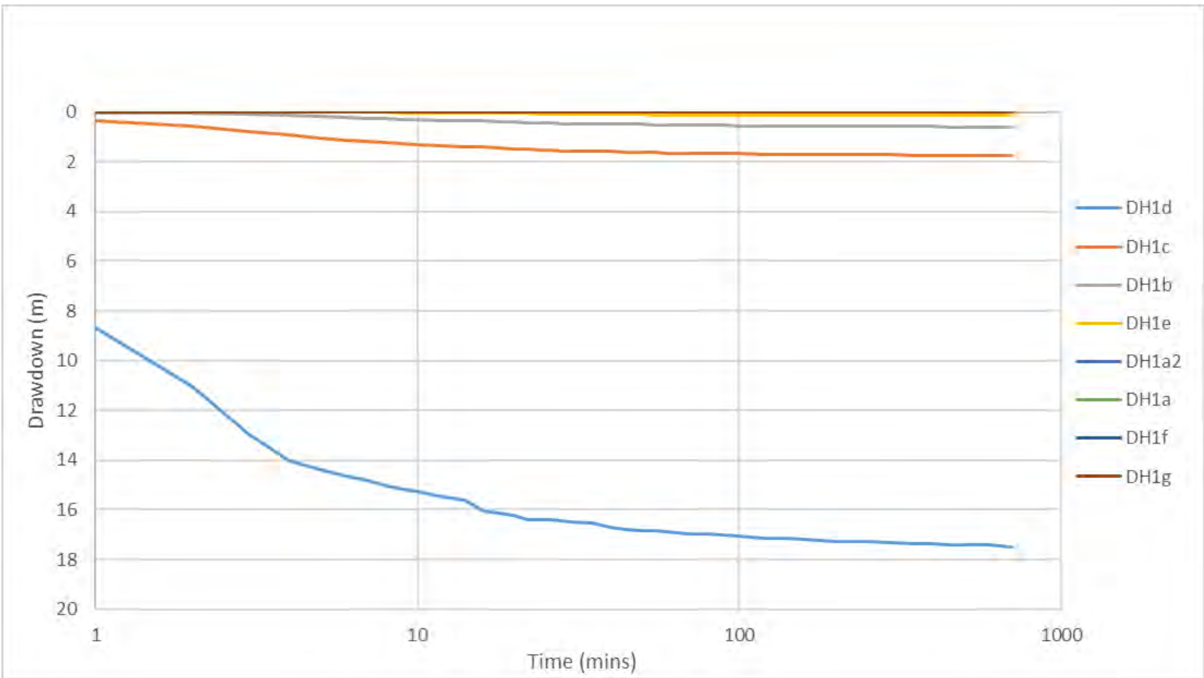


**Figure 3-8. Drawdown shown for pumping well (DH1d) and observation wells during the pumping phase of the CRD test.**

A drawdown plot as a function of time on a semi-log axis (Fig. 3-9) shows a slight deviation below the typical theis curve. This may indicate one of two mechanisms: (a) leakage from above; or (b) delayed yield. To determine what the dominant process is a longer-term pumping phase is required. A longer pumping phase duration is required to assess any boundary affects that may impact of long term-well sustainability. As there is no obvious confining bed above the main water bearing zone (unit 1b) we favour the response of an unconfined aquifer with delayed yield, however future work, as well as additional aquifer testing, would need to examine the nature of the indurated (consolidated) sandstone between 30-50 mBNS as wells as any clay horizons. As detailed in the following sections the distribution of tracers collected in the palaeovalley favour that of an unconfined aquifer. Future coring and aquifer testing should evaluate the hydraulic parameters of this zone with more rigorous testing since results here are preliminary at best.

In consideration of above , and whilst theoretical, interpretation undertaken using the Eden and Hazel[2] (1973) method which calculates drawdown as a function of extraction rate and duration (Kruseman and de Ridder 1994) determined that the well could be pumped at a rate of 10 L/sec continuously for 2 years with a resultant drawdown of approximately 20 m. If the pumping rate was increased to 15 L/sec, the predicted drawdown would be 33 m. Given well DH1d has an available drawdown

[2] The Eden Hazel method is a variant of the Jacob (1947) and Rorabaugh (1953) solutions.

calculated to be 43 m, these pumping durations and rates are theoretically possible unless hydraulic boundaries are encountered beyond the tested 12 hours of pumping.

In a practical sense, wells would not be pumped continuously for two years so the resulted drawdowns calculated here would represent maximum drawdowns. One of the largest unknowns in this kind of calculation is that we do not know what boundary conditions may or may not occur at long pumping times. Nevertheless, these results are extremely promising, for not only does this well have a large sustainable pumping rate, but its water quality (salinity) is potable with a value of 870 mg/L. Future work should include additional drilling and longer-term pump testing as well as development of a numerical model to further assess the long-term sustainable pumping and viability of the resource.

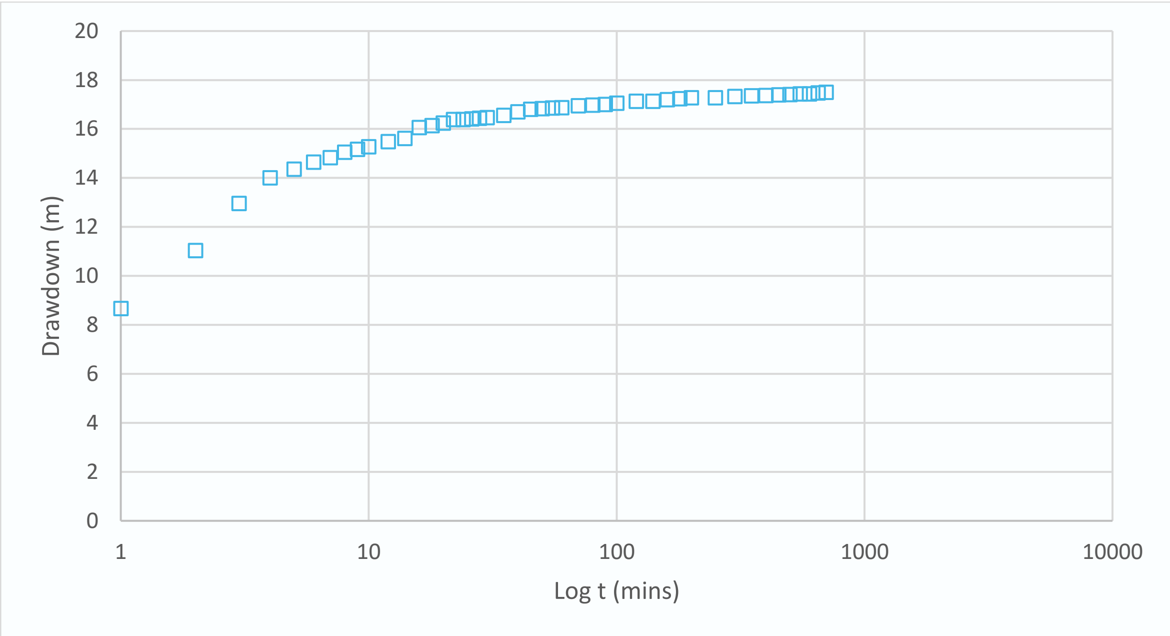


**Figure 3-9. Specialised plot (semi-log axis) of drawdown as a function of log time (Log t) for pumping well (DH1d) during the pumping phase of the CRD test.**

### 3.1.6 AIR PERMEABILITY OF THE CORE

#### Introduction

The TinyPerm® was used to measure permeability in the core. The instrument directly measures air permeability and once the air permeability is correlated with hydraulic conductivities of the core, the TinyPerm® provides hydraulic details of the core log at very high space resolutions. It has advantages of quick measurement for batch samples with small disturbance of the samples. Therefore, the method offers a very handy upscaling tool for hydrogeological investigations.

#### Methodology

The air permeability ($k_a$) was determined in two directions of the core. When the rubber nozzle is pressed to the surface of the cross-section of the core, the vertical permeability ($k_v$) is measured; when it is pressed to the side walls of the core, the horizontal permeability ($k_h$) is measured. The procedures of how to use the TinyPerm® is shown in Appendix A. Figures 3-10 and 3-11 show the setup for $k_v$ and $k_h$ measurements of the core.

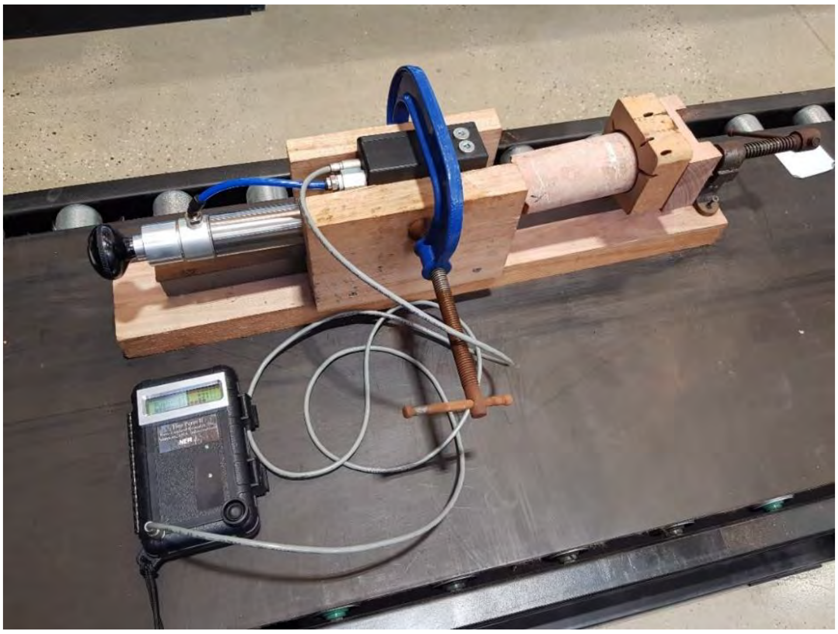

Figure 3-10. TinyPerm® setup for measuring $k_v$ of the core sample.

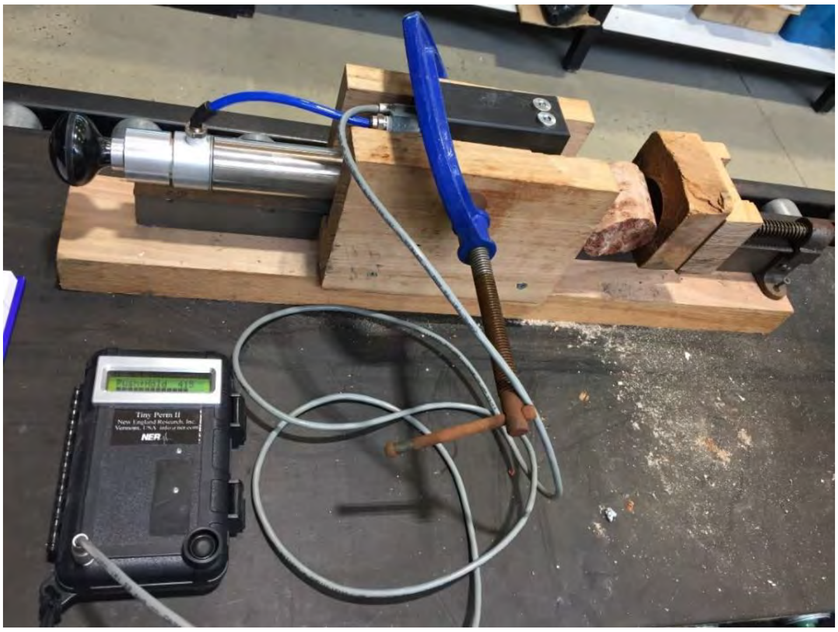

Figure 3-11. TinyPerm® setup for measuring $k_h$ of the core sample.

When performing measurements, an airtight connection between the instrument and core is most important. In order to achieve this, an application of 0.5-1 cm (thickness) of putty surrounding the nozzle tip of the instrument and surface of the core with pressure was employed to keep an airtight connection. Issues did arise since the putty does not stick to the core; in parts a friable surface. Therefore, plastic wrap was applied around the putty and the core (Fig. 3-12).

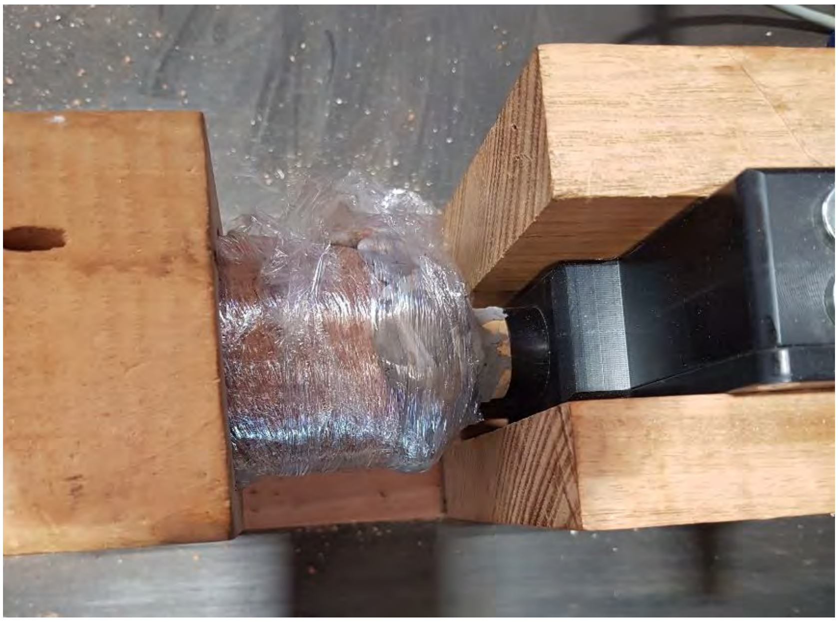

Figure 3-12. Airtight preparation of the core sample.

Small fragments of the friable core proved to be another issue for the inlet nozzle allowing these to be consumed by the instrument and influence the measurement. To prevent this occurrence, a filter (0.45 µm) paper was placed between the nozzle and the core surface. However, no difference between measurements with and without a filter were noted.

In order to limit cutting of core repeatedly, the cored piece chosen was relatively flat or a gentle scratch to the area was applied. Again, no difference between a trimmed surface or a rough surface was found in the measurements as the seal was maintained.

Each cored sample was measured twice. If small variations in the two measurements were recorded, the measurement was repeated as a leak of the seal was suspected.

### Results

The air permeability in $k_a$ (m/day) is shown in Figure 3-13. The methodology of this technique is discussed in Appendix A. Raw data is shown in the Appendix B.

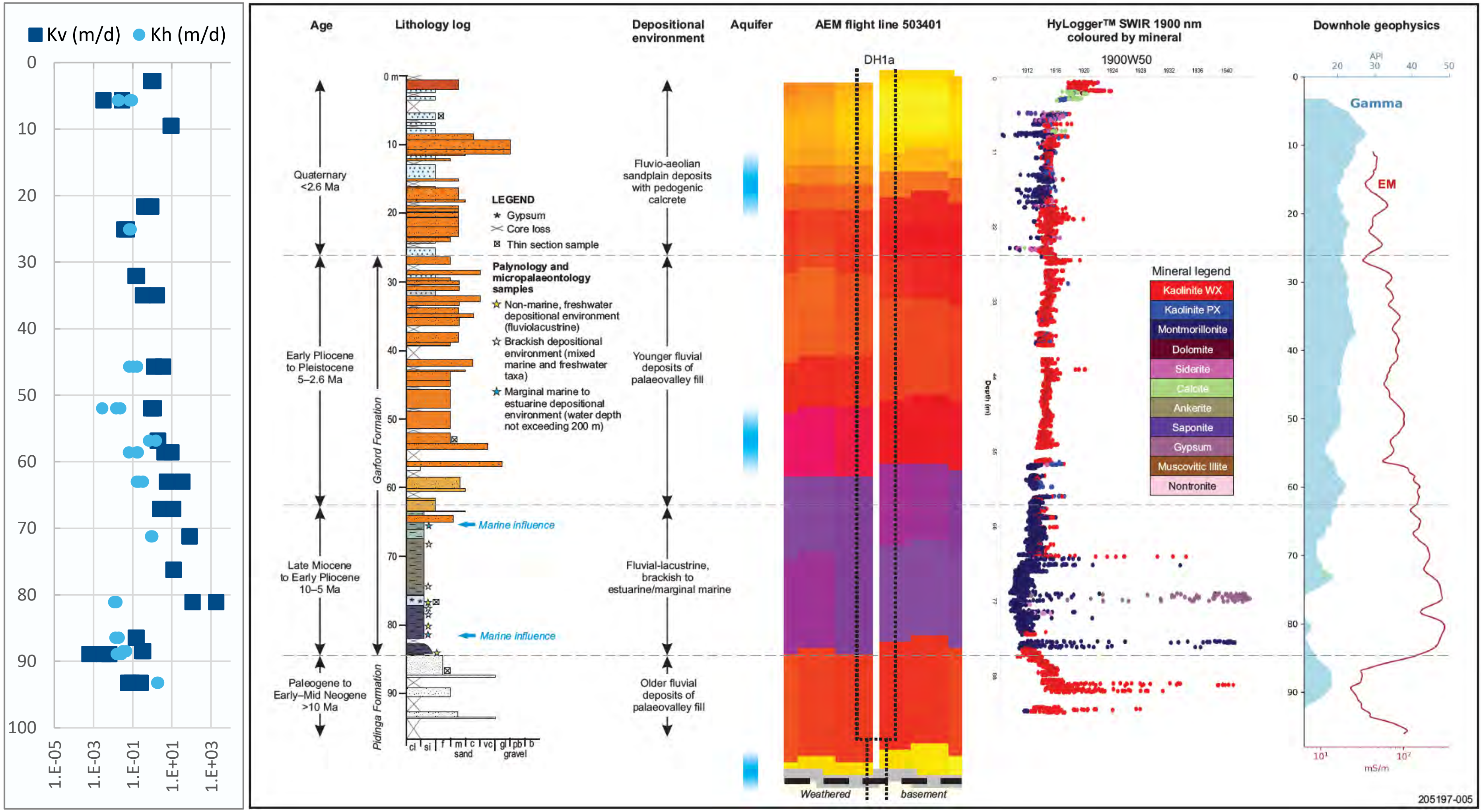


**Figure 3-13. Measured air permeability for DH1a core (left); aligned lithology, mineralogy spectral scan (HyLogger) and downhole geophysics (right).**

### Discussion

Both $k_v$ and $k_h$ reveal the more conductive aquifer (fluvial deposits) at depth 10 mBNS, between 60-80 mBNS and 90 mBNS which match with the results of the lithology study (Fig. 3-13). However, $k_v$ seems to be 1-2 magnitudes higher than $k_h$, which is opposite to the expectation. This is likely due to the incorrect treatment of samples for $k_h$ measurement. Since the side wall of the core was smooth, and not cut flat (in order to conserve core) the nozzle was directly pressed the surface of the core for the measurement. Measurements were attempted on several different locations of the side wall. All $k_h$ measurements yielded much lower results than $k_v$ which may mean that the variability could not be explained for the lower value of $k_h$ than $k_v$. $k_v$ is measured on a cross section which is exposed to fresh surface. $k_h$ however, is measured on the side of the soil core, which may be squashed during the drilling, thus yielding a much smaller measured value. Therefore, on this basis it is considered that $k_v$ is more reliable measurement and $k_h$ may need to be scaled.

## 3.2 Lindsay East Palaeovalley architecture

The acquired, processed and interpolated AEM datasets (Munday et al. 2020) are an important tool in determining the architecture of the substructure; is this case the Lindsay East Palaeovalley. Figures 3-15, 3-16 and 3-17 show AEM (SkyTEM) depth slices of conductivity variability across the wider hydrogeological control site DH1 at 10-20, 50-60 and 80-90 mBNS. These depths were chosen as they represent average values of conductivity over that interval as well as the covering the major water bearing units of the upper unconfined aquifer, deep unconfined aquifer and confined aquifer respectively.

The palaeovalley drainage system (which includes the Lindsay East Palaeovalley) hidden from the surface can be mapped. It was this data that was used to map the palaeovalley extent (main Lindsay East Palaeovalley and eastern and western palaeovalley tributaries) by Krapf et al. (2020) and is shown as an overlay on Figures 3-14, 3-15 and 3-16.

The AEM depth slice (10-20 mBNS) is spatially the most conductive zone (red) and the boundary of this zone approximately coincides with the palaeovalley outline. More resistive (blue) rocks occur outside of this zone. The 50-60 mBNS AEM depth slice represents the average conductivity for this depth. Areas in red denote high conductivity zones. These are interpreted to represent the major sand/sandstone unit in the palaeovalley. The confined aquifer slice from 80-90 mBNS shows a pattern of decreasing conductivity with depth. The deep conductive sand zone can also be observed having the largest values of conductivity representing the palaeovalley thawleg, i.e. the deepest part of the palaeovalley. High conductivity zones occur at 75 km along the main transect as well as at the 7.5 km point along the western tributary where palaeovalley sediments become thicker. These represent zones of high potential for good yielding aquifers.

The values of the intermediatory conductivity can be observed in yellows and greens, while the light to dark blue represent the more resistive zones. Dramatic changes in conductivity indicate a change in lithology. These changes are often related to a shallower depth of the basement as can be observed along the profiles (Fig. 3-18). Furthermore, these changes correspond to the orientation of the east–west structures. These zones may represent faults, shear zones or similar geological features that cause a change in the hydraulic properties of the rock that may either enhance or reduce groundwater recharge.

The boundary between the more resistive basement rocks and the palaeovalley sediments may represent major zones of recharge to the palaeovalley (this is discussed below). A good example of this is the northern boundary of the palaeovalley and the fractured rocks near Umuwa.

Note the above discussion refers to groundwater resource potential, however, more drilling is required to obtain a greater understanding of the system (Chapter 4).

Figures 3-17a, 3-17b and 3-17c show an elevation cross-section along these transects. The upper boundary represents the watertable which was determined to be on average 10 metres below the topography (i.e. DEM minus 10 m). As discussed in the previous section, the lower boundary was chosen to be at the value of conductivity at 50 mS/m. The difference between these cross-section profiles represent the thickness of the porous media aquifer.

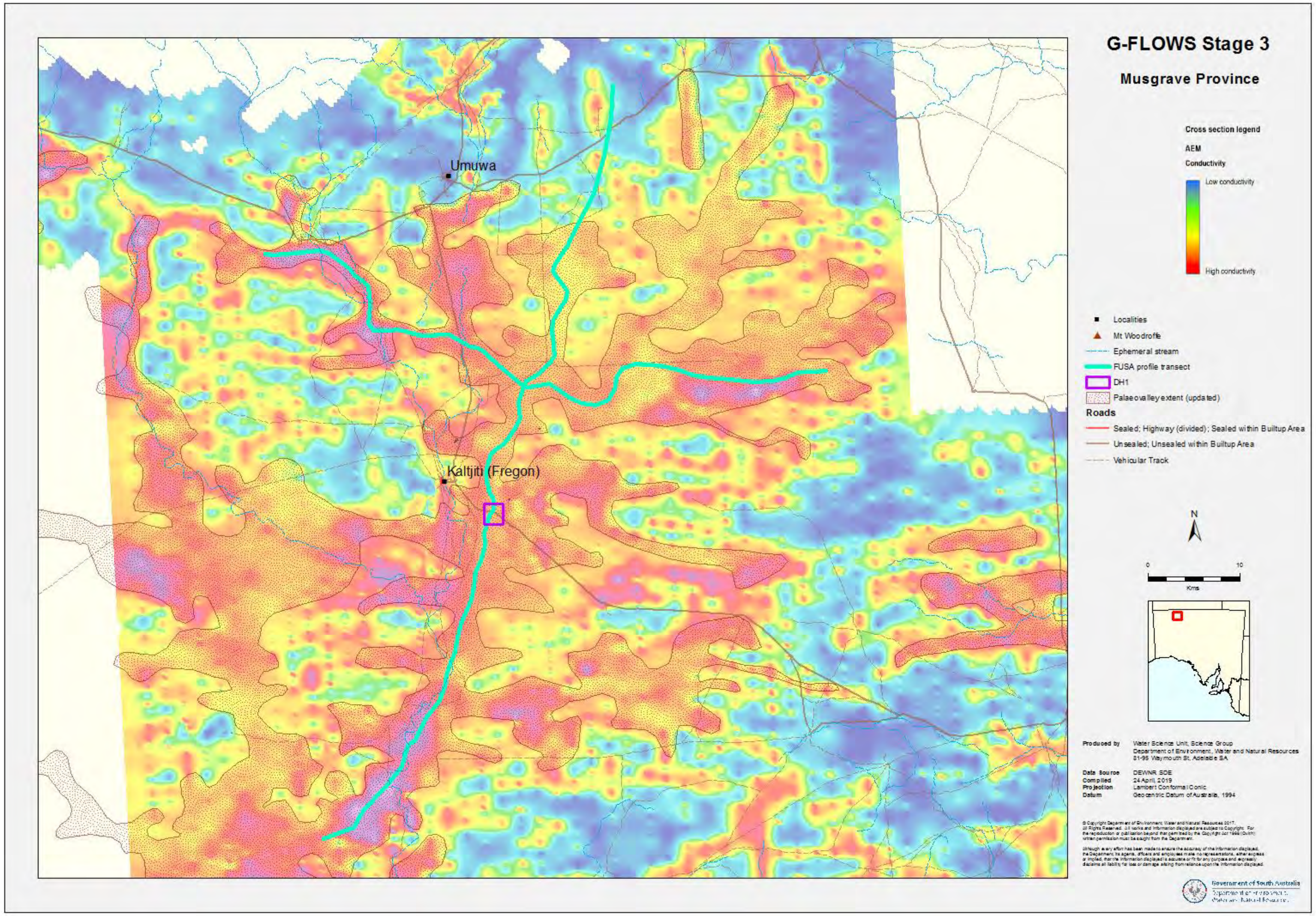


**Figure 3-14. AEM depth slice 10-20 mBNS (SkyTEM data) showing conductivity (red) and resistive (blue) variations over hydrogeological control site DH1.**

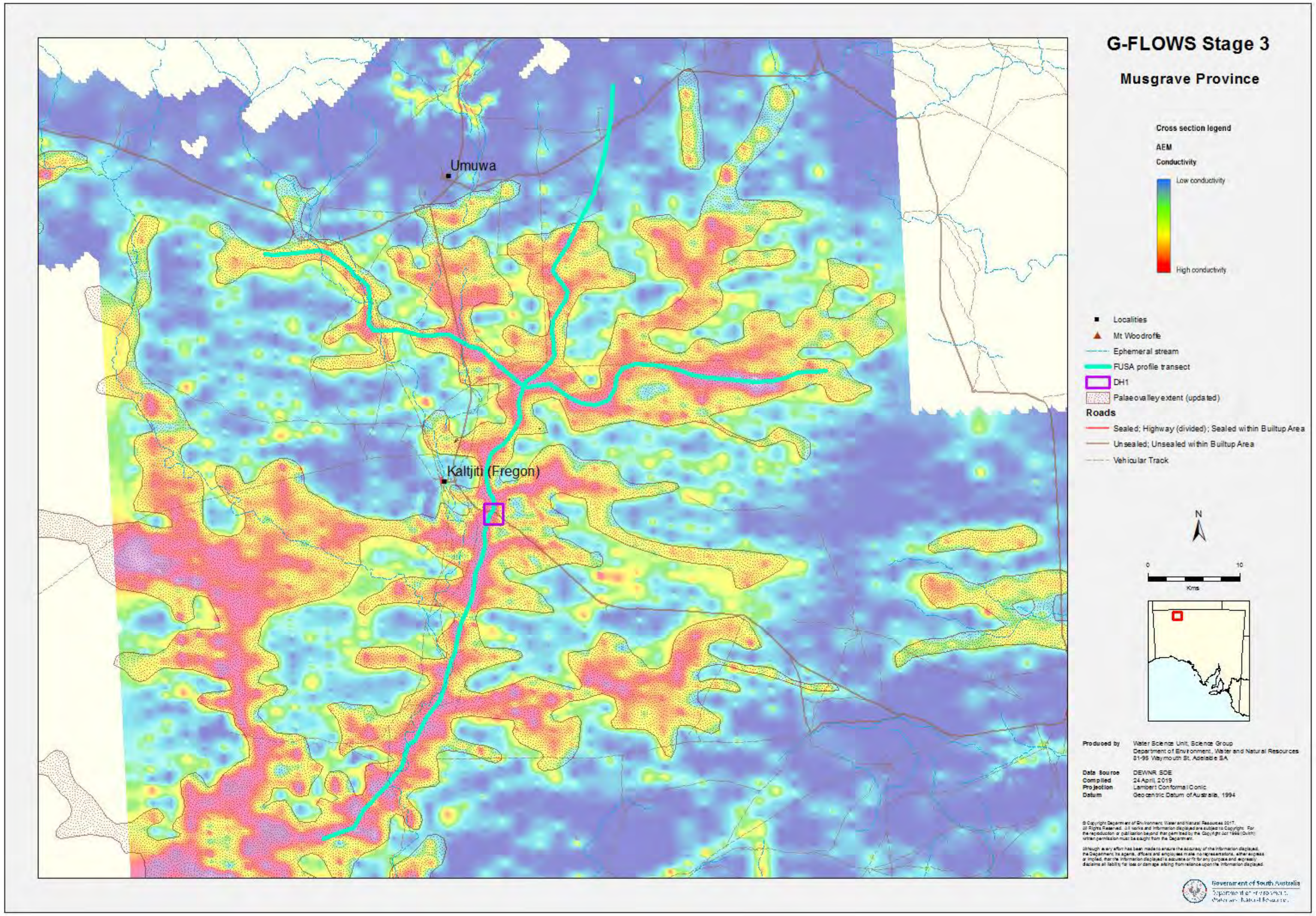


**Figure 3-15. AEM depth slice 50-60 mBNS (SkyTEM data) showing conductivity (red) and resistive (blue) variations over hydrogeological control site DH1.**

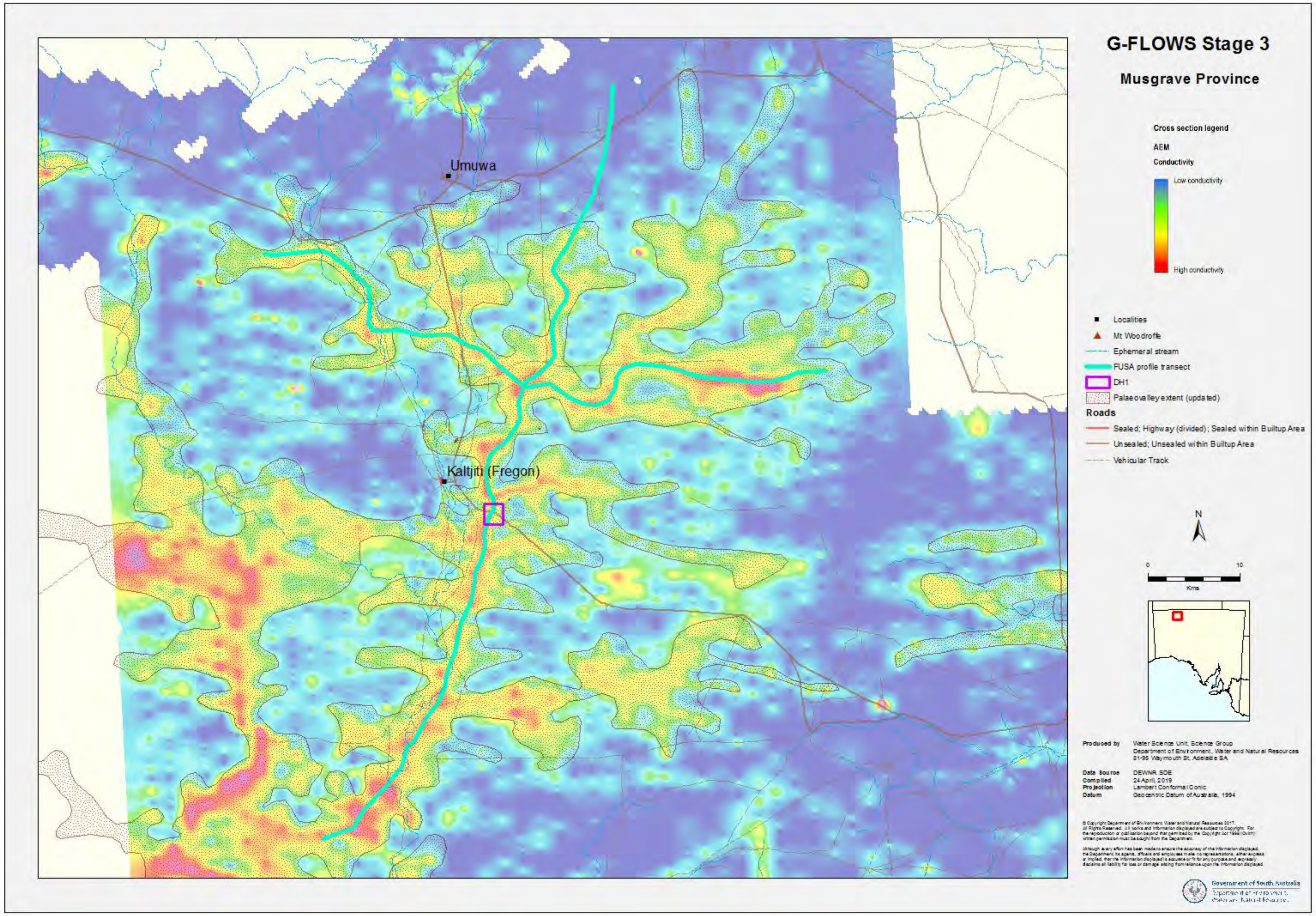


**Figure 3-16. AEM depth slice 80-90 mBNS (SkyTEM data) showing conductivity (red) and resistive (blue) variations over hydrogeological control site DH1.**


**Figure 3-17. Cross-section profiles across the Lindsay East Palaeovalley showing the watertable and the boundary between the porous media and weathered fractured rock: (a) N-S along Lindsay East Palaeovalley; (b) W-E along the western tributary of the palaeovalley; (c) E-W along the eastern tributary of the palaeovalley.**

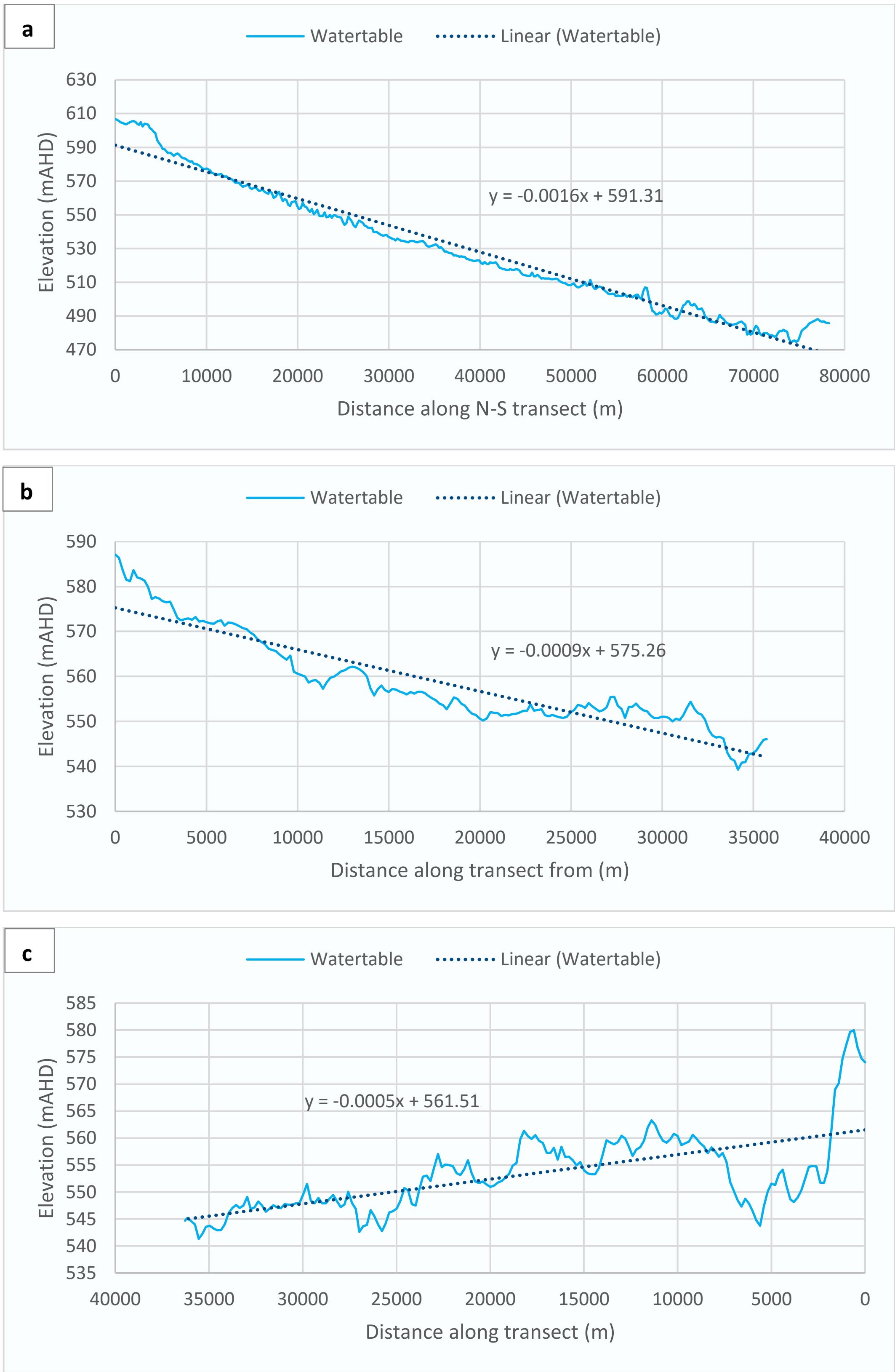


**Figure 3-18. Cross-section profiles across the Lindsay East Palaeovalley, showing the regional groundwater slope as well variations of the watertable: (a) N-S along Lindsay East Palaeovalley; (b) W-E along the western tributary of the palaeovalley; (c) E-W along the eastern tributary of the palaeovalley.**

Figure 3-18 provides more detail of the watertable. The following discussions provides some generalised comments, however, more detailed modelling of the thalweg profiles of the main Lindsay East Palaeovalley and its tributaries are required for future work. These would include smoothing of the watertable plus addition of vertical conductivity depth slices. Nevertheless, the following observations/comments will still be valid.

All transects have a flat regional hydraulic gradient of 0.0016, 0.0009 and 0.0005 (for the main western and eastern transects respectively). The watertable shows considerable undulations when compared to the regional slope of the watertable. Variations in amplitude of the watertable with reference to the regional slope can vary from a few meters to in excess of 10 m. These variations in the watertable suggest that flow cells of different scales and magnitude are occurring (Toth 1963, Toth 2009). This also indicates the importance of vertical as well as horizontal flow.

The aspect ratio of these transects is approximately 1:75, 1:35 and 1:35 for the main, western and eastern transects, respectively. Note aspect ratio is defined as the thickness of the aquifer versus the length of transect. If we assume homogeneous and isotropic condition for the aquifer material then aspect ratios of >1:10 will generate local flow systems and the so called "nested flow systems" will not occur (Robinson and Love 2012). The above is discussed by Love et al. (2020).

This analyses strongly supports the numerical strip modelling in Chapter 2 and further confirms that the groundwater system in the APY Lands is dominated by local flow systems and that this is not only confined to the mountainous regions (ranges) but occurs throughout the whole of the APY Lands. Future field work is required to validate this work and would include drilling along the thalwegs of the main and tributaries of the palaeovalleys to determine the location of the watertable. Additional drilling and nested piezometers should also be drilled.

### 3.2.1 POTENTIAL ZONES OF LARGE WATER RESOURCES

A comparison of the thickness map of the porous media (Chapter 2) with the AEM depth slices (Figs. 3-14, 3-15 and 3-16) as well as the thalweg transects (Fig. 3-17) provides areas of large water resource potential that should be considered for future drilling:

- Lindsay West Palaeovalley (south of Amata) (Fig. 2-14)
- N-S feature parallel to Lindsay East Palaeovalley approximately 30 km west of Kaltjiti a large conductivity feature is observed in all three AEM slice depths. This area represents a significant palaeovalley feature which has a depth of up to 200 m (Fig. 2-14)
- Lindsay Easter Palaeovalley – eastern tributary. Approximately 7.5 km from the origin (right-left) a large conductivity feature is observed. This area represents a significant palaeovalley feature which has a depth of up to 150 m (Fig. 3-17)

## 3.3 Hydrochemistry and environmental tracers

Groundwater chemistry for the DH1 site was sampled on three separate occasions. The first sampling occurred after the well was initially constructed and then a few days later after development; note this sampling occurred by air lifting from the rotary rigs compressor (28 July to 3 September 2018). Between 17 and 19 November 2018 all wells were sampled for full chemical analyses as well as a variety of environmental tracers. All wells were pumped for at least three casing volumes and groundwater samples were only collected once field parameters of electrical conductivity (EC) and pH were stable.

### 3.3.1 HYDROCHEMISTRY

Most samples yielded water of good to fair quality based on the total dissolved solids (TDS/salinity) concentration. The water type is consistently a Na-Cl water (Fig. 3-21) of alkaline nature (pH >8). The dissolved oxygen concentrations measured in the field suggest anoxic conditions for most samples.

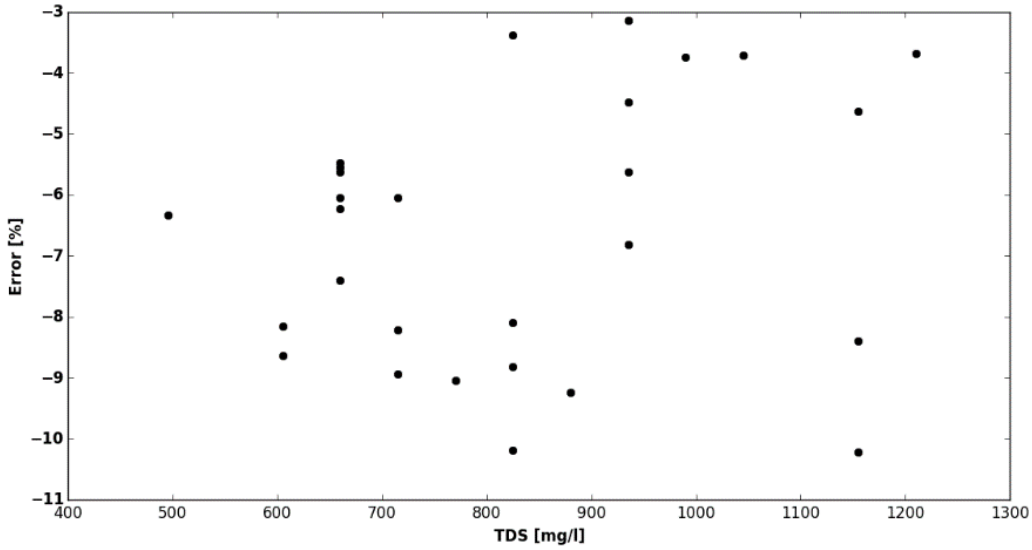


**Figure 3-19. Salinity and charge balance error of analysis. Salinity estimated as Total Dissolved Solids ≈ Electrical Conductivity * 0.55.**

Accordingly, iron and manganese are elevated in many samples owing to the generally anoxic conditions, however only one sample, taken immediately after drilling, was above the taste threshold level for iron of 0.3 mg/L. Following sufficient well development, this value decreased to below <0.1 mg/L. All waters proved to be oversaturated in respect to iron oxide ($Fe(OH)_3$). No water samples exceeded the guideline value for manganese of 0.5 mg/L. Groundwater's with a manganese concentration above 50 µg/L proved to be oversaturated in respect to rhodochrosite. Other trace metal concentrations were generally low, below detection limit for most waters.

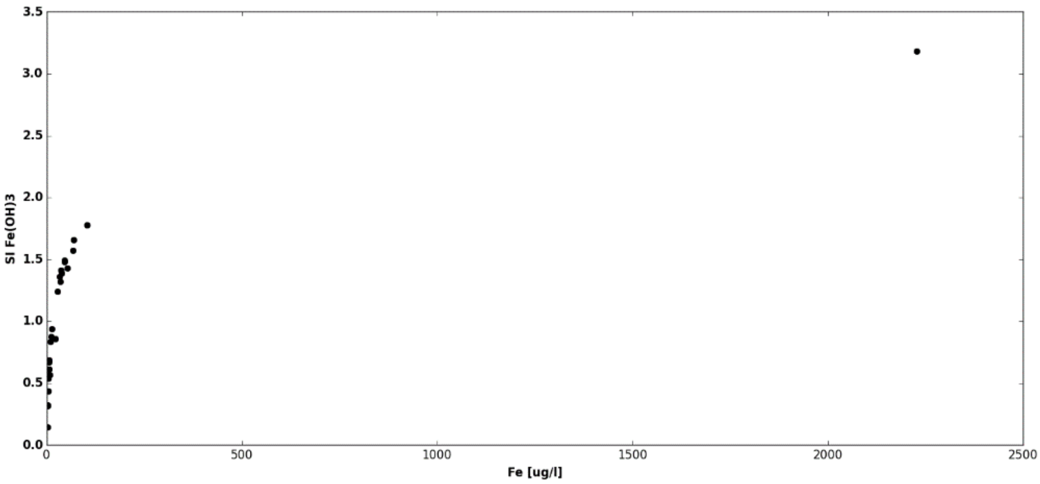


**Figure 3-20. Fe vs saturation index of $Fe(OH)_3$.**

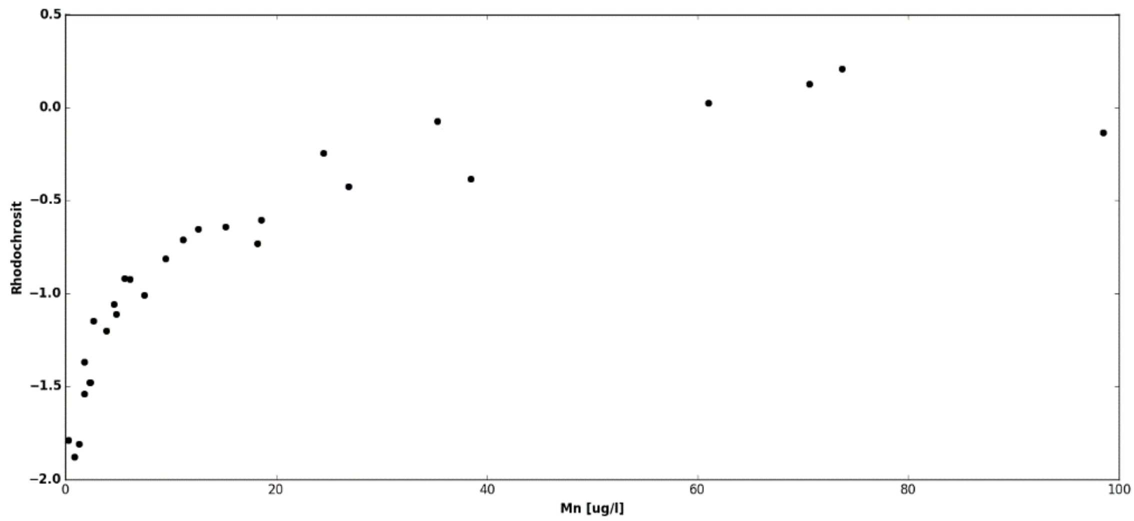


**Figure 3-21. Rhodochrosite ($MnCO_3$) vs Mn.**

The majority of waters exceed the $NO_3$ guideline value of 50 mg/L, but remain below 100 mg/L of nitrate, which is regarded a safe level for adults and children over three months old. The elevated nitrate levels may reflect evaporative enrichment in the soil zone as well as the potential for occasional flushing and downward leaching during periods of recharge.

Most samples exceed the taste threshold value of 250 mg/L Cl. The elevated Cl and sodium values are due to evaporative –transpiration enrichment with elevated concentrations possibly transported into the saturated zone through occasional downward flushing during periods of recharge. Alternatively, elevated Cl may also represent differential recharge rates due to different soil properties or evapotranspiration (ET) during discharge processes.

Seven out of 10 sampled wells during the November 2018 sampling event exceeded the guideline value for fluoride of 1.5 mg/L. Maximum concentrations thereby reach 2.6 mg/L with highest concentrations correlated to low calcium levels. Saturation in respect to fluorite is not attained in any of the waters, however, waters high in fluoride approach saturation. Fluoride levels in groundwater largely depend on reaction times with aquifer minerals and may indicate prolonged residence times and slow groundwater movement of the tested waters. Some of the fluoride-bearing rocks thereby include gneissic and granitic rocks, with fluorspar ($CaF_2$), apatite, and hornblende being some of the most important fluoride-bearing minerals.

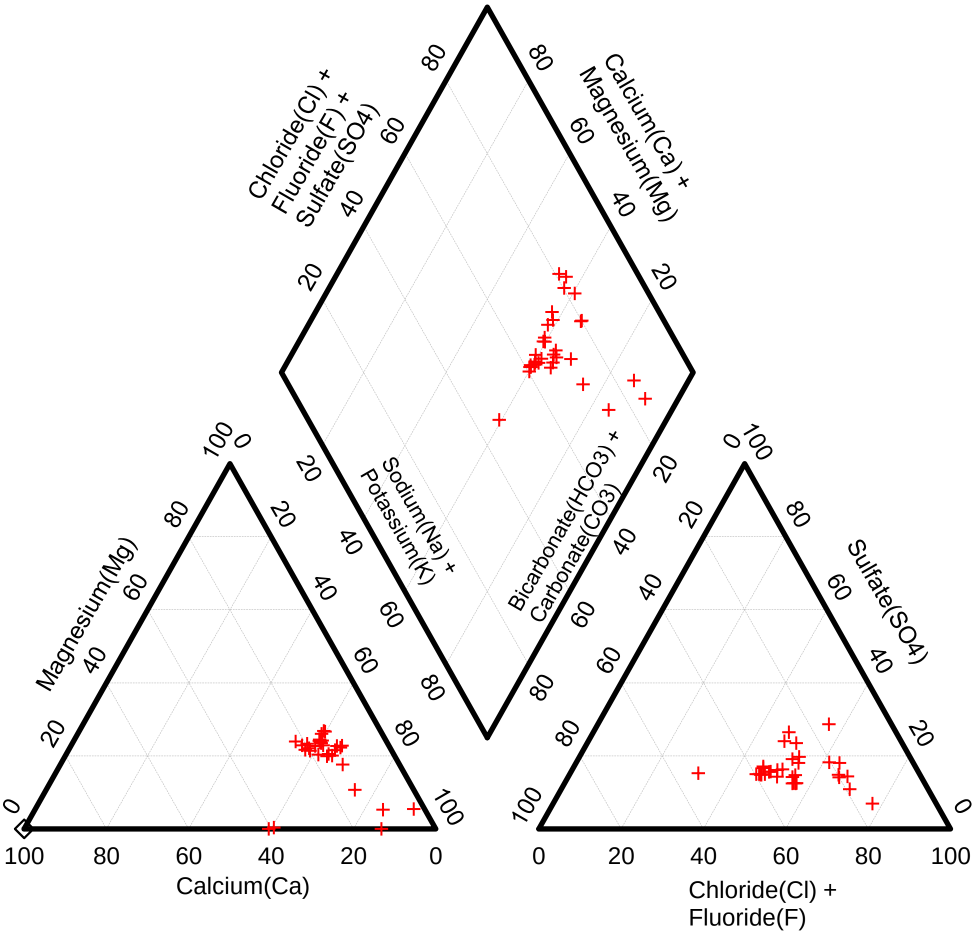


**Figure 3-22. Piper Diagram. The analysis reflect a Na-Cl type water.**

### Table 2. Summary of statistics of water quality data.

| Parameter | Unit of | Average | Median | Minimum | Maximum | n |
|---|---|---|---|---|---|---|
| Field pH | | 8.60 | 8.46 | 7.91 | 9.48 | 20 |
| Field Alkalinity | mg/L | 207.99 | 212.00 | 126.00 | 294.00 | 20 |
| Field EC | mS/cm | 1364.40 | 1204.00 | 1009.00 | 2094.00 | 20 |
| Field DO | mg/L | 2.43 | 0.08 | 0.03 | 13.20 | 20 |
| Lab pH | | 8.29 | 8.19 | 7.57 | 9.23 | 29 |
| Lab EC | dS/m | 1.49 | 1.45 | 0.90 | 2.19 | 29 |
| Total Alkalinity | meq/L | 4.36 | 4.42 | 2.76 | 5.74 | 29 |
| F- | mg/L | 0.88 | 0.62 | 0.18 | 2.59 | 29 |
| Cl- | mg/L | 284.33 | 268.54 | 159.43 | 555.95 | 29 |
| Br- | mg/L | 2.07 | 1.98 | 0.92 | 4.48 | 29 |
| NO3- | mg/L | 48.27 | 52.68 | 0.03 | 89.09 | 29 |
| SO4= | mg/L | 114.98 | 100.86 | 81.05 | 241.62 | 29 |
| Ca | mg/L | 44.77 | 38.84 | 24.28 | 88.02 | 29 |
| K | mg/L | 18.72 | 18.16 | 9.31 | 35.69 | 29 |
| Mg | mg/L | 36.54 | 34.04 | 7.56 | 57.86 | 29 |
| Na | mg/L | 183.80 | 165.87 | 141.74 | 283.13 | 29 |
| S | mg/L | 43.84 | 35.64 | 29.31 | 77.89 | 29 |
| B | mg/L | 0.31 | 0.33 | 0.16 | 0.40 | 29 |
| Si | mg/L | 29.35 | 30.30 | 15.63 | 48.75 | 29 |
| Sr | mg/L | 0.53 | 0.55 | 0.34 | 0.98 | 29 |
| Al | µg/L | 64.57 | 8.20 | 1.20 | 1425.00 | 29 |
| V | µg/L | 23.23 | 24.80 | 5.40 | 61.00 | 29 |
| Cr | µg/L | 4.50 | 4.90 | 0.50 | 15.00 | 29 |
| Mn | µg/L | 19.49 | 7.50 | 0.25 | 98.50 | 29 |
| Fe | µg/L | 102.28 | 13.00 | 2.00 | 2228.00 | 29 |
| Co | µg/L | 0.15 | 0.05 | 0.05 | 0.40 | 29 |
| Ni | µg/L | 2.11 | 1.00 | 0.10 | 15.50 | 29 |
| Cu | µg/L | 1.17 | 0.50 | 0.10 | 11.10 | 29 |
| Zn | µg/L | 23.16 | 15.00 | 2.50 | 130.00 | 27 |
| As | µg/L | 0.96 | 0.70 | 0.20 | 4.60 | 29 |
| Se | µg/L | 3.83 | 3.50 | 2.20 | 6.40 | 29 |
| Mo | µg/L | 2.12 | 1.60 | 0.80 | 9.00 | 29 |
| Cd | µg/L | 0.36 | 0.05 | 0.05 | 2.90 | 29 |
| Pb | µg/L | 1.77 | 0.10 | 0.05 | 33.20 | 29 |
| U | µg/L | 1.19 | 0.80 | 0.10 | 4.10 | 29 |

## 3.4 Environmental tracers

Environmental tracers, including major solutes and $^{14}C$, $^{13}C$, $^{3}H$, $\delta^{2}H$ and $\delta^{18}O$, were sampled 17-19 November 2018. All wells were pumped at least three casing volumes and samples were only taken when field parameters of EC and pH were stable (Table 3 and Table 4, for results). As discussed previously the wells were specially designed and constructed for sampling environmental tracers in that they were completed over small screen intervals, hence we avoided potential mixing processes and in this way, we obtained relatively consistent depth weighted sampling.

**Table 3. Field data at the time of sampling at sites DH1 and S22. BNS denotes below natural surface. FRA denotes fractured rock aquifer.**

| Unit No | Name | Screen interval (mBNS) | SWL (m) | pH | EC (µS/cm) | Alkalinity (mEq/L) | Geology | Aquifer type |
|---|---|---|---|---|---|---|---|---|
| 5344-78 | DH1a2 | 108.7-111.7 | 7.91 | 7.95 | 1580 | 4.91 | sandstone | confined |
| 5344-80 | DH1c | 51-57 | 7.51 | 8.16 | 1140 | 4.67 | sandstone | unconfined |
| 5344-83 | DH1e | 10.5-13.5 | 7.686 | 8.12 | 1340 | 4.42 | sand | unconfined |
| 5344-85 | DH1f | 70.35- 76.35 | 8.06 | 9.97 | 1330 | 2.13 | sand | unconfined |
| 5344-86 | DH1g | 11.61-14.61 | 7.88 | 8.14 | 2050 | 4.65 | basement | FRA |
| 5344-89 | DH1b | 57-60.4 | 8.4 | 8.11 | 1140 | 4.72 | sandstone | unconfined |
| 5344-79 | S22a | 31.3-34.3 | 27.05 | 8.87 | 900 | 2.76 | sand | unconfined |
| 5344-81 | S22c | 16-19 | 12.19 | 8.12 | 1530 | 5.24 | sand | unconfined |
| 5344-84 | S22b | 31.5-34.5 | 31 | 7.57 | 1350 | 5.74 | sand | unconfined |
| 5344-88 | S22i | 44-47 | 13.2 | 8.04 | 1350 | 5.74 | sand | unconfined |

**Table 4. Environmental tracer data for sites DH1 and S22. $^{13}C$ are expressed as per mil relative to PDB (Pee Dee Belomite), $\delta^{2}H$ and $\delta^{18}0$ are expressed in per mil relative to VSMOW (Vienna standard mean ocean water). $^{3}H$ expressed in Tritium units (TU) where one TU = one $^{3}H$ atom in $10^{18}$ atoms of hydrogen.**

| Unit No | Name | Screen interval (mBNS) | Screen mid-point (mBNS) | %MC | $^{13}C$ | $^{3}H$ TU | $\delta^{18}0$ | $\delta^{2}H$ | Cl (mg/L) |
|---|---|---|---|---|---|---|---|---|---|
| 5344-78 | DH1a2 | 108.7-111.7 | 110.2 | 17.27 | -6.5 | -0.009 | -6.06 | -44.63 | 316 |
| 5344-80 | DH1c | 51-57 | 54 | 39.79 | -7.1 | 0.012 | -5.85 | -42.98 | 203 |
| 5344-83 | DH1e | 10.5-13.5 | 12 | 45.16 | -8.1 | 0.019 | -5.84 | -42.78 | 270 |
| 5344-85 | DH1f | 70.35- 76.35 | 73.4 | 8.67 | -11.9 | 0.019 | -6.16 | -45.44 | 277 |
| 5344-86 | DH1g | 11.61-14.61 | 13.1 | 62.57 | -7.6 | 0.003 | -6.26 | -45.62 | 494 |
| 5344-89 | DH1b | 57-60.4 | 58.7 | 39.27 | -6.6 | 0.01 | -5.81 | -42.64 | 204 |
| 5344-79 | S22a | 31.3-34.3 | 32.8 | 53.2 | -8.9 | 0.035 | -6.01 | -45.01 | 159 |
| 5344-81 | S22c | 16-19 | 17.5 | 66.8 | -6.2 | 0.011 | -6.02 | -45.12 | 334 |
| 5344-84 | S22b | 31.5-34.5 | 33 | 58.58 | -13.1 | 0.234 | -6.36 | -51.05 | 292 |
| 5344-88 | S22i | 44-47 | 45.5 | 54.38 | -9.2 | 0.057 | -6.04 | -45.41 | 556 |

### 3.4.1 CHLORIDE

As discussed in Chapter 2, the Cl anion is chemically conservative in the APY Lands, therefore the Cl ion can be used to provide both qualitative information on the nature of the groundwater flow system as well as quantitative values of recharge. In a way Cl is neither added nor removed by chemical means it can only be altered by physical processes. The spatial distribution of Cl for the Lindsay East Palaeovalley and adjacent regions is shown in Figure 3-23. As can be observed, there is large spatial variability in the values of Cl, low Cl concentrations are indicative of high recharge rates (denoted by blue and light green dots), while higher concentrations of Cl may represent lower rates of recharge or even local discharge features. Low Cl concentrations often <150 mg/L occur near Pukatja (Ernabella) as well adjacent to Ernabella Creek. Groundwater with Cl <100 mg/L as well some wells <50 mg/L occur on the boundary between the fractured rock and the porous media fill of the palaeovalley. The best example of this is near Umuwa ~2-3 km north of the palaeovalley boundary.

This zone corresponds to a change in the geology from sedimentary units in the palaeovalley to fractured rock aquifers. This area corresponds to a break in the AEM where we observe a transition from a zone of high conductivity to a more resistive zone of low conductivity. We have interpreted this to be a zone of high recharge from the fractured rock aquifer to the porous media aquifer into the paleovalley. This is also supported by modern groundwater as evident by above background $^{14}C$ data (Chapter 2). It is inferred that these zones also represent a mechanism for recharge to the deeper confined aquifer of the palaeovalley.

Inside the palaeovalley the Cl concentrations increase in concertation compared to the adjacent fractured rock indicating lower rates of recharge. Although there is a paucity of data inside the upper palaeovalley sediments, Cl values still show large spatial variability which suggests differential inputs of recharge or alternatively different recharge and discharge zones.

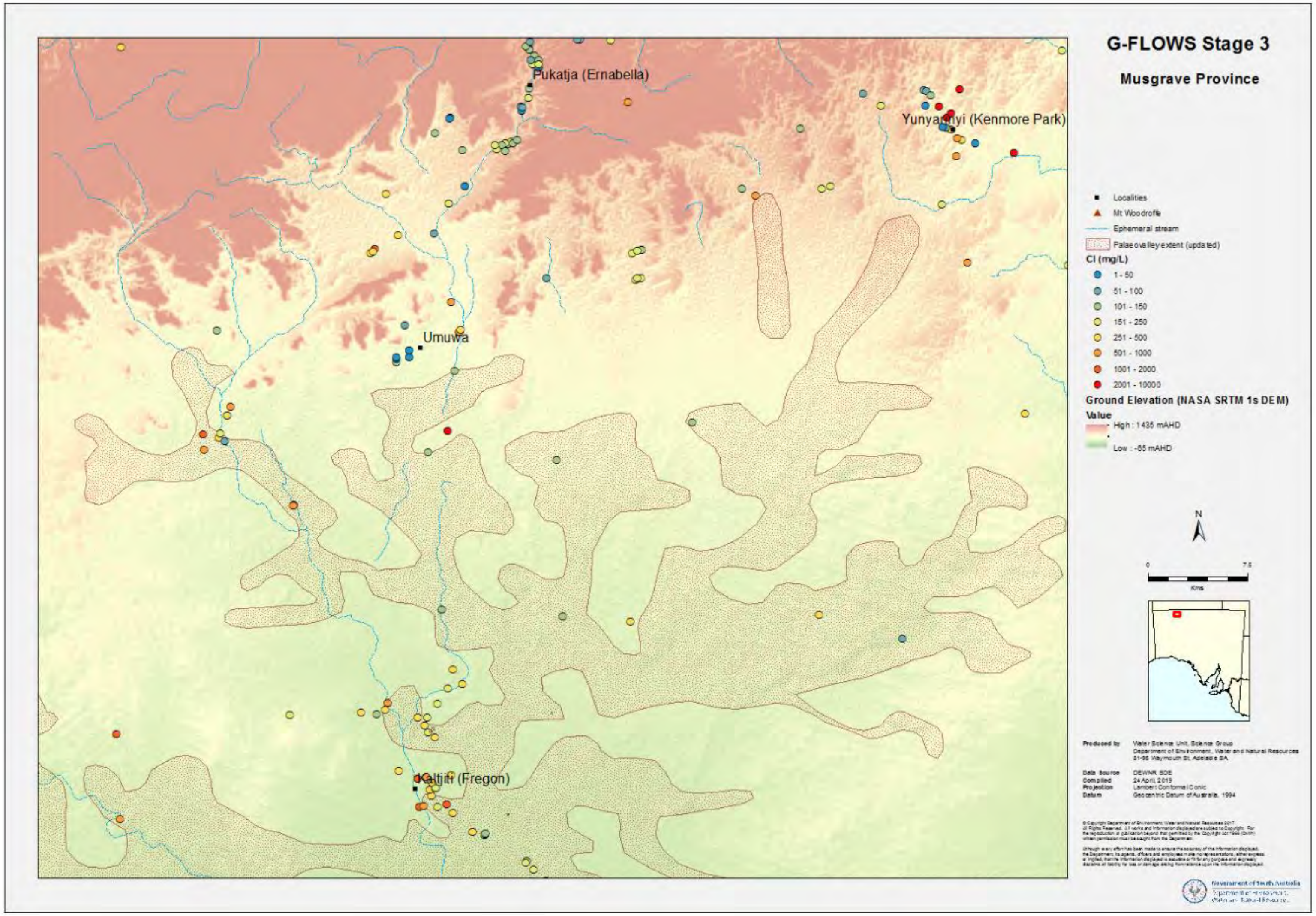


Figure 3-23. Cl concentrations located across the Lindsay East Palaeovalley.

### 3.4.2 TRACER VS TRACER PLOTS

Tracers versus tracers plots presented in Chapter 2 are presented here again along with the sampling data for sites DH1 and S22 (Fig. 3-24).

The $^{14}C$ versus Cl plot shows a wide scatter of data (Fig. 3-24a). There is a slight tendency for older groundwater to have a higher values of Cl but it can be observed that many of the groundwater >75 %MC have Cl > 1000 mg/L. This is not indicative of rapid recharge as low Cl concentrations would have been observed, but rather it could represent either differential recharge, with different soil properties, or alternating recharge and discharge zones. This data plots in the transpiration window on the Cl versus $\delta^{18}O$ plot (Fig. 3-24c). Groundwater for DH1 and S22 generally plot in the middle of the cluster. The two oldest groundwater's (DH1a2 and DH1f) represent groundwater from the deep confined aquifer in the palaeovalley and the adjacent fractured rock, respectively.

The $^{14}C$ – $\delta^{18}O$ space shows the characteristic high $^{14}C$ activities depleted $\delta^{18}O$ which also corresponds to low Cl concentrations indicative of rapid recharge. The data for the local sites shows constant values of $\delta^{18}O$ for a wide range of $^{14}C$ activities. The data for DH1 and S22 corrects to mean residence times between modern and approximately 2000 years BP for the unconfined aquifer (see Section 3.4.5).

$\delta^{18}O$ varies from -10 to -8 per mil without any significant enrichment of Cl (Fig. 3-24c). This suggests that this young, low salinity groundwater were recharged via rapid infiltration of large rainfall events. These rainfall events are likely to occur with rainfall intensities of 60-70 mm/month. Compared to Alice Springs rainfall, this would represent recharge occurring between January and March. The slight enrichment between in $\delta^{18}O$ from -8 to -6 per mil corresponds to an increase in Cl concentrations up to 1000 mg/L. This trend could be characteristic of evapotranspiration processes. The more significant increase in Cl concentrations from ~500 to 3500 mg/L is indicative of transpiration being a dominant process (Fig. 3-24c).

The typical plot of rainfall and groundwater data in $\delta^{18}O$ –$\delta^{2}H$ space is shown in Figure 3-25. The rainfall data is taken from the decommissioned IAEA rainfall station at Alice Springs. The graph shows both the global meteoric water line of $\delta^{2}H = 8\delta^{18}O + 10$ (dashed line) as well as the local meteoric water line for Alice Springs, $\delta^{2}H = 6.96\delta^{18}O + 4.96$. The rainfall data has been sorted into monthly values of intensity that vary 0-20, 20-40, 40-60, 60-80, 80-100 and >100 mm/month.

Previously collected groundwater sample data from the APY Lands is shown in blue data points (Leaney et al. 2012, Kretschmer and Wohling 2014). Data collected for this project (2018) is represented by the red data points. The line of best slope through all the groundwater data is represented by $\delta^{2}H = 5.9\delta^{18}O -9.1$. Previous authors have assumed that this equation is representative of an evaporative trend and that where the groundwater line intersects the Local Meteoric Water Line (LMWL) is indicative of a recharge threshold of 100 mm/month.

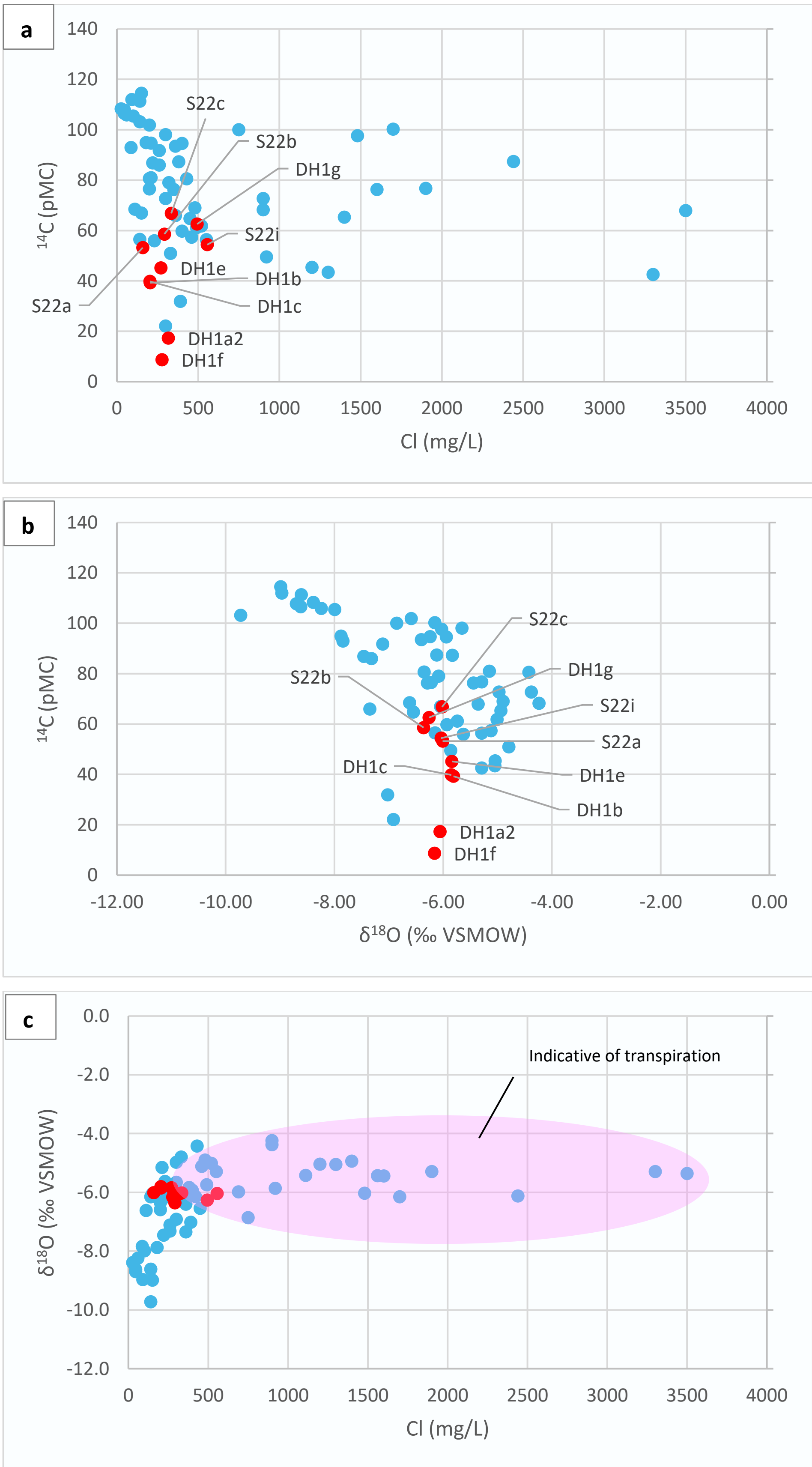


**Figure 3-24. Tracer vs tracer plots. (a) $^{14}C$ vs Cl; (b) $^{14}C$ vs δ$^{18}$O; and (c) δ$^{18}$O vs Cl. Blue data points represent data from Leaney et al. (2012) and Kretschemer and Wohling (2014). Red data points represent data from the project sampling event (2018).**

However, the reference line for evaporation is the LMWL and as both the LMWL and groundwater line have a similar slope of 6.96 and 5.9 respectively (Fig. 3-25) it does not appear that the groundwater trend is representative of evaporation. Otherwise a much flatter slope (around 3-4) for groundwater would be expected but this is not observed.

The range of groundwater's in $\delta^{18}O$ –$\delta^{2}H$ space plot with the range of monthly rainfall at Alice Springs between 60 to 100 mm/year. This suggest that rainfall of this intensity > 70 60 mm/month is required for groundwater recharge. The monthly average values of $\delta\ ^{18}O$ in rainfall from Alice Springs suggest that the majority of recharge occurs in the summer months between January and March (Fulton et al. 2013). It is also worth noting that no groundwater's have $\delta^{18}O$ and $\delta^{2}H$ that correspond to rainfall values less than <60 mm/month, which suggest that no small rainfall events result in recharge and that recharge is totally dominated by these large events.

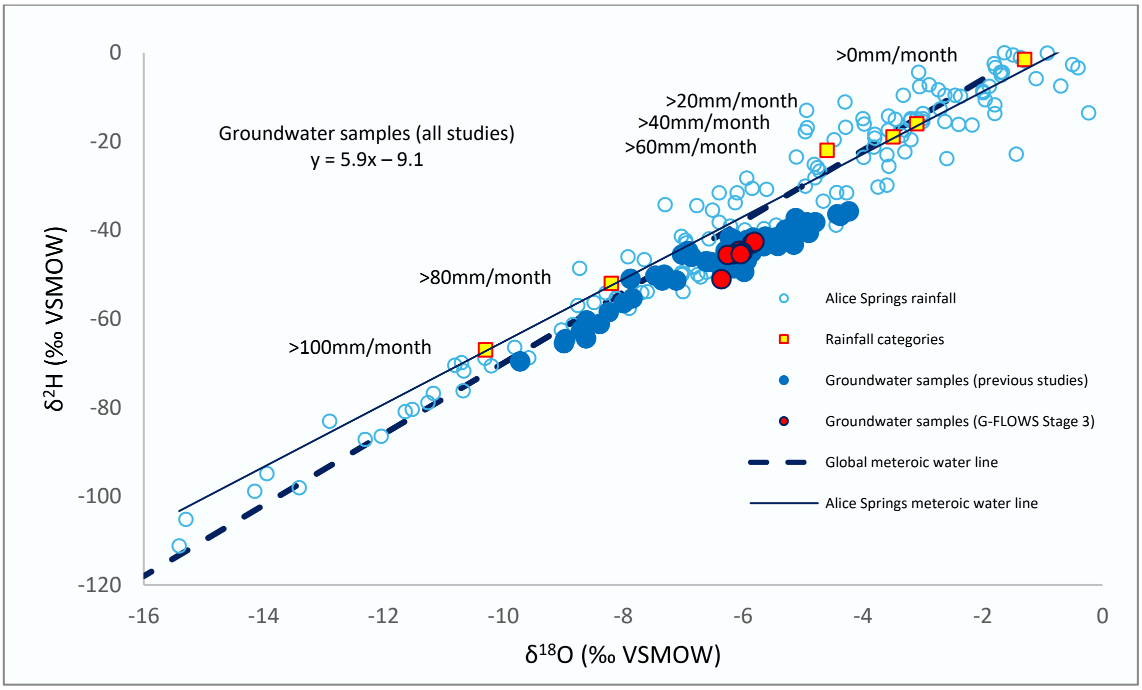


**Figure 3-25. Groundwater stable isotope ratio relative to amount weighted-mean monthly rainfall volume categories. VSMOW = Vienna Standard Mean Oceanic Water**

A plot of monthly rainfall from 2013 until 2019 for Pukatja can be instructive (Fig. 3-26). Given there are 49 events over 70 mm/month over the 106-year record, and if 70 mm/month is the threshold rainfall value required for recharge, then recharge to the APY Lands groundwater would occur approximately every two years.

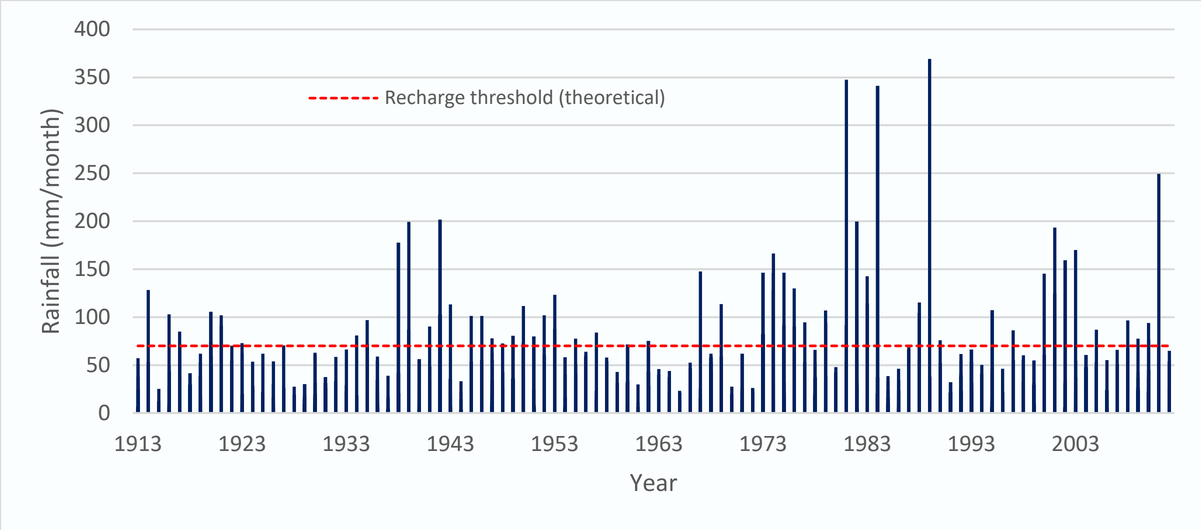


**Figure 3-26. Monthly rainfall for Pukatja (Ernabella) from 1913-2019.**

### 3.4.3 RECHARGE ESTIMATION IN PALAEOVALLEY

Groundwater recharge across the Lindsay East Palaeovalley has been estimated from CMB and by application of the Vogel method for $^{14}C$. CMB recharge was estimated from the following:

$$R = \frac{Cl_P P}{Cl_{gw}}$$

where *R* = recharge, $Cl_p$ = Cl concentration in precipitation, *P* = annual precipitation, *Clgw* = Cl concentration in groundwater.

Cl concentrations at site DH1 vary from 203 to 556 mg/L with an average of 294 mg/L. If it is assumed an average precipitation of 260 mm/year (precipitation average at Pukatja from 1913-2019) and $Cl_p$ = 0.72 mg/L (rainfall chemistry data at Alice Springs, Crosbie 2012). Groundwater recharge may vary from 0.38 to 0.92 mm/year with an average recharge of 0.64 mm/year. In a similar manner for site S22, if a Cl concentration of 0.72 mg/l is assumed and annual precipitation of 260 mm/year is used, then recharge rates vary from 1.1 to 0.34 with an average of 0.7 mm/year.

Even lower values of recharge will be obtained if we used other Cl values in rainfall in adjacent areas where the mean weighted Cl concentrations from rainfall at Alice Springs and Wintana station was calculated to be 0.63 and 0.4 mg/L respectively (data from Keywood 1997). This would convert to 12.5% to 45% less recharge.

The discussion above shows the importance of rainfall chemistry in estimating recharge in the arid zone. Unfortunately, data is very sparse in the region with no (or limited) rainfall data in the APY Lands. Furthermore, rainfall chemistry in the rangeland and the plains is expected to be different (Guan et al. 2009). Weather stations that collect rainfall chemistry amongst other data in the APY Lands in both the plains and the ranges would prove most useful.

Although there are relatively low recharge rates at the study sites (DH1 and S22), the spatial distribution of Cl in the Lindsay East palaeovalley suggests a variable recharge rate. Throughout the upper zones of the palaeovalley (where the depth to groundwater is relatively shallow) Cl concentrations vary from 26 to 490 mg/L. The uneven and spatially variable distribution of Cl suggests differential inputs of recharge at least to the upper palaeovalley system. The variability of input is most likely related to different variations of soils in the unsaturated zone. Using the above values of precipitation and Cl in precipitation we obtain recharge values of 0.38 to 7.2 mm/year. An alternative to this could be discharge in zones of low elevation where the dominant mechanism to concentrate salinity is by water up-take by plants during transpiration.

The highest value of recharge occurs at the proposed recharge zone near Umuwa with values ranging from 3 to7 mm/year. Recharge in the palaeovalley varies from 0.5 to 4 mm/year.

### 3.4.4 RADIOCARBON AND TRITIUM

#### Radiocarbon ($^{14}C$)

There are three isotopes of carbon, the most common is stable $^{12}C$ (~98.8%). $^{13}C$ is far less abundant but still stable (~1.1 %) and $^{14}C$ is radioactive and the least abundant (<0.01 %). $^{14}C$ is produced in the atmosphere by cosmic ray bombardment with $N_2$ (Libby 1952). The $^{14}C$ atoms rapidly oxidise to $CO_2$ and mix with atmospheric $CO_2$. From its atmospheric reservoir, $^{14}CO_2$ is introduced into the hydrosphere via precipitation. Radiocarbon can be introduced into groundwater via three main processes, namely (a) exchange between the soil and atmosphere, (b) dissolution of carbonates in the soil or aquifer zone, and (3) decomposition of plants and root respiration produces $^{14}CO_2$. Once removed from its atmospheric source $^{14}C$ can decrease due radioactive decay, mixing with other waters, as well as decay and dilution with carbonate materials of zero $^{14}C$.

Provided that the initial radiocarbon activity ($A_0$) at the time of recharge can be determined we can estimate the "radiocarbon age" from the law of radioactive decay from the following:

$$A = A_{0\,.}e^{-\lambda t}$$

where, $A$ = activity at time t (activity of the sample), $A_0$ = is the $^{14}C$ activity at initial time, $t$, and $\lambda$ = decay constant (years$^{-1}$).

Rearranging the law of radioactivity and substituting the $^{14}C$ decay constant ($\lambda$ =1/8033 yr$^{-1}$), the groundwater age can be calculated from the following:

$$t = -8033.\,ln\, {}^{A}\!/_{A_0}$$

#### Tritium ($^3H$)

Tritium ($^3H$) is the radioactive isotope of hydrogen. It has a ½ life of 12.43 years and is measured in Tritium Units (TU), where 1 TU = one $^3H$ atom in $10^{18}$ atoms of hydrogen. Tritium is an ideal tracer as it is part of the water molecule and does not require any chemical corrections for its application. The concentrations of $^3H$ in the atmosphere increased dramatically as a result of thermonuclear testing reaching an atmospheric peak in 1963. Since then, $^3H$ has declined due to decay and as a result, current concentrations in groundwater (<1 TU) are difficult to detect due to the existing laboratory methodology. However, recently new analytical techniques have resulted in much lower detection limits which increases the potential of this isotope as a tracer of groundwater systems.

#### Results

The raw analytical results for $^3H$ and radiocarbon are presented to determine what can be understood about these environment tracers at face value. The section that follows corrects the raw $^{14}C$ data into groundwater residence times.

$^3H$ concentrations at site DH1 are all extremely low and within the error of measurement. We therefore interpret that all the samples here do not contain any thermonuclear component and were recharge prior to 1963 and must be in excess of 60 years. For S22 all the sampled wells have thermonuclear $^3H$ and therefore would have been recharged in the last 60 years, the exception being S22c which has $^3H$ values that indicate recharge >60 years

The radiocarbon data indicate increases in age with depth in the palaeovalley. There is a wide range of $^{14}C$ activities at DH1 ranging from 8.7 to 62.6 pMC. This converts to an uncorrected radiocarbon age of between 3,710 to 19,615 years BP.

In the middle of the palaeovalley, four wells were sampled. The upper well (DH1e) has a $^{14}C$ activity of 45.2 pMC which converts to an uncorrected age of 6380 years BP at a depth of 4.3 m below the watertable (reference midpoint of screen). Wells DH1c and DH1b represent the high yielding aquifer and have $^{14}C$ activities of 39.8 and 39.3 pMC respectively. This converts to an uncorrected age of 7420- and 7510-years BP at 46.5 and 50 m respectively below the watertable. The last production zone in the central paleovalley is well DH1a2 which is the confined well with a $^{14}C$ activity of 17.3 pMC and an uncorrected age of 14,090 years BP. At the edge of the palaeovalley (DH1g and DH1f) we observe that $^{14}C$ activities decrease from 62.6 to 8.7 pMC at 5.1 and 65.4 m respectively below the watertable.

There is zero head difference between the mid and deeper unit, and at least locally there is no hydraulic connection. Furthermore, at the DH1 site it appears that there is no hydraulic connection between the surrounding fractured rock/alluvium and palaeovalley sediments. This is based on two pieces of evidence: (1) groundwater is more brackish compared to palaeovalley salinity and (2) groundwater is older than the palaeovalley. Furthermore, our limited data indicates that the groundwater flow paths may be parallel to the palaeovalley (Fig. 2-17).

The raw data suggest that we have both modern water as well as groundwater that is >2000 years. $^3H$ and thermonuclear $^{14}C$ are good indicators of modern groundwater. For older groundwater $^{14}C$ is ideal for ages >5,730 years (one half-life). However, there is an age gap between 60-5730 years BP where $^{14}C$ is not ideal. The tracer to fill this time gap is $^{39}Ar$ which has a half-life of 269 years BP. $^{39}Ar$ is expensive and complicated to sample but previous studies have shown that it is an ideal tracer for studying sand aquifers in this time range (Loosli 1983).

### 3.4.5 $^{14}C$ "GROUNDWATER AGES"

#### Radiocarbon ages

Radiocarbon determinations of the total dissolved inorganic carbon (TDIC), $HCO_3$ and $CO_2(aq)$ plus stable $^{13}C$ were used in a number of correction models (Ingerson and Pearson 1964, Pearson and Hanshaw 1970, and Tamers 1970). The first process to consider is whether to use an open system or closed system model with respect to carbon. Open system models are generally driven by high $CO_2$ concentrations and high partial pressure of $CO_2$ ($PCO_2$) in the soil gas. If these conditions occur prior to recharge then open system conditions occur and there is no need for any correction models to be used for $^{14}C$, and uncorrected values from accelerator mass spectrometer (AMS) can be used. The initial $^{14}C$ would be in the order of ~100 pMC, with $^{13}C$ varying depending on the soil and vegetation type.

Closed system models usually apply to relatively low porosity media, low organic content and low values of $PCO_2$ (all of these conditions occur in the APY Lands). Cartwright et al. (2020) suggested that some form of closed systems behaviour occurs for most groundwater.

Recent studies have shown that the values of $^{14}C$ may decay with conditions of thick soil zones and low recharge rates in the arid zone (Wood et al. 2015). However, as the watertable in our study area is relatively shallow we assume that $^{14}C$ values in the soil zone are in equilibrium with the atmosphere.

Estimating groundwater ages or residence times in groundwater is difficult due to the many uncertainties in the dissolved inorganic carbon (DIC) reservoirs. This is especially true in the arid zone, where the input of $^{14}C$ and $^{13}C$ into the groundwater system is uncertain. We have applied three different correction schemes for estimating the initial value of $^{14}C$ (*Ao*).

## Chemical mixing model (Tamers)

Tamers (1970) is a closed system model often referred to as a chemical mixing model. The model does not use $\delta^{13}C$ to account for carbonate dilution. Instead of this the model accounts for dilution of carbonate minerals from the major species of TDIC. The model does not account for isotopic fractionation between $CO_2$ and $HCO_3$. The initial radiocarbon activity can be calculated from the following:

$$Ao = \frac{mCO2aq + 0.5mHCO3}{mCO2 + mHCO3}$$

## Isotope mixing model (Pearson model)

The Pearson model (Ingerson and Pearson 1964, Pearson and Hanshaw 1970) is a closed system mixing model that accounts for the reaction between biogenic $CO_2$ and solid carbonates. The model is similar to the Tamers model, but it uses the $^{13}C$ content of soil $CO_2$ and solid carbonate as end members.

$$Ao = \frac{\delta d - \delta c}{\delta g - \delta c}(Ag - Ac) + Ac$$

## International Atomic Energy Model IAEA model

The IAEA model is a closed system isotopic mixing model open to $CO_2$ in the unsaturated zone (Gonfiantini 1972). Dissolved $CO_2$ is allowed to equilibrate with soil $CO_2$ in the unsaturated zone. The model is similar to the Pearson model except that it is open to $CO_2$ in the unsaturated zone. This model accounts for the fractionation between gaseous $CO_2$ and dissolved $HCO_3$. The initial $^{14}C$ content can then be calculated from the following:

$$Ao = \frac{\delta d - \delta c}{\delta g - \varepsilon g - \delta c}(Ag - Ac) + Ac$$

The nomenclature for the above equations are *Ao* = initial activity of radiocarbon at recharge, m = molarity, δmd = $\delta^{13}C$ per mil measured in groundwater (i.e. dissolved $HCO_3$, δc = $\delta^{13}C$ in solid carbonate, δg = $\delta^{13}C$ of gaseous soil $CO_2$, Ag = $^{14}C$ in gaseous phase.

**Table 5. $^{14}C$ correction schemes. For the calculations we have assumed the following values. *δd* = $^{13}C$ measured. *δc* = 2, per mil, *δg* = -16 `per mil, *eg* +=-8 per mil, *Ag* = 100, *Ac* = 0. When values of the initial $^{14}C$ activity (*Ao*) are determined then they can be substituted into the radioactive decay. The "ages" in red text represent modern groundwater with a recharge component in the in the last 60 years.**

| Unit No | Name | $^{14}C$ | $^{13}C$ | mCO2 | mHCO3 | pCO2 | Uncorrected | Tamers | Pearson | IAEA |
|---|---|---|---|---|---|---|---|---|---|---|
| 5344-78 | DH1a2 | 17.27 | -6.5 | 9.02E-05 | 4.63E-03 | 2.66E-03 | 14108 | 8692 | 8080 | 5128 |
| 5344-80 | DH1c | 39.79 | -7.1 | 5.52E-05 | 4.42E-03 | 1.63E-03 | 7403 | 1933 | 1924 | -1030 |
| 5344-83 | DH1e | 45.16 | -8.1 | 6.48E-05 | 4.15E-03 | 1.91E-03 | 6386 | 940 | 1744 | -1219 |
| 5344-85 | DH1f | 8.67 | -11.9 | 1.38E-07 | 6.95E-04 | 4.08E-06 | 19643 | 14077 | 17567 | 14619 |
| 5344-86 | DH1g | 62.57 | -7.6 | 6.59E-05 | 4.31E-03 | 1.95E-03 | 3767 | -1681 | -1283 | -4242 |
| 5344-89 | DH1b | 39.27 | -6.6 | 7.01E-05 | 4.45E-03 | 2.07E-03 | 7509 | 2064 | 1575 | -1373 |
| 5344-79 | S22a | 53.2 | -8.9 | 5.87E-06 | 2.32E-03 | 1.73E-04 | 5070 | -478 | 1040 | -1918 |
| 5344-81 | S22c | 66.8 | -6.2 | 7.62E-05 | 4.91E-03 | 2.25E-03 | 3241 | -2205 | -3075 | -6039 |
| 5344-84 | S22b | 58.58 | -13.1 | 2.73E-04 | 5.52E-03 | 8.06E-03 | 4296 | -902 | 2885 | -66 |
| 5344-88 | S22i | 54.38 | -9.2 | 7.35E-05 | 3.82E-03 | 2.17E-03 | 4893 | -525 | 1082 | -1867 |

The model that best fits the carbonate evolution is the Tamers or Pearson model. The IAEA model gives unrealistic young groundwater. In all these models we assume that all of the alkalinity ($HCO_3$) is derived from carbonates. However, it is possible that part of the alkalinity could be derived from reaction with silicate minerals. For the IAEA model to be plausible we would require an additional source of $HCO_3$. We also assume that a +8 per mil fractionation between DIC and gaseous $CO_2$ does not occur. The Tamers model is preferred over the Pearson model as all groundwater at S22 is modern which is consistent with the $^3H$ data.

## Groundwater recharge rates

Groundwater ages were converted to recharge rates using the Vogel method (refer to Chapter 2 for further details as well as the original source Vogel (1967)) using the following equation:

$$R = \frac{H\theta}{t} ln\left(\frac{H}{H - z}\right)$$

where *R* = recharge, *H* = total thicknees of aquifer, *ϑ* = porosity, *t* = "groundwater age" or mean residence time (taken from the Tamers model, Table 5), and *z* = sampling interval below watertable.

When *H* >> *z*, then above can be approximated by.

$$R = v\theta$$

## Site DH1

For the following we assume, watertable is 8 mBNS, *H* is 57 metres (saturated thickness of unconfined aquifer) and *ϑ* is 0.2. In the central palaeovalley, the shallowest piezometer (DH1e) has a completion interval of 4 m (+/-1.5 m) below the watertable with a $^{14}C$ "groundwater age" of 940 years BP. This converts to a recharge rate of 0.66 mm/year which compares a CMB value of 0.69 mm/year.

The wells completed in the main unconfined aquifer in the palaeovalley at depth of 46 m (+/-3 m) below the watertable (DH1c) and 50.7 m (+/-2.2 m) below the watertable (DH1b) have similar corrected ages of 1933 and 2064 years BP respectively. These values convert to recharge rates of 9.7 mm/year (DH1c) and 12.2 mm/year (DH1b). In contrast, the CMB recharge is significantly less with 0.92 mm/year for both wells.

For the nested pair located just outside the palaeovalley extent (DH1g and DH1f) we assume that both wells are unconfined, with a sand aquifer grading into highly weathered basement. Here $H$ is 100 m, $\vartheta$ is 0.2 and watertable is 8 mBNS. For the shallow well (DH1g) all the $^{14}C$ correction schemes have a thermonuclear component indicating modern groundwater. If we assume an age of 60 years BP this would convert to a recharge rate of 17 mm/year, however if the age was assumed to be 30 years BP this would convert to a recharge rate of 34 mm/year. However, the recharge calculated using CMB is very low at 0.38 mm/year. The $^{3}H$ data for this well is below detection limit.

## Recharge zone

As discussed previously the major proposed recharge location to the unconfined and confined palaeovalley occurs at the beginning of transects where the sediments are in contact with the more indurated fractured rock aquifer. A good example of this is the east-west truncation near Umuwa. Well 5345-79 has a Cl concentration of 26 mg/L that converts to a CMB recharge rate of 7.2 mg/L. This well has an uncorrected $^{14}C$ of 108 pMC indicating that it has been recharged in the last 60 years. For an average completion interval of 4 m below the watertable, a recharge rate of 13.3 mm/year is obtained. However, if the groundwater had an age of 30 years BP this would double recharge to 26.6 mm/year.

Groundwater recharge calculated using the CMB method is either similar to or much less than environmental tracer approach such as $^{14}C$. One of the major assumptions of the CMB method is that it only has one source of Cl, namely the atmosphere. Any other additional sources of Cl from rocks or clay horizons will result in minimum Cl values. This assumption should be tested in future work. A similar result was found in the saprolite and fractured rock aquifers of the Clare Valley in South Australia (Love et al. 2000). For $^{14}C$ estimates of recharge we assume a porous media aquifer, however, if the sample came from a more indurated fractured rock aquifer or discrete fractures, the value of porosity would be much less than that of the porous media. Estimating recharge in distribution of lithologies, i.e. porous media to purely fractured rock is complex. For more information the reader is referred to Love et al. (2000) and Cook et al. (2005).

Further investigation is required to ascertain the nature of the aquifers before reliable recharge rates can be estimated. This report presented a range of recharge values that serve as a first pass until additional work is completed. Given this, findings to date for estimated recharge rates for the region can be summarised:

- 10-20 mm/year in the ranges
- <2 mm/year in the plains and recharge to local community supply
- 8-20 mm/year to the palaeovalleys which are recharged from the fractured rock aquifers

Note the above recharge rates are calculated across the entire landscape, and so they do not consider the net recharge since discharge is not accounted for. It is recommended that future studies in the APY Lands consider both the location and the quantification of groundwater recharge and discharge.

## 3.5 Numerical modelling of the Lindsay East Palaeovalley at the hydrogeological control site

Flow and groundwater age modelling were undertaken in order to test different plausible conceptual models of the groundwater regime within the palaeovalley to aid the understanding of the available resource.

The purpose of modelling was to use the available data, namely hydraulic head data and groundwater age data at the hydrogeological control site (DH1), to assess various conceptualisations of the system. In other words what are the plausible scenarios that fit the data? This model is an initial attempt to model the palaeovalleys, however, it must be mentioned that further data collection would be required to provide more confidence and extend our results to obtain sustainability parameters. As a first pass, this two-dimensional (2D) model assumes a flat sloping watertable.

However, this approximation of the watertable and 2D assumptions need further investigation. For example, it can be observed that for even for small variations in the watertable local flow systems can occur (reference Chapter 2).

### 3.5.1 DESIGN AND CONSTRUCTION

The groundwater flow model was constructed as a 2D vertical transect model. The model domain was aligned along the main trunk of the Lindsay East Palaeovalley, following the deepest recorded basement elevations based on the AEM conductivity depth profiles (Fig. 3-27). The top elevation followed the DEM.

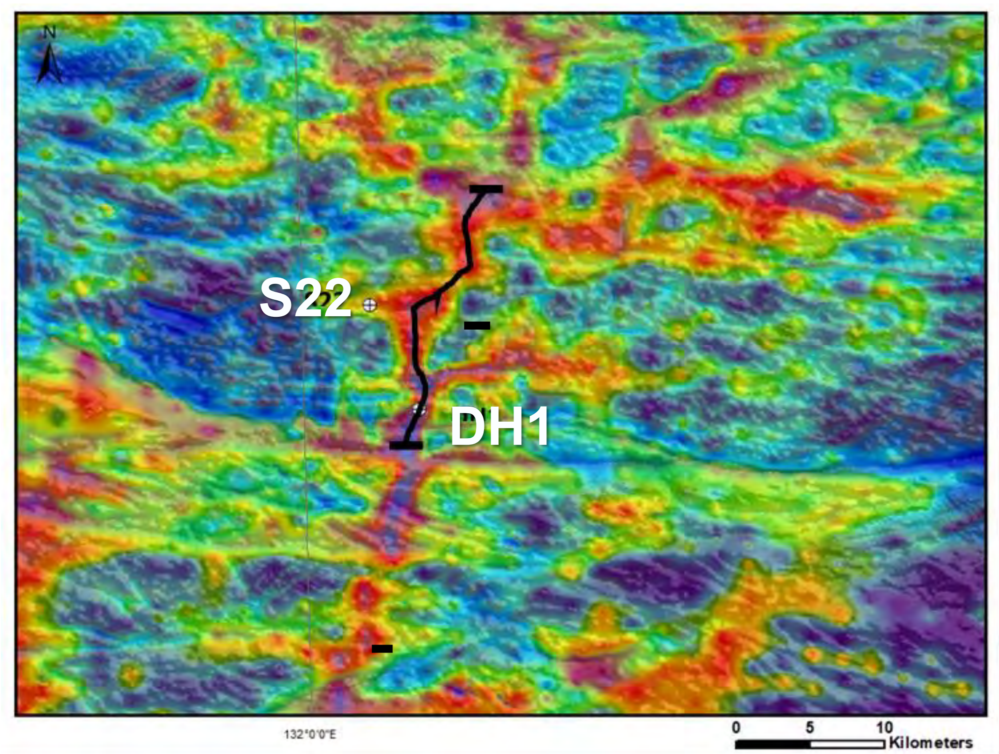


**Figure 3-27. Location of the model profile across hydrogeological control sites DH1 and S22 including AEM depth slice 60-70 mBNS and TMI (textured).**

Overall, the selected model domain covers a flow distance of 17 km from the north to south, originating at a prominent AEM feature, where an east-west trending tectonic feature intersects the main trunk of the palaeovalley (Fig. 3-27). Site DH1 is intersected at the downstream extend of the model.

Based on the hydrogeological site characterisation and $^{14}C$ data at site DH1, a range of plausible conceptual models for the physical flow processes within the palaeovalley were formulated. These were translated into a corresponding numerical model using the USGS MODFLOW (Harbaugh 2005) model as the basis for the flow simulation, while the reactive transport model code PHT3D (Prommer et al. 2003) was applied for the simulation of groundwater age.

The palaeovalley aquifers, including a 20 m thick marine mud formation, were discretised into 5 model layers in order to obtain a sufficient vertical resolution of the lithology (Figs. 3-27 and 3-28). Thereby, layers 1 to 3 covered the upper 65 m thick fluvial sandstones,. layer 4 is the mud that overlies the base layer (Layer 5) represents the basal fluvial sandstone aquifer (Fig. 3-28 and 3-29). The horizontal cell discretisation was homogeneous at 200 m cell width. Recharge was approximated to be 5 mm/year over the model domain. Influx via the northern boundary was allowed in model variants 2 and 6 via a general-head boundary in the upper fluvial sandstones (Layer 1 to 3), while rainfall recharge was the sole influx for all other conceptual models. Outflow via model boundaries was allowed via the upper fluvial sandstone aquifer at the downstream southern extend of the model domain, implemented through a general-head boundary condition (Fig. 3-30). Lateral groundwater flux perpendicular to the main trunk of the palaeovalley was considered negligible on the basis of the AEM depth profile at site DH1 and the $^{14}C$ age data at site S22, which indicated old water at the shallow margin of the palaeovalley, suggesting a limited hydraulic connectivity.

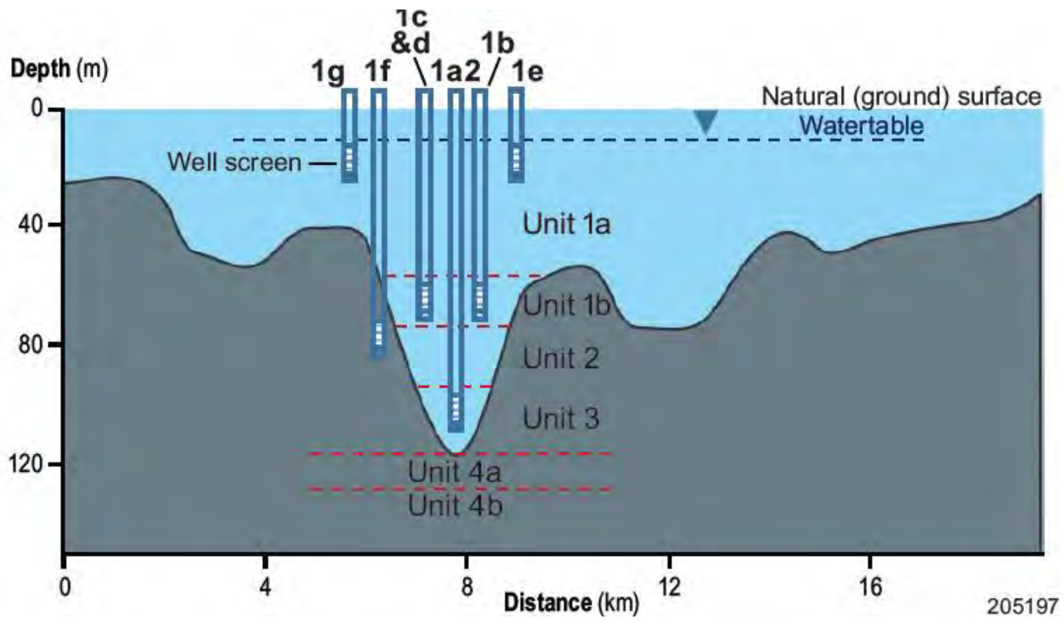


**Figure 3-28. Schematic profile through site DH1 depicting location of sample horizons (Costar et al. 2019) as shown earlier.**

The initial head distribution was based on the surface elevation along the profile, while the age of groundwater was assumed uniform (0 years) within the model domain. The model was run over a sufficiently long time period to obtain a steady-state head and age distribution throughout the model. The simulation period was set to 8M years, discretised into 6000 time steps of 1333 years. The age simulation of groundwater was implemented via a zeroth-order rate reaction, which increased the age of water by 1 year every 365 days. Dispersion was set to 1 m, while the Total Variation Diminishing (TVD) scheme was selected as the solution scheme for the advective flow component.

A suite of plausible conceptual and numerical model variants for the sites groundwater flow regime were investigated (conceptual model variants 1 to 6, see Table 1). The flow and solute transport model head and groundwater age results were compared to measured groundwater heads and corrected $^{14}C$ groundwater ages at site DH1 and the regional head distribution (Fig. 2-17) for each scenario. The comparison between model simulation results and observations thereby allowed us to prioritise some conceptual models above others for their potential to represent a realistic flow regime and with that, aided in the understanding of the sustainability of the resource. Clearly, at this stage, the numerical implementation of the palaeovalley geometry and lithology is idealised and based on depth records from site DH1, while spatially more distributed observation data is lacking. The available measured data along the profile is currently not sufficient to constrain these conceptual models more tightly. The conceptual models presented here could be verified in the future through additional age and water level data at various distances along the profile.

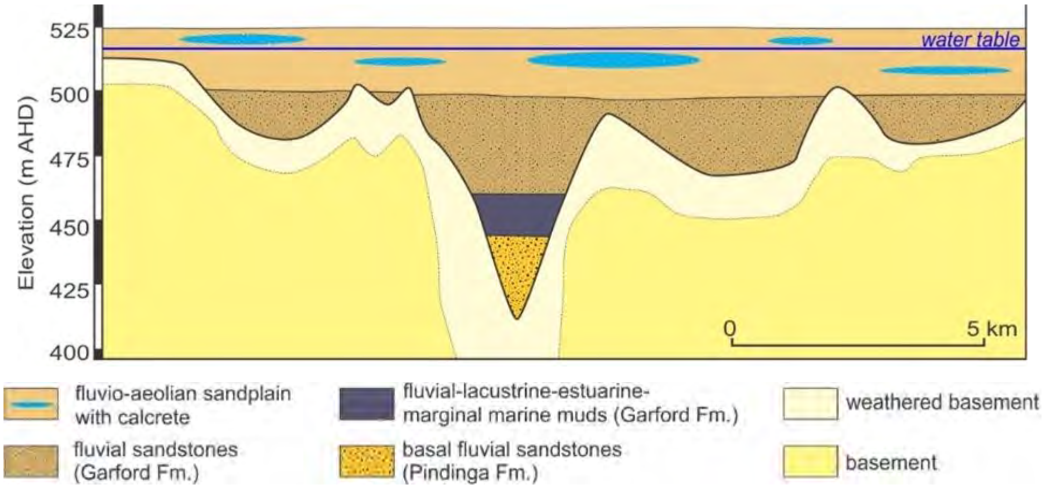


**Figure 3-29. Schematic cross section through palaeovalley at site DH1 (Krapf et al. 2019), which forms the basis of the model set-up.**

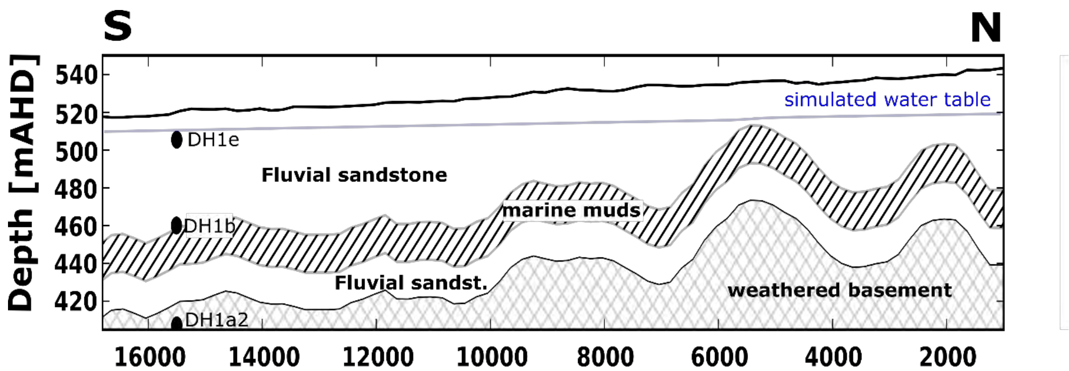


**Figure 3-30. Dimension of model domain and spatial distribution of lithology along model transect form N-S.**

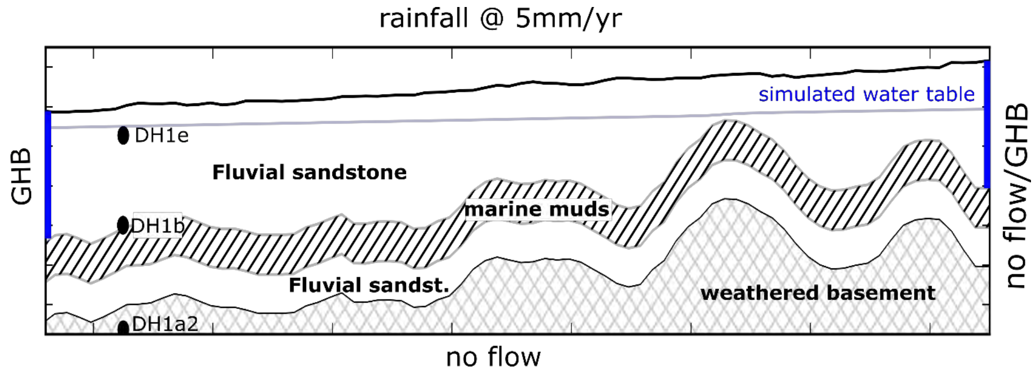


**Figure 3-31. Model boundaries (see also Table 6).**

**Table 6. Model variants No. 1 to No. 6.**

| Model variant | Model features | Comment |
|---|---|---|
| No. 1 | Aquifer properties:<br>Kh fluvial sands: 25m/day; Kh clay: 0.00001 m/day<br>Flux:<br>Rainfall recharge sole influx | Aquifer properties according to pump tests data at DH1. Clay horizon continuous over model domain. |
| No. 2 | Aquifer properties:<br>Kh fluvial sands: 25m/day; Kh clay: 0.00001 m/day<br>Flux:<br>Rainfall recharge and influx via general head boundary at northern end of model domain within upper fluvial sandstone (Layers 1-3) | Aquifer properties according to pump tests data at DH1. Clay horizon continuous over model domain. Influx into model domain via lateral groundwater flow and rainfall recharge. |
| No. 3 | Aquifer properties:<br>Kh fluvial sands: 1.8m/day; Kh clay: 0.00001 m/day<br>Flux:<br>Rainfall recharge sole influx | Aquifer properties adjusted to reflect the lateral head distribution along the model profile under rainfall recharge conditions. Clay horizon continuous over model domain. |
| No. 4 | Aquifer properties:<br>Kh fluvial sands: 1.8m/day; Kh clay: 0.00001 m/day<br>Flux:<br>Rainfall recharge sole influx | Aquifer properties adjusted to reflect the lateral head distribution along the model profile under rainfall recharge conditions. Clay horizon not continuous to reflect the vertical head distribution at site DH1. |
| No. 5 | Aquifer properties:<br>Kh fluvial sands: 1.8m/day; Kh clay: 0.00001 m/day<br>Flux:<br>Rainfall recharge sole influx | Aquifer properties adjusted to reflect the lateral head distribution along the model profile under rainfall recharge conditions. Clay horizon not continuous to reflect the vertical head distribution at site DH1. |
| No. 6 | Aquifer properties:<br>Kh fluvial sands: 25m/day; Kh clay: 0.00001 m/day<br>Flux:<br>Rainfall recharge and influx via general head boundary at northern end of model domain within upper fluvial sandstone (Layers 1-3) | Aquifer properties according to pump tests data at DH1<br>Clay horizon not continuous to reflect the vertical head distribution at site DH1. Influx into model domain via lateral groundwater flow and rainfall recharge. |

## 3.5.2 RESULTS AND DISCUSSION

Model variant No. 1 (Table 6) was implemented on the basis of the established hydraulic conductivities within the fluvial sands via a 12 hour pumping phase CRD (Constant rate discharge test) at site DH1 (up to 25 m/day). The conductivities of the marine clays at the site were approximated based on the recorded lithology ($10^{-5}$ m/day). The ratio of horizontal to vertical conductivity was set at 1:100. Based on this conductivity distribution and assuming rainfall recharge to be the sole influx to the palaeovalley within the model domain, the groundwater head and age distribution is shown in Figure 3-32. The high conductivities in the fluvial sands in combination with the rainfall recharge of 5 mm/year result in a subdued hydraulic gradient. Hydraulic heads vary in this model scenario by ~3 m over the model distanced of 17 km, which is contrary to the observed regional head difference of ca. 25 m over the same distance (Fig. 2-17). This could mean that either: i) the established conductivities for the fluvial sands at site DH1 are not continuous along the model profile, but rather lower at least in parts of the transect (model variant No. 3), or ii) the model domain receives lateral groundwater influx at the northern model extend in addition to rainfall recharge (model variant No. 2). Both these scenarios would result in more realistic hydraulic head gradients along the valley.

If influx of water in the upper fluvial sands is allowed of the order of 12 L/d/$m^2$ of cross-sectional area (model variant No. 2), a realistic hydraulic gradient results (Fig. 3-32). At the same time, this results in relatively young waters if the flux across the northern model domain is assumed to be recently recharged waters (0 years old), i.e. if the northern boundary is assumed to be a recharge area. This is contrary to what is observed in DH1. Under the assumed aquifer properties, for groundwaters to obtain approximately the age recorded in DH1, recently recharged waters would have to enter the palaeovalley ca 30 kms further to the north, i.e. ca 50 km north of DH1 in the area of the Musgrave Ranges. Then, under the relatively high flow velocities (~0.05 m/day), groundwater would attain an age of >3000 years BP within the upper fluvial sands at DH1, as observed.

If it is assumed that rainfall recharge is the sole influx to the palaeovalley, a realistic hydraulic gradient can only be achieved if the hydraulic conductivity of the fluvial sands is reduced by a factor of ~10 (model variant No. 3). Under this scenario the hydraulic gradient approximates the observed regional gradient, while the reduced flow velocity results in simulated groundwater ages within the upper fluvial sandstone aquifer of between 3000 and 7500 years at DH1, which is in the order of what is observed (Fig. 3-32).

Model variant No. 3, however, also highlights, that the simulation of a continuous clay layer results in very old waters in the basal fluvial sands, several orders of magnitude older than observed (>100 000 years BP). Also, high vertical hydraulic gradients would develop as a consequence of a continuous aquitard. However, site DH1 documents negligible vertical gradients between the upper and basal fluvial sandstone units. This suggests that the clay layer is very likely discontinuous along the length of the palaeovalley (model variant No. 4 and No. 5).

Assuming a discontinuous clay layer along the main trunk of the palaeovalley, by implementing multiple narrow (model variant No. 4) or wider (model variant No. 5) windows within the clay, the vertical hydraulic gradients reduce, while the overall regional hydraulic gradient is maintained. The age distribution clearly highlights the conduits through the clay layer which convey younger waters into the lower fluvial sandstone unit. This results in an age distribution which is much more aligned to the observed age data range within the upper and lower fluvial sands (Fig. 3-32).

Based on the findings of model variants No. 1 to No. 5 in combination with the evidence from the discharge tests conducted at DH1, the most plausible conceptual model (model variant No. 6) recognises the hydraulic conductivities for the fluvial sandstones determined through aquifer testing (up to 25 m/day) and conceptualises the clay aquitard as discontinuous. This, in combination with lateral influx of groundwater into the palaeovalley in addition to rainfall recharge, allows the regional head gradient, the vertical head gradient at DH1 and the observed $^{14}C$ age distribution to be reasonably replicated (Fig. 3-32).

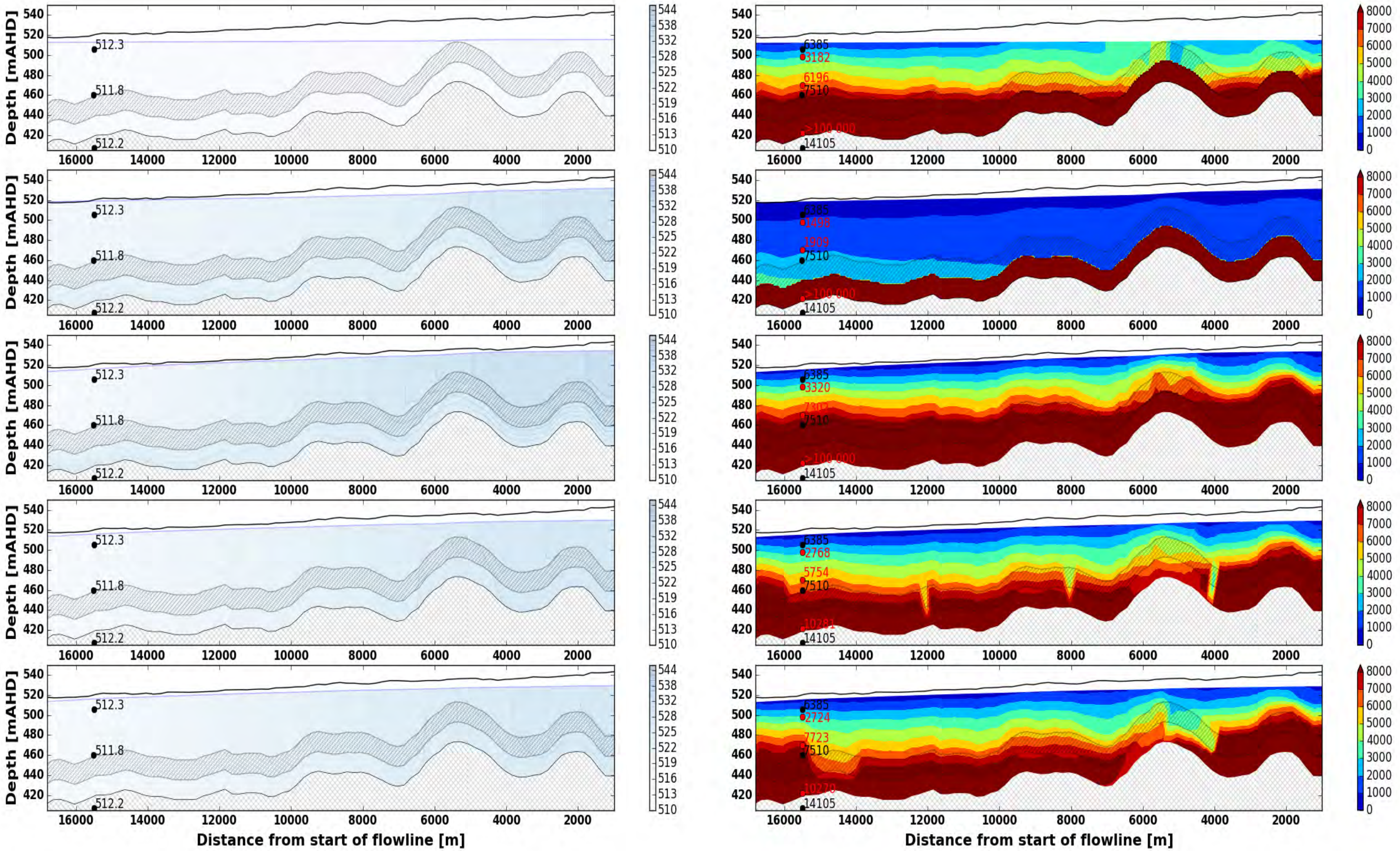


**Figure 3-32. Simulated groundwater heads (mAHD) and groundwater age (years BP) for model variants No. 1 to No. 5. Observed groundwater age data based on $^{14}C$ measurements are marked in black for DH1e, DH1b and DH1a2, while the vertical simulated age distribution at site DH1 is provided in red for three depths.**

# 4 Conclusions and recommendations

A novel understating of the hydrogeological conceptualisation (Fig. 3-33) both at the regional and local scale has been developed with the collective use of different datasets that include geophysical, geological, hydrogeological and hydrochemical data. The ability to drill new groundwater wells that were study specific was a significant and crucial component in gathering groundwater data in the Lindsay East Palaeovalley at the local scale. While more drilling is required, historically, geological and hydrogeological interpretation has largely relied upon airborne datasets due to the difficulty in accessing the APY Lands as result of the remoteness of the area and permissions required for accessing the land.

Greater understanding of geological unit distribution across the study area (a subset of the APY Lands) as well as the evolution of the palaeovalleys has been achieved. In particular, the discovery of recurrent marine influences turned the Lindsay East Palaeovalley into an estuarine system during the Late Miocene – Early Pliocene and marine influence reached close to the foothills of the Musgrave Ranges more north than was previously observed and anticipated.

The geology of this region is extremely complex as the basement units contain highly metamorphosed rocks that have been intruded, folded and faulted, overlain by Adelaidean sediments that have also been influenced by subsequent deformation. In addition, erosion of and sedimentation onto the basement palaeosurface and the erosional and depositional processes that led to the evolution and preservation of the palaeovalley drainage system added to the complexity.

Converting geological information into a meaningful hydrogeological model and hence understanding is a difficult process. This is even more difficult in the APY Lands due to the complex nature of the geology as well as the overall data sparsity.

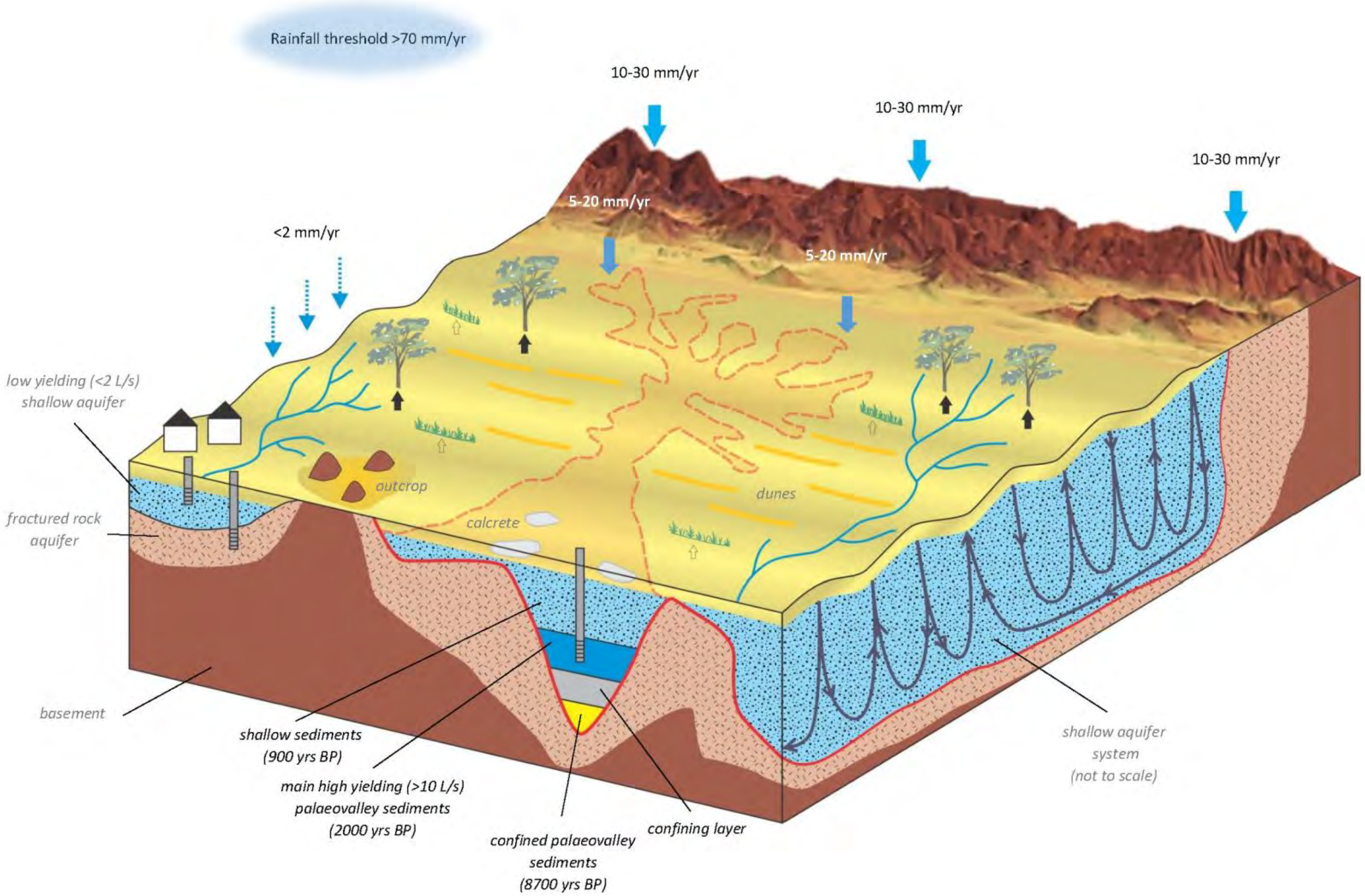


**Figure 4-1**. Conceptual understanding schematic of the hydrogeological processes in the APY Lands.

## Hydrogeology

Figure 3.33 Summarises the important features of the hydrogeology of the APY Lands.

The upper porous media aquifer consists of unconfined sand, silts clays and occasional sandstones. The yield and salinity of these units is highly variable. Geologically these sediments are of undifferentiated Quaternary to Neogene age, The main sand /sandstone horizon below the mud confining bed in the palaeovalleys is pre- Miconee and therefore of Palaeogene age. This major paleovalley unit contains confined groundwater of high hydraulic conductivity and yields with salinity less than 1000 mg/L. Local community and town water supplies occur in the shallow porous media aquifer or the fractured rock aquifer outside of the major paleovalley resources. At these sites groundwater supplies can be unreliable due to the low yielding nature of the aquifers.

## Recharge

All groundwater is derived from meteoric rainfall as indicated by the stable isotopes of the water molecule. The vast majority of groundwater recharge occurs for rainfall events in excess of 70 mm/ month. Rapid recharge occurs in the Musgrave Ranges that is derived from monsoonal rainfall that transgress the continent from the north. Episodic recharge from this process occurs approximately every 2 years, predominately occurring from January to March.

Rapid recharge to the aquifers occurs from monsoonal activity in the north of the continent that deposits intense rainfall events with depleted values of the stable isotopes of groundwater. This rapid recharge mechanism is also supported by modern radiocarbon as well as low Cl concentrations. High rates of groundwater recharge (~10-30 mm/year) occur in the Musgrave Ranges and are associated with fractured rock aquifers

Recharge to the palaeovalleys occurs where the fractured rock aquifer abuts the porous media sediments of the palaeovalley resulting in an angular unconformity. This region corresponds to the surface headwaters of the palaovalleys as well as a change in conductivity. At these locations recharge has been estimated to be in the range of 5-20 mm/yr. A good example of this occurs near the community location of Umuwa. Elsewhere in the plains recharge is by slow diffuse mechanisms and is generally less than 2 mm/yr. This area corresponds to many off the local town water community supplies.

## Groundwater Flow

The watertable follows the topographic surface at a relatively shallow depth, indicating that topographic driven flow is the dominate driving mechanism for groundwater flow. Undulations of the watertable combined with relatively large aspect ratios result in cellular groundwater flow systems. The new watertable map illustrates this point as it shows a mixture of groundwater flow at different scales, i.e. local, intermediate and an occasional regional flow. This includes a general gradient of the watertable towards the south, however, this is superimposed by several local groundwater flow cells as indicated by large and small scale watertable undulations. In these local areas groundwater will flow from local high topographic zones to local depressions in the topographic surface, which corresponds to zones, of potential recharge and discharge, respectively. An example of a regional system occurs along the modem day drainage pattern such as the Ernabella Creek Catchment.

Because the groundwater system has an aspect ratio of approximately 1:1000 with relatively shallow water table that follows a subdued form of the topography large scale regional flow is unlikely to occur. As a result, of this aspect ratio the groundwater flow systems are dominated by local flow cells Because of this a number of reversals of groundwater flow occur against the overall regional gradient.

Discharge

Groundwater discharge occurs via evapotranspiration in the low lying local topographic depressions that correspond to local and to a lesser extent intermediate discharge zones. In these regions discharge occurs via evapotranspiration, the majority of this discharge occurs via transpiration of groundwater dependent plants. The majority of discharge is thought to occur within the APY regional with only minor lateral discharge to the Officer Basin to the south.

Estimate of Lindsay East Palaeovalley resource

A first order estimate of the volume of groundwater in the Lindsay East Palaeovalley has been attempted. The outline of the Lindsay East Palaeovalley superimposed on the thickness of the porous media shown in Figure 3-35. The maximum thickness of the porous media in this zone is 172 m with a mean thickness of 56 m. The total number of cells in this zone is 253,849 with a cell size of 90m x 90m. This results in the total area of the main trunk equal to 2,056 $km^2$ (2,056, 176,900 $m^2$). If we multiple this by an average thickness of 56 m this equals a volume of 115 $km^3$. If we assume that only 20 % of this volume is available as a groundwater resource, we obtain a volume of 23 $km^3$ This converts to 23,000 gigalitres of groundwater which is approximately 46 times the volume of water stored in Sydney Harbour.

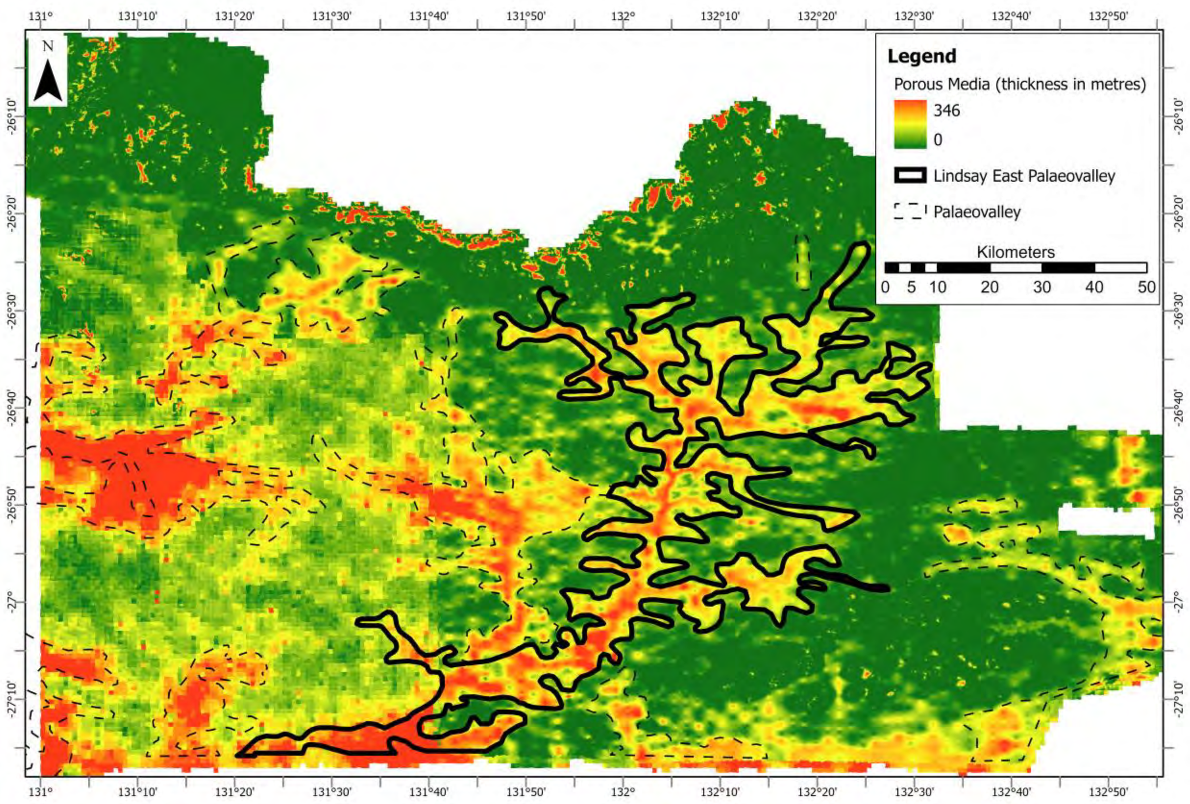


Figure 4-2. Outline of the main trunk of the Lindsay East Palaoevalley.

**Summary**

The discovery of a new fresh groundwater resource (<1,000 mg/L TDS) in the APY Lands has enormous potential for the future development of this remote region in outback South Australia. Availability of a high yielding groundwater resource within the Lindsay East Palaeovalley could unlock the potential for economic development in the region. However, it is vital to follow up with additional hydrogeological investigations to determine the size and sustainability of this groundwater resource.

Future work is required to assess the full potential of these palaeovalley resources. This work includes drilling, aquifer testing and geochemical sampling, for both a greater understanding of the sustainability of the system as well as the potential targeting of new untapped greenfield water resources. Specifically:

- Deep drilling (<120 mBNS) along the course of the Lindsay East Palaeovalley, i.e. to the north and south of the hydrogeological control site DH1, including the detailed establishment of nested piezometers.
- Shallow drilling (<20 mBNS) to map the watertable along the thalweg (thickest part) of the Lindsay East Palaeovalley.
- Long-term aquifer testing designed to assess pumping sustainability of the resource.
- Establishment of nested piezometers in recharge zones.
- Establishment of weather stations (i.e. rainfall) in the ranges and plains to assess the local climate. Sample for major ions to improve Chloride mass balance recharge esimates
- Hydrogeological and geological mapping of the land surface to assess any groundwater manifestations (i.e. what the landscape tells us about the groundwater flow).
- Drilling into other palaeovalley systems, such as the Lindsay West Palaeovalley (west of the project study area) to help determine the feasibility of other palaeovalleys as potential water targets and resources and verify characteristics of the wider palaeovalley drainage distribution across the APY Lands.
- Extending the groundwater environmental tracer suite to argon 39 and krypton 85 (100-3,000 years BP) that is more conducive to the groundwater age windows within the APY Lands.
- Extension of the numerical modelling, once more data (temporal and spatial) is available.
- Mapping of recharge and discharge zones in combination with numerical modelling.

This research to uncover a palaeovalley drainage network in the APY Lands has identified the location of a potentially significant new water resource. Finding reliable water resources under cover in arid environments is challenging but by having a suitable water target, such as the palaeovalleys, ensures a greater probability of success.

A considerable amount of data and analysis has been achieved by this project to further understand the groundwater system, in particular the palaeovalley system. More work and targeted investigations are required to add to the findings and to prove up the groundwater resource for the region.

# References


Australian Bureau of Statistics 2016. 2016 Census QuickStats, APY Lands, code 406021138 SA2. Australian Bureau of Statistics, viewed 7 May 2019, <https://quickstats.censusdata.abs.gov.au/census_services/getproduct/census/2016/ quickstat/406021138>.

Australian Bureau of Statistics 2017. APY Lands (SA2) (406021138). Australian Bureau of Statistics, viewed 5 June 2018, <http://stat.abs.gov.au/itt/r

Bureau of Meteorology 2018. Climate statistics for Australian locations, Summary statistics ERNABELLA, Monthly mean maximum temperature. Bureau of Meteorology, viewed 5 June 2018, <http://www.bom. gov.au/climate/averages/tables/cw_016013.shtml>.

Bureau of Meteorology 2019. Climate statistics for Australian locations, Summary statistics ERNABELLA, Daily rainfall. Bureau of Meteorology, viewed 2 May 2019, <http://www.bom.gov.au/climate/averages/ tables/cw_016013.shtml>.

Bell J.G., Kilgour P.L., English P.M., Woodgate M.F., Lewis S.J. and Wischusen J.D.H. comps 2012. WASANT Palaeovalley Map - Distribution of palaeovalleys in arid and semi-arid WA-SA-NT, 1:4,500,000 scale, Geoscientific thematic map. Geoscience Australia, Canberra.

Bell J.G., Kilgour P.L., English P.M., Woodgate M.F., Lewis S.J. and Wischusen J.D.H. comps 2012. WASANT Palaeovalley Map - Distribution of palaeovalleys in arid and semi-arid WA-SA-NT, 1:4,500,000 scale, Geoscientific thematic map. Geoscience Australia, Canberra.

Bureau of Meteorology 2018. Climate statistics for Australian locations, Summary statistics ERNABELLA, Monthly mean maximum temperature. Bureau of Meteorology, viewed 5 June 2018, <http://www.bom. gov.au/climate/averages/tables/cw_016013.shtml>.

Bureau of Meteorology 2019. Climate statistics for Australian locations, Summary statistics ERNABELLA, Daily rainfall. Bureau of Meteorology, viewed 2 May 2019, <http://www.bom.gov.au/climate/averages/ tables/cw_016013.shtml>.

Cartwright I., Cendon D., Currell M. and Meredith K. 2017. A Review of Radioactive Isotopes and other Residence Time Tracers in Understanding Groundwater Recharge: Possibilities, Challenges, and Limitations, Journal of Hydrology 555:797-811

Conor C.H.H., Camacho A., Close D., Goode A., Major R.B. and Scrimgeour I. 2006. 16th Australian Geological Convention, Musgrave Block Excursion C2, Proterozoic and Palaeozoic geology, Report Book 2002/00020.

Close, D.F., Edgoose, C.J., Scrimgeour, I.R., 2003. Hull and Bloods Range Special, Northern Territory. 1:100 000 geological map series explanatory notes, 4748, 4848. Northern Territory Geological Survey, Darwin. Coats, R.P., 1962. The geology of the Alberga

Cook P G and Herczeg A L editors 2000 Environmental tracers in sub surface hydrology

Cook P.G. and Bohlke J.K. 2000. Determining timescales for groundwater flow and solute transport, In. Cook, P. & Herczeg A.L. ed. Environmental tracers in subsurface hydrology, pg. 1–30.

Cook P.G. and Solomon D.K. 1997. Recent advances in dating young groundwater: chlorofluorocarbons, 3H/3He and 85Kr. J. Hydrol. 191, 245–265.

Cook, P.G., Love, A.J., Robinson, N.I., and Simmons, C.T., 2005. Groundwater ages in fractured rock aquifers, *Journal of Hydrology*, 308(1-4), 284-301.

Cooper H.H. and Jacob C.E. 1946. A generalized graphical method for evaluating formation constants and summarizing well field history, Am. Geophys. Union Trans., vol. 27, pp. 526-534.

Costar A., Krapf C., Keppel M., Love A., Inverarity K., Munday T. and Soerensen C. 2018. G-FLOWS S3 – drilling for community in the APY Lands. In Reid AJ, Geological Survey of South Australia Discovery Day 2018: presentation abstracts and posters, Report Book 2018/00034. Department for Energy and Mining, South Australia, Adelaide.

Costar A., Howles S. and Love A. 2020 (in press). G-FLOWS Stage 3, APY Lands Aquifer Testing, north-western South Australia, Technical Report Series. Goyder Institute for Water Research, Adelaide.

Costar A., Love A., Krapf C., Keppel M., Munday T., Inverarity K., Wallis I. and Soerensen C. 2019. Hidden water in remote areas – innovative exploration to uncover the past in the Anangu Pitjantjatjara Yankunytjatjara Lands. MESA Journal 90:23–35. Department for Energy and Mining, Adelaide.

Cresswell R., Wischusen J., Jacobsen G. Fifield K. 1999. Assessment of recharge to groundwater systems in the arid southwestern part of Northern Territory, Australia, using chlorine-36, Hydrogeology Journal, 7, pg 393-404.

Cresswell R.G., Hostetler S., Jacobson G. and Fifield L.K. 2002. Rapid, episodic recharge in the arid north of South Australia. Proceedings of International Association of Hydrogeologists Groundwater Conference “Balancing the Groundwater Budget”, May 14-17 2002, Darwin.

Crosbie R., Morrow D., Cresswell R., Leaney F., Lamotagne S., Lefournour M. 2012. New insights to the chemical and isotopic composition of rainfall across Australia, CSIRO Water for a Healthy Country Flagship, Australia.

Custance H.E. 2012. Hydrochemistry of shallow regolith hosted aquifers in the eastern Musgrave Province of South Australia. Honours Thesis. Flinders University

Davis A., Flinchum B., Munday T., Cahill K., Peeters L., Martinez J., Blaikie T., Gilfedder M., and Ibrahimi T. 2020. Characterisation of a palaeovalley system in APY Lands of South Australia using ground-based hydrogeophysical methods: Stage 1. Goyder Institute for Water Research Technical Report Series No. 20/xx.

Dodds A.R., Hostetler S.D., and Jacobson G. 2001. Community water supplies in the Anangu Pitjantjatjara Lands, South Australia: sustainability of groundwater resources. Bureau of Rural Sciences, Canberra.

Eden R.N. and Hazel C.P. 1973. Computer and graphical analysis of variable discharge pumping tests of wells. Civ Eng Trans Inst of Eng Australia; CE 15 (1), 5–10.

Edgoose, C.J., Close, D.F., Stewart, A.J., Duncan, N., 2002. UMBEARA, Northern Territory. 1:100 000 geological map series explanatory notes, 5646. Northern Territory Geological Survey,

Edgoose, C.J., Scrimgeour, I.R., Close, D.F., 2004. Geology of the Musgrave Block, Northern Territory, Report 15. Northern Territory Geological Survey, 44 pp. Evins, P.M. et al., 2010. Devil in the detail; The 1150–1000 Ma magmatic and structural evolutiDFH

Eriksson E., Khunakasem V. 1969. Chloride concentration in groundwater, recharge rate and rate of deposition of chloride in the Israel coastal plain. J Hydrol 7:178–197.

Fulton, S.A, Wohling, D, Love, A.J, Berens, V. 2013. Chapter 3, Ephemeral river recharge - Allocating Water and Maintaining Springs in the Great Artesian Basin, Volume II: Groundwater Recharge, Hydrodynamics and Hydrochemistry of the Western Great Artesian Basin, National Water Commission, Canberra. ISBN (volume II): 978-1-922136-07-0

Glikson, A.Y. et al., 1996. Geology of the western Musgrave Block, central Australia, with particular reference to the mafic-ultramafic Giles Complex, Bulletin 239. Australian Geological Survey Organisation, 206 pp.

Glorie S, Agostino K and Pawley M 2017. Low-temperature exhumation history of the eastern Musgrave Province. MESA Journal 84:19–22. Department of the Premier and Cabinet, South Australia, Adelaide.

Gonfiantini R., 1972. Notes on isotope hydrology, internal publication. Vienna, International Atomic Energy Agency.

Guan H., Simmons C.T. and Love A.J. 2009. Orographic controls on rain water in the Mt Lofty Ranges. Journal of Hydrology, Vol 374 Issue 3-4 pp 255-264.

Harbaugh, A.W., Banta, E.R., Hill, M.C., and McDonald, M.G., 2000, MODFLOW–2000, the U.S. Geological Survey Modular Ground-Water Model—User guide to modularization concepts and the Ground-Water Flow Process: U.S. Geological Survey Open-File Report 00–92, 121 p.

Harrington G.A., Cook P.G. and Herczeg A.L. 2002. Spatial and temporal variability of ground water recharge in central Australia: a tracer approach. Ground Water, 40(5): 518-528.

Harrington G., and Herczeg A. 2003. The importance of silicate weathering of a sedimentary aquifer in arid Central Australia indicated by very high 87Sr/86Sr ratios. Chemical Geology, 199: 281-292.

Heath P., Wilcox C. and Davies T. 2017. Musgraves water and mineral potential. MESA Journal News 2017:59–60. Department of the Premier and Cabinet, South Australia, Adelaide.

Hou B., Frakes L.A., Alley N.F. and Clarke J.D.A. 2003. Characteristics and evolution of the Tertiary Palaeovalleys in the North-west Gawler Craton, South Australia, Australian Journal of Earth Sciences, 50: 215-230.

Howard, H.M. et al., 2011. The geology of the west Musgrave Province and the Bentley Supergroup – a field guide, Record 2011/4. Geological Survey of Western Australia, Perth, Western Australia, 116 pp

Hutton J.T. 1983. Soluble ions in rainwater collected near Alice Springs, N.T., and their relationship to locally derived atmospheric dust. Transactions of the Royal Socisty of South Austrlia 107, part 2: 138.

Hou B., Zang W., Fabris A., Keeling J., Stoian L., Michaelsen B. and Fairclough M. comps 2012. Palaeodrainage and Cenozoic coastal barriers of South Australia, 1:2,000,000 Series, DIGIMAP 00002. 2nd edn. Geological Survey of South Australia, Adelaide.

Howles, Gogoll and Vasilic 2017. APY Lands and Yalata water search 2015-17, DEWNR Technical note 2017/15, Government of South Australia, Department of Environment, Water and Natural Resources, Adelaide.

Ingerson, E. and Pearson F.J. Jr 1964. Estimation of age and rate of motion of groundwater by the $^{14}C$ method, Recent Researchers in the fields of Hydrosphere, Atmosphere and Nuclear Geochemistry, Maruzen, Tokyo: 263.

Keppel M., Costar A., Krapf C. and Love A. 2019. G FLOWS Stage 3, APY Lands Drilling Program, north-western South Australia, Technical Report Series. Goyder Institute for Water Research, Adelaide.

Keywood M.D. 1995. Origins and sources of atmospheric precipitation from Australia: Chlorine 36 and major element chemistry. PhD dissertation. Research School of Earth Sciences, Australian National University, Canberra.

Korsch R.J., Kositcin N. (Eds.), 2010. GOMA (Gawler Craton-Officer Basin-Musgrave Province-Amadeus Basin) Seismic and MT Workshop 2010, Record 2010/39. Geoscience Australia, 162 pp.

Krapf C., Costar A., Stoian L., Keppel M., Gordon G., Inverarity K., Love A. and Munday T. 2019. A sniff of the ocean in the Miocene at the foothills of the Musgrave Ranges – unravelling the evolution of the Lindsay East Palaeovalley. MESA Journal 90:4–22. Department for Energy and Mining, Adelaide.

Krapf C.B.E., Irvine J.A., Cowley W.M. 2012, Compilation of the 1:2 000 000 State Regolith Map of South Australia – a summary, Report Book 2012/00016, Department of Manufacturing, Innovation, Trade, Resources and Energy, South Australia, Adelaide.

Krapf C., Costar A., Stoian L., Keppel M., Gordon G., Inverarity K., Love A. and Munday T. 2019. A sniff of the ocean in the Miocene at the foothills of the Musgrave Ranges – unravelling the evolution of the Lindsay East Palaeovalley. MESA Journal 90:4–22. Department for Energy and Mining, Adelaide.

Krapf C.B.E., Costar A., Munday T., Irvine J.A., Ibrahimi T. 2020. Palaeovalley map of the Anangu Pitjantjatjara Yankunytjatjara Lands (1st Edition), 1:500 000 scale. Department for Energy and Mining.

Kretschmer P. and Wohling D. 2014. Groundwater recharge in the eastern Anangu Pitjantjatjara Yankunytjatjara (APY) Lands DEWNR Technical Report (2014).

Kruseman G.P. and Ridder N.A. 1994. Analysis and evaluation of pumping test data. 2nd edition, International Institute for Land Reclamation and Improvement, Wageningen, Netherlands, 372p.

Leaney F W., Herczeg, A.L and Walker, G.R., 2003. Salinisation of a fresh palaeo-ground water resource by enhanced recharge, Ground Water Vol 41 (1) pp 84-92.

Leaney F.W., Taylor A.R., Jolly I.D., Davies P.J. 2013. Facilitating long term outback water solutions (G-FLOWS), Task 6: Groundwater recharge characteristics across key priority areas, Goyder Institute for Water Research Technical Report Series No. 12/8.

Libby W.F. 1965. Radiocarbon Dating, University of Chicago Press, Chicago, 111, 175p.

Loosli H. 1983. A dating method with39Ar, Earth Planet. Sci. Lett., 63(1), 51– 62, doi:10.1016/0012-821X(83)90021-3.

Love, A.J., Herczeg, A.L., Leaney, F.W., Stadter, M.F., Dighton, J.S., and Armstrong, D., 1994. Groundwater residence time and palaeohydrology in the Otway Basin, South Australia:2H, 18O and 14C data. Journal of Hydrology, 153: 157-187.

Love, A.J., Herczeg, A.L., Sampson, L., Cresswell, R.G. and Fifield, L.K., 2000. Sources of chloride and implications for 36C1 dating of old groundwater, southwestern Great Artesian Basin, Australia. Water Resources Research 36 (6): 1561-1574

Love et al. (eds) 2013. Allocating Water and Maintaining Springs in the Great Artesian Basin, Volume II: Groundwater Recharge, Hydrodynamics and Hydrochemistry of the Western Great Artesian Basin, National Water Commission, Canberra.

Love, A.J., Robinson, N.I., Yueqing, X., Costar, A., 2020 Groundwater flows systems in the APY (in prep)

Major R.B. and Conor C.H.H. 1993. 'Musgrave Province', in Drexel, JF & Preiss, WV (eds), The Geology of South Australia, Vol. 1, The Precambrian, Bulletin 54, Geological Survey, Adelaide, pp.156-167.

Magee J.W. 2009. Palaeovalley groundwater resources in arid and semi-arid Australia – a literature review, Record 2009/03. Geoscience Australia, Canberra.

Munday T., Adbat T., Ley-Cooper Y. and Gilfedder M. 2013. Facilitating Long-Term Outback Water Solutions (G-FLOWS) Stage-1: Hydrogeological framework, Technical Report Series No. 13/12. Goyder Institute for Water Research, Adelaide.

Munday T., Taylor A., Raiber M., Soerensen C., Peeters L., Cui T., Cahill K., Flinchum B., Smolanko N., Martinez J., Ibrahimi T. and Gilfedder M. 2020. Integrated hydrogeophysical conceptualisation of the Musgrave Province, South Australia. Goyder Institute for Water Research Technical Report Series No. 20/xx.

Pearson F.J. Jr and Hanshaw B.B. 1970. Sources of dissolved carbonate species in groundwater and their effects on carbon 14 dating. In Isotope Hydrology 1970, pp271-285 International Atomic Energy Agency, Vienna.

Pawley M.J. and Krapf C.B.E. 2016. Investigating the potential for bedrock aquifers in the APY Lands, Report Book 2016/00021. Department of State Development, South Australia, Adelaide.

Prommer, H., Barry, D.A. and Zheng, C. (2003) MODFLOW/MT3DMS Based Reactive Multicomponent Transport Modelling. Groundwater, 41, 247-257.

Robinson N.I. and Love A.J. 2013. Hidden channels of groundwater flow in Tóthian drainage basins. Adv Water Resource. 62:71-78.

Rockwater 2012. Nyikukura Palaeochannel Investigation (unpublished company report).

Rogers P.A. 1995. Hamilton Basin. In JF Drexel and WV Preiss eds, The geology of South Australia, Volume 2, The Phanerozoic, Bulletin 54. Geological Survey of South Australia, Adelaide, p. 198.

Rorabaugh M.J. 1953. Graphical and theoretical analysis of step-drawdown test of artesian well, Proc. Amer. Soc. Civil Engrs., vol. 79, separate no. 362, 23 pp.

Soerensen C.C., Munday T.J., Ibrahimi T., Cahill K. and Gilfedder M. 2017 (in press). Musgrave Province, South Australia: Processing and inversion of airborne electromagnetic (AEM) data: preliminary results, Technical Report Series. Goyder Institute for Water Research, Adelaide.

Scanlon B.R. 2000. Uncertainties in estimating water fluxes and residence times using environmental tracers in an arid unsaturated zone, Water Resources Research, 36, pg 395-409.

Scanlon B.R., Healy R.W. and Cook P.G. 2002. Choosing appropriate techniques for quantifying groundwater recharge. Hydrogeology Journal 10, 18–39. https://doi.org/10.1007/s10040-001-0176-2

Smithies, R.H. et al., 2011. High-temperature granite magmatism, crust–mantle interaction and the Mesoproterozoic intracontinental evolution of the Musgrave Province, Central Australia. Journal of Petrology, 52(5): 931-958

Tamers M.A. Stipp J.J., Weiner R. 1975. Radiocarbon ages of ground water as a basis for the determination of safe limits of aquifer exploitation, Environmental Research, 9, pg 250-264.

Tewkesbury P. and Dodds A.R. 1997. An appraisal of the water resources of the Musgrave Block, South Australia, Department of Mines and Energy Resources, Geological Survey of South Australia, Report book 97/22, DME 93/526.

Tóth J. 1963. A theoretical analysis of groundwater in a small drainage basins. Geophysical Research Letters 68(16) pp, 4795-4812.

Tóth J. 2009. Gravitational systems of Groundwater Flow Theory, Evaluation, Utilization. Cambridge Universal Print. ISBN 978-0-521-88638-3 hardback.

Varma S. 2012. Hydrogeological review of the Musgrave Province, South Australia, Goyder Institute for Water Research Technical Report Series No. 12/8.

Vogel J.C. 1967. Investigation of groundwater flow with radiocarbon: Isotopes in Hydrology, International Atomic Energy Agency, Vienna, pp 355–369.

Watt E.L. and Berens V. 2011. Non-prescribed groundwater resources assessment – Alinytjara Wilurara Natural Resource Management Region. Phase 1 – Literature and Data Review, DFW Technical Report 2011/18, Department for Water, Government of South Australia, Adelaide.

Werner, M., Dutch, R.A., Pawley, M.J., Krapf, C.B.E., 2014. Mafic intrusions in the East Musgraves: new geochemical data set available now!, Unlocking SA's Mineral Wealth Technical Forum. Department for Manufacturing, Innovation, Trade, Resources and Energy, Adelaide, South Australia, pp. 37-40.

Wood C., Cook P.G., Harrington G.A., Meredith K. and Kipfer R., 2014. Factors affecting carbon-14 activity of unsaturated zone CO2 and implications for groundwater dating. J. Hydrol. 519, 465–475, Part A.

Woodhouse A.J. and Gum J.C. 2003. Musgrave Province —geological summary and exploration history, Report Book 2003/00021. Department of Primary Industries and Resources South Australia, Adelaide.

# Appendix A: Measurement procedure for Tiny Perm®

Note: Author Rose Deng (modified from the manual with contribution from Eddie Banks)

Manual available at URL: https://www.vindum.com/wp-content/uploads/TinyPermManual.pdf

**Take measurement**

1. Turn on
2. Screen show "ready!"
3. Pull the plunger all the way out, screen show "push and hold"
4. Number should be centred on 0 (no vacuum)
5. Press the nozzle to the surface, put 'blue tack putty' as the seal (create a small sausage worm, coil it around the rubber tip ensuring nothing goes inside the tip and then firmly place it up against the core material)
6. Depress plunger completely. hold until value is 0
7. Record the value on screen
8. Repeat from 3-7 for another measurement

**Generate air permeability values**

1. For kh (horizontal conductivity), the core needs to be sliced in axial direction (see figure below)

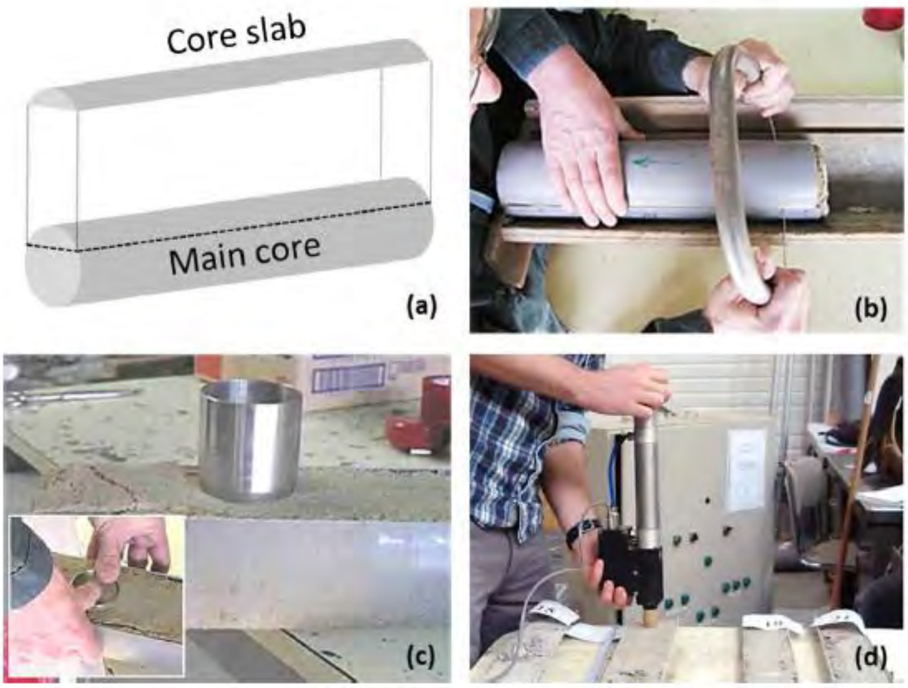


Appendix Figure A-1. Measure the horizontal K. Source: Figure 2 from Rogiers, B., Winters, P., Huysmans, M., Beerten, K., Mallants, D., Gedeon, M., ... & Dassargues, A. (2014). High-resolution saturated hydraulic conductivity logging of borehole cores using air permeability measurements. Hydrogeology Journal, 22(6), 1345-1358.

2. For kv (vertical conductivity), the core needs to be sliced in radial direction.

**Convert readings to air permeability (ka)**

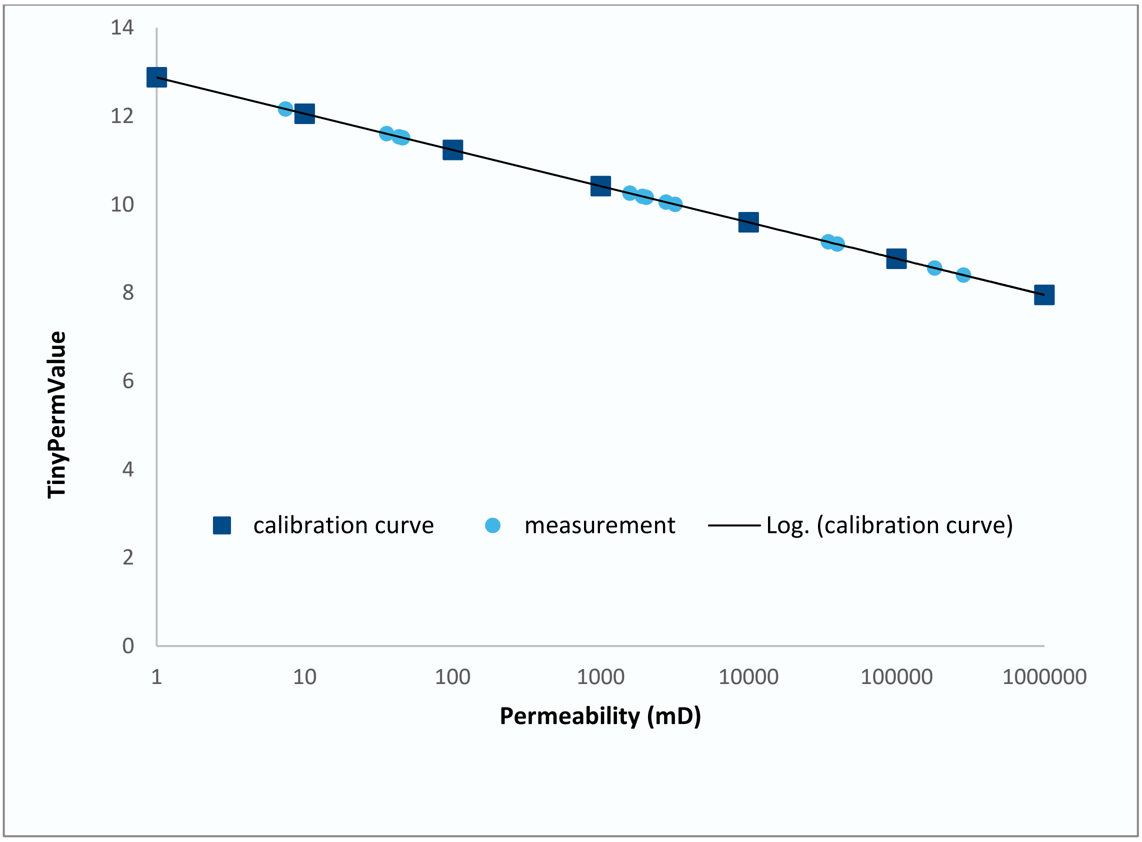


Appendix Figure A-2. Calibration curve from the manual and measurement points.

Follow the equation below to get K

K=10^((D2-12.8737)/-0.8206) (mD)

where, mD=0.001 Darcy; 1 Darcy =0.831 m/day.

**Cautions**

1. Use putty, but not suck the putty into the plunger
2. Fully pull out plunger before measurement

# Appendix B: Air permeability raw data - DH1a core sample

### Appendix Table B-1. Summary of groundwater parameters for the palaeovalley sediments

| Sample No | Depth (m) | Actual Depth (m) | Measurement value | Comment | k group ($k_v$ or $k_h$) | k (mD) | k (m/day) |
|---|---|---|---|---|---|---|---|
| 1 | 88.9 | 99 | 12.98 | with rubber | kv | 0.742096936 | 6.17E-04 |
| 1 | 88.9 | 99 | 12.16 | with rubber | kv | 7.408486029 | 6.16E-03 |
| 1 | 88.9 | 99 | 12.14 | without rubber | kv | 7.83613441 | 6.51E-03 |
| 1 | 88.9 | 99 | 12.39 | without rubber | kv | 3.885498506 | 3.23E-03 |
| 2 | 86.46 | 88.6 | 11.03 | | kv | 176.5105449 | 1.47E-01 |
| 2 | 86.46 | 88.6 | 11 | | kv | 192.0123979 | 1.60E-01 |
| 3 | 88.5 | 88.6 | 10.77 | | kv | 366.110337 | 3.04E-01 |
| 3 | 88.5 | 88.6 | 10.73 | | kv | 409.5970424 | 3.40E-01 |
| 4 | 25.1 | 25.2 | 11.41 | | kv | 60.77078655 | 5.05E-02 |
| 4 | 25.1 | 25.2 | 11.51 | | kv | 45.90212648 | 3.81E-02 |
| 5 | 21.65 | 21.73 | 10.63 | | kv | 542.2741025 | 4.51E-01 |
| 5 | 21.65 | 21.73 | 10.68 | | kv | 471.2895804 | 3.92E-01 |
| 5 | 21.65 | 21.73 | 10.38 | with filter 0.45um | kv | 1093.639014 | 9.09E-01 |
| 5 | 21.65 | 21.73 | 10.4 | with filter 0.45um | kv | 1033.954873 | 8.59E-01 |
| 6 | 93.25 | 93.3 | 11.21 | | kv | 106.5170087 | 8.85E-02 |
| 6 | 93.25 | 93.3 | 10.83 | zeroing is not standard | kv | 309.3817986 | 2.57E-01 |
| 6 | 93.25 | 93.3 | 11.36 | | kv | 69.92393872 | 5.81E-02 |
| 7 | 81.1 | 81.2 | 8.66 | | kv | 136427.3024 | 1.13E+02 |
| 7 | 81.1 | 81.2 | 7.66 | | kv | 2256949.352 | 1.88E+03 |
| 8 | 76.25 | 76.35 | 9.46 | | kv | 14454.55994 | 1.20E+01 |
| 8 | 76.25 | 76.35 | 9.45 | | kv | 14865.89564 | 1.24E+01 |
| 9 | 71.25 | 71.35 | 8.78 | | kv | 97424.19571 | 8.10E+01 |
| 9 | 71.25 | 71.35 | 8.77 | | kv | 100196.6114 | 8.33E+01 |
| 10 | 67.1 | 67.2 | 10.01 | | kv | 3088.613658 | 2.57E+00 |
| 10 | 67.1 | 67.2 | 9.47 | | kv | 14054.6058 | 1.17E+01 |
| 11 | 63 | 63.1 | 9.08 | | kv | 41983.69639 | 3.49E+01 |
| 11 | 63 | 63.1 | 9.73 | | kv | 6776.061416 | 5.63E+00 |
| 12 | 58.6 | 58.7 | 9.83 | | kv | 5118.176772 | 4.25E+00 |
| 12 | 58.6 | 58.7 | 9.54 | | kv | 11548.22489 | 9.60E+00 |

| | | | | | | | |
|---|---|---|---|---|---|---|---|
| 13 | 56.85 | 57 | 10.1 | | kv | 2399.317605 | 1.99E+00 |
| 13 | 56.85 | 57 | 10.12 | | kv | 2268.377497 | 1.89E+00 |
| 14 | 52 | 52.1 | 10.39 | | kv | 1063.37829 | 8.84E-01 |
| 14 | 52 | 52.1 | 10.28 | | kv | 1447.891594 | 1.20E+00 |
| 15 | 45.7 | 45.8 | 10.27 | | kv | 1489.094474 | 1.24E+00 |
| 15 | 45.7 | 45.8 | 9.89 | | kv | 4325.118892 | 3.59E+00 |
| 16 | 35 | 35.1 | 10.74 | | kv | 398.2635924 | 3.31E-01 |
| 16 | 35 | 35.1 | 10.15 | | kv | 2085.243205 | 1.73E+00 |
| 17 | 32.1 | 32.15 | 10.98 | | kv | 203.0961458 | 1.69E-01 |
| 17 | 32.1 | 32.15 | 11.05 | | kv | 166.8776768 | 1.39E-01 |
| 18 | 9.5 | 9.6 | 9.57 | | kv | 10615.89507 | 8.82E+00 |
| 18 | 9.5 | 9.6 | 9.54 | | kv | 11548.22489 | 9.60E+00 |
| 19 | 5.7 | 5.85 | 11.61 | calcrete | kv | 34.67135008 | 2.88E-02 |
| 19 | 5.7 | 5.85 | 12.39 | | kv | 3.885498506 | 3.23E-03 |
| 20 | 2.8 | 2.9 | 10.3 | | kv | 1368.87451 | 1.14E+00 |
| 20 | 2.8 | 2.9 | 10.4 | | kv | 1033.954873 | 8.59E-01 |
| 21 | 5.7 | 5.85 | 11.29 | without putty | kh | 85.09995296 | 7.07E-02 |
| 21 | 5.7 | 5.85 | 11.19 | without putty | kh | 112.6656099 | 9.36E-02 |
| 21 | 5.7 | 5.85 | 11.78 | with putty | kh | 21.51816654 | 1.79E-02 |
| 21 | 5.7 | 5.85 | 11.74 | with putty | kh | 24.07410139 | 2.00E-02 |
| 22 | 93.25 | 93.3 | 10.1 | | kh | 2399.317605 | 1.99E+00 |
| 22 | 93.25 | 93.3 | 10.14 | | kh | 2144.5833 | 1.78E+00 |
| 23 | 56.85 | 57 | 10.48 | | kh | 826.0606648 | 6.86E-01 |
| 23 | 56.85 | 57 | 10.19 | | kh | 1863.854016 | 1.55E+00 |
| 24 | 25.1 | 25.2 | 11.31 | | kh | 80.45571701 | 6.69E-02 |
| 24 | 25.1 | 25.2 | 11.25 | | kh | 95.20815317 | 7.91E-02 |
| 25 | 88.9 | 89 | 11.84 | | kh | 18.18394182 | 1.51E-02 |
| 25 | 88.9 | 89 | 11.63 | | kh | 32.77919944 | 2.72E-02 |
| 26 | 88.5 | 88.6 | 11.44 | | kh | 55.86454189 | 4.64E-02 |
| 26 | 88.5 | 88.6 | 11.58 | | kh | 37.71632495 | 3.13E-02 |
| 27 | 86.46 | 86.6 | 11.75 | | kh | 23.40797689 | 1.95E-02 |
| 27 | 86.46 | 86.6 | 11.89 | | kh | 15.8036356 | 1.31E-02 |
| 28 | 81.1 | 81.2 | 11.85 | | kh | 17.6807966 | 1.47E-02 |
| 28 | 81.1 | 81.2 | 11.94 | | kh | 13.73491516 | 1.14E-02 |
| 29 | 71.25 | 71.35 | 10.4 | | kh | 1033.954873 | 8.59E-01 |

| | | | | | | | |
|---|---|---|---|---|---|---|---|
| 29 | 71.25 | 71.35 | 10.34 | | kh | 1223.541813 | 1.02E+00 |
| 30 | 63 | 63.1 | 10.74 | | kh | 398.2635924 | 3.31E-01 |
| 30 | 63 | 63.1 | 10.99 | | kh | 197.4765251 | 1.64E-01 |
| 30 | 63 | 63.1 | 10.91 | | kh | 247.1753275 | 2.05E-01 |
| 31 | 58.6 | 58.7 | 10.95 | | kh | 220.9328512 | 1.84E-01 |
| 31 | 58.6 | 58.7 | 11.32 | | kh | 78.229527 | 6.50E-02 |
| 31 | 58.6 | 58.7 | 10.99 | | kh | 197.4765251 | 1.64E-01 |
| 32 | 52 | 52.1 | 12.44 | | kh | 3.376880718 | 2.81E-03 |
| 32 | 52 | 52.1 | 11.86 | | kh | 17.19157328 | 1.43E-02 |
| 32 | 52 | 52.1 | 11.69 | | kh | 27.70008562 | 2.30E-02 |
| 33 | 45.7 | 45.8 | 11.31 | | kh | 80.45571701 | 6.69E-02 |
| 33 | 45.7 | 45.8 | 10.98 | | kh | 203.0961458 | 1.69E-01 |
| 33 | 45.7 | 45.8 | 11.14 | | kh | 129.6350377 | 1.08E-01 |

NA – not available

# Appendix C: Chemistry simulations at hydrogeological control site DH1

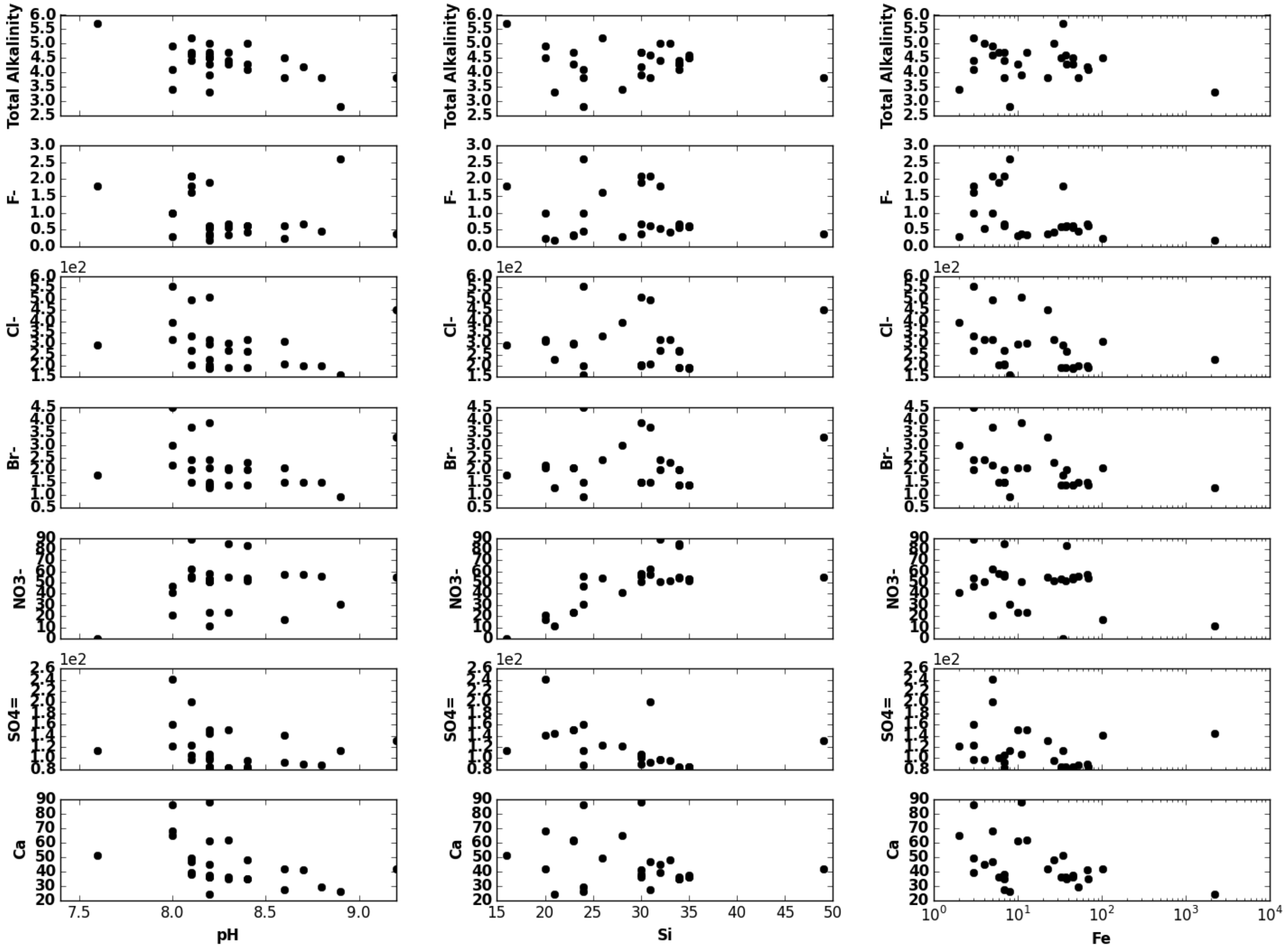


**Appendix Figure C-1. Correlation matrices with pH, Si [mg/L] and Fe [ug/L]. Major ions in [mg/L], except alkalinity in [meq/L]. Minor ions in [ug/L].**

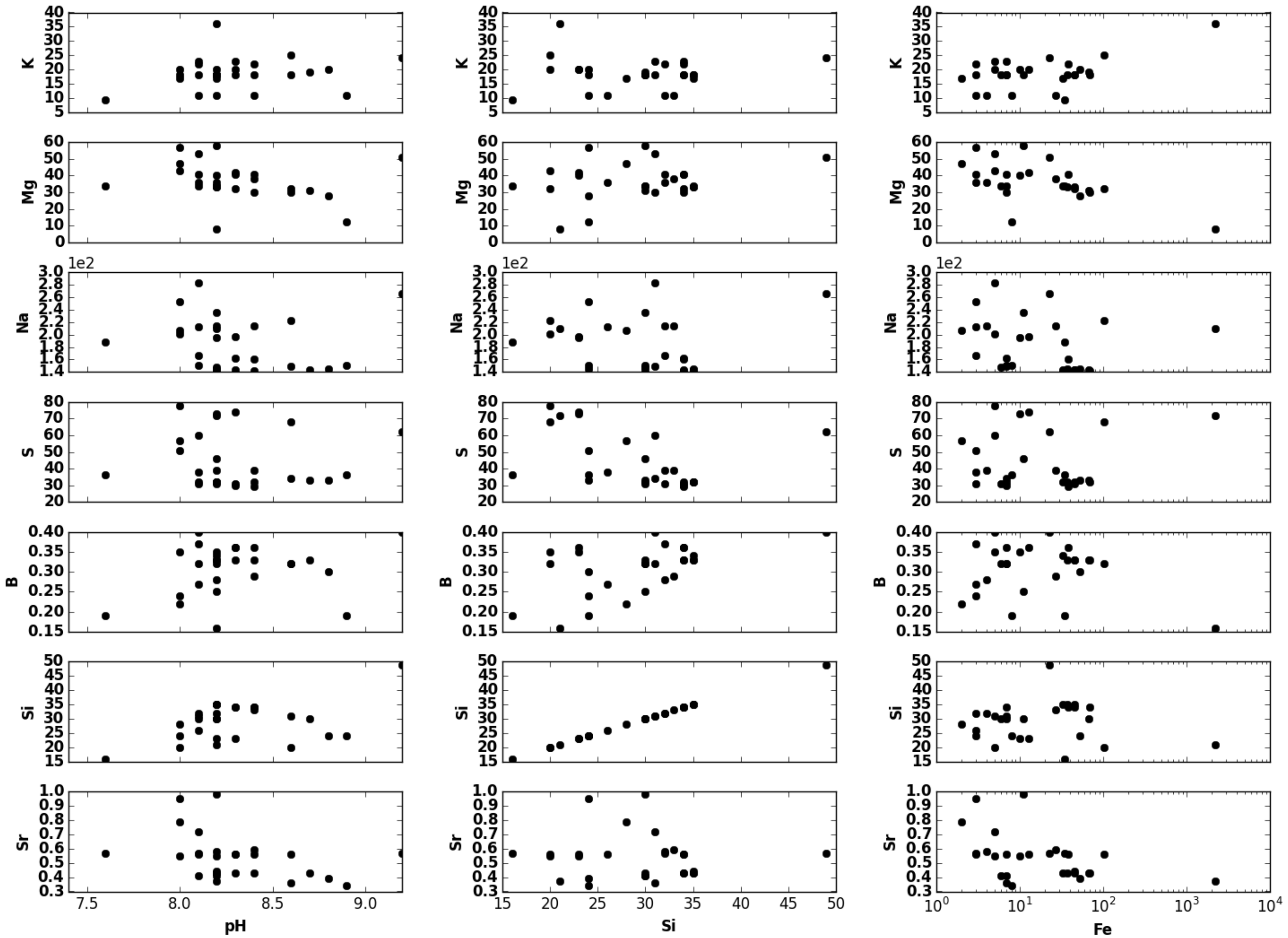


**Continued Appendix Figure C-1. Correlation matrices with pH, Si [mg/L] and Fe [ug/L].**

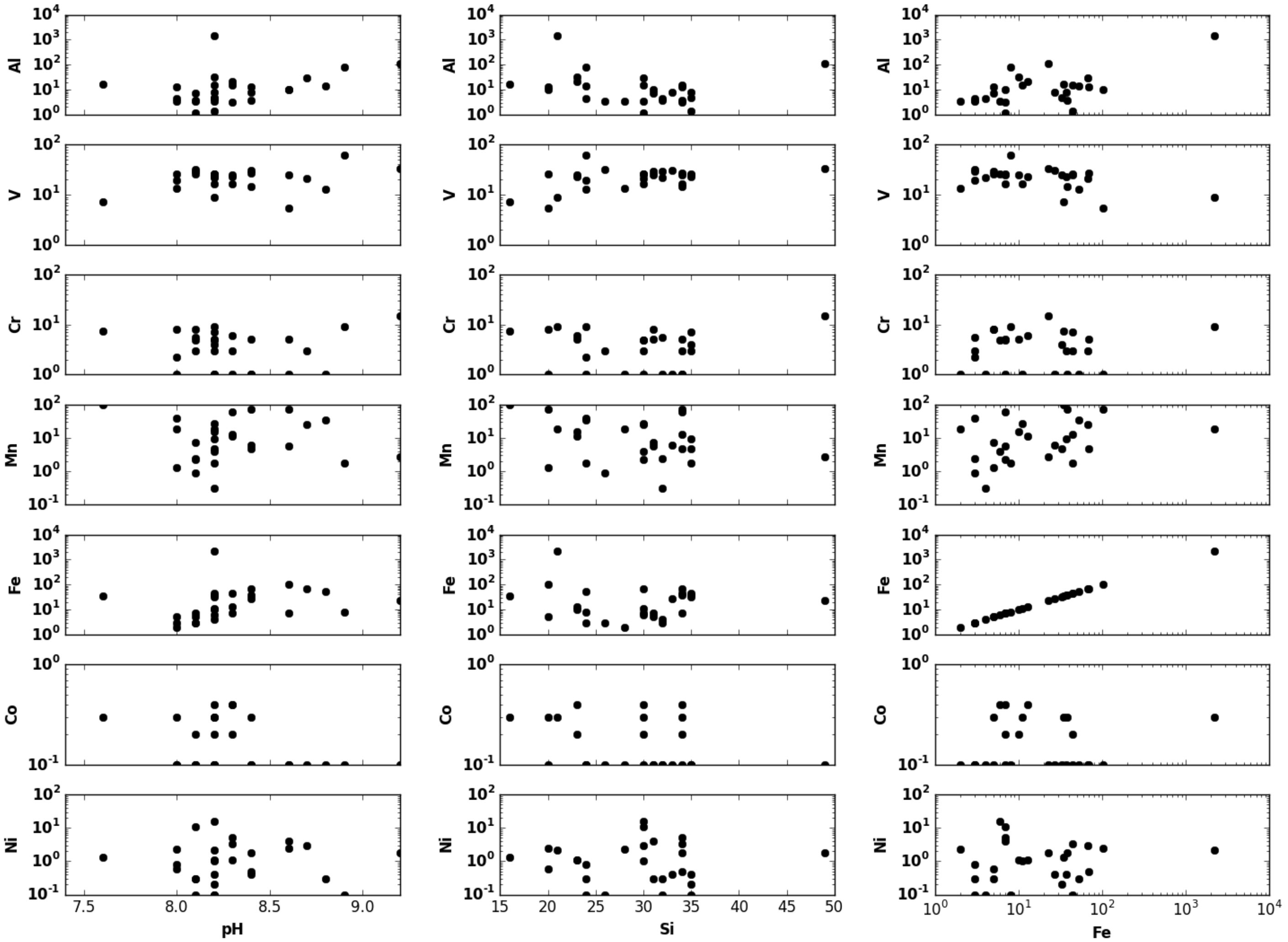


Continued Appendix Figure C-1. Correlation matrices with pH, Si [mg/L] and Fe [ug/L].

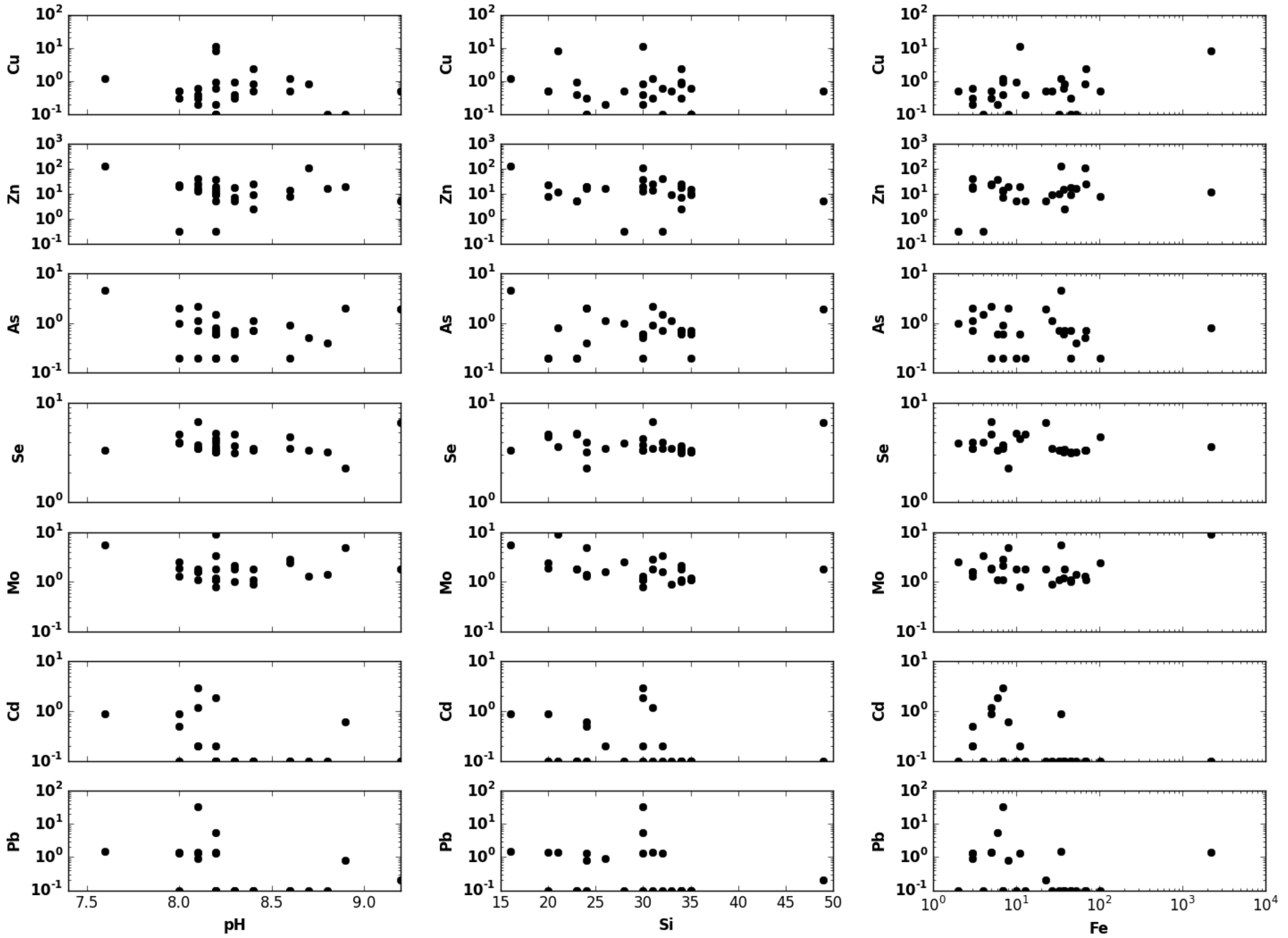


**Continued Appendix Figure C-1. Correlation matrices with pH, Si [mg/L] and Fe [ug/L].**

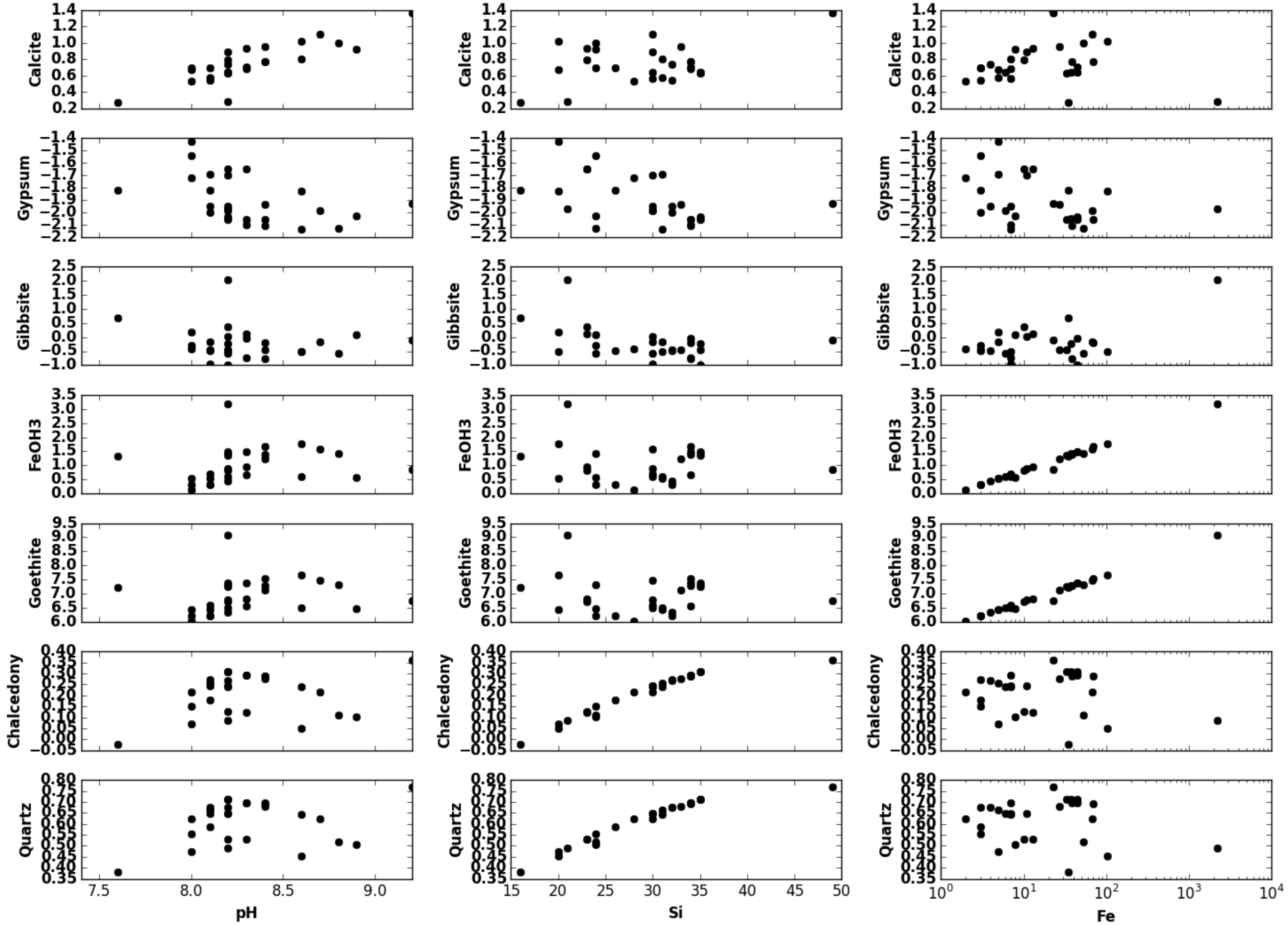


**Appendix Figure C-2. Correlation matrices of saturation indices of major minerals and pH, Si [mg/L] and Fe [ug/L].**

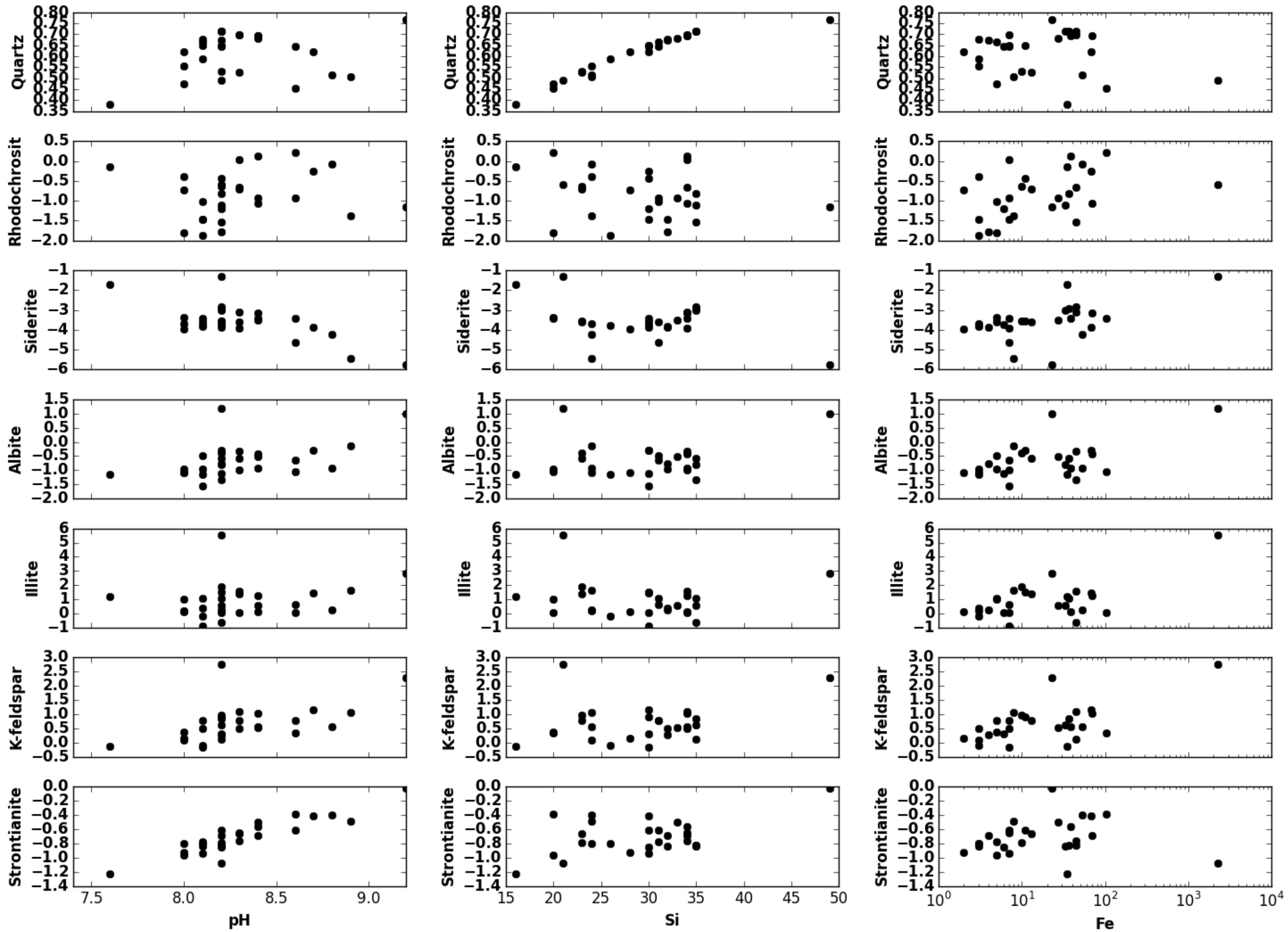


**Continued Appendix Figure C-2. Correlation matrices of saturation indices of major minerals and pH, Si [mg/L] and Fe [ug/L].**

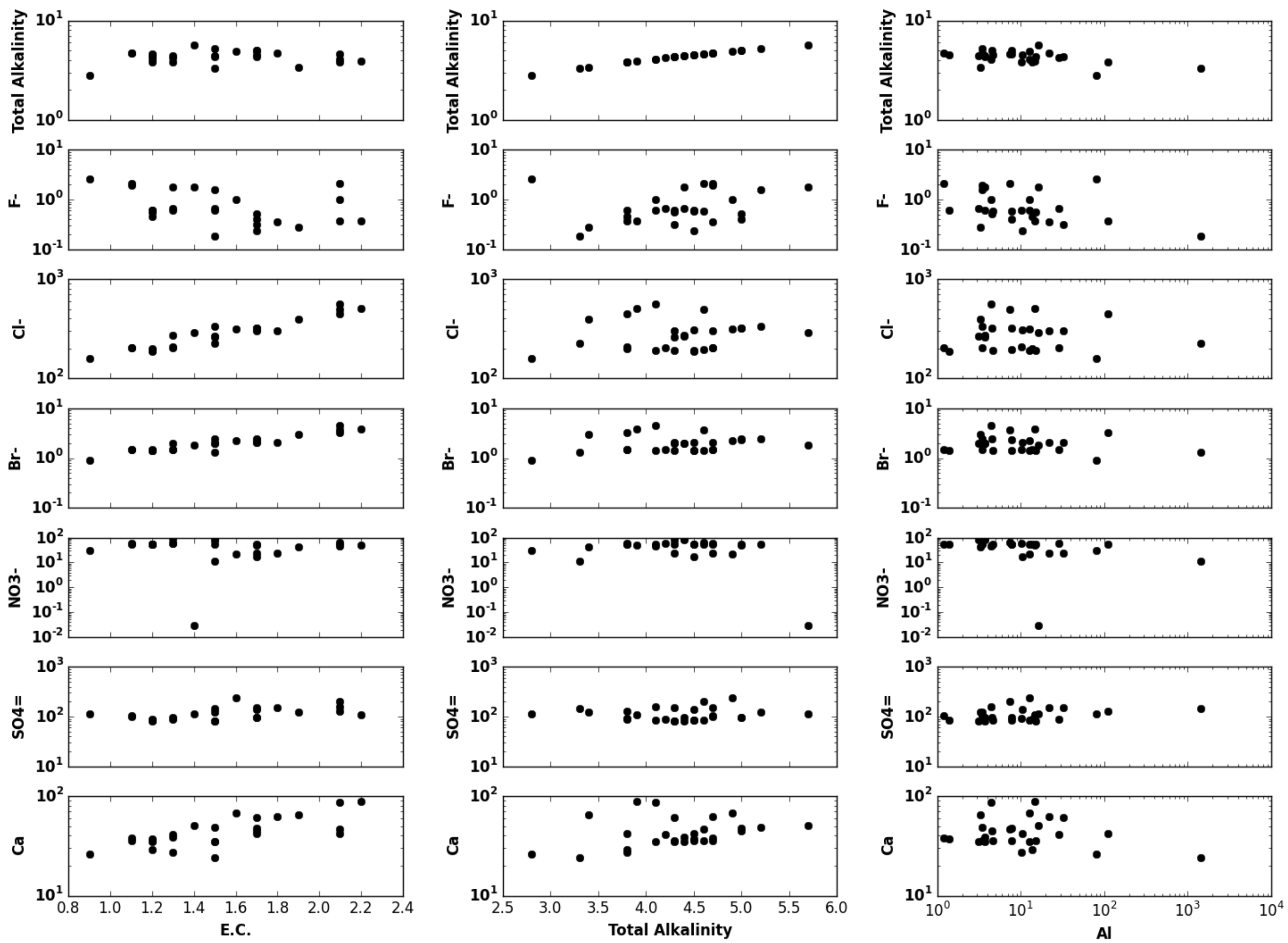


**Continued Appendix Figure C-2. Correlation matrices with EC [mS/m], total alkalinity [meq/L] and Al [ug/L].**

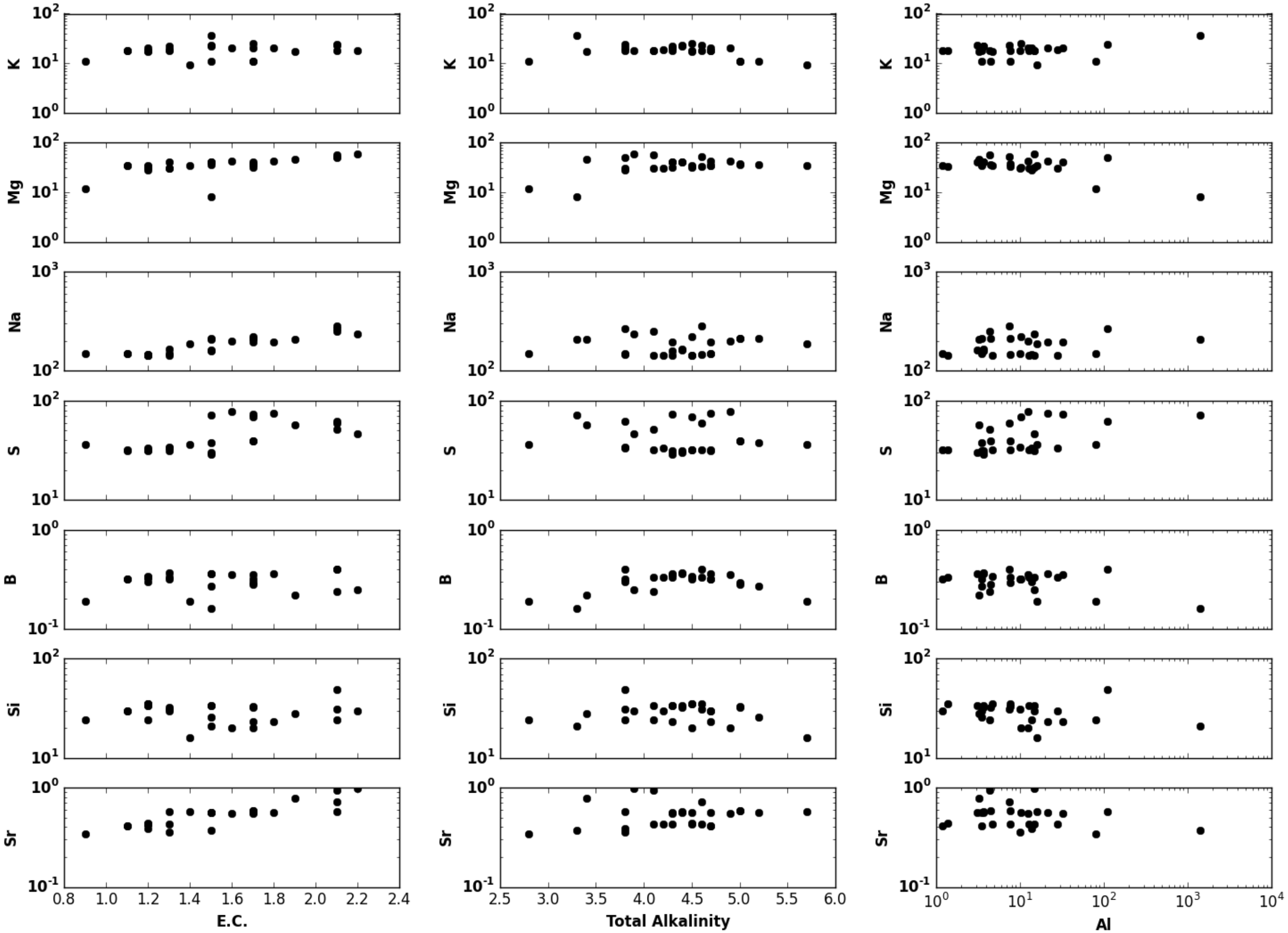


**Continued Appendix Figure C-2. Correlation matrices with EC [mS/m], total alkalinity [meq/L] and Al [ug/L].**

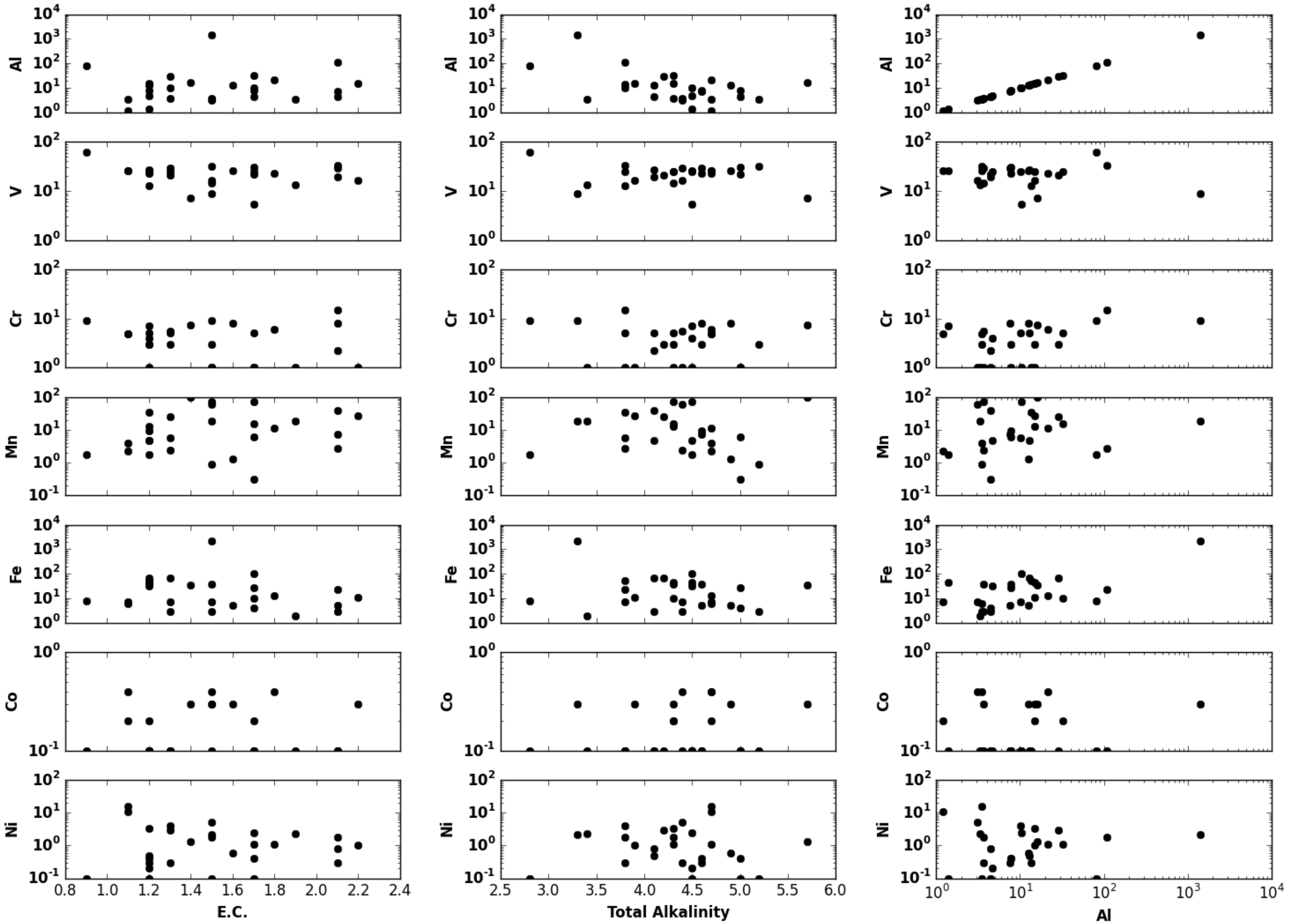


Continued Appendix Figure C-2. Correlation matrices with EC [mS/m], total alkalinity [meq/L] and Al [ug/L].

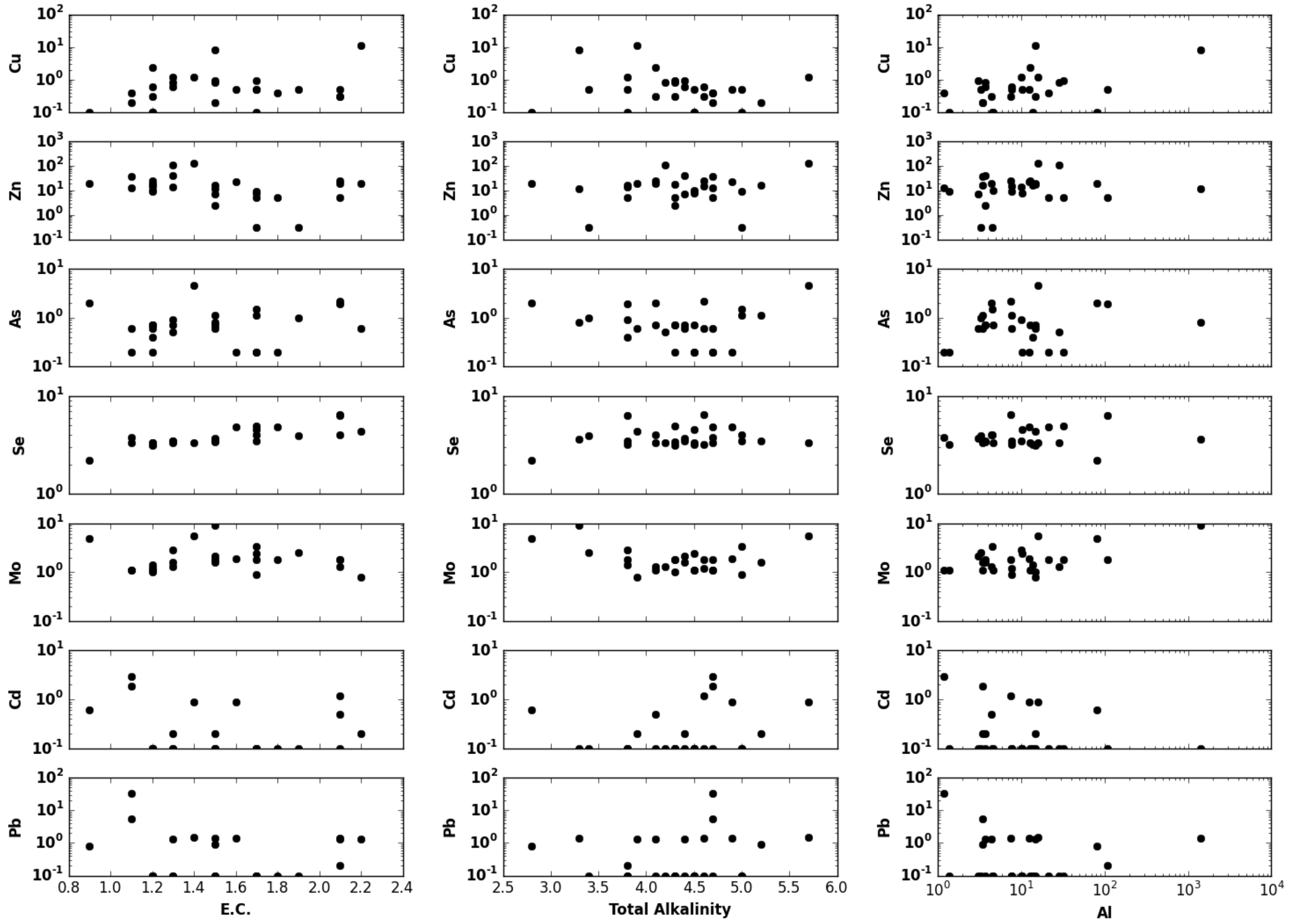


Continued Appendix Figure C-2. Correlation matrices with EC [mS/m], total alkalinity [meq/L] and Al [ug/L].

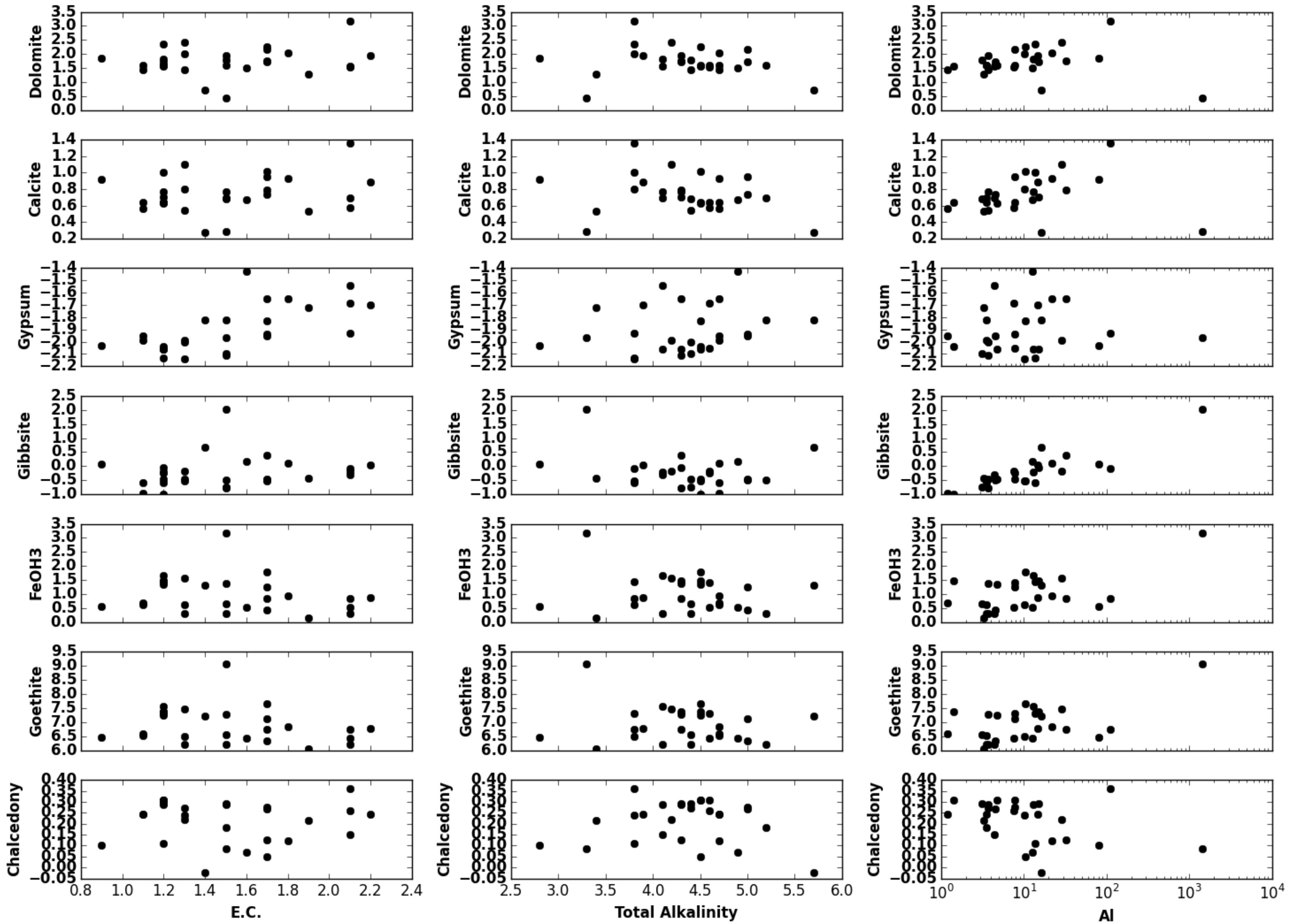


**Continued Appendix Figure C-2. Correlation matrices of saturation indices of major minerals and EC [mS/m], total alkalinity [meq/L] and Al [ug/L].**

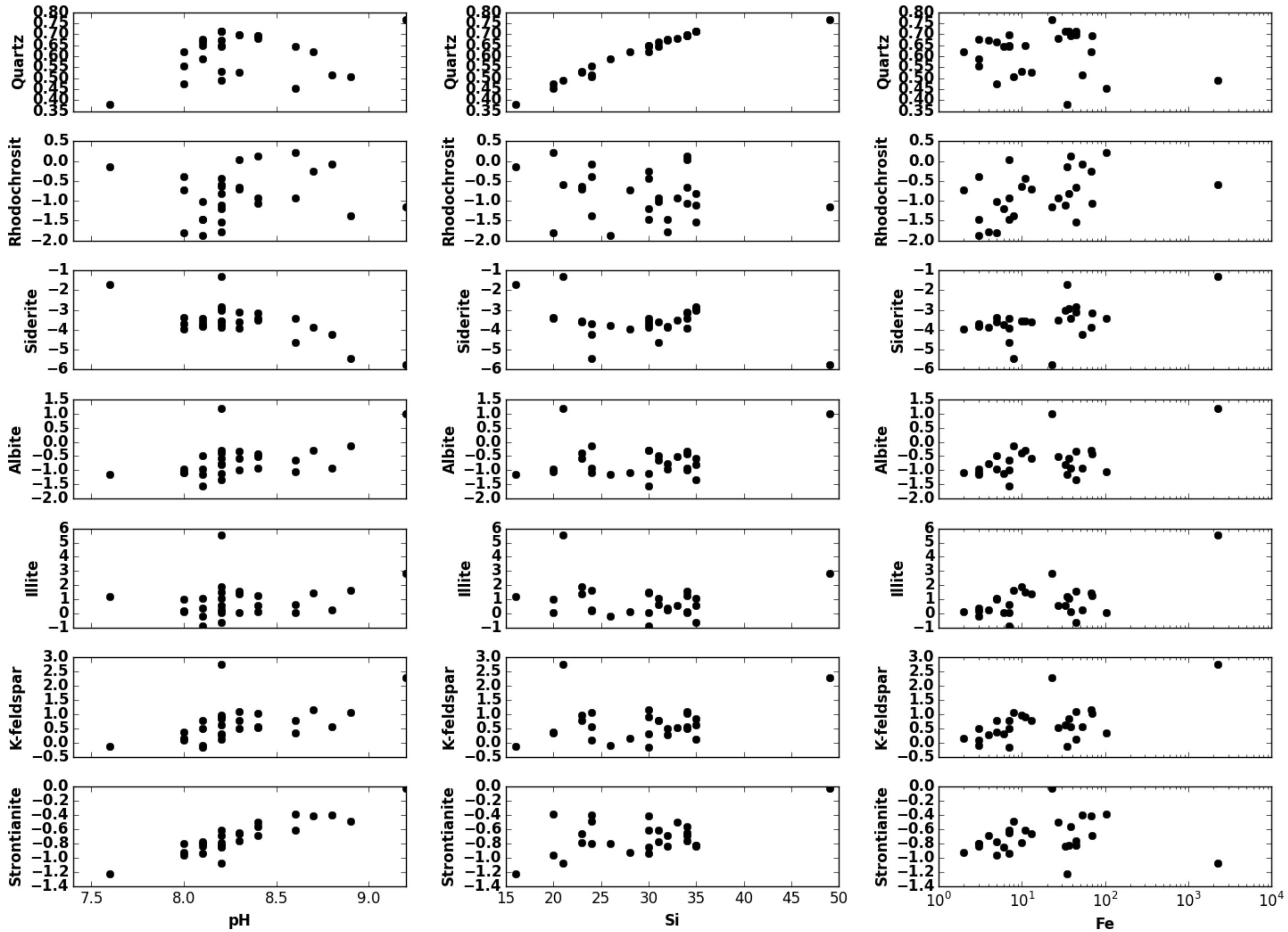


**Continued Appendix Figure C-2. Correlation matrices of saturation indices of major minerals and EC [mS/m], total alkalinity [meq/L] and Al [ug/L].**